DTU Library

Passive Loads Control in the Preliminary and Conceptual Design of Wind Turbine Blades

Pavese, Christian

Publication date:
2017

Link back to DTU Orbit

Citation (APA):
Pavese, C. (2017). Passive Loads Control in the Preliminary and Conceptual Design of Wind Turbine Blades. DTU Wind Energy. DTU Wind Energy PhD

Passive Loads Control in the Preliminary and Conceptual Design of Wind Turbine Blades

Christian Pavese

DTU

Summary (English)

This thesis deals with the development of methodologies for the implementation of passive control strategies in the preliminary and conceptual design process of a wind turbine blade.

Reducing the cost of energy is a key concern for wind energy research and the ultimate goal for both academia and industry. An effective path to achieve this goal is to scale down the increase in total mass of the blades while designing rotors with increasing size and energy yield. In this context, the capability to mitigate loads on the structure during operation becomes an attractive characteristic for the design of modern wind turbine blades.

One of the family of methods for the alleviation of loads on a wind turbine is called passive control, as it relies on the idea of designing a structure that, without any active mechanisms, deforms so as to reduce the unsteady loading generated by turbulent fluctuating wind inflow. The concept behind passive control for wind turbine blades is to produce a structural coupling between flapwise bending towards the tower and torsion towards feathering. This coupling mitigates loads dynamically on the wind turbine structure due to a decrease in the angle of attack.

Researchers have been fascinated by the possibility to embed a form of control directly into the structural design of a wind turbine blade for decades. A wind turbine rotor that can mitigate loads passively can be considered a cost effective solution because the load mitigation effects allow the employment of lighter components without the addition of actuators and mechanical actively-controlled parts. The load mitigation effects can be also used to stretch the size

of the rotor, increasing the energy yield by the machine.

Our contribution to the research in the topic of passive control for wind turbines is articulated as follows. First, we provide a validation of the aero-servo-elastic model used to perform the analysis throughout the work. Once the accuracy of the nonlinear aeroelastic models has been established, we focus on the subtle and complex interactions arising during the design process of passively controlled rotors, due to the mutual effects of aerodynamics, structure, and control. The aim is to provide a fair estimation of the load alleviation potential of different categories of passive control methods.

The parametric study approach, where design parameters which trigger favourable structural coupling effects are changed individually, is not enough to ensure that the full potential of passive control is exploited. Even though parametric studies offer an estimation of load mitigation effects, they do not allow any control on whether standard design requirements have been met or not. Furthermore, these type of studies are not suited to convert the reduction in loads into factors that have a direct impact on the cost of energy, such as the decrease in blade mass or the increase in annual energy production.

We overcome these shortcomings by formulating the passively controlled wind turbine blade design process as an optimization problem using a multidisciplinary design optimization framework. From the application studies reported, we demonstrate how the integration of passive control as a design variable can open the path to the preliminary design of wind turbine rotors with not only considerable load alleviation potential, but also with substantially decreased blade mass or increased annual energy production.

Summary (Danish)

Formålet med denne afhandling er at udvikle metoder der kan direkte anvendes til at implementere passive kontrol egenskaber i vindmølle vinge på et tidligt tidspunkt i den konceptuelle design fase.

Et helt centralt element for forskning i vindenergi er at sænke prisen på vindenergi. En effektiv måde at opnå dette er ved at sænke den samlede vægt samtidig med at vindmølle rotorerne mht. størrelse og ydelse øges. I denne sammenhæng er evnen til at begrænse lasterne under drift en attraktiv egenskab for design af moderne vindmølle vinger.

En måde til at begrænse lasterne på vindmøllen er passiv kontrol, der fundamentalt baseres på at strukturen i sig selv aflastes når den deformeres, så de varierende aerodynamiske kræfter fra det turbulente vindfelt reduceres. Konceptet bag passiv kontrol er med direkte ord at skabe en strukturel kobling mellem den flapvise udbøjning af vingen til vridning af vingen. Det giver en dynamisk aflastende effekt da indfaldsvinklen reduceres når vingens vridning ændres.

Muligheden for at indføre passiv kontrol i vinger har været et centralt punkt i aero-elastisk forskning i årtier. En vindmølle rotor, der kan aflastes passivt, er en kost effektiv løsning, da det muliggør et lettere design uden at tilføre behov for aktive systemer i form at aktuatorer og andre mekaniske løsninger. De mindre laster muliggør også at kan vingen forlænges, hvilket dermed forbedrer produktionen og kosteffektiviteten af hele møllen.

Som det første gives en validering af den aero-servo-elastiske model der benyttes til senere analyser. Derefter fokuseres den komplekse sammenhæng i vingens

design gennem den samlede effekt af aerodynamik, struktur og kontrol. Målet er at opnå et reelt estimat for potentialet af den lastreducerende effekt fra flere typer af passive metoder.

At det er muligt at skabe fordelagtige koblinger i strukturen ved at ændre på enkelte design parametre er i sig selv ikke nok til at sikre at det fulde potentiale udnyttes. Selvom man kan demonstrere at lastreduktion i visse situationer kan opnås, er det vanskeligt at se om strukturen overholde alle krav. Derudover er denne type af undersøgelser ikke velegnet til at omsætte den mulige lastreduktion til faktorer der direkte påvirker kosteffektiviteten, såsom reduktion af vingens egenvægt eller forøget energiproduktion.

Ved i stedet at formulere den design processen som et multidiciplinært optimeringsproblem er det muligt at udnytte potentialet af passiv kontrol fuldt. Fra de udførte studier, demonstreres hvordan integration af passiv kontrol som en design variabel kan åbne vejen til vindmøllevinger, hvor der via passiv lastreduktion kan opnås betydelig lavere vægt af vingerne eller forøget energiproduktion af vindmøllen.

Preface

This thesis was prepared at the Department of Wind Energy at the Technical University of Denmark (DTU) in partial fulfilment of the requirements for acquiring a Ph.D. degree.

The thesis addresses the implementation of passive control methodologies in the preliminary and conceptual design of wind turbine blades. Methods are investigated and developed to include parameters which trigger passive control effects in the design of wind turbine blades.

The thesis consists of a summary report and seven research papers, detailing the research conducted over the period of January 2014 to December 2016.

Lyngby, 15th Decemeber-2016

Christian Pavese

Christian Pavese

Acknowledgements

Thanks to my girlfriend, Niamh, for her constant encouragement and unquestioned support. Thanks for reading my thesis cover to cover. I am sure that this was not the most entertaining experience of our relationship. I like to think that I would have done the same if you asked me, but we will never be sure! Thanks to my friends and family in Italy for all their support through the years. Thanks to all my friends here in Denmark and in the Risø Campus (if my experience here in Denmark has been nothing but great and fun, it's thanks to you!). Thanks to my football team and my squash companions, who helped soften the frustrations of this PhD. All these people might have not contributed that much to my technical knowledge, but they made me the person I am today (I hope a good one!).

Finally, thank You, Reader. I hope that you will not stop at the acknowledgements, but that you will take the time to learn a little something about the cost of wind energy (Chapter 2), and what is passive control for wind turbines (beginning of Chapter 3). I cannot promise you that you will like it, but as my professor of Italian and Latin always reminded me when I did not want to learn something that sounded uninteresting

Considerate la vostra semenza:
fatti non foste a viver come bruti,
ma per seguir virtute e conoscenza.

Consider well the seed that gave you birth:
you were not made to live as brutes,
but to follow virtue and knowledge.

Canto XXVI, Divina Commedia, Dante Alighieri

List of Publications

Scientific Research Publications in this Thesis

A Christian Pavese, Qi Wang, Taeseong Kim, Jason Jonkman, Michael A. Sprague (2015). "HAWC2 and BeamDyn: Comparison Between Beam Structural Models for Aero-Servo-Elastic Frameworks," In Proceedings of European Wind Energy Association Annual Conference 2015, Paris, France.

B Christian Pavese, Carlo Tibaldi, Taeseong Kim (2015). 'Study on Controller Tuning of Wind Turbines with Backward Swept Blades," In Proceedings of AIAA SciTech 2015 - 33rd Wind Energy Symposium. Kissimmee, Florida, USA

C Christian Pavese, Taeseong Kim, Juan Pablo Murcia (2015). 'Design of a Wind Turbine Swept Blade Through Extensive Load Analysis,", Renewable Energy Journal, Elsevier, 2016, DOI: 10.1016/j.renene.2016.10.039

D Christian Pavese, Taeseong Kim (2014). 'Implementation of Passive Control Strategies Through Swept Blades,", in: Proceedings of the 10th PhD Seminar on Wind Energy in Europe, 28-31 October 2014, Orleans, France

E Christian Pavese, Vladimir Fedorov, Kim Branner (2015). 'New lightweight structural blade designs and blade designs with build-in structural couplings - New Structural Solutions, sec. 2.3", in: Innovative Wind Conversion Systems (10-20MW) for Offshore Applications (INNWIND), Deliverable 2.22, Agreement n. 308974, supported by EU 7th Framework Programme

F Christian Pavese, Carlo Tibaldi, Torben J. Larsen, Taeseong Kim, Kenneth Thomsen (2016). 'Reduced Design Load Basis for Ultimate Blade Loads Estimation in Multidisciplinary Design Optimization Frameworks", in: Journal of Physics: Conference Series - The Science of Making Torque from Wind 2016, IOP publishing

G Christian Pavese, Carlo Tibaldi, Frederik Zahle, Taeseong Kim (2016). 'Aeroelastic Multidisciplinary Design Optimization of a Swept Wind Turbine Blade", Journal Paper, Under Revision

Other Works and Co-authorships Not Included in this Thesis

H Christian Pavese, Flemming Rasmussen (2014). 'New concepts to control the load along the span of the blade, passive, active or mixed, sec. 5", in: Innovative Wind Conversion Systems (10-20MW) for Offshore Applications (INNWIND), Deliverable 2.31, Agreement n. 308974, supported by EU 7th Framework Programme

I Wilfried Njomo Wandji, Christian Pavese, Anand Natarajan, Frederik Zahle (2016). 'Reduction of fatigue loads on jacket substructure through blade design optimization for multi-megawatt wind turbines at 50 m water depths", in: Journal of Physics: Conference Series - The Science of Making Torque from Wind 2016, IOP publishing

J Frederik Zahle, Carlo Tibaldi, Christian Pavese, Michael K. McWilliam, Jose P. A. A. Blasques, Morten H. Hansen (2016). 'Design of an Aeroelastically Tailored 10 MW Wind Turbine Rotor", in: Journal of Physics: Conference Series - The Science of Making Torque from Wind 2016, IOP publishing

Contents

Part I

Summary Report

CHAPTER 1

Introduction

1.1 Context and Motivation

Reducing the cost of energy is a key concern for wind energy research and the ultimate goal for both academia and industry. An effective path to achieve this goal is to scale down the increase in total mass of the blades while designing rotors with increasing size and energy yield [1]. In this context, the capability to mitigate loads on the structure during operation becomes an attractive characteristic for the design of modern wind turbine blades [2].

A variety of techniques have been exploited in the last two decades to achieve load reduction on wind turbines, and they can be generally categorized in two branches: active and passive loads control methods. The first consists of technologies able to reduce loads by actively controlling the machine, e.g. blade pitch actuators [3], moving flaps [4], etc. The second is based on the idea of designing a structure that, without any additional components, deforms so as to induce a load reduction when it is loaded [5].

Researchers have been fascinated by the possibility to embed a form of control directly into the structural design of a wind turbine blade for decades [5, 6, 7, 8, 9]. A wind turbine rotor that can mitigate loads passively can be considered a cost effective solution [10], as it allows the employment of lighter components due

to the load mitigation effects without the addition of actuators and mechanical actively controlled parts.

The concept behind passive loads control for wind turbine blades is to produce a structural coupling between flapwise bending towards the tower and torsion towards feathering. This coupling mitigates loads dynamically on the wind turbine structure due to a decrease in the angle of attack [5].

For a long time, the theoretical model of couplings on highly tailored composite structures, which has been in development since the 70s [11], has been considered too complex and computationally expensive for the tools used to simulate wind turbines in operation. In fact, the computation of loads on a wind turbine is a field that involves interlaced disciplines such as aerodynamics, structural dynamics, and control theory (**aero-servo-elasticity**). The tools capable of performing this computation need incorporate modelling simplifications to keep the computational time in a reasonable range.

Recently, the development of models more suitable to be integrated in the modern aero-servo-elastic codes [12, 13], and the possibility of accessing high-performance computing clusters, opened up a path to the modelling of passive loads control. The benefits of this are twofold; firstly, the potential of the employment of this type of control can be explored using more accurate and appropriate tools; secondly, the design problem of a passively controlled blade can be approached in a more systematic way, using tools able to handle the interconnecting disciplines involved in a practical amount of time.

The implementation of passive loads control methodologies for modern wind turbine blade design is a problem that can finally be fully addressed. The beneficial effects of the employment of tailored structural coupling on a wind turbine rotor in operation have been already demonstrated [8, 14, 15], but its full potential never investigated. The reason is the aforementioned complexity and multidisciplinarity of the blade design problem. This problem can now be properly tackled, not only further highlighting the multiple connections between the disciplines involved using the recently developed aero-servo-elastic models, but also using ad hoc frameworks capable of streamlining the design of a wind turbine blade considering all the necessary design requirements and limitations [16, 17, 18, 19]. These frameworks include all the significant steps for the preliminary and conceptual design of a wind turbine blade. The process is fully automated and an optimizer can be included in the framework's workflow, so that the blade design process can be formulated as an optimization problem.

Multidisciplinary design optimization frameworks are the key to providing a blade design able to fully benefit from the passive loads control concepts, which can be implemented in multiple configurations and multiple combinations. The

formulation of an optimization problem is the best way to completely take into account the interlaced disciplines involved in the blade design process and the conflicting objectives that a rotor design is subjected to.

1.2   Thesis Objectives

The objective of this thesis is to develop methods for the implementation of passive loads control strategies for the preliminary and conceptual design of wind turbine blades. In the interest of narrowing the scope of this work and developing specialised aeroelastic methods, detailed structural and fluid dynamics computations, as well as details related to the manufacturing process of blades are not considered.

Two central research questions are addressed in this thesis, each consisting of a number of secondary research tasks:

I. How can the effects of passive loads control strategies be fairly estimated?

Addressing this research question necessitates consideration of the multiple interactions between the disciplines that constitute the wind turbine blade design process. The investigated methodologies for the design of passively controlled rotors have to take into account how tailored changes in the blade structure affects the aerodynamic performance, the structural behaviour, and the dynamics of the controller of the wind turbine. If these interactions are taken into account, a more accurate estimation of the beneficial and negative effects brought by the employment of passive loads control can be provided.

II. How can the full potential of passive loads control for wind turbines be explored?

Once the multidisciplinary nature of the design of passively controlled rotors is highlighted, together with its extreme complexity, a method must be investigated to include passive loads control in the design process while retaining a complete view over the design requirements for wind turbine blades. Passive loads control strategies cannot be drily implemented on an existing design, but the blade properties need to be tailored to accommodate the passive loads control method chosen. If the blade design is optimized according to the particular passive loads control strategy selected, the full potential of these control methodologies can be explored, and translated in material reductions or increase

in annual energy production.

This thesis is motivated by a lack of existing academic research addressing the multidisciplinary nature and significant complexity of the design of modern wind turbine blades employing passive loads control strategies. This thesis seeks to remedy this lack of research by investigating the interactions between the disciplines involved in the process of designing a passively controlled rotor. When these interactions are evaluated, a method is developed to take into account the multiple design requirements and the conflicting objectives that take part in the process of designing a blade employing passive loads control strategies.

1.3   Thesis Contributions

As an initial step, we assessed the accuracy of the model needed to properly simulate the behaviour of wind turbines employing passive loads control strategies. Modern wind turbine blades are highly tailored composite structures that have been growing in size and flexibility to increase energy yield while containing material costs. They undergo large deflections and rotations without exceeding their specific elastic limit. To accurately compute these deformations, appropriate structural models for aero-servo-elastic frameworks have been developed. In Paper A, we provide a demonstration of the accuracy and capabilities of the model used in this thesis.

The aim of introducing passive loads control strategies on a wind turbine blade is to mitigate loads on the structure. The employment of passive loads control on the design of a modern wind turbine blade adds complexity to a problem that is already characterized by the interactions of multiple disciplines, such as aerodynamics, structural dynamics, and control theory. Due to these interactions, a design parameter that is changed to generate a passive loads control behaviour, can trigger changes in the controller dynamics of the wind turbine (which, in turn, can produce an effect on the wind turbine loading) or in the performance of the system, among others. We addressed the interaction of a passively controlled rotor with the dynamics of a wind turbine controller in Paper B, and with the aerodynamic performance of the system in Paper D.

We started performing parametric studies with the intention of investigating the potential of passive loads control. We have taken into account the changes in the dynamics of the controller and the performance of the wind turbine, offering a fair comparison of the effects of the implementation of a passive loads control strategy with respect to an initial design. Investigating an easy-to-implement passive loads control method such as sweep in Paper C, we show that a para-

metric study approach provides useful information about the effects of passive loads control, but does not give the possibility to deal with all the standard design requirements for a wind turbine blade. To compensate for negative effects on the design requirements brought about by the implementation of a single passive loads control method, we have performed a parametric study involving combined passive loads control techniques. In Paper E, we demonstrate that negative effects on the design requirements can be compensated by exploiting the synergy between the different passive loads control strategies. We highlight that even though certain negative effects can be mitigated, the parametric implementation gives no control on whether all the standard design requirements can be met or not. Furthermore, parametric studies offer only an estimation of load mitigation effects, but they are not suited to convert the reduction in loads into factors that have a direct impact on the cost of energy, such as the decrease in blade mass or the increase in annual energy production. The design of a passively controlled rotor is a multidisciplinary problem, and it has to be treated at such.

The multidisciplinary nature of blade design is a complex challenge that cannot be addressed with parametric studies because it compels the designer to simultaneously satisfy several constraints while evaluating trade-offs between conflicting objectives. In this context, multidisciplinary design optimization (MDO) frameworks are used to develop wind turbine blades. Design parameters are optimized with respect to a cost function, subjected to constraints that encompass standard design requirements for wind turbines. MDO is the method that we have used to provide a blade design that can fully explore the potential of different passive loads control techniques.

The main contribution of our work in relation to multidisciplinary design optimization of a wind turbine blade is the implementation of passive loads control as a design variable. There is a lack of research related to the use of design parameters capable of triggering passive loads control as design variable in an optimization framework. The reason being that the employment of a passive loads control strategy has a large impact on the wind turbine loading. A considerable number of aero-servo-elastic simulations are needed to properly capture the effect of passive loads control methods on the loads. The main issue is that a large number of simulations represent an excessively expensive computational effort for an optimization framework. We addressed this problem in Paper F, where we develop a method to reduce the size and number of computationally expensive simulations.

The final section of Paper F, Paper G, and the final part of this summary report show the efficacy of an MDO applied to the problem of designing a blade with different forms of passive loads control.

As a final note, we need to stress that the methods investigated in this thesis involve the **preliminary** and **conceptual** design a wind turbine blade. The successive steps of a blade design process, which involve the detailed structural and fluid dynamic design, as well as the manufacturing and production, are not part of the research detailed in these pages.

1.4 Thesis Structure

This thesis is structured as follows. Part I is a summary report outlining the main contributions of this thesis and how these contributions can fit into the larger wind energy picture. Chapter 2 provides an insight on the cost of wind energy and the impact of the design of wind turbine blades on the levelised cost of electricity. Chapter 3 describes the concept of passive loads control methods for wind turbines. The implementations of these control strategies are presented through Chapter 4 to Chapter 7 along with selected research results from Part II. Chapter 8 provides conclusions and perspectives.

Part II consists of the publications that contribute to this thesis. The contribution of each author is listed to ease the assessment of the Ph.D. candidate.

Paper A is a peer-reviewed article published in *Proceedings of European Wind Energy Association Annual Conference 2015*. It consists of a comparison between structural beam models for aero-servo-elastic frameworks.

Paper B is a peer-reviewed article published in the *Proceedings of AIAA SciTech 2015 - 33rd Wind Energy Symposium*. It consists of a study on the dynamics and the tuning of a controller of wind turbine employing backward swept blades.

Paper C is a journal article published in *Renewable Energy* in which a detailed load analysis of a parametric study of wind turbine swept blades is carried out to explore the potential of this passive loads control strategy.

Paper D is a peer-reviewed article published in *Proceedings of the 10th PhD Seminar on Wind Energy in Europe*. This publication describes the effects of the employment of backward swept blades on the aerodynamic performance of a wind turbine.

Paper E is a peer-reviewed technical report published as part of the *Innovative Wind Conversion Systems (10-20MW) for Offshore Applications (INNWIND), Deliverable 2.22*. It consists of a parametric study focused on the evaluation of the synergy and the discord in the employment of different combinations of passive loads control strategies on a wind turbine.

Paper F is a peer-reviewed journal article published in *Journal of Physics: Conference Series - The Science of Making Torque from Wind 2016*. We describe a method that reduces the computational time in optimization frameworks for the estimation of the ultimate blade load envelopes. We apply this method for the optimization of a blade employing material bend-twist coupling.

Paper G is a journal article submitted for consideration in *Wind Energy*. In this article, the methodology for a multidisciplinary design optimization of swept blades is presented and validated.

CHAPTER 2

The Cost of Wind Energy

2.1 There are no shortcuts...

Wind power is one of the oldest sources of energy known to mankind. Since the mass production of Danish wind turbines started in 1979, wind power technologies have experienced an incredible growth. This forty-year successful progress has been driven by cutting edge research and the strive to develop the best possible ways of extracting energy from the wind.

When we talk about technology improvements in wind energy, we always weigh them against their potential for reducing the cost of energy (COE). There are no ways around this, and there are no shortcuts. The cost of energy is a determining factor. The analysis of its trend is of critical importance to establish whether innovative concepts for the generation of wind energy are worth pursuing.

If we look at the statistics, after 20 years of steady reduction, the wind power generation costs have stabilized, showing attenuated capacity for further reductions of COE [1, 20]. On a global scale, using the levelised cost of electricity (LCOE)[1] as criterion for comparison, we can observe that during the last 5 years

---

[1]"The LCOE of a given technology is the ratio of lifetime costs to lifetime electricity generation, both of which are discounted back to a common year using a discount rate that

2014 USD/kWh
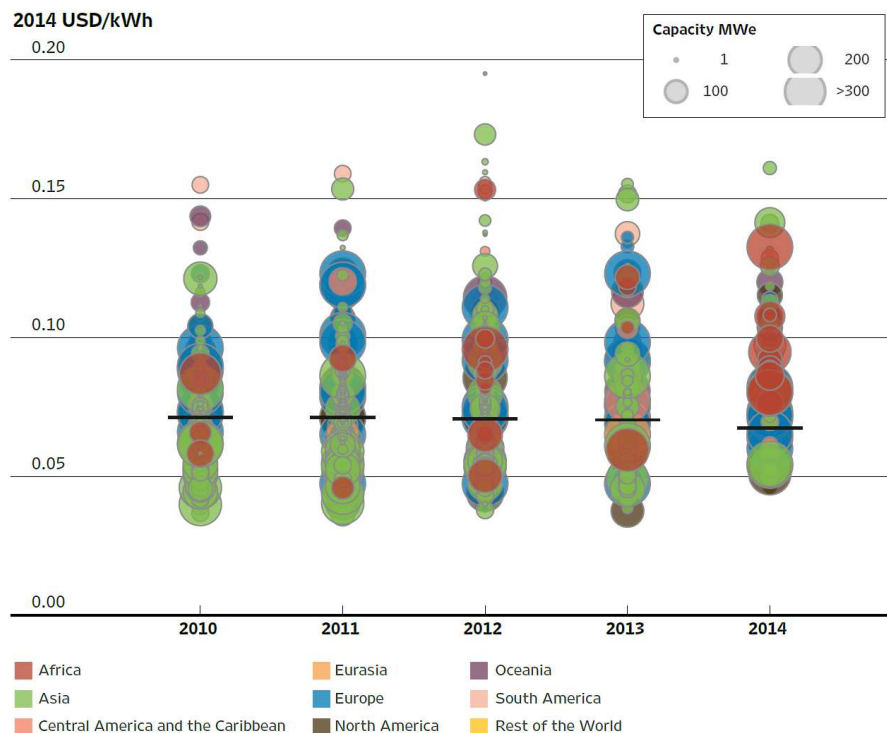
Figure 2.1: Global LCOE and weighted average of commissioned and proposed large wind farms (>5 MW) from 2010 to 2014 [1, p. 73].

the cost of energy of wind farm projects followed a stable trend (Figure 2.1).

According to the International Renewable Energy Agency (IRENA), "the global weighted average LCOE of wind has fallen by 7% between 2010 and 2014" [1, p.73], but this decrease cannot be attributed exclusively to technology improvements. In fact, the global LCOE for wind power has been driven down mostly by the low installation costs typical of large and fast-growing markets like China, where the availability of cheap labour and materials creates a significant impact on the global LCOE (Figure 2.2).

This observation is related to the combined onshore and offshore wind energy sectors. If we look exclusively at the offshore sector, where fast-growing economies have not yet left their mark, we can observe a dramatic increase in the global average LCOE in the decade from 2002 to 2012 (Figure 2.3). This incre-

---

reflects the average cost of capital." [1, p. 3]
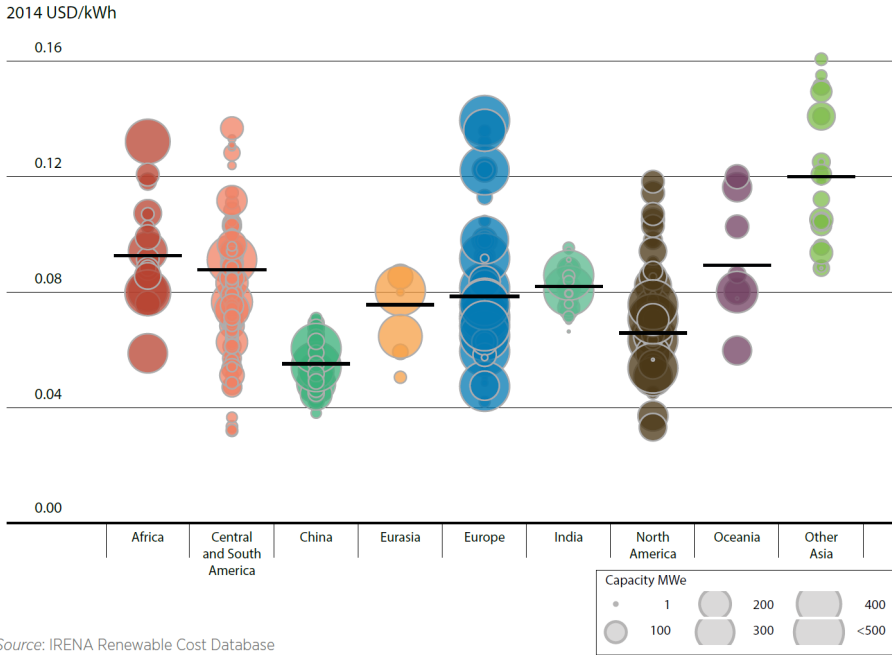
Figure 2.2: Global LCOE and weighted average of commissioned and proposed wind projects by country and region (>5 MW), 2013 to 2014 [1, p. 73].

ment is due to several reasons, including operation and maintenance costs, and large capital investments in offshore cables, foundations, offshore transportation and installation of equipment and turbines, etc.

Even though the LCOE has decreased by the aforementioned 7%, the general picture shows an onshore industry relying on the expansion in new and more affordable markets, and an offshore sector that languishes unable to value and drive technological breakthroughs.

Let us bear in mind that most wind power projects developed today are characterized by electricity generation costs well within the range of fossil fuel-fired LCOE (0.045-0.14 USD/kW h) [1], and offshore wind farms planned to 2020 are expected to deliver even lower average costs. However, a question arises: how can we keep driving down the COE, while liberating the onshore sector from the short-term dependency on emerging markets, and lowering offshore wind power generation costs?
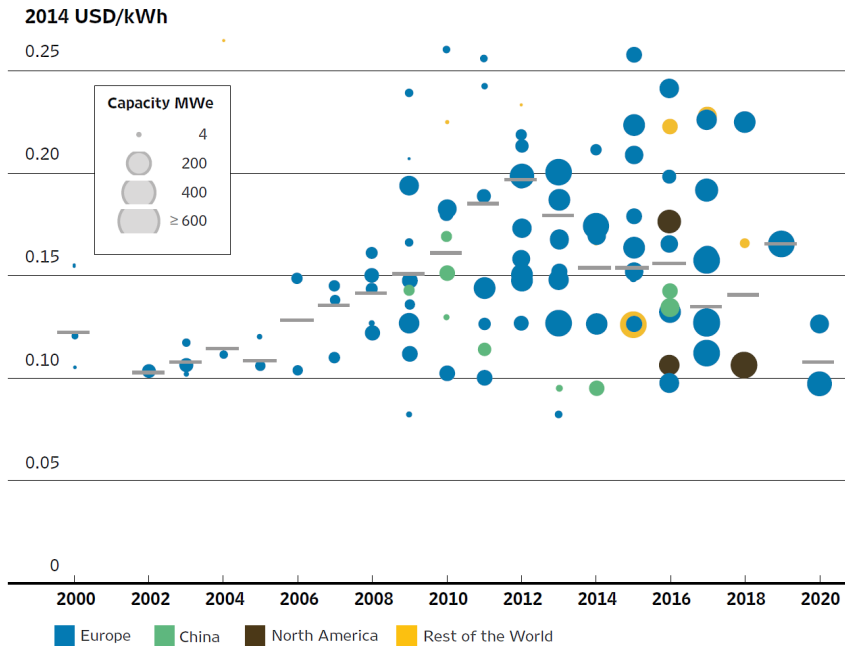
Source: IRENA Renewable Cost Database

Figure 2.3: Global LCOE and weighted average of commissioned and proposed offshore wind projects, 2000 to 2020 [1, p. 73].

We will take things one step at the time. We established that the analysis of the LCOE is an extremely useful metric, able to provide the necessary information to discern the factors that drive the development of wind energy. We will now show that a more detailed and tailored definition of this metric can be used to ratify the impact of research and technological improvements in wind power generation.

The final goal is to reveal how particular aspects of wind energy R&D can drive down the COE independently from factors like cheap labour and materials availability.

2.2 The Levelised Cost of Electricity in Wind Energy

The general definition of LCOE relates the lifetime costs of a generic power plant to its production of electricity. The danish consortium Megavind[2] provides a specific definition of the LCOE that can be applied to all the wind farms: "LCOE expresses the "levelised" unit cost of 1 MW h over the lifetime of the wind farm by taking the sum of the discounted lifetime costs relative to the sum of the discounted energy production at the time of the financial investment decision." [21, p. 6]

More details on the Megavind's LCOE model can be found in the respective report [21]. For the sake of clarity, we will report the basic mathematical expressions behind this model. The purpose is to present to the reader a clear, yet simplified, overview of the economic factors that drive the research exposed in these pages.

The wind-energy-tailored definition of LCOE is described by a very simple equation:

$$LCOE = \frac{C_{t_0}}{P_{t_0}} \tag{2.1}$$

where the numerator C_{t_0} is the value of all the expenditures associated with the wind farm at the present time (time of investment decision t_0), and the denominator P_{t_0} is the present value of the energy production. Specifically:

$$C_{t_0} = \sum_{year=k_c}^{T} \frac{I_{year} + O_{year} + A_{year}}{(1 + W_n)^{year}} = \frac{I_0 + O_0 + A_0}{(1 + W_n)^0} + ... + \frac{I_T + O_T + A_T}{(1 + W_n)^T}$$

$$P_{t_0} = \sum_{year=k_p}^{T} \frac{AEP_{year}}{(1 + W_r)^{year}} = \frac{AEP_0}{(1 + W_r)^0} + \frac{AEP_1}{(1 + W_r)^1} + ... + \frac{AEP_T}{(1 + W_r)^T}$$
$$\tag{2.2}$$

Cost and production are summed annually over a lifetime period T, which starts from the earliest year with cash flows k_c or the earliest year with energy production k_p, respectively. The present value of the expenditures includes:

---

[2]Established in 2006, Megavind is Denmark's national partnership for wind energy. Its steering committee is formed by a public-private cooperation between the state, private enterprises, and knowledge institutions. The role of Megavind is to act as a catalyst and initiator for a stronger strategic agenda for research, development, and demonstration within several areas of wind energy technology. [21]

- I_{year}, the initial investment costs including

  – the development expenditures (DEVEX), all the costs spent from idea and development to design and planning;

  – the capital expenditures (CAPEX), the "first power" costs spent from construction to commission;

- O_{year}, the operational expenditures (OPEX), the costs related to maintaining the wind farm in operation;

- A_{year}, the abandonment cost (ABEX), the expenditures related to the decommissioning of the wind farm.

AEP_{year} is the annual energy production of the wind farm, which ultimately represents the annual revenues from the project.

Finally, W_n is the nominal weighted average cost of capital, and W_r is the real weighted average cost of capital, connected by the following equation:

$$W_r = \frac{1 + W_n}{1 + I} - 1 \tag{2.3}$$

where I is the inflation rate.

Equations from 2.1 to 2.3 help us understand which factors affect the cost of energy and how we can produce an impact on these factors to lower the LCOE.

Previously, we posed a question about how particular aspects of wind energy R&D can drive down the cost of energy independently from cheap labour and cheap materials availability. It is time to be more specific and go back to the title of this work. In particular, it is now time to discuss **wind turbine blade design**, one of the "aspects of wind energy R&D", and how we can relate it to the cost model presented in this chapter.

2.3 The Cost of Wind Turbine Rotor Blades Design

How does the design of wind turbine rotor blades impact Equations 2.1 and 2.2? If we look at the present value of the energy production P_{t_0}, the answer is clear: the characteristics and the performance of the rotor are strictly connected to the energy extracted by the turbine. The design of rotors for a wind farm needs to comply to several requirements dictated, for instance, by the standards, the site

selected, and the availability of wind resources. Even if these requirements limit the amount of energy that can be produced, the concept is still straightforward: the higher the AEP produced by the rotor during its lifetime, the lower the LCOE (assuming, of course, that the expenditures C_{t_0} do not increase as the AEP increases).

The evaluation of the impact of the rotor design on the expenditures C_{t_0} is more complex. The design of wind turbine blades, specifically, influences the initial investment costs (I_{year}), and it might have an impact on the operational (O_{year}) and abandonment expenditures (A_{year}). In this work, we will give a quantification of this influence on the CAPEX and DEVEX. The impact on OPEX and ABEX is not considered, due the complexity of the detailed estimation of the operation, maintenance, and decommissioning costs, to which more specialized branches of wind energy research are dedicated.

Wind farms investment costs take into account several aspects. We can get an idea of the costs that constitute I_{year} by looking, for example, at the comparison between the breakdown of typical initial investments for onshore and offshore projects in UK before 2007 (see Figure 2.4 and Figure 2.5, respectively). The data, provided by the Department of Trade and Industry [22], shows which are typically the main contributors to the total investment costs of wind farm projects. Even though the cost of the foundations for offshore wind farms accounts for a significant proportion of costs, the largest part of the investment is represented by the wind turbines. This observation is supported by more recent studies, summarized in Table 2.1 [1, 20, 23, 24, 25]. The cost share of the wind turbines can vary between 65 and 84% for onshore projects, and 30 and 50% for offshore projects. If we further breakdown the wind turbines share of the investment costs, we can see that the blades account for approximately 20% of that share (Figure 2.6). An effective way to lower the share of this investment cost is to reduce the cost or the quantity of materials used for the manufacturing of the wind turbine blades [26].

The analysis presented here is based on data from publicly available reports. The economic aspects of a wind farm business case are more complex than described here, but the information presented in Figures 2.4, 2.5, and 2.6, and Table 2.1 provide a clear quantification of the influence that the design of rotor blades can have on the investments costs.

We need to highlight a crucial point before continuing our discussion: while the design of rotor blades has a direct impact on the LCOE through the annual energy production, it can only influence the total expenditures by acting on a percentage of a percentage of one out of three parameters (initial investment, operational, and abandonment costs).
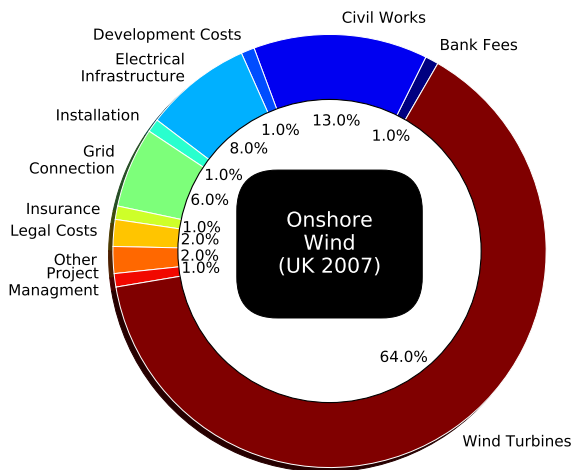
Figure 2.4: Comparison between typical breakdown investment costs of on-
shore wind farms in UK before 2007 [22, p. 21].
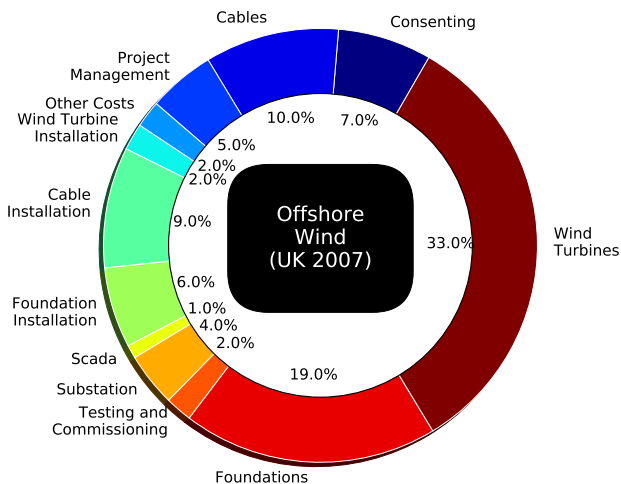
Figure 2.5: Comparison between typical breakdown investment costs of off-
shore wind farms in UK before 2007 [22, p. 21].

Table 2.1: General comparison between the broken down investment costs of onshore and offshore wind farms in developed countries in 2011 [1, 20, 23, 24, 25].

	ONSHORE	OFFSHORE
Investment Costs (USD/kW)	1700 - 2450	3300 - 5000
Wind Turbine Cost Share[a] (%)	65 - 84	30 - 50
Grid Connection Cost Share[b] (%)	9 - 14	15 - 30
Construction Cost Share[c] (%)	4 - 16	15 - 25
Other Capital Cost Share[d] (%)	4 - 10	8 - 30

[a] Wind turbine costs includes the turbine production, transportation, and installation.
[b] Grid connection costs include cabling, substations, and buildings.
[c] The construction costs includes transportation and installation of wind turbine and tower, construction of the foundations and the infrastructures required for the installation of the wind turbines.
[d] Other investment costs include development and engineering costs, licensing procedures, consultancy and permits, SCADA (Supervisory Control and Data Acquisition) and monitoring systems.
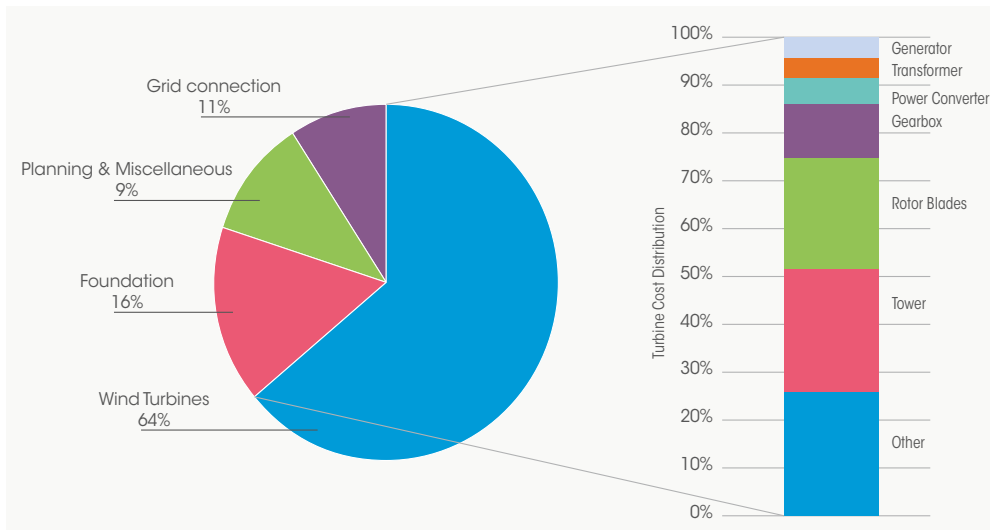
Figure 2.6: Onshore wind farm investment cost breakdown. In turn, the broken down cost of the wind turbines is highlighted [1, 20].

In the next chapter, we describe how we should act on the design of wind turbine blades to lower the LCOE. The understanding of the factors in the blade design process that can positively influence the trend of the LCOE is crucial, as the cost modelling presented in the current chapter will not take directly part in the wind turbine blade design studies carried in this dissertation.

Passive Loads Control for Wind Turbines

In the following chapter, we describe a concept that, when implemented properly in the design of a wind turbine blade, can lower the cost of energy. We introduce the concept of **passive loads control**.

3.1 Reduce Wind Turbine Loads to Reduce the LCOE

We established that the LCOE is the most important criterion to establish the value of wind energy research and development. Giving a more detailed description of the LCOE, we saw how the design of wind turbine rotors can produce a positive impact to lower the cost of wind energy. Specifically, wind turbine rotor design can: increase the annual energy production without incrementing the cost of the wind turbine and its components; decrease the wind turbine investment costs by providing blades with lower mass without lowering the energy produced by the wind turbine; or both the aforementioned [1, 7, 10, 26, 27, 28, 29]. To do so, the regulation and mitigation of the loads acting on the structure plays a fundamental function. We have seen a development of wind turbine loads

regulation systems through the years (an example is the passage from stall-regulated wind turbines to variable-speed pitch-regulated machine), but to keep decreasing the LCOE, load **mitigation** strategies must be used on top of the necessary control methods. Control methods for wind turbine loads mitigation can be generally classified in two branches:

- **active methods**, a category that consists of technologies that reduce loads by actively controlling certain components of the rotor; individual blade pitch control [3] and trailing edge flaps [4, 30] fall into this classification;

- **passive methods**, based on the idea of designing a structure that, without any additional components, deforms so as to induce a load reduction when it is loaded [5, 8].

The current work focuses exclusively on the latter.

3.2   Mechanisms for Passive Loads Control

The term "passive" describes the idea of conceiving a structure that mitigates loads deforming in a certain manner. The wind turbine blade is designed to be able to reduce loads "by itself". Even though modern blades are highly complex composite structures, the concept behind passive loads control is straightforward: introducing structural changes in the blade so that when the blade is bending flapwise, it also twists in a direction that lowers the angle of attack. The reduction in angle of attack causes a decrease in the aerodynamic loads acting dynamically on the rotor. How these loads are distributed on the rotor and how the angle of attack varies along the blade span during the lifetime of a wind turbine is a complicated matter and we won't go further into that. The important piece of information is that it is possible to introduce structural changes to the blade and play around with its deformations to alleviate loads on the wind turbine through tailored changes in the angle of attack along the blade span. If these structural changes are properly introduced, the loads acting on the wind turbine can be alleviated throughout its entire lifetime.

In modern multi-megawatt horizontal-axis three-bladed rotors, passive loads control is achieved by making the blade twist towards feathering when it is bending in the direction of the tower. This behaviour of the blade is generated by a so-called **structural coupling**, and it can be referred to specifically as **bend-twist coupling** (**BTC**). The structural changes necessary to achieve bend-twist coupling can be classified in several ways. We chose to divide them

into three categories based on the type of change that needs to be implemented in the blade design to generate passive loads control. These three categories are listed below together with a brief description.

1. **Variation of the geometry of the blade shape** or, simply, **blade sweep**: this method consists of introducing a blade shape variation in the rotor plane; such a change in blade geometry produces a distribution of aerodynamic forces along the blade span that constrains part of the blade to twist, in case of load alleviation techniques, towards feather (reduction of the angle of attack, **backward sweep**). Figure 3.1 provides a visual description of the blade sweep concept. The aerodynamic lift force L applied along the blade span is proportional to the angle of attack, AoA, which, in turn, is proportional to the inflow angle, ϕ. When a part of the blade is "swept", a torque, T, proportional to the lift and the amount of sweep, Δ, is generated due to a variation in the cross-sectional shear centre. This torque will cause a local variation of the inflow angle, ϕ, along part of the blade span, l. This change in inflow angle will also depend on the structural properties of the blade, which in this case can be approximated to the torsional stiffness, GJ. The $\partial\phi/\partial l$, if the sweep is **backward** (curling over the trailing edge of the blade), causes a reduction in the angle of attack with a consequent load alleviation effect.
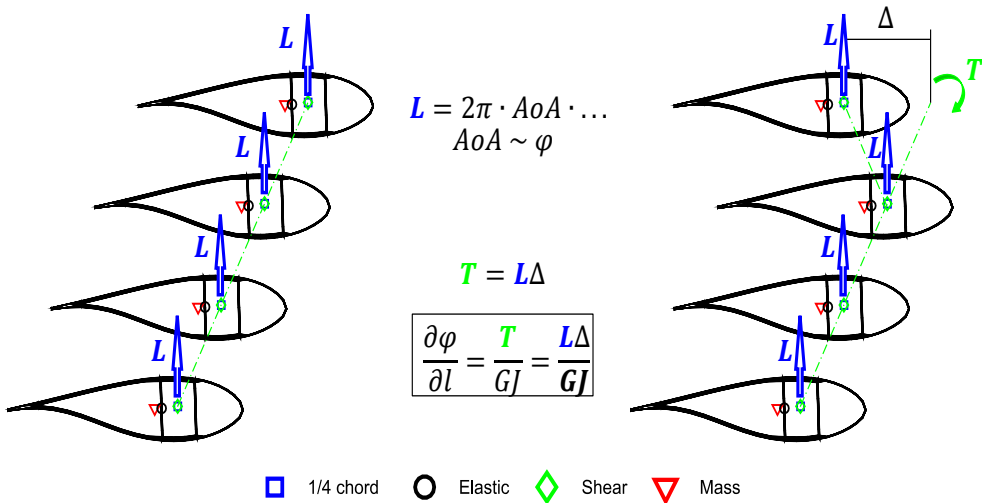
Figure 3.1: Blade sweep concept applied for passive loads control.

2. **Tailoring of the blade internal structure to achieve structural properties prone to bend-twist coupling**: we already saw from Figure 3.1, that the variation of inflow angle/angle of attack also depends on the structural properties of the blade. Consequently, passive loads control can be achieved by changing the internal structure of the blade, namely, cross-section geometry, number of webs, thickness of the blade layups, and materials. An example is changing the characteristics of the blade internal structure to **lower the torsional stiffness** GJ, allowing the blade to twist further when it bends toward the tower. Another case that falls into this category is **changing in the location of the shear centre** through changes in the location of the spar caps and webs. The latter, visually shown in Figure 3.2, can also be tailored to **move the principal bending axes**, which can be rotated to introduce a coupling between the two bending directions while the structure deforms.

3. **Exploitation of the properties of composite materials**: blade layups can be modified to create bend-twist coupling; specifically, the direction of the fibres in the layers can be rotated and oriented to generate a structural coupling capable of producing load alleviation (see sketch in Figure 3.3). For brevity, we refer to this type of coupling as **material bend-twist coupling**. As with item two above, this approach has a significant impact on the structural properties of the blade. We decided to keep these two methodologies separated because the variation of the orientation of the fibres can be applied without introducing major changes in the design of the blade. In the modelling phase, the angle of the fibres in the blade layups is not a challenging parameter to implement, as a variation in cross-
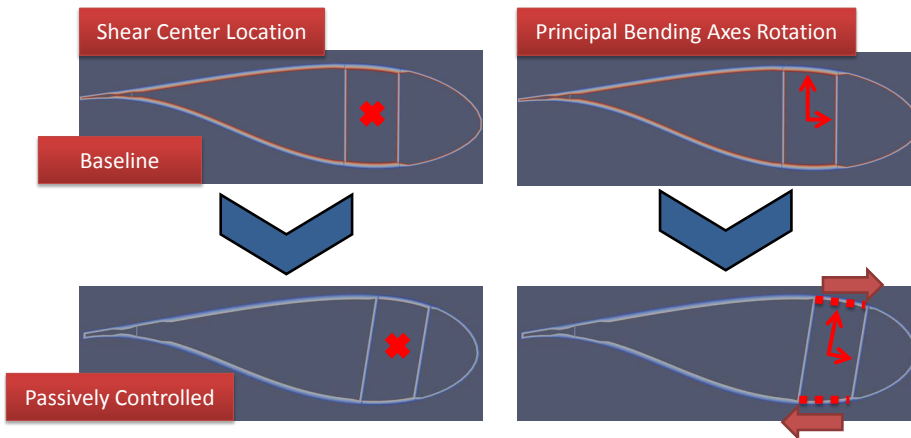
Figure 3.2: Tailoring-of-the-blade-internal-structure concept applied for passive loads control.
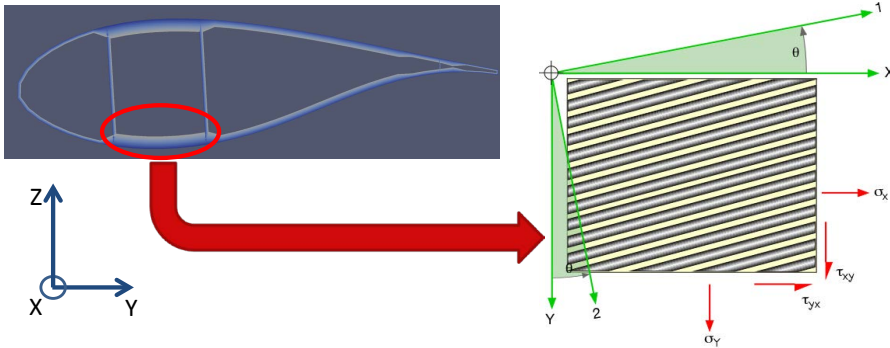
Figure 3.3: Rotation-of-the-fibres concept applied for passive loads control.

section geometry, thickness of the blade layups, position of spar caps and webs, etc. can require a higher design effort.

3.3   Almost 30 years of Research: a Literature Review

Passive loads control methodologies applied on wind turbines are neither new nor innovative concepts. As the title of this section states, many years of research and resources have been dedicated to the topic. We are going to present an overview of the most relevant works carried on the subject. As evident below, there is a significant body of work already dedicated to the topic of passive loads control. However, it must be stressed that this does not invalidate the work present in this thesis. On the contrary, we will demonstrate in the work comprising this dissertation that the progresses made in the development of more sophisticated tools and models for the analysis of wind turbine designs have made the concept of passive loads control more mature and applicable to modern wind farms.

We have divided passive loads control strategies in three categories: swept blades, design of tailored blade internal structure and properties, and employment of ad hoc blade layups. Before diving into each one of the three different categories, we need to mention that a vast literature on aeroelastic tailoring in aeronautics functioned as precursor for passive loads control for wind turbine blades.

According to Shirk et al. [31], the first study on aeroelastic tailoring is dated

back to 1949, when Munk [32] investigated changes in the orientation of the grain of his wooden propeller blade to create desirable deformation couplings during operation. In the late 1960s, aeroelastic tailoring research was fueled by studies on the forward swept wings of the X-29 [33] and on the Active Aeroelastic Wing project [34]. In this context, the work of Weisshaar [35, 36, 37, 38, 39] and Librescu [40, 41, 42] represents a great contribution on the study of elastic couplings between wing bending and torsional deformations through the employment of laminated composites. We cannot explore this vast research literature in details, but the reader can refer to Jutte [43] for a complete and thorough review of aeroelastic tailoring in aeronautics.

In the next part of this section, we are going to go through the three passive loads control categories, highlighting step by step the most relevant research contributions published in the last three decades. The overview of the publications that we provide on these three subjects is far from being complete. Our aim is not to supply a full detailed list of all the work carried on wind turbine passive loads control, but to present the publications that inspired the research reported in these pages.

3.3.1 Variation of the Geometry of the Blade Shape

In the decade 2000s, we can find one of the most complete studies conducted and published on wind turbine swept blades. This project is called Sweep-Twist Adaptive Rotor Blade (STAR) and it was conducted by the Knight & Craver Wind Group in SANDIA National Laboratories between 2004 and 2010 [8, 44, 45]. The project started following two initial feasibility studies: one by Ashwill et al. [6] and the other by Zuteck [46]. These studies prove that a blade planform curvature can produce substantial twist, thus reducing fatigue loads. This load alleviation capability allows for longer blades with the same fatigue spectrum. As part of the STAR project, Larwood and Zuteck [44] used a 28 m blade model (STAR6) with 2.2 m of backward tip sweep to run aeroelastic simulations. Results were compared with a baseline turbine model. The swept rotor had a 25% wider area compared to the baseline to compensate the power loss below rated due to the sweep. The study shows that the swept-bladed turbine increases the amount of annual energy captured by 5-10%. The swept blade has similar or higher flapwise root bending moments to the original straight 25-m blade due to the coupling. For the conclusive part of the STAR programme, Ashwill et al. [45] designed, fabricated, and tested a new swept 27.1-m blade. They showed the capability of a sweep-adaptive blade to passively reduce operating loads. An increased production of energy was detected comparing the prototype to a baseline 23.5 m blade mounted on a 48-m-diameter Zond 750 kW turbine. The new rotor showed an increase of 10-12% of the an-

nual energy production without increasing the blade root bending moments. A complete overview of the STAR project was provided in a final project report by the Knight & Craver Wind Group [8].

A first detailed parametric study involving geometric parameters for swept blades was conducted by Verelst and Larsen [14]. This study is based on several swept blade configurations involving variations on both sweep curvature and sweep offset at the tip. The authors showed that flapwise fatigue and extreme loads can be reduced up to 10% and 15%, respectively, for a backward swept blade, whereas the edgewise fatigue and extreme loads can increase up to 6%. Verelst and Larsen also mapped the blade root torsional moment, which registered an increase up to 400%. This parametric study is based on a simple load case (10-minute time series with fixed turbulence intensity of 0.18 and no wind shear).

Hansen [47] investigated aeroelastic properties of backward swept blades using a linear model obtained from a nonlinear co-rotational finite beam element formulation coupled with the Blade Element Momentum method (BEM) including an unsteady aerodynamic model. He computed frequencies, damping, and mode shapes of the aeroelastic blade modes. Hansen concluded that the backward sweep creates torsion towards feathering for downwind flapwise deflection in the first flapwise bending mode. This torsional component causes the frequency of the first aeroelastic bending mode to increase compared to the corresponding structural frequency, and this increase is larger for larger sweep. Furthermore, Hansen found that the frequency response of the flapwise blade root bending moment from wind excitation decreases below the increased first flapwise frequency. This drop of the flapwise blade root moment explains the reduced flapwise loads observed in other studies of backward swept blades. Hansen also provided an overview of the steady states of a wind turbine with swept blades, showing the deviation of pitch angles below rated and the inevitable increase in blade root torsional moment. The observations on the steady states show positive and negative effects of designing a rotor with backward swept blades for passive loads control.

Important contributions to the topic were also given by European projects such as Upwind, funded under the EU's Sixth Framework Programme (FP6), which ran from 2006 to 2011 [48]. Under "Work Package 2 – Task 1 Structural Dynamics – Large Deflections and non-linear effects" [49], simulations and investigations with uniform inflow were done to estimate the significance and the effect of geometrical variations of the blade properties on loads and stability. The analyses focused mostly on pre-bent rather than swept blades. Concerning swept blades, the study concluded that fore sweep degrades the stability of the blade and that an optimum sweep for the reference wind turbine blade with respect to loading and stability can be found.

3.3.2   Design of Tailored Blade Internal Structure and Properties

Passive loads control related to the tailoring of the blade internal structure have always been well-known and implemented in the wind turbine design process. The manufacturers always had the know-how on creating a blade with tailored structural properties capable of withstanding specific requirements. Nonetheless, in recent times, designing a blade with properties particularly prone to mitigation of loads has gained more attention. A number of key works are described here to inform the interested reader of crucial advances in this area.

Zahle et al. [18, 19] performed a simultaneous aerodynamic and structural optimization of a 10 MW wind turbine rotor with respect to the blades inner structure and outer shape. The work does not directly relate to passive loads control, but the material distribution and, consequently, blade structural properties obtained from the optimization design process are inclined towards loads alleviation purposes. For instance, the final designs have a lower torsional stiffness that allows the blade to be more prone to the beneficial effect of bend-twist coupling. Furthermore, the location of the caps can vary, moving the shear center and rotating the principal bending axes, and hence triggering a tailored reduction of the angle of attack to reduce loads in certain parts of the blade. The results show that, separately, the blade mass can be reduced by up to 20%, and the AEP can be increased by up to 1.7%. Both blade outer shape and inner structure were re-designed, but it is important to remark that the choice of certain parameters for the internal structure have contributed to control the loading on the wind turbine allowing for blade mass reduction and higher AEP.

The work by Capuzzi et al. [50, 51] provides another valid example of passive loads control strategies applied through tailoring of blade structural properties. They show that a proper tailoring of the blade's elastic response through displacement of the spar caps along the blade length, can increase the energy harvest by the turbine while mitigating extreme loading conditions due to gusts. The passive loads control methodology used is actually a combination of variation of the blade planform with backward sweep and displacement of the caps. Nonetheless, the authors demonstrate the possibility of tailoring the wind turbine blade structural properties to achieve a target performance alleviating simultaneously the loads on the wind turbine.

3.3.3 Exploitation of the Properties of Composite Materials

The last of the three passive loads control categories listed in the previous section is the implementation of load alleviation techniques exploiting the properties of composite materials. Specifically, the fibres in the blade layups can be oriented to induce bend-twist coupling.

Kooijman [5] published one of the first and most complete studies on the use of material bend-twist coupling as a passive loads control method on wind turbines. He developed a model based on the coupling theory for a thin walled monocoque structure described by Karaolis [52, 53], showing that a wind turbine blade can achieve bend-twist coupling, preferably using a hybrid laminate layup of carbon and glass epoxy. His preliminary calculations show that bend-twist coupling towards feathering can improve blade stability through dynamic reductions of the angle of attack of the blade elements.

Lobitz, Veers, et al. carried out several studies on material bend-twist coupled blades [54, 55, 56, 57]. These studies range from preliminary investigations concerning the possibility of using coupled blades on wind turbines [54] to technical research involving the computation of the stability of coupled blades [55] and their potential for load mitigation [56], even on horizontal axis wind turbines using modern control strategies [57]. First, Lobitz, Veers, et al. showed that a tailored twisting achieved through structural coupling has a payoff in increased power production or in vibration alleviation or both [54]. Even if the critical stability rotor speeds were always above their wind turbine design limit, they show that the coupled blades examined are less stable as extreme values of the coupling coefficient are approached [55]. Improved power productions and vibration alleviation potential were not the only targets of their studies. The authors designed a material-coupled rotor with physically attainable levels of coupling coefficients to perform wind turbine load analyses. They show that significant reductions in damage across the spectrum of applied wind loading can be achieved [56]. Looking at turbulent wind inflow aeroelastic simulations, material bend-twist coupling triggers also substantial fatigue load reductions in variable-speed pitch controlled rotors [57].

In SANDIA National Laboratories, the work by Lobitz, Veers, et al. resulted in a series of numerical and experimental design studies concerning structural coupling and involving manufacturing of material-coupled blades. Ashwill [45] provides a complete description of the design and manufacturing work carried out at SANDIA on passively controlled blades. Ashwill shows not only the potential of employing blades with passive loads control, but also the feasibility of the manufacturing process and the accuracy of the model developed to study

the topic.

A validation of the tools developed in recent times to model material bend-twist coupling for wind turbine blades is also provided by the work of Berring [58], Branner [59], and Fedorov [9]. The first two used an 8-m section from a 23-m blade from Vestas Wind Systems A/S for both dynamic and static tests. The original blade section was tested and then modified with four layers of UD1200 (unidirectional glass fibre, $1200 \ \mathrm{g \, m^{-2}}$), which were laminated on the pressure and suction side of the blade with an angle of $25°$ to the blade axis to create a measurable bend-twist coupling. The results and comparison with numerical analyses showed that a valid coupling can be easily introduced and measured by adding angled unidirectional layers on the blade section [58, 59]. Fedorov [9] used the same Vestas blade section to present a method for the evaluation of the material coupling magnitude. The method is tested and validated against both experimental results and finite element modelling, demonstrating the importance of accurately estimating the bend-twist coupling effect in wind turbine blades.

Orientation of the fibres as a passive loads control method has also been integrated with active control methods. Bottasso et al. [15] presented an extensive analysis of the combination of this passive loads control technique with active load control. They produced a set of passively controlled blade designs through multi-disciplinary optimization, demonstrating how different types of material bend-twist coupling can reduce extreme and fatigue loads on a wind turbine. The integration of passive and active load control is studied using a cyclic pitch controller with two different sets of gains: the first has lower gains and moderate actuator duty cycle, whereas the second one has higher gains and more aggressive behaviour. They conclude that the combination of passive and active methods leads to higher load reductions than one would obtain using separately only one of the two approaches.

This literature review highlights that the beneficial effects of employing passive loads control techniques on wind turbines were already largely demonstrated using several numerical tools and experiments. Nonetheless, the amount of resources that researchers and engineers have dedicated in the last three decades to passive loads control denotes one important thing: the design of modern wind turbine blades is an extremely complicated problem, that can be approached from many different angles. Such a complex problem does not have a unique solution, and almost 30 years of dedicated effort might not be enough after all. In the next chapter, we are placing our research effort in context, outlining the key contributions that we brought to this field.

CHAPTER 4

The Implementation of Passive Loads Control on Wind Turbine Blade Design

The theory of modelling bend-twist coupling on slender and twisted composite structures was initially developed in the 70s [11]. So, why is the implementation of passive loads control on wind turbine blades still relevant?

The problem is aero-servo-elastic, as a wind turbine has to be regulated with a controller while exposed to stochastic turbulent loading throughout its entire lifetime. To properly capture all the effects of the exposure to a turbulent wind inflow in the many different situations that a wind turbine encounters once installed (start-up, shut-down, controller faults, storm conditions, etc.), the design standards for the structure require thousands of simulations [60, 61].

An extensive computational effort is necessary to accurately simulate the aero-servo-elastic behaviour of wind turbines with highly flexible blades that extensively employ structural couplings. This computational effort can be impractical for a blade designer, as it requires the solution of a highly nonlinear problem in thousands of loading conditions. To reduce the time spent in running several expensive computations, the structural models of the aero-servo-elastic design tools are simplified. These aero-servo-elastic computer programs use

mainly Timoshenko-based multi-body formulations [62, 63] capable of handling large displacements and rotations with sufficient accuracy [64, 65], or modal-expansion-based approaches [66].

What kept passive loads control of wind turbine blades relevant and alive is the unending improving of aero-servo-elastic design tools able to model such sophisticated structures accurately and at low computational costs. The wind energy community, even though the benefits of bend-twist coupling on blades was extensively demonstrated, is making an effort to include these control strategies as a common design feature for modern wind turbine blades. Widely used aero-servo-elastic tools have been upgraded to properly include structural couplings in the blade design process. Furthermore, comparing to 30 years ago, many more companies and academic institutions have access to high-performance computing clusters (HPCC). The possibility of using HPCCs has facilitated the blade design process because the many nonlinear aero-servo-elastic simulations required by the standards can be run with practical computation time.

4.1   Aero-Servo-Elastic Framework to Model Passive Loads Control

The aero-servo-elastic framework used to study the implementation of passive loads control methods on wind turbine blades is the code HAWC2 [67], developed by DTU Wind Energy. The framework couples an aerodynamic model, a structural model, and a model for the wind turbine controller. In this section, we focus specifically on the structural part of the framework. Before that, we provide a general description of the models that constitute the framework to clarify the analysis capability provided by the code.

The aerodynamic part of the code is based on the blade element momentum (BEM) theory. The unsteady aerodynamic forces and moments on an airfoil section undergoing arbitrary motion are computed using 2D models. The classical BEM approach is extended to handle dynamic inflow, dynamic stall, skew inflow, shear effects on the induction, and effects from large deflections. For example, when the blades undergo large flapwise deflections, the effective rotor diameter is reduced and the blade forces are no longer perpendicular to the rotor plane. Consequently, the rotor thrust is reduced causing variations in the induced velocities and vice versa. The dynamic stall model [68] is a modified Beddoes–Leishmann model [69] that includes the effects of shed vorticity from the trailing edge (Theodorsen theory [70]), as well as the effects of stall separation lag caused by a non-stationary trailing edge separation point. Taking into

account these effects is fundamental not only for flutter analysis, but also to calculate loads and stability of highly-flexible non-straight wind turbine blades with low torsional stiffness. The calculation of the induced velocities is based on the local inflow velocities causing different inductions in the upper and lower parts of the rotor, as in the case of a large wind shear [71]. The validation of the unsteady BEM method used by the aerodynamic component of the program can be found in [72, 73, 74].

The structural model is based on a multi-body formulation as described in [12] using the floating frame of reference method. In this formulation, the wind turbine main structures are represented by bodies, where each body is an assembly of Timoshenko beam elements with six degrees-of-freedom at each node. The motion of the bodies is limited by kinematic constraints formulated as algebraic equations. Internal inertial loads are accounted for when the coordinate system of each body is moved in space. External forces are placed on the structure in the deformed state, which is especially important for pitch loads and twist of the blades. Large rotations and deflections can be handled by a proper subdivision of bodies. Recently, the capability to provide fully populated cross-sectional stiffness matrices for the beam elements has been introduced. This addition allows the modelling of complex composite structures with anisotropic lay-ups. Even if an initial validation of this new anisotropic beam element is provided in [12], we carried out a more thorough comparison against another structural model: BeamDyn, a nonlinear beam model for the aeroelastic moduralization framework FAST v8 [75]. This comparison is reported in the next section. We would like to remark that before the addition of the capability to model anisotropic lay-ups, the structural module of HAWC2 could still handle nonlinear effects due to large deflections, large rotations, and geometric coupling. The structural model took part to several validation campaigns of aeroelastic codes for wind turbines. Other than the ones already cited for the aerodynamic part of the code, we can mention the reports in Ref. [48, 76, 77].

Finally, the controller system is included through Dynamic Link Libraries. The controller used throughout the project is described in [78]. The three-dimensional Mann turbulence model [79] is used in all the simulations with turbulent wind. A manual of the code can be found in [64].

4.2 Benchmarking of Beam Structural Models

Highly flexible composite structures, such as wind turbine blades, can undergo large deflections without exceeding their specified elastic limit. Due to the geometry of their deformation, the behaviour of such structures is nonlinear and

the solution becomes very complex. For this reason, and to face the complexity of these deformations, BeamDyn uses GEBT [80][81]. Exhaustive details related to the theory behind BeamDyn and its implementation in the FAST v8 state-space formulation are provided by [13, 82]. This approach enables very high accuracy in solving highly nonlinear structural problems, but it has a high computational cost. To address the computation cost, BeamDyn has been implemented with LSFEs, which characteristically have exponential convergence rates for smooth solutions, as opposed to low-order FEs that have algebraic convergence (requiring fewer nodes for the same accuracy). HAWC2 uses a different method to face nonlinear effects due to large deflections, large rotations, and structural couplings. As reported in the previous section, the beam model of HAWC2 is based on a multi-body formulation assembled with linear anisotropic Timoshenko beam elements. A detailed description of this type of element is provided by [12]. The accuracy of this approach is, in general, lower than that of the GEBT. The advantages, with respect to a nonlinear beam model, are the much lower computational cost required to model a nonlinear problem and the possibility of augmenting the accuracy by increasing the number of bodies.

These two methods are compared using a series of benchmarking cases. The main purpose is to evaluate the accuracy of the two structural codes against highly nonlinear problems. It is important to remark that the first four cases investigated in this work are "extreme." The deflections and rotations computed for these nonlinear problems are not comparable to those typical of operating wind turbine blades. Nonetheless, the two structural codes have been used to simulate these limit cases to prove the suitability of both approaches to provide valid solutions related to the behaviour of twisted and curved structures and composite beams with complex layups.

The cases are listed below:

- Case 1: Static analysis of a cantilever beam under five bending moments applied at its free end

- Case 2: Static analysis of an initially twisted and an initially curved beam

- Case 3: Static analysis of a composite beam with a force applied at the free end

- Case 4: Dynamic analysis of a composite beam with a sinusoidal force applied at the free end

- Case 5: DTU 10-MW reference wind turbine (RWT) [83] blade natural frequencies.

The analysis of the performances and responses of the two beam models start from a simple and very common case (static bending of a cantilever beam) and move to a complex tailored wind turbine blade. Except for the DTU 10-MW RWT blade natural frequencies, the cases were already used to verify BeamDyn and are presented by [13, 82]. Nonetheless, these cases were selected as the basis for this study, because they are suited to demonstrate the capabilities of the two codes to model structures that show nonlinear responses due to geometric and material couplings. The results obtained from the two codes were compared to results found in the literature or high-fidelity models generated using commercial, three-dimensional (3D), FE software such as ANSYS, Patran-Marc and Dymore.

4.3 Results

In this section, results for the each of the benchmarking cases are reported and discussed. Discrepancies between the two structural codes are highlighted and analyzed. The section is divided into five parts, one for each of the cases computed. Except for the last part of the study, which reports results concerning a wind turbine blade, very large displacements and composite beams with complex layups are taken into account.

4.3.1 Case 1: Static analysis of a cantilever beam under five bending moments applied at its free end

Case 1 concerns the static deflection of a cantilever beam that is subjected at its free end to a constant negative moment around the x_2 axis. A system schematic is shown in Figure 4.1.

The length of the beam is 10 m and the input cross-sectional stiffness matrix is defined in Equation 4.1. In this paper, the stiffness matrices are presented in the coordinate system adopted by [81].

$$K = 10^3 \begin{bmatrix} 1770 & 0 & 0 & 0 & 0 & 0 \\ 0 & 1770 & 0 & 0 & 0 & 0 \\ 0 & 0 & 1770 & 0 & 0 & 0 \\ 0 & 0 & 0 & 8.16 & 0 & 0 \\ 0 & 0 & 0 & 0 & 86.9 & 0 \\ 0 & 0 & 0 & 0 & 0 & 215 \end{bmatrix} \tag{4.1}$$

where the units associated with the stiffness values are $K_{i,j}$ (N) and $K_{i+3,j+3}$ ($\mathrm{N\,m^2}$) for $i, j = 1, 2, 3$. Further details on the data used are fully provided by [82]. The BeamDyn model is composed of two 5th- order LSFEs, whereas
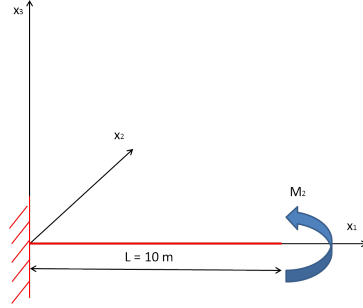
Figure 4.1: Description of the beam and the coordinate system for Case 1
[Paper A].

HAWC2 models uses 30 and 50 bodies, respectively. The negative moment
applied around the x_2 axis is defined in Equation 4.2.

$$M_2 = \lambda \pi \frac{EI_2}{L} \tag{4.2}$$

where λ is a parameter used to scale M_2, from 0 to 2; E is the Young modulus;
I_2 is the moment of inertia with respect to the axis x_2, and L is the total length
of the beam. Table 4.1 shows the tip displacements computed by BeamDyn
and HAWC2 compared to the analytical solution. The solution, reported in
Equation 4.3, can be found in [84].

$$u_1(x_1) = \rho \sin\left(\frac{l(x_1)}{\rho}\right) - l(x_1)$$
$$u_3(x_1) = \rho \cos\left(1 - \frac{l(x_1)}{\rho}\right) \tag{4.3}$$

where $\rho = \frac{EI_2}{M_2}$ and u_1 and u_3 are the displacements along the x_1 and x_3 axes,
respectively, calculated at each node $l(x_1)$.

In Table 4.1, *Sol.* indicates the analytical solution, *BD* the beam model Beam-
Dyn, and *H2-30b* and *H2-50b* the HAWC2 structural model assembled with 30
and 50 bodies, respectively. For $\lambda = 2$, because the analytical solution of u_1 is
0.0, the results are reported in absolute values instead of percentages.

Figure 4.2 provides a visual representation of the beam displacement in lon-
gitudinal, x_3, and axial directions, x_1. As the moment applied to the free end
increases, the geometrically nonlinear effects of the benchmark problem become
relevant. The tip displacement computed by BeamDyn is indistinguishable from
the analytical solution; two 5th-order LSFEs is more than enough to achieve
high accuracy and fewer nodes/elements is likely possible. Due to the use of

linear elements, the structural model of HAWC2 is not fully able to catch this highly nonlinear behaviour. The increase in the number of bodies in HAWC2 to model the beam reduces the error and improves the accuracy of the computed displacements.

Table 4.1: Comparison of the beam tip displacements for all the applied bending moments.

λ	Sol. (u_3)	BD	H2-30b	H2-50b
0.4	-2.432 m	0.0%	0.5%	0.2%
0.8	-7.661 m	0.0%	1.3%	0.5%
1.2	-11.56 m	0.0%	1.2%	0.4%
1.6	-11.89 m	0.0%	1.3%	0.5%
2.0	-10.00 m	0.0%	5.1%	2.0%
λ	Sol. (u_1)	BD	H2-30b	H2-50b
0.4	5.50 m	0.0%	0.1%	0.0%
0.8	7.20 m	0.0%	0.3%	0.1%
1.2	4.80 m	0.0%	4.5%	1.7%
1.6	1.37 m	0.0%	22.7%	9.7%
2.0	0.00 m	0.00	-0.008 m	-0.01 m

Figure 4.2: Bending of the cantilever beam in the x_1-x_3 plane. Five growing negative bending moments around the x_2-axis are applied at the free end on the beam. Circles: HAWC2 beam model with 30 bodies. Triangles: HAWC2 beam model with 50 bodies [Paper A].

4.3.2   Case 2: Static analysis of an initially twisted and an initially curved beam

Beams characterized by initial twists and curvatures are analyzed for Case 2. First, a straight beam with an initial twist is considered (Figure 4.3). The beam is linearly twisted in the positive θ_1 direction from 0 degrees at the root to 90 degrees at the tip. Table 4.2 shows the material properties for A36 steel, the beam geometry, and the force applied at the free end along the negative x_3 axis. As in Case 1, the beam in BeamDyn is meshed with two 5th-order LSFEs, and the HAWC2 beam model is meshed with 30 bodies.

The full description of the beam is also provided by [13]. The results for the twisted beam are shown in Table 4.3 and compared to the baseline results obtained from an extremely refined 3D ANSYS SOLID186 elements model.

The second part of Case 2 involves an initially curved beam. The benchmark problem for pre-curved beams was proposed by Bathe in 1979 [85]. Figure 4.4 shows the configuration of the curved cantilever beam. The beam lies in the plane defined by the positive x_1 direction and the negative x_2 direction. A force
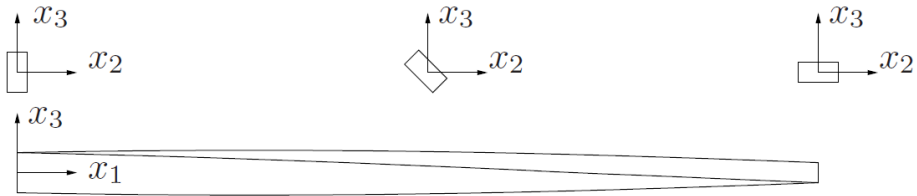
Figure 4.3: Schematic of the twisted beam and the coordinate system for Case 2 [Paper A].

Table 4.2: Material properties (A36 steel), geometry (rectangular section), and tip force applied on the beam.

Property	Value
Elastic Modulus	200 GPa
Shear Modulus	79.3 GPa
Height	0.5 m
Width	0.25 m
Length	10 m
Force	4000 kN

Table 4.3: Comparison of the twisted beam tip displacements: ANSYS
SOLID186 Model, BeamDyn, and HAWC2.

	u_1 [m]	u_2 [m]	u_3 [m]
ANSYS	-1.134	-1.714	-3.584
BeamDyn	0.13%	0.04%	0.15%
HAWC2	2.42%	1.92%	1.05%
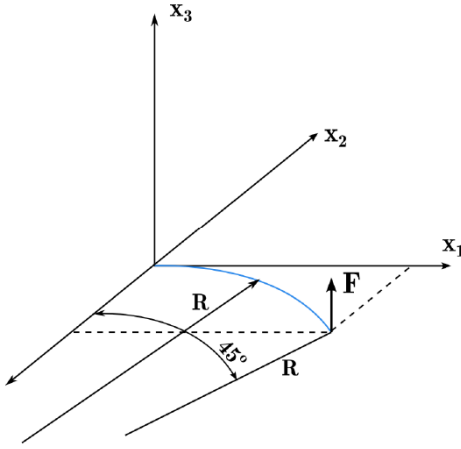
Figure 4.4: Schematic of the initially curved beam and the coordinate system
for the second part of Case 2 [Paper A].

of 600 N is applied in the positive x_3 direction. The beam is defined by the
45-degree arc with 100-m radius centered at 100 m in the negative x_2 direction.
The beam has a square cross-section geometry. As in Case 1, the cross-sectional
stiffness matrix of the beam, computed using the geometry and the material
properties provided by [85], is diagonal. The computed displacements for the
static analysis are reported in Table 4.4 and a comparison to the results pub-
lished by [85] is provided.

The tendency of the results computed by the two structural codes is the same for
both the pre-twisted beam problem and the pre-curved benchmark cases. With
the discretization applied, BeamDyn is able to better represent the nonlinear
behaviour of twisted and curved beams (differences below 1%). HAWC2 com-
putes tip displacements that are between 2% and 3% away from the solutions.
Even though HAWC2 uses linear beam elements, the multi-body approach is

Table 4.4: Comparison of the curved beam tip displacements: Ref.[85], Beam-Dyn, and HAWC2.

	u_1 [m]	u_2 [m]	u_3 [m]
Bathe-Bolourchi [85]	-23.7	-13.4	53.4
BeamDyn	0.8%	0.8%	0.0%
HAWC2	2.1%	3.1%	0.0%

able to provide sufficiently accurate solutions for the large displacements considered in these two geometrically nonlinear problems.

4.3.3 Case 3: Static analysis of a composite beam with a force applied at the free end

The purpose of Case 3 is to compare the capability of HAWC2 to BeamDyn to simulate the behaviour of composite beams with an elastic coupling. A 10-m long cantilever composite box beam is considered. The coordinate system is the same as Case 1 (see Figure 4.1). BeamDyn and HAWC2 use the same meshes described for Case 2 (BeamDyn: two 5th-order LSFEs; HAWC2: 30 bodies). The cross-sectional stiffness matrix is shown in Equation 4.4.

$$K = 10^3 \begin{bmatrix} 1368.17 & 0 & 0 & 0 & 0 & 0 \\ 0 & 88.56 & 0 & 0 & 0 & 0 \\ 0 & 0 & 38.78 & 0 & 0 & 0 \\ 0 & 0 & 0 & 16.96 & 17.61 & -0.351 \\ 0 & 0 & 0 & 17.61 & 59.12 & -0.370 \\ 0 & 0 & 0 & -0.351 & -0.370 & 141.47 \end{bmatrix} \tag{4.4}$$

where the units associated with the stiffness values are $K_{i,j}$ (N), $K_{i,j+3}$ (N m) and $K_{i+3,j+3}$ (N m^2) for $i, j = 1, 2, 3$.

A concentrated dead force of 150 N is applied in the positive direction of x_3 at the free tip of the beam. The displacements and rotations along the beam axis are plotted in Figure 4.5 and Figure 4.6, respectively. Due to the properties of the composite materials, coupling effects exist between the twist and the two bending modes (see Equation 4.4). For this reason, a consistent rotation around the x_1 axis can be observed in Figure 4.6.
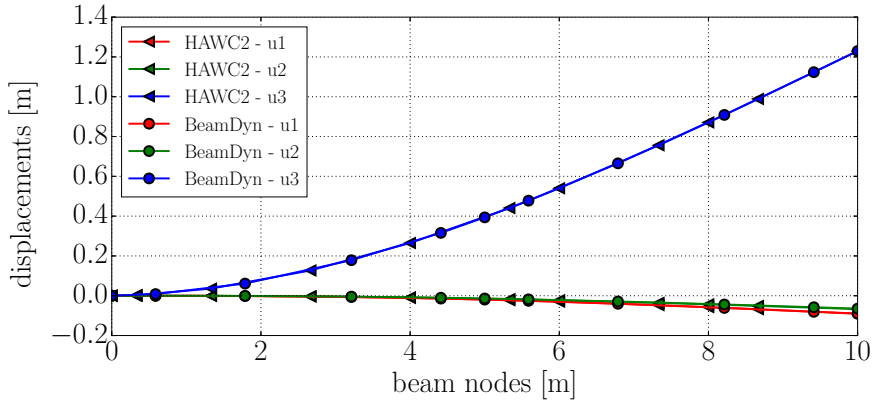
Figure 4.5: Displacements of the composite beam with respect to the nodal positions. Red: beam displacement of the nodes along the u_1 axis. Green: beam displacement of the nodes along the u_2 axis. Blue: beam displacement of the nodes along the u_3 axis. Triangles: HAWC2. Circles: BeamDyn [Paper A].
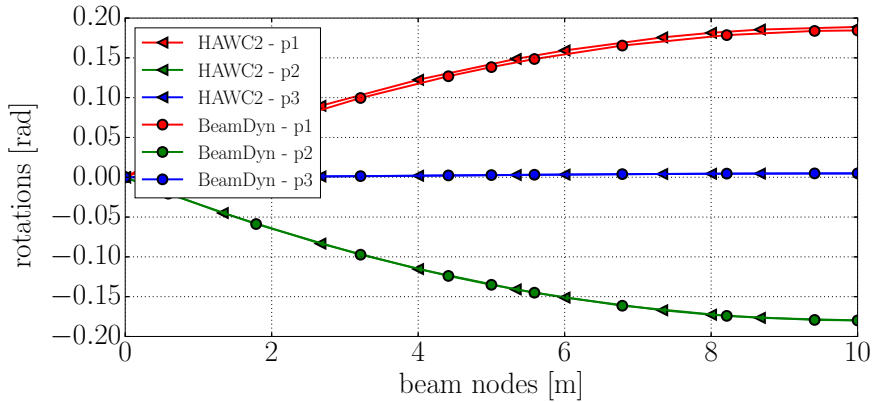
Figure 4.6: Rotations of the composite beam with respect to the nodal positions. Red: beam rotation of the nodes around the u_1 axis. Green: beam rotation of the nodes around the u_2 axis. Blue: beam rotation of the nodes around the u_3 axis. Triangles: HAWC2. Circles: BeamDyn [Paper A].

The tip displacements and rotations are compared to Dymore [86], a finite-element-based multi-body dynamics code. Results are shown in Table 4.5.

In Table 4.5, p_1, p_2, and p_3 indicates the rotation of the free-end node of the beam around the axis x_1, x_2, and x_3 respectively. BeamDyn is able to perfectly match the displacements and rotations computed by Dymore. The tip deflections and rotations computed by the structural beam model of HAWC2 are in good agreement with Dymore, with a maximum discrepancy of approximately 3%.

4.3.4   Case 4: Composite beam with a sinusoidal force applied at the free end

The objective of Case 4 is to compare HAWC2 and BeamDyn to composite beams under dynamic loading. The cantilever beam used is the same as that described in Case 3 as are the meshes used for the beam models. The coordinate system is the same as that used in Case 1 and shown in Figure 4.1. The cross-sectional mass matrix is presented in Equation 4.5.

$$M = 10^{-2} \begin{bmatrix} 8.538 & 0 & 0 & 0 & 0 & 0 \\ 0 & 8.538 & 0 & 0 & 0 & 0 \\ 0 & 0 & 8.538 & 0 & 0 & 0 \\ 0 & 0 & 0 & 1.4433 & 0 & 0 \\ 0 & 0 & 0 & 0 & 0.40972 & 0 \\ 0 & 0 & 0 & 0 & 0 & 1.0336 \end{bmatrix} \tag{4.5}$$

The units associated with the mass matrix values are $M_{i,i}$ $(\mathrm{kg\,s^2\,m^{-2}})$ and $M_{i+3,i+3}$ $(\mathrm{kg\,s^2})$ for $i = 1, 2, 3$. A sinusoidal point dead force is applied in the x_3 direction. The force is described by Equation 4.6.

$$F_3(t) = A_F \sin \omega_F t \tag{4.6}$$

Table 4.5: Comparison of tip displacements and rotations for Case 3.

	u_1 [m]	u_2 [m]	u_3 [m]
Dymore	-0.09064	-0.06484	1.22998
BeamDyn	0.0%	0.0%	0.0%
HAWC2	1.1%	3.7%	0.0%

	p_1 [rad]	p_2 [rad]	p_3 [rad]
Dymore	0.18445	-0.17985	0.00488
BeamDyn	0.0%	0.0%	0.0%
HAWC2	2.4%	0.01%	2.3%

where the signal amplitude $A_F = 100\ N$ and the frequency $\omega_F = 10\ rad\ s^{-1}$. The displacements and rotations along the beam axis are plotted in Figure 4.7. Root forces and moments are plotted in Figure 4.8.

On this dynamic benchmark case, BeamDyn and HAWC2 show good agreement, particularly in relation to the dynamics of the tip displacement and rotation in the direction where the force is applied. The most noticeable differences are registered for the displacement on the x_2 direction and the rotation around the x_3. These discrepancies are also the reason for the differences reported
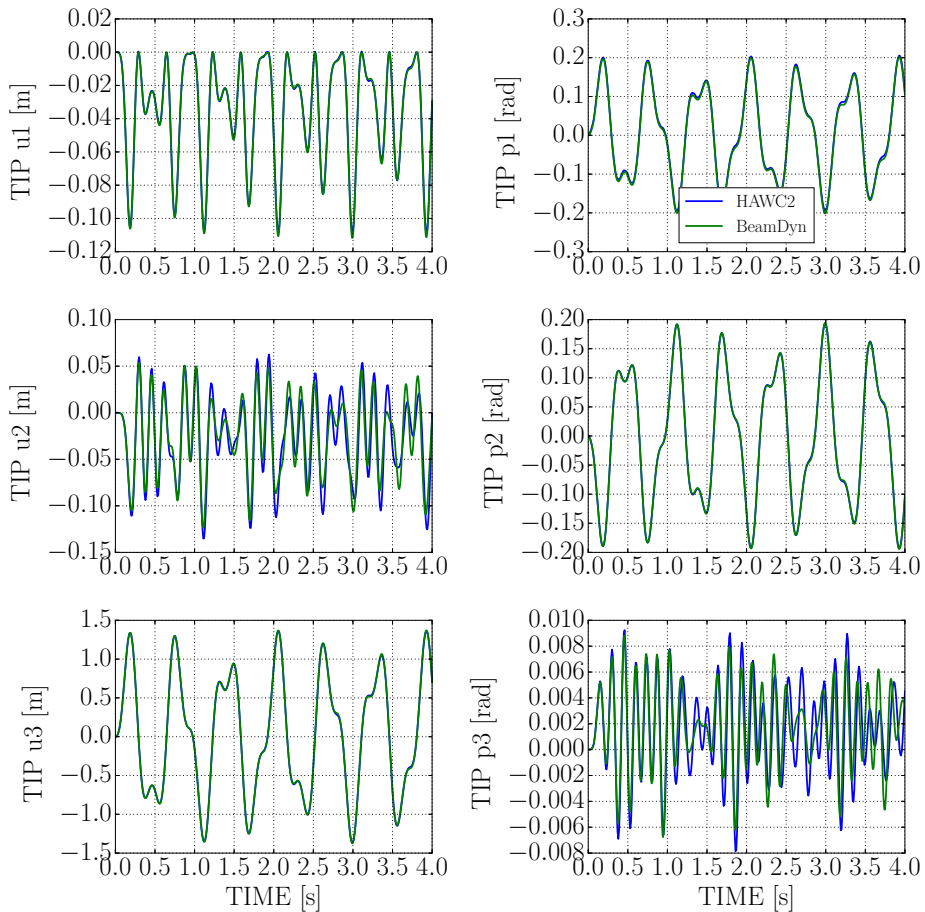
Figure 4.7: Tip displacements (left side, u_1, u_2, and u_3 from top to bottom) and rotations (right side, p_1, p_2, and p_3 from top to bottom) for 4-second simulations [Paper A].
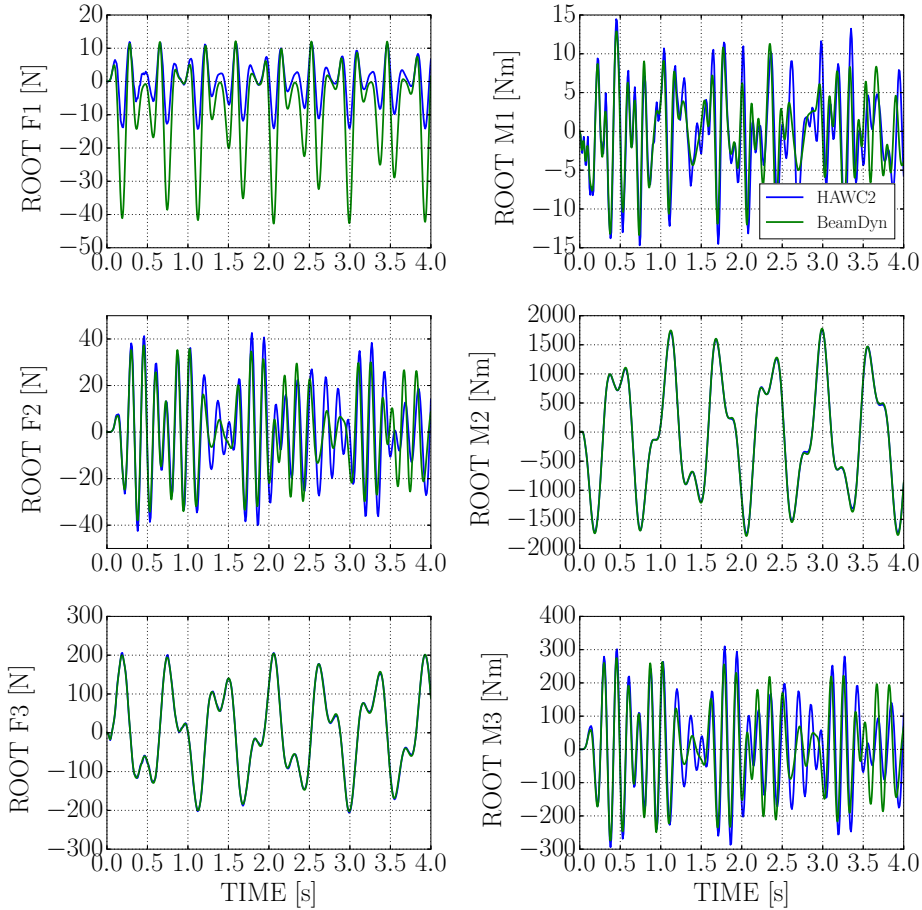
Figure 4.8: Root forces (left side, F_1, F_2, and F_3 from top to bottom) and moments (right side, M_1, M_2, and M_3 from top to bottom) for 4-second simulations [Paper A].

for the axial force F_1 (see Figure 4.8). The forces are projected on a fixed coordinate system placed at the root of the beam. BeamDyn and HAWC2 compute slightly different rotations around the x_3 direction and slightly different deflections on the x_2 direction, and these have an impact on the component of the force projected on the x_1 axis. No other relevant discrepancies are registered between the forces and moments computed by HAWC2 and those computed by BeamDyn (see Figure 4.8).

4.3.5 Case 5: DTU 10-MW RWT blade natural frequencies

For the last case, the natural frequencies of the isolated DTU 10-MW RWT blade [83] are compared. In HAWC2, the natural frequencies of the blade are obtained directly from its eigenvalue solver. The beam is assembled with 26 bodies. The version of BeamDyn used for the current work was not developed with an eigenvalue solver. Therefore, two impulse forces of 4 kN are applied on the blade tip in the edgewise and flapwise directions. Power spectral densities (PSDs) are then computed from the tip displacement time series. The beam is meshed assembling 13 2nd-order elements. For this case study, more elements than the previous cases were used to better represent the complexity of such a tailored structure. The results obtained from HAWC2 and BeamDyn are compared to the natural frequencies computed with a Patran-Marc 3D FE model (20-noded layered continuum elements). This 3D FE model was developed by the candidate for a benchmark of blade structural models [87].

Figure 4.9 shows the PSDs of the two BeamDyn impulse test cases. Table 4.6 identifies the natural frequencies using the Patran model compared to those computed by BeamDyn and HAWC2.

The results show good agreement between HAWC2 and BeamDyn. The differences between the natural frequencies of the beam models from the full 3D FE model are in the same range. The largest discrepancy is registered for the first edgewise mode, with an approximate 4% difference between the beam models and the FE model. This discrepancy is because of the strategy used to model the trailing edge in the FE model, in which the 20-noded layered continuum elements allowed for a higher degree of tailoring compared to the input data

Table 4.6: Comparison of the DTU 10-MW RWT natural frequencies.

	FEM [Hz]	H2 [%]	BD [%]
1st Flap	0.615	-0.6%	0.0%
1st Edge	0.971	-4.2%	-3.8%
2nd Flap	1.764	-1.4%	-1.7%
2nd Edge	2.857	-3.7%	-2.2%
3rd Flap	3.592	-0.4%	-0.5%
1st Torsion	5.753	-1.7%	-0.1%
4th Flap	6.124	-1.1%	-0.1%
3rd Edge	6.151	-0.3%	-0.2%
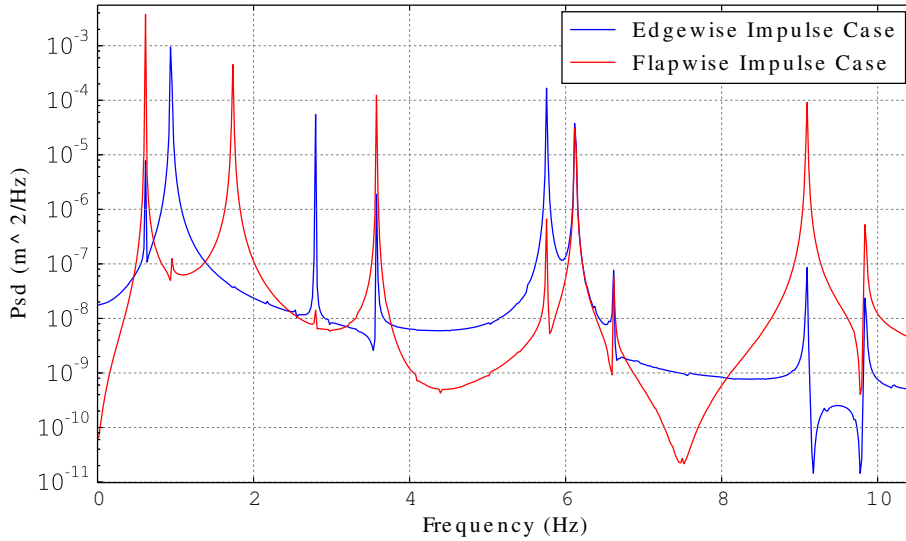
Figure 4.9: BeamDyn PSD of tip displacement in flapwise and edgewise directions for impulse load case. Blue curve: Flapwise tip displacement for an impulse force applied on the tip in the flapwise direction. Red curve: Edgewise tip displacement for an impulse force applied on the tip in the edgewise direction [Paper A].

provided in [83]. Consequently, this FE-modeling strategy resulted in a stiffer blade in the edgewise direction.

Given the results generated by both codes to simulate highly nonlinear structural problems, both approaches are considered suitable to properly model the complex behaviour of a wind turbine blade in operation.

Passive Loads Control: A Multidisciplinary Problem

The design a wind turbine rotor is an aero-servo-elastic problem. A modern wind turbine blade is subject to large deflections and non-negligible rotations driven by wind inflow conditions of a stochastic nature. Moreover, the wind turbine has to be regulated to provide a prescribed performance. Aerodynamics, structural dynamics, and control theory are the interconnected disciplines that drive the design of a wind turbine blade. The links between these three fields of study become even more crucial for the implementation of passive loads control methods on a wind turbine rotor. Even though these control strategies are implemented through the structure, they are tailored to produce a considerable impact on the wind turbine loading. Blade structural changes cause variations in the dynamic behaviour of the rotor. Consequently the aerodynamic performance of the turbine and the dynamics of the controller used to regulate the machine are also going to be affected by the implementation of passive control strategies. In particular, the way the controller is set to regulate the performance of the turbine also has an effect on rotor loads.

In other words: we want to change the design of the structure to alleviate loads on turbine components; these structural changes have an impact on the dynamics of the controller, which will react differently to accommodate the new structural behaviour of the rotor and its new aerodynamic performance; these

variations in the reaction of the controller will, in turn, affect the regulation of the turbine producing an impact on the loading.

As a first step to implement passive loads control on blades, we focused on understanding the interaction between the employment of a passive loads control strategy and the dynamic behaviour of the controller. The purpose is to isolate load variations caused by the passive loads control from the loading differences brought about by the controller's actions, providing a fair estimation of the potential of the passive loads control strategy chosen.

5.1   Effects of Backward Swept Blades on the Dynamics of a Wind Turbine Controller

We chose an easy-to-implement passive loads control strategy to perform this study (see Paper B): backward swept blades. As a matter of fact, this passive loads control strategy can be modelled by simply changing the external shape of the blade directly in the aero-servo-elastic model, without performing more invasive interventions, such as changes in the material properties or distributions, that would require detailed calculations for the structural input parameters of the aero-servo-elastic framework.

The aim of this investigation is to consider the effects of backward swept blades on the dynamics of the controller, highlighting how the dynamics of the mode that represents the controller (**regulator mode**) are affected by variation of the geometrical properties of the blade.

We first selected two backward swept shapes to implement on the blade of the DTU 10-MW RWT (Figure 5.1). We performed an analysis of the aero-servo-elastic properties of the full wind turbine in closed-loop using a model implemented in HAWCStab2 [47], a tool developed for eigenvalue and stability analysis of wind turbines.

The aero-servo-elastic framework HAWCStab2 is based on an analytical linearization of a linear finite element beam model in a nonlinear corotational formulation. As for HAWC2, the wind turbine model is constituted by a series of bodies. Each body is an assembly of Timoshenko beam elements similar to the one previously described in Section 4.2, without the capability of including fully populated cross-sectional stiffness matrices. Pitch and shaft bearings are included with frictionless bearing. This structural model is coupled with an unsteady BEM model of the blade aerodynamics. The aerodynamic part of the framework takes into account shed vorticity, dynamic stall, and dynamic inflow.
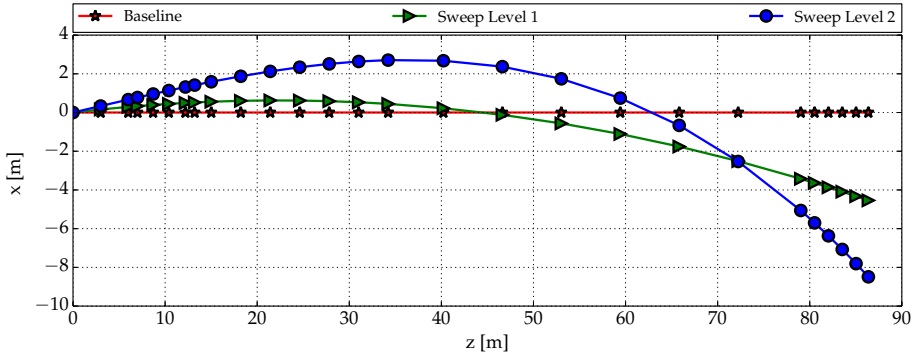
Figure 5.1: Backward swept blade shapes compared to the pitch axis of the baseline blade [Paper B].

The analytical linearization is performed around steady-state conditions. The steady states are obtained to balance elastic, aerodynamic, and inertial forces. This computation does not include gravitational forces. In the computation of the steady states, the multi-body formulation allows to capture nonlinear effects due to large deflections and rotations. An extensive validation and analysis of the open-loop performances of the tool without dynamic inflow are provided by Sønderby and Hansen [88]. As a final note, the framework has been already used to study the aero-elastic properties of backward swept blades [47].

We analyzed the interaction between the controller and the employment of backward swept blades, and the consequent effects on the dynamics of a wind turbine.

5.1.1 Closed-loop Wind Turbine Modes

Results are computed above rated wind speed where the action of the controller produces an effect on the turbine modes. Operational points are calculated for each of the benchmarked wind turbine.

Figure 5.2 shows the first 11 aero-servo-elastic frequencies. The baseline model (star symbol) is compared against the Level 2 swept configuration (circle). Only results for the most extreme swept shape, Level 2, are reported, since variations from the baseline are more pronounced and easier to spot than the differences registered for the mild case. However, the discrepancies of Level 1 frequencies
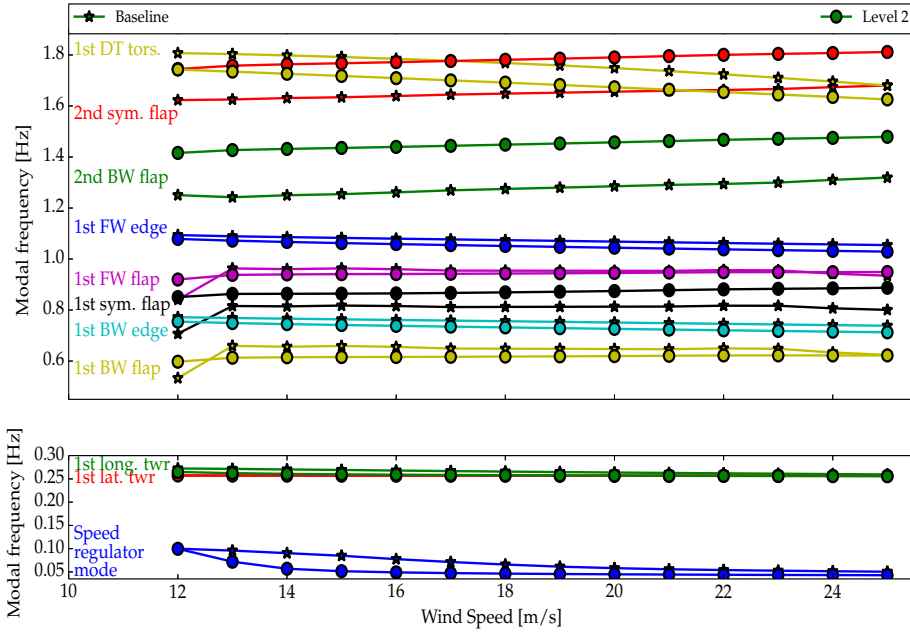
Figure 5.2: Closed-loop frequencies of the aero-servo-elastic turbine modes as a function of the wind speed. Star: Baseline turbine modes . Circle: Passive-controlled (Sweep Level 2) turbine modes. Mode descriptions are labeled and distinguished by color [Paper B].

with the baseline are qualitatively the same as to Level 2. Description of the modes can be found on the left part of the plot. Different colors help the association between descriptions and corresponding curves.

The first flapwise frequencies of Baseline and Level 2 show a different trends at $12\,\mathrm{m\,s^{-1}}$ and $13\,\mathrm{m\,s^{-1}}$. The difference is caused by the fact that the two configurations are using different operational points at $12\,\mathrm{m\,s^{-1}}$ and $13\,\mathrm{m\,s^{-1}}$. The backward sweep affects the first symmetric and the second asymmetric flapwise blade modes, drivetrain torsion and speed regulator mode more than tower, the first asymmetric flapwise and the first edgewise blade modes. The aero-servo-elastic frequencies of the first symmetric, the second backward, and the second symmetric flapwise blade modes are increased when sweeping the blade, whereas the frequencies of the drivetrain torsion and the regulator mode decrease. An explanation concerning the differences reported for flapwise blade modes is given by Hansen[47]. The aerodynamic lift (which points mainly downwind) is reduced when the blades deflects toward the tower because of the structural coupling between torsion towards feathering and downwind flapwise deflection. Conse-

quently, the lift acts as a stiffening restoring force. This results in increased aero-servo-elastic flapwise frequencies of the turbine with swept blades, as observed in Figure 5.2. The modal frequencies of the drivetrain torsion mode of the swept configuration decrease compared to the baseline. Due to the change in geometry and the increase in length, the backward swept blade are heavier than the baseline. Therefore, the passive-controlled rotors have a higher inertia. The increase in rotor inertia justifies the drivetrain aero-servo-elastic frequency decreases.

Since the analysis focuses on the dynamics of the speed regulator mode, a detailed explanation of the differences in aero-servo-elastic frequencies of the tower, the first asymmetric flapwise, and first edgewise blade modes will be the object of other more detailed studies. Figure 5.3 shows a comparison between the first 11 closed-loop aeroelastic modes dampings of the Baseline and the Level 2 sweep configuration.

Damping ratios and modes are indicated in the same manner as in Figure 5.2.
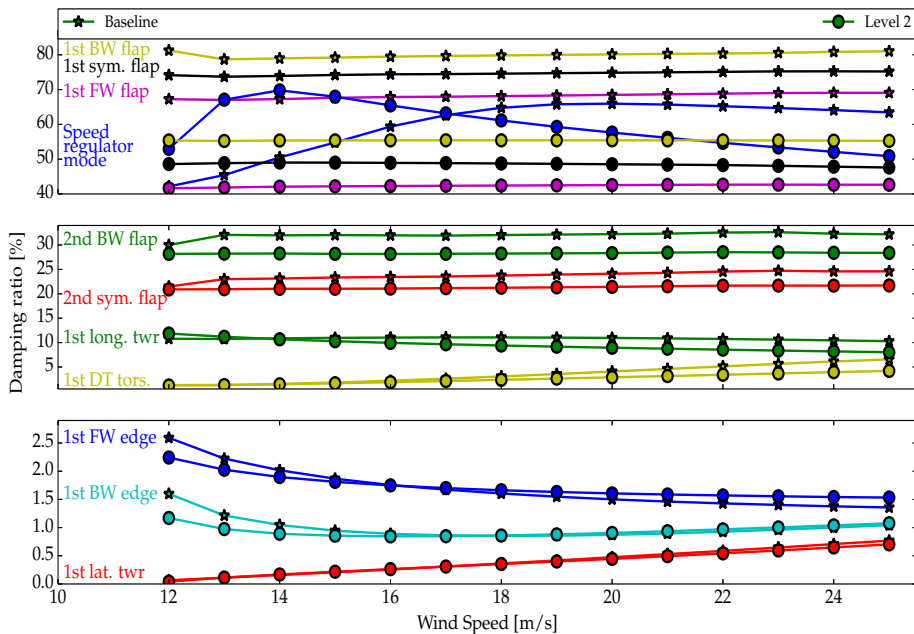
Figure 5.3: Closed-loop damping ratios of the aero-servo-elastic turbine modes as a function of the wind speed. Star: Baseline turbine modes. Circle: Passive-controlled (Sweep Level 2) turbine modes. Mode descriptions are labeled and distinguished by color [Paper B].

Except for the flapwise blade modes and for the speed regulator mode, the damping of the wind turbine modes are almost unchanged by the sweep. The damping ratios of the regulator mode of the passive-controlled turbine increases close to the rated wind speed and decreases for high wind speeds. The damping ratios of the flapwise blade modes drastically decrease due to the sweep. As for the aeroelastic frequencies, a detailed explanation for the decreased damping of the flapwise modes is provided by Hansen [47]. For the Baseline, the torsional component of the flapwise blade modes is out of phase with the flapwise motion therefore adding to the damping. Wind turbines with backward swept blades have a torsional component of the flapwise blade modes around 180 degrees out of phase with the flapwise motion, therefore consistently reducing the effect of the torsional motion on the damping ratio of the flapwise blade modes.

The comparison between the aeroelastic frequencies and damping ratios of the speed regulator mode for the different configurations is discussed in detail below. Figure 5.4 and Figure 5.5 respectively show the modal frequencies and damping ratios of the regulator mode of the different configurations. The baseline is denoted by a star symbol, while Sweep Level 1 and Sweep Level 2 are denoted by triangles and circles respectively. The three regulator modes start at 0.1 Hz. As the wind speed increases, the frequency of the regulator mode of the turbines with swept blades drops compared to the baseline.

The effect, shown in Figure 5.4, is increased for a larger sweep. The damping ratios of the regulator mode of the passively controlled turbines increases close to the rated wind speed and decreases for high wind speeds. The explanation for the differences registered for the dynamic properties of the speed regulator
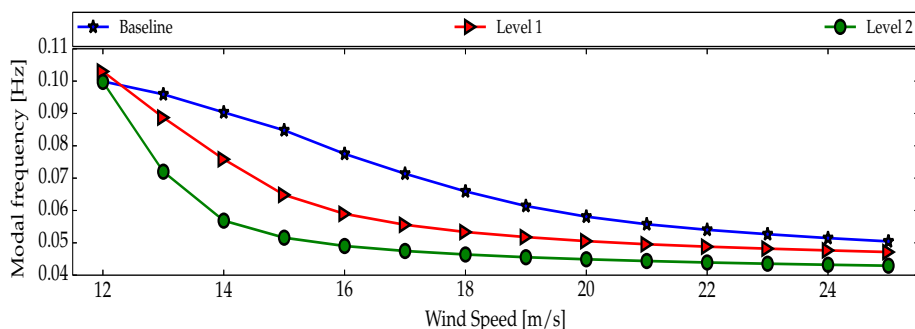
Figure 5.4: Speed Regulator Mode frequency as a function of the wind speed. Star: Baseline regulator mode. Triangle: Sweep Level 1 configuration. Circle: Sweep Level 2 configuration - Baseline Controller Tuning [Paper B].
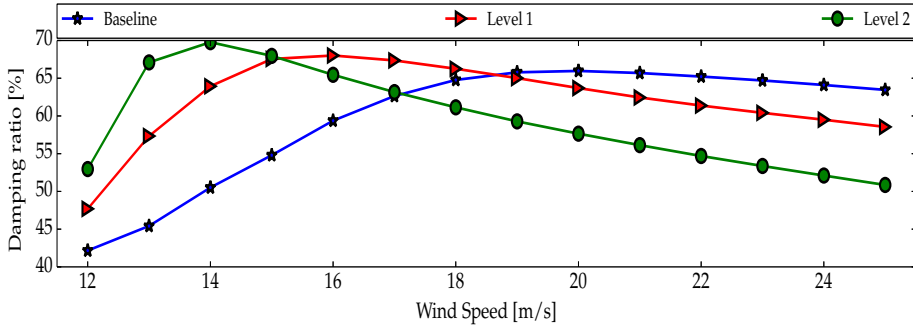
Figure 5.5: Speed Regulator Mode damping as a function of the wind speed. Star: Baseline regulator mode. Triangle: Sweep Level 1 configuration. Circle: Sweep Level 2 configuration - Baseline Controller Tuning [Paper B].

mode lies in the the partial derivatives of the aerodynamic torque with respect to the pitch angle (the so-called *aerodynamic gain*) and with respect to the rotor speed (the so-called *aerodynamic damping*) [89]. The first, $\frac{\partial Q}{\partial \theta}$, is shown in the left plot Figure 5.6 , while the second, $\frac{\partial Q}{\partial \omega}$, is plotted on the right in Figure 5.6. Both partial derivatives are plotted with respect to the pitch angle.
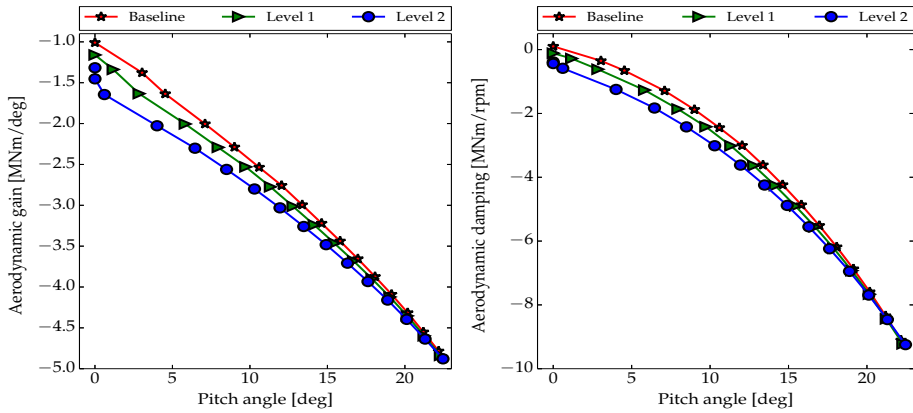
Figure 5.6: Comparison of the aerodynamic gain (left plot) and damping (right plot) of the different turbine configurations with respect to the pitch angle. Star: Baseline regulator mode. Triangle: Sweep Level 1 configuration. Circle: Sweep Level 2 configuration [Paper B].

The higher the sweep level, the greater the difference in aerodynamic gains and damping from the baseline. These discrepancies are due to the variation of the pitch angle, which varies according to the amount of bend-twist coupling provided by different backward swept blade shapes. Because of the different aerodynamic gains and damping, the tuning process, done exclusively for the Baseline, has to be performed again for the passively controlled wind turbines.

5.1.2 Controller Tuning of a Wind Turbine with Backward Swept Blades

Using a gain scheduling technique implemented for HAWCStab2 [89], the Sweep Level 1 configuration is re-tuned to compensate the discrepancies in aerodynamic gain and damping. The calculations of the gains for the controller is not sufficient to obtain a regulator mode with dynamic behaviour similar to the baseline. For this reason, the poles for the tuning of the PI controller need to be placed accordingly.

Figure 5.7 shows the comparison between the regulator modes of: the Baseline, Sweep Level 1 with baseline controller tuning, Sweep Level 1 with controller tuned, Sweep Level 1 with controller tuned and poles placed ad hoc target. If the passively controlled configuration controller is tuned using the described gain scheduling technique and the poles are placed accordingly, the discrepancies on the dynamic properties of the speed regulator mode are partially eliminated, as shown by Figure 5.7.
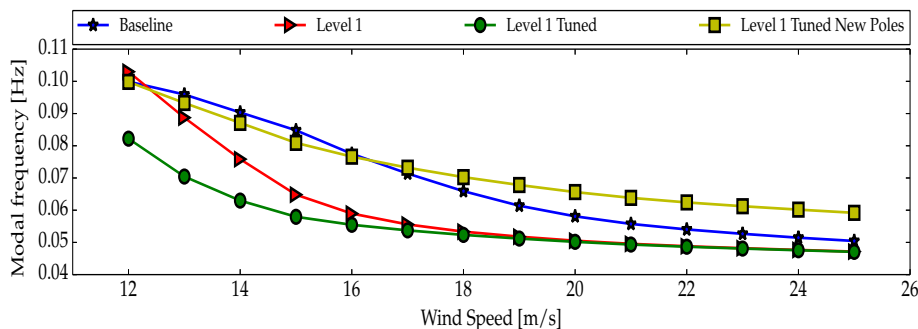
Figure 5.7: Comparison of Speed Regulator Mode frequencies as a function of the wind speed. Modes are computed varying the controller tuning. [Paper B].

Relevant differences can be observed when the wind speed increases further away from the rated wind speed. The differences at high wind speeds are due to the gain scheduling technique used. A tuning method based only the aerodynamic gain and damping cannot accurately reproduce the behaviour of the baseline controller for all the wind speeds.

When performing a benchmarking between turbines with passive loads control, it is important to properly select the procedure for tuning the controller, since the regulator mode performance has an effect on the overall dynamic response of the system. To provide a proper evaluation of the load variations brought by the passive loads control, the effects of the use of backward swept blades need to be separated from the influence of the controller. This can be achieved by ensuring that the dynamic properties of controllers of the benchmarked wind turbines are similar. The reader can refer to Paper B for a detailed description of the closed-loop dynamic behaviour of the wind turbines that took part to this study.

In conclusion, this study shows the importance of considering the wind turbine blade design problem as a multidisciplinary process. A simple change in blade shape has a relevant impact on the dynamics of the system, and this impact has to be taken into account to provide an accurate evaluation of the potential of the implementation of passive loads control.

Parametric Studies for Wind Turbine Blades Employing Passive Loads Control

In this chapter, we are going to implement passive loads control strategies more systematically using a parametric study approach. We are going to show that even though load alleviations can be achieved, several design requirements for the wind turbine need to be taken into account. The implementation of passive control on a blade has to compromise with other conflicting objectives and single changes of a single blade design variable are not sufficient to explore the full potential of passive control methodologies.

6.1   A Parametric Study on Backward Swept Blades

As in the investigation carried out in the previous chapter, we decided to start from an easy-to-model passive control method: backward swept blades (see Paper C).

6.1.1 Models Description

Changes in the external blade planform are implemented systematically using Bezier Polynomials [90] and varying the control points of these polynomials. Three parameters are selected to describe the shape of the swept blades. Each of these parameters is associated to a letter (s, b or f) and a sequence of numbers having three or four digits (three digits for the integer part and an optional forth digit for the fractional):

- *sxxx*: location of the first control point on the centerline; it roughly describes the spanwise length where the sweep starts;

- *bxxxx*: backward sweep at the tip in percentage of the total blade length;

- *fxxxx*: maximum forward sweep in percentage of the total blade length.

The parametric study involves a total of 25 blade geometries. Figure 6.1 shows a sample of the selected backward swept blade shapes.

6.1.2 Methodology

The aim of this study is to explore the backward swept blades full potential for load alleviations. To achieve this objective, we performed extensive load analyses using the DTU 10-MW RWT coupled to the DTU Wind Energy Controller [78] as baseline turbine, and the DTU Design Load Basis (DLB) [91] as the baseline DLB. More importantly, we provide a **fair** comparison between the different passively controlled wind turbines analysed. We compensate for two effects
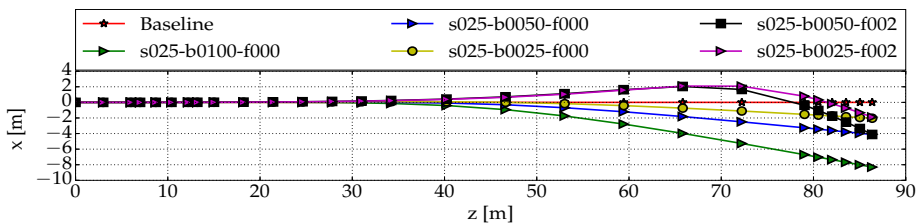
Figure 6.1: Backward swept shapes of Family 1. z is the coordinate along the blade centerline, whereas x is the coordinate oriented in the edgewise direction. The first control point is located at 25% span of the total blade length [Paper C].

that influence the analysis of the loads and the mitigation potential of backward swept blades:

- due to the geometric structural coupling, turbines with backward swept blades have a lower AEP compared to a turbine with a straight-bladed rotor because of the decrease in the angle of attack along the blade span during operation (see Paper D);

- due to the changes in the structural and aerodynamic response of the blade, i.e. bend-twist coupling effect and change in the angles of attack, respectively, frequencies and damping ratios of the speed regulator mode of turbines with swept blades are significantly different compared to a baseline with straight blades (see Paper B).

To compensate the loss of AEP below rated wind speed, the aerodynamic twist of each blade design selected is optimized using the HAWTOpt2 framework [18, 19]. The numerical optimization problem is defined as:

$$
\begin{aligned}
\max_{\mathbf{x}_p(\beta)} \quad & f(\mathbf{x}_p(\beta), \mathbf{p}) \\
\text{s.t.} \quad & \mathbf{g}(\mathbf{x}_p(\beta)) \leq \mathbf{0}
\end{aligned}
\tag{6.1}
$$

The cost function f depends on a set of variable $\mathbf{x}_p(\beta)$ and a set of constant parameters $\mathbf{p}$. For this simple optimization, the design variables are exclusively the parameters that describe the aerodynamic twist of the blade β. A free form deformation spline (FFD) with 5 control points is used to parametrize the aerodynamic twist as a design variable. The parameters $\mathbf{p}$, including the blade planform, the layups of the blades, and the other components of the wind turbine, are kept constant throughout the optimization. The design variables are normalized, such that when they are equal to zero they correspond to the baseline value. The cost function, defined in Equation 6.2, is subject to a set of nonlinear constraints $\mathbf{g}$.

$$
f(\mathbf{x}_p(\beta), \mathbf{p}) = \frac{AEP(\mathbf{0}, \mathbf{p})}{AEP(\mathbf{x}_p(\beta), \mathbf{p})}
\tag{6.2}
$$

$AEP(\mathbf{0}, \mathbf{p})$ is the annual energy production of the baseline design.

The constraints $\mathbf{g}$ include:

- the rotor thrust, so that the swept-bladed turbines cannot exceed the operational rotor thrust of the baseline;

- the operational lift coefficients that, along the blade span, are limited to avoid stall.

The controllers of wind turbines that take part in the investigation have similar dynamics. The behaviour of the controllers are set following the methodology summarized in the previous chapter and reported in Paper B.

As a final note, we need to remark that because of the number of blade designs involved in the study (25), the amount of simulations required by the chosen DLB (1800), and the computational time required to simulate a 10-minute time series with HAWC2 (from 10 to 20 minutes depending on the load case), this investigation would not have been completed in a practical amount of time without the use of an HPCC. The latter observation underlines the importance of the availability of high-end computing capability to carry research studies on the subject of passive loads control techniques.

6.1.3 Results Highlights

The impact of each geometry parameter and its potential for load reductions is analysed through a comparison of distributions of absolute maxima and lifetime equivalent fatigue loads (LTEFL) on the blade root. Figure 6.2 and 6.3 respectively show a sample of the extreme and fatigue load analysis performed on backward swept blades. For the complete set of results and discussion, the reader can refer to Paper C.

The results obtained from the extensive load analysis can be summarized as follows:

- "sxxx": the choice of the first control point location parameter is driven by the large increase in extreme and fatigue blade root torsional moment, and the increase of the edgewise LTEFL due to the increase in blade length more pronounced as the sweep starts closer to the root;

- "bxxxx": the parameter has to be chosen considering the minimum increase in torsional extreme and fatigue loading, and taking into account the increase in blade mass due to the increment in blade length brought about by the swept shape;

- "fxxxx": the presence of forward sweep helps by compensating excessive increments of the torsional moment, but it also reduces or cancels the beneficial effects due to the sweep; moreover, the location of the forward sweep along the blade span does not have a relevant influence on the loading.

The conclusion of the investigation is that mildly and purely backward swept shapes are the best option for the design of passively controlled wind turbines

because they can achieve load alleviations without causing large increases in blade root torsional moment.

Annual energy production and tower clearance were monitored as well. The optimization of the aerodynamic twist to maximize AEP produces negative effects on the tower clearance of some of the designs analyzed. The optimizer increases the aerodynamic twist at the blade tip to fulfil the loss in AEP below rated wind speed, resulting in higher angles of attack and higher loads at the tip around rated wind speed compared to the baseline design. This process causes a reduction of the tower clearance with respect to the RWT and a different distribution of the loading along the blade span.

In Paper C, we chose to focus on an individual passive control category. Previous studies have already demonstrated the beneficial load alleviation effects of utilizing blades that use a single form of bend-twist coupling. In our next investigation, we expand the work described in this section to consider wind turbine blade designs that employ all the three categories of passive control simultaneously (see Paper E).

6.2 Parametric Combination of Passive Loads Control Strategies

The purpose of this study is to evaluate the load alleviation potential effects of each of the three methods separately, and then in different combinations. Extensive load and strength analyses are performed in order to demonstrate the possibility of exploiting the synergy between these methods. The idea is to enhance the benefits from each of the strategy applied alone and to reduce the negative effects by combining the methods.

6.2.1 Passive Loads Control Methods Selection and Description

A summary of the passive methods considered here is given in Figure 6.4. Each column in Figure 6.4 describes a different method, classified by a three letters code (SSW for the blade design with single shear web, SWP for the swept blade and BTC for the blade with material bend-twist coupling). The rows contain information regarding:
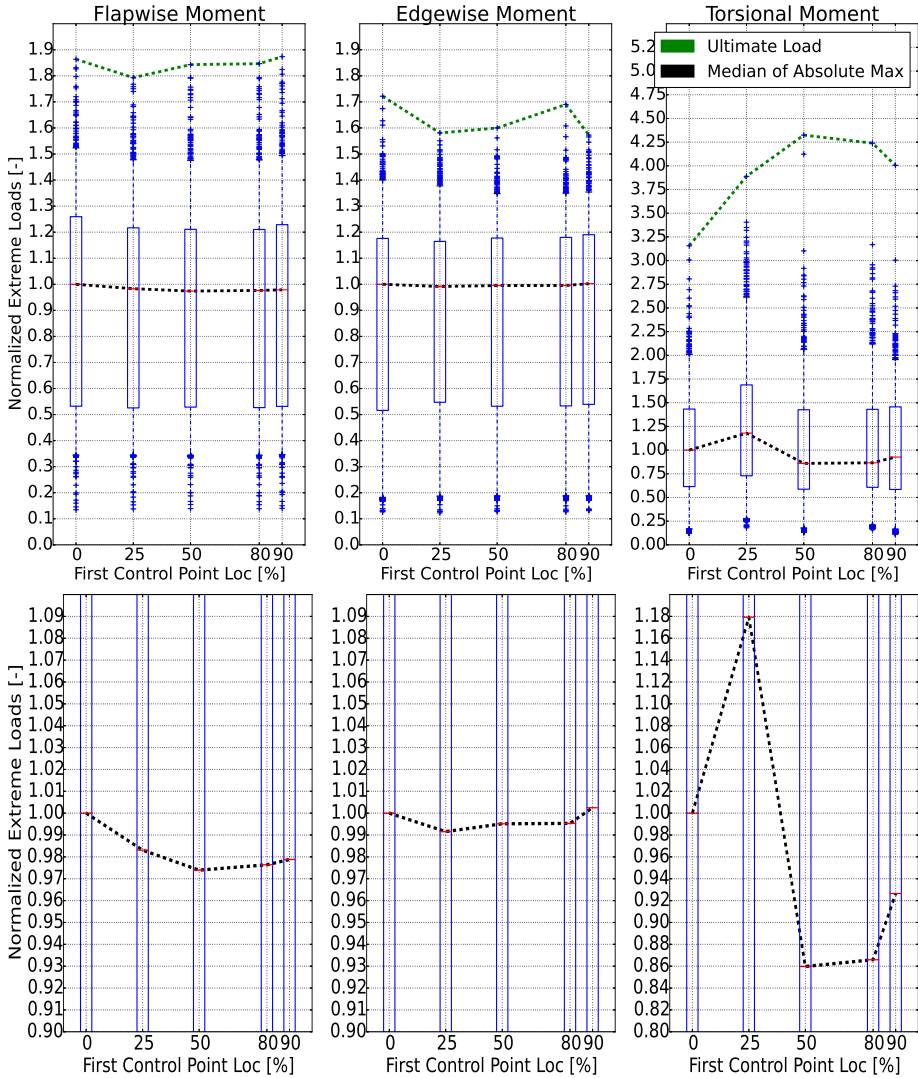
Figure 6.2: Normalized absolute maxima distributions for baseline and swept
blades with ascending first control point location along the blade
span. Extreme flapwise, edgewise, and torsional moments are plot-
ted on the left, center, and right, respectively. Bottom plots show
a close-up on the medians of the distributions. The loads are
non-dimensionalized by the median of the respective baseline dis-
tribution [Paper C].
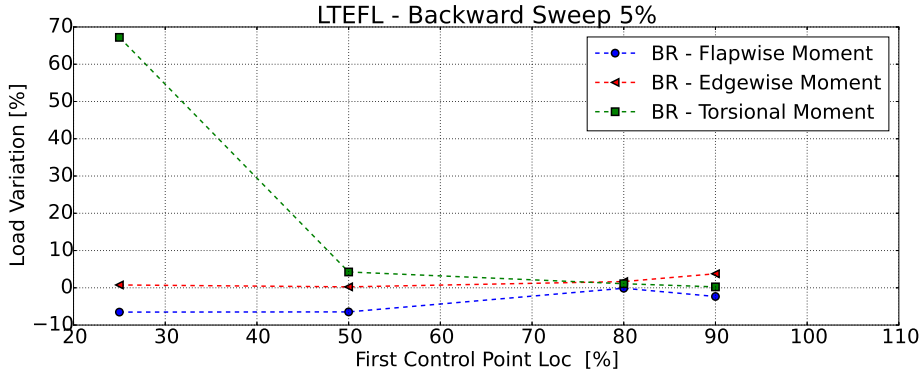
Figure 6.3: LTEFL blade root moments deviations in percentage from the baseline straight blade (blue circle - flapwise, red triangle - edgewise, green square - torsional). The backward sweep parameter at the tip is fixed at 5% of the blade length. No forward sweep is considered. Different blade radius along the span are taken into account [Paper C].

- application zone - area where the control strategy is applied according to the span-wise position;

- mechanism of the passive control strategy;

- outcome - the qualitative effect of each control strategy;

- required design corrections - general design adjustments to be considered for implementing the method on the blades.

The following points have to be highlighted in order to clarify some of the presented choices for the passive control strategies applied in each blade design:

- the application zones for the different methods have been chosen based on the analysis of the possible outcomes;

- the application of the SSW on the full blade span is bounded to manufacturing constraints;

- the swept blade design is selected according to a parametric study performed by the authors, taking into account load alleviation potential and a restrained increase in extreme and fatigue blade root torsional loads (see Paper C); the shape for the swept blade is chosen to be a pure backward sweep where the change in the shape starts at 80% of the blade length with the maximum sweep of around 2m at the tip;

- the application zone for the BTC is chosen after preliminary consideration of the blade strength and structural properties; after few design iterations, we selected an angle of 8° for biasing of the unidirectional layers in the spar caps.

The full list of the wind turbine blade design analysed within the present investigation is reported hereby together with their acronyms in the parenthesis:

- Baseline straight blade

- Swept blade (SWP)

- Blade with material bend-twist coupling (BTC)

- Straight blade with single shear web (SSW)

- Swept blade with single shear web (SWP+SSW)

- Swept blade with material bend-twist coupling (SWP+BTC)

- Straight blade with single shear web and material bend-twist coupling (BTC+SSW)

	Single Shear Web (SSW)	Sweep (SWP)	Bend-twist coupling (BTC)
Application zone	Full Blade	Blade tip - s80-b0025-f0000 (80% radius, 2m tip back)	UD layers of spar caps - 8° UD bias for entire blade
Mechanism	Twist to feather due to lower torsional stiffness	Twist to feather by extra torque	Twist to feather due to bending moment and BTC
Positive Outcome	Passive load alleviation due to decreased angles of attack in operation, Slightly higher tower clearance	Passive load alleviation due to decreased angles of attack in operation, Higher tower clearance	Passive load alleviation due to decreased angles of attack in operation, Higher torsional stiffness
Negative Outcome	Risk of aeroelastic instabilities Structural stability (buckling)	Higher torque load along the blade length Higher torque load at the pitch actuator	Lower tower clearance due to lower bending stiffness Lower strength of the biased UD layers
Required Design corrections	Pitch toward stall to compensate AEP loss below rated wind speed Check for buckling	Pitch toward stall to compensate AEP loss below rated wind speed	Pitch toward stall to compensate AEP loss below rated wind speed

Figure 6.4: Passive control methods description [Paper E].

• Swept blade with single shear web and material BTC (SWP+BTC+SSW)

6.2.2   Synergy and Discord

All the choices relating to the design parameters are made with the general intention of exploiting the synergy between the three passive control methods. Consider for example tower clearance: a backward swept blade is able to increase the tower clearance due to its structural properties, at the same time providing beneficial load alleviations on the blades. BTC can reduce the loads acting on the structure, but it also decreases the bending stiffness of the blade, lowering the tower clearance. Hence, a combination of SWP and BTC can result in a favourable load alleviation effect, while still maintaining the tower clearance required by the design standards (see Figure 6.5).

Another interesting synergistic effect is shown in Figure 6.6. The flapwise bend-twist coupling coefficient β is calculated along the blade length in accordance to the method described in [9]. The figure shows that generally higher coupling can be achieved for the original two-shear-web blade than for the modified single-shear-web blade. This fact agrees well with the results obtained for the coupled box- and I-beams in [9]. Thereby, the BTC and single-shear-web methods for passive load control seem to interfere with each other and are not recommended for combination in the same blade design when the BTC effects are prioritized.
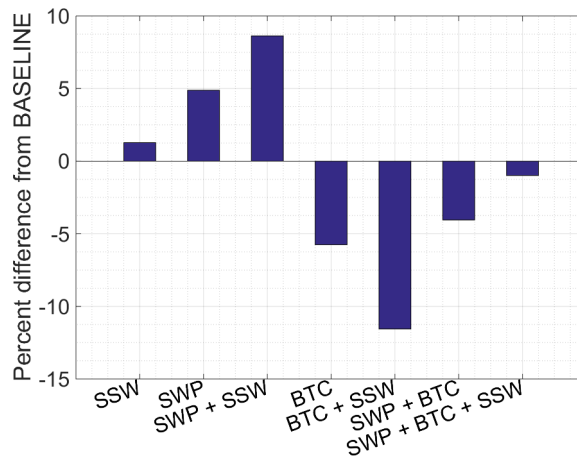
Figure 6.5: Variation of the tower clearance of considered blade designs compared to the baseline configuration [Paper E].
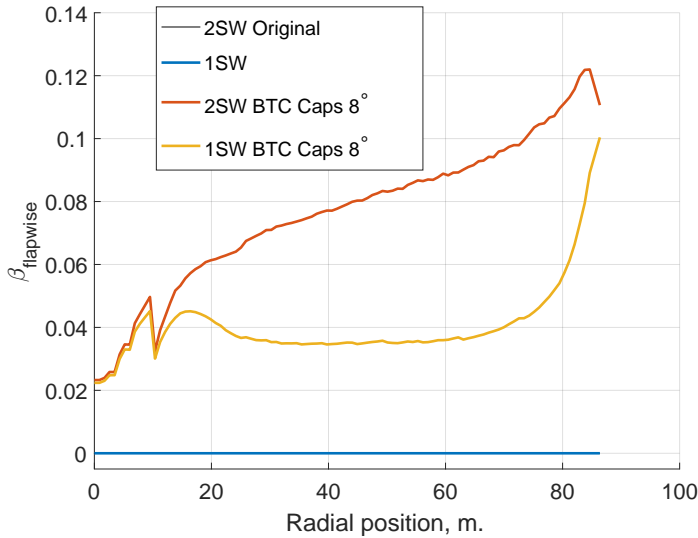
Figure 6.6: Flapwise bend-twist coupling coefficient β for different blade designs [Paper E].

Figures 6.7, 6.8, and 6.9 show blade root flapwise, edgewise, and torsional loads respectively. In general, all passive control strategies produce alleviations for both extreme and fatigue bending loads in the range of 5 to 10%. In the flapwise case, the combination of all the three control methods demonstrates the highest drop in both extreme and fatigue loads (6% for extreme and approximately 11% for fatigue values). The flapwise load alleviation for the combined designs is stronger than for the isolated passive control designs.

The swept blade design is the most efficient for the extreme edgewise blade root loads. The single shear-web design and its combinations prove to be the most effective choice for the lifetime equivalent blade root edgewise fatigue load. This outcome is due to the fact that these loads are mostly driven by gravity forces which are linked to the total mass of the blade. The SSW designs have lower blade mass, which is reduced by 7.5% compared to the DTU 10-MW RWT blade due to the presence of only a single shear-web against the three used for the baseline design.

The backward swept blade has a negative impact on the blade root torsional moment (1.5% increase in extreme and 5% increase in fatigue), due to the extra torque generated by the swept tip of the blade. BTC shows a strong alleviation of the extreme blade root torque (11%) and a large increase in the lifetime
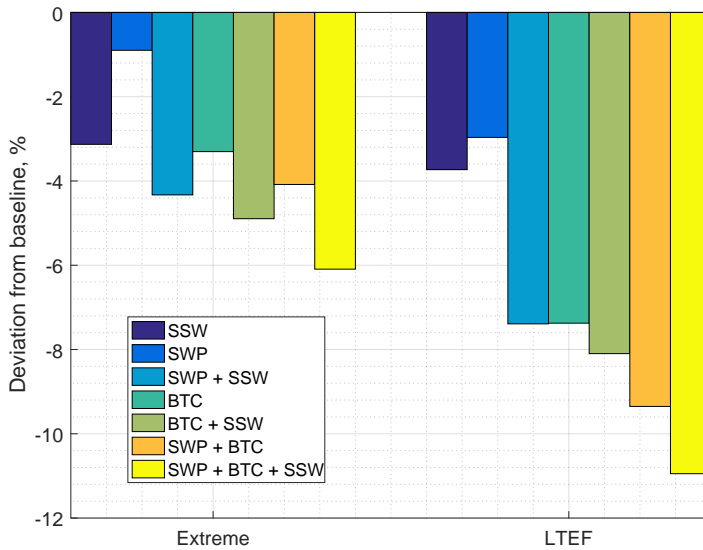
Figure 6.7: Extreme and life-time equivalent fatigue (LTEF) flapwise bending moment for the blade root [Paper E].
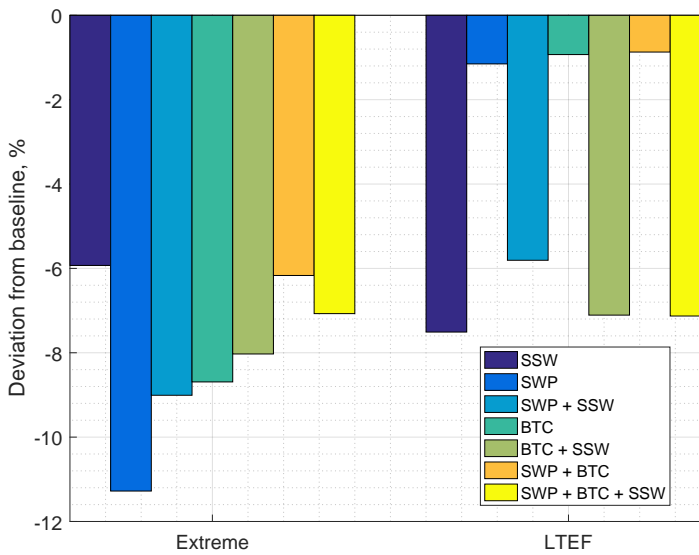
Figure 6.8: Extreme and life-time equivalent fatigue (LTEF) edgewise bending moment for the blade root [Paper E].
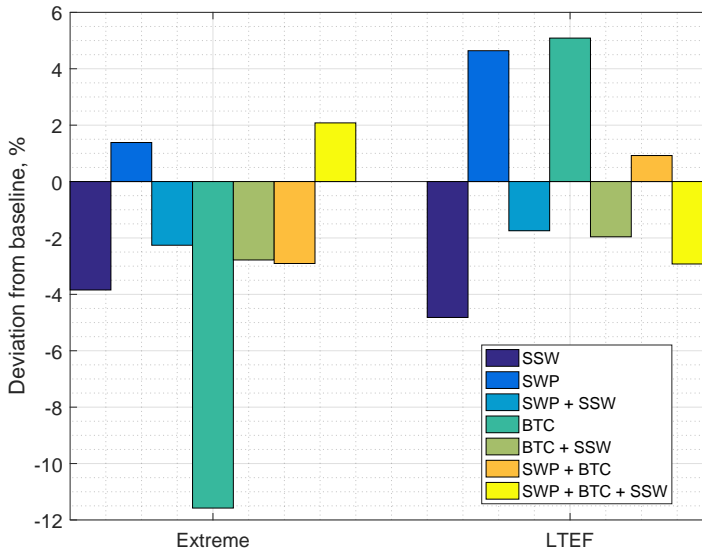
Figure 6.9: Extreme and life-time equivalent fatigue (LTEF) torque values for
the blade root [Paper E].

equivalent fatigue load (around 5%).

The results showed that the right combination of passive control strategies can
lead to a blade design capable of enhancing the load alleviations and diminish-
ing negative effects from each of the passive control strategies. An example is
the combination of the BTC and the backward sweep in the same blade, re-
sulting in the blade root flapwise fatigue loads being lower with respect to the
baseline (4%) and with respect to the only-swept blade design (6% extra load
alleviation) and the BTC-only design (2% extra load alleviation). At the same
time, combining the swept blade design with the BTC helped to compensate
for the decrease in minimum tower clearance caused by the loss in bending stiff-
ness due to the rotation of the fibres of the unidirectional layers in the spar caps.

Other than observations on the effects of different passive control parameters
or different concepts combinations on the wind turbine loading, these studies
brought to light another question: is this the best methodology to fully explore
the potential of the employment of a passive control methodology? Not only
did we have to take into account interactive effects like controller dynamics and
loss of annual energy production, but we also ended up battling, among others,
with blade root torsional moments and tower clearance. Even basic changes in
blade external planform such as sweep that are not as invasive as changing, for
instance, materials and structural properties, have multiple implications on a

complex system such as a wind turbine.

Analysing the synergistic effects brought about by combinations of different passive control strategies helped in fulfilling certain design requirements by reducing negative effects. The problem is that a parametric study approach does not give full control on any of the requirements demanded by the designer. These investigations are a demonstration that parametric studies are a great aid to study the principles behind passive control, but they cannot fully explore passive control potential while fulfilling the many design limitations imposed by the certification standards. More importantly, we were able to give an estimation of the load mitigation effects of different implementations of passive control, but we could not directly relate the load reduction to what creates an impact on the LCOE: a decrease in the rotor mass and an increase in the annual energy production.

The design of a wind turbine blade is a multidisciplinary problem, and it needs to be treated as such. We have demonstrated here that parametric studies are not sufficient to fully explore the potential behind the implementation of passive control methods because they cannot take into account all the right trade-offs to achieve a cost effective design. Consequently, we now turn to a discussion on multidisciplinary design optimization (MDO) and its application to passively controlled rotors.

Multidisciplinary Design Optimization of Passively Controlled Rotors

Through a number of parametric studies, we confirmed that the design of passively controlled blades is a complex process, involving a deep understanding of the interlaced disciplines involved. The multidisciplinary nature of blade design is a challenge from an early stage of the process, as it compels the designer to simultaneously satisfy several constraints while evaluating trade-offs between conflicting objectives. In this context, multidisciplinary design optimization (MDO) frameworks can be used to develop wind turbine blades. Design parameters are optimized with respect to a cost function, subjected to constraints that encompass standard design requirements for wind turbines. These design parameters can be several and generally refer to different components of the wind turbine and its operational characteristics. If the focus of the MDO process is exclusively the wind turbine rotor, the design variables are the internal structure and the outer shape of the blades.

Several MDO frameworks have been presented in recent years. Martins provides a good overview of the state-of-the-art of MDO framework architectures [92]. These frameworks can be used for a diverse range of applications, but for the sake of conciseness, we will focus exclusively on the frameworks used in wind

energy.

Common objectives for the wind-energy optimization frameworks is the minimization of the COE, or the maximization/minimization of its main drivers, such as annual energy production (AEP) and component mass. MDO of wind turbines can be done at several levels and using models of various fidelities. For example, the design process of wind turbines can be done on a wind farm scale where the characteristics of the installation site are incorporated in the optimization [93]. In this case, the modelling of the components and costs are done based on simplified design principles to avoid the high computational costs that a more detailed model of the wind turbine would require. If the representation of the wind turbine system is done at high-fidelity, integrated aero-structural metrics can be used to achieve better designs [17]. Aeroelastic MDO requires a complex set of interfacing tools and computationally expensive procedures. In particular, the need to run a large number of nonlinear aero-servo-elastic simulations constitutes a practical issue to successfully perform an MDO [94]. This challenge was tackled by developing a multi-stage process that alternates between a purely aerodynamic blade optimization loop and a structural one, to then obtain a final optimum solution with the combination of the two [16]. Alternatively, the aeroelastic MDO can be done sequentially, stripping the number of aero-servo-elastic simulations involved to a bare minimum [95].

Even though the MDO frameworks available today are sufficiently robust to produce reliable wind turbine blade designs, we have not found any previous work where passive loads control is used as a design variable for wind turbine blades optimization. In the past, an optimized passively controlled wind turbine design was developed [15], where the loading on the rotor was mitigated through the employment of bend-twist coupled blades (orientation of the fibres in the layups is tailored to create structural coupling between flapwise bending and torsion), but the passive loads control method was imposed a priori and not as a variable in the MDO.

This lack of research is due to the fact that the employment of a passive loads control strategy has a significant impact on the wind turbine loading. A considerable number of aeroelastic simulations are needed to properly capture the effect of the structural coupling induced by passive loads control methods on the loads. The first issue is that a large number of simulations represent an excessively expensive computational effort for an optimization framework. The second problem is that large variations in wind turbine loading are not suited for the assumption that loads change slowly with respect to changes in the design variables (*frozen loads* assumption), i.e. a small change in the blade sweep can produce large loading modifications, as shown in Paper C. In particular, an inaccurate estimation of the loads on a blade can produce an incorrect evaluation of the strength constraints, compromising the quality of the final design.

Our major research contribution to the topic of aeroelastic MDO is the introduction of passive loads control design variables in the wind turbine blade optimization process. Before diving into the MDO problem formulation for passively controlled rotors, we need to describe how we addressed the two issues reported above: excessively expensive computational effort and accurate estimation of large loading variations due to the use of passive loads control.

In the first part of the chapter, we describe the MDO framework used to perform the passive loads control design studies. We then report the summary of a method developed to face the problem related to the computationally expensive estimation of aeroelastic wind turbine loads in an MDO framework (see Paper F). This method can be used exclusively for the estimation of blade ultimate loads. The fatigue loads are computed using a method developed, validated, and used by Tibaldi et al. [96, 97]. We present the results of the implementation of passive loads control methods in MDO, along with a description of the optimization problem, in the second part of the chapter (see the final part of Paper F and Paper G for further details).

7.1   MDO Framework and Models

The optimization process is implemented in the HawtOpt2 framework [18]. Built on the platform provided by OpenMDAO (Open-source Multidisciplinary Design, Analysis, and Optimization Framework) [98, 99, 100, 101], the tool is used to handle the definition of the optimization problem, workflow, dataflow, and parallelization of simulation cases. OpenMDAO provides an interface to PyOpt [102], a container for several optimization algorithms. In this work, the gradient-based sequential quadratic programming optimizer SNOPT is used [103].

The core of the MDO framework is constituted by three tools: a finite element cross sectional code, BECAS [104, 105, 106], the already introduced aeroelastic solvers HAWC2, and HAWCStab2. These three codes are connected to the optimization platform through interfaces that allow the state-of-the-art analysis required to tackle the complexity of the blade design process. BECAS, HAWC2, and HAWCStab2 are not set to provide the estimation of analytic gradients. For this reason, the MDO framework relies on the computation of finite difference (FD) gradients.

BECAS is a cross section analysis tool for anisotropic and inhomogeneous beam sections of arbitrary geometry. In the workflow, BECAS is used for the evaluation of the cross sectional stiffness and mass properties of the blade, and for

the computation of stresses and strains. The geometry of each section is exactly described through a 2D finite element formulation, which allows a description of the various layups. The cross sectional stiffness and mass properties are used to extract the inputs for the linear Timoshenko beam element model implemented in HAWC2 and HAWCStab2.

As previously mentioned, HAWCStab2 performs analytical linearizations of high-order aero-servo-elastic models. The tool is used for frequency analysis, controller tuning, and evaluation of fatigue damage equivalent load rates using a frequency domain based approach [96]. Ultimate loads simulations within the optimization loop are carried out using the nonlinear aeroelastic solver HAWC2 on a reduced set of design load cases. The latter approach is described in details in the next section. We remark that the final designs coming out of the optimization loop are checked against a full design load basis described in [91]. The loads obtained through the aeroelastic solvers are provided back to BE-CAS, which has a stress recovery module that the framework uses for the blade strength and failure analysis.

Figure 7.1 provides a visual overview of the general workflow using the so-called extended design structure matrix diagram (XDSM) [107]. The connections between the tools aforementioned are highlighted. HawtOpt2 selects design variables (surface and internal geometry) based on a cost function subjected to constraints evaluated by the aeroelastic solvers and the cross section analysis tool.
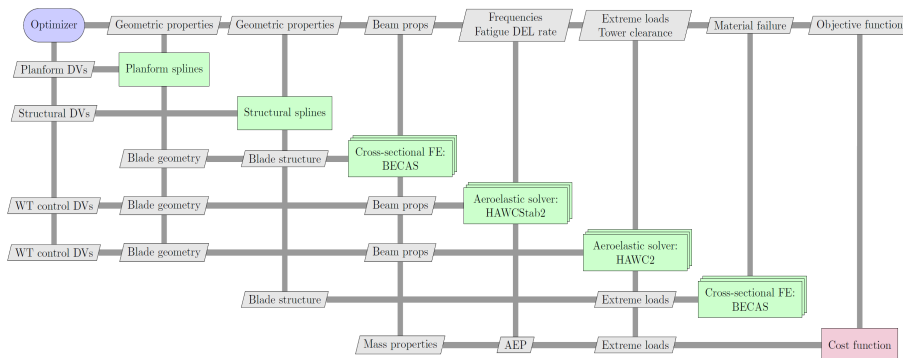
Figure 7.1: General overview of the MDO framework. The link between the three tools (BECAS, HAWC2, and HAWCStab2) and the pre/post-processing phases are highlighted [108].

The framework used for the MDO performed in this chapter is built as a Monolithic Architecture (see Figure 7.1), as the MDO problem, described in Section 7.3, is cast as a single optimization problem. Specifically, we use the Multidisciplinary Feasible Architecture (MFA) because the aeroelastic solvers and BECAS are connected in OpenMDAO as black boxes to avoid the complex task of intervening on their source codes to adapt them to more complex MDO architectures (as SAND or AAO for instance). A complete overview of the different types of available MDO architectures is provided by Martins and Lambe [92].

7.2 The Reduced DLB

The stochastic nature of the turbulence adds complexity to the estimation of the ultimate loads. As briefly mentioned in this section's introduction, to face the intricate matter of simulating wind turbine loading in turbulent inflow conditions, a standard DLB requires a large number of simulations (the DTU DLB counts up to 1880 DLCs). The number of simulations depends on the amount of turbulence seeds considered, which is usually as large as possible to obtain wind turbine loads with sufficient accuracy. Taking into account such a number of simulations in an MDO can become impractical due to the computational effort and time required to perform each cost function evaluation. Moreover, turbulent DLCs are lengthy simulations (usually the standard simulated time is 10 minutes), which can represent a further obstacle to keep the optimization time reasonable. Another issue is the fact that the interaction of a changing turbine design with different parts of the same turbulent field during an MDO might compromise the quality of the optimization process [89].

In the light of these problems, the main idea behind the formulation of the reduced DLB for the estimation of ultimate loads in MDO frameworks is to use a "deterministic" set of load cases able to mimic the effects of turbulence on the blade loading. These "deterministic" DLCs are characterized by the presence of a custom-made shear zone or extreme operating gusts. A detailed description is provided in the next part of the section.

The absence of turbulence from the DLB gives the possibility to greatly shorten both the amount of simulations (no turbulence seeds need to be considered) and the simulation time of each DLC selected (without turbulence a simulated time of 10 minutes is no more a requirement). This translates to a consistent advantage with respect to computation time, which is consistently shortened for the aero-servo-elastic code used in the study (HAWC2).

In the next part of this section, a full description of the reduced DLB is pro-

vided, along with an explanation of the aforementioned "deterministic" set of load cases. The section concludes with a description of how this reduced DLB concept can be integrated in an wind turbine blade MDO problem.

7.2.1   Description of the Concept

The main characteristic of the reduced DLB is the substitution of turbulent load cases with a set of "determistic" ones. The substitution brings about a significant reduction in the number of DLCs and simulation time. Moreover, as the presence of stochastic inflow conditions can compromise the results of the MDO process, the ultimate blade load envelopes are computed through simulations that use deterministic changes in the inflow. In this manner, a blade design changing during the MDO will always interact with the same wind field structure, ensuring a more robust evaluation of the variations in wind turbine loading due to a change in a design variable. At each cost function evaluation, the new design undergoes the same wind loading excitations as its predecessor, ensuring, for example, that the optimization process is not depending on the position occupied by the blade in a stochastic inflow field.

Two wind flow conditions are used to substitute the turbulent inflow load cases:

- a custom-made shear zone for production, fault, start-up, and shut-down load cases;

- an extreme operating gust (EOG) for parked and maintenance DLCs.

Figure 7.2 provides a visual representation of the first deterministic wind field variation used by the reduced DLB. When a blade rotates towards the upward positioning, it passes through a custom-made shear zone, formed by a combination of a linear horizontal shear and a linear vertical shear. At the center of the hub, the wind speed, defined by the coordinate system $< u, v, w >$ that follows the notation in the HAWC2 manual [64, p. 21], is equal to the uniform wind speed selected for the specific DLC ($u_1 = V_{hub}$ and $v_1 = V_{hub}$). Above the hub height, the wind speed increases towards the outer part of the rotor until it reaches the value defined in Equation 7.1. The rest of the wind inflow is uniform and it has a constant value of V_{hub}.

$$u_2 = V_{hub} + 3\sigma_1; \quad v_2 = V_{hub} + 3\sigma_1 \tag{7.1}$$

where V_{hub} is the wind speed at hub height selected for a specific DLC, and σ_1 is the representative value of the turbulence standard deviation as defined by

the IEC standard [60, p.24-27] and reported in Equations 7.2 and 7.3 for normal and extreme turbulence models, respectively.

$$\sigma_1 = I_{ref}(0.75V_{hub} + b); \quad b = 5.6\text{m s}^{-1} \tag{7.2}$$

$$\sigma_1 = c\, I_{ref}\left[0.072\left(\frac{V_{ave}}{c} + 3\right)\left(\frac{V_{hub}}{c} - 4\right) + 10\right]; \quad c = 2\text{m s}^{-1}; \quad V_{ave} = 0.2\, V_{ref} \tag{7.3}$$

V_{ref} and I_{ref} are the reference wind speed and turbulence intensity, respectively, which depend on the turbine class. Since the DTU 10-MW RWT belongs to the class IA, $V_{ref} = 50\text{m s}^{-1}$ and $I_{ref} = 0.16$.
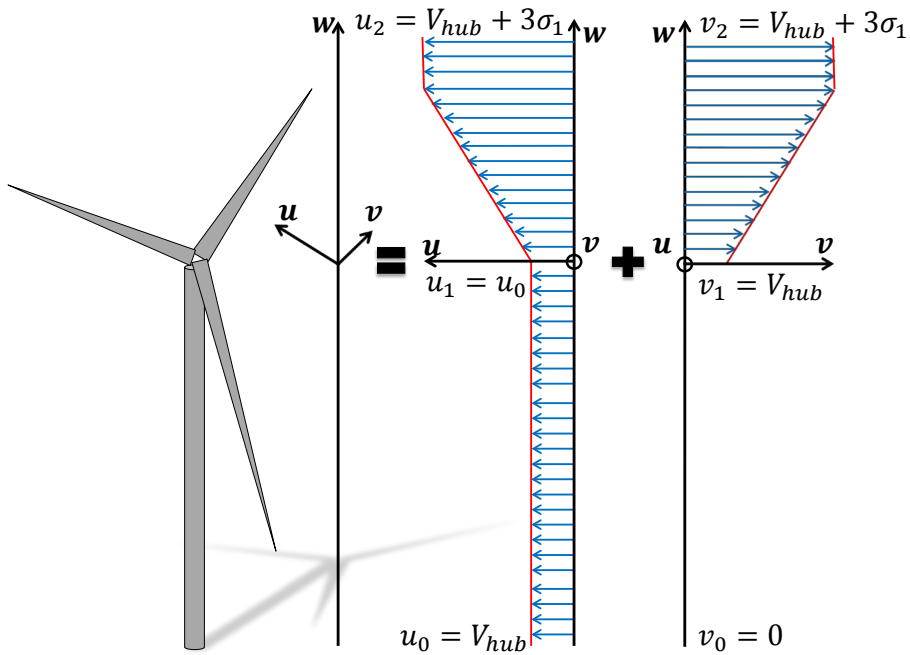
Figure 7.2: Visual representation of the custom-made shear zone used to mimic ultimate blade loading generated by turbulent inflow. The sheared wind inflow is assembled by the combination of a linear horizontal shear and a linear vertical shear in the upper part of the rotor. Values of the wind speed in the different areas of the shear zone are highlighted in the equations [Paper F].

The idea behind the use of the described custom-made shear zone is to apply a loading to each blade with the highest peak at 1P, both in the flapwise and the edgewise directions. This type of loading is typical for wind turbines due to shear, tower shadow, and nacelle tilt, and it represents the most important contribution to blade loads in turbulent inflow conditions. The wind profile in the custom-made shear zone (Equations 7.1, 7.2, and 7.3) is selected to take into account the maximum wind speed variations present in the turbulence DLCs.

The second deterministic wind field variation is an EOG, which is implemented in the reduced DLB following the formulation provided by the IEC standard in [60, p. 26].

The effect of turbulence on the loads cannot be exactly replicated, but the maximum and minimum flapwise and edgewise blade loads can be captured with a sufficient accuracy, as shown in the next section. Furthermore, the proposed scheme to mimic turbulent DLCs is based on general observations of typical wind turbine loads, and it can be therefore applied to different wind turbine designs and classes.

A complete summary of all the load cases that constitute the reduced DLB used for the RWT is reported in Paper F. Only the ultimate DLCs are part of the DLB (label "U" in [91, p. 7]). The partial safety factors used for each DLC are the same used in [91]. The load cases that do not consider turbulence in the DTU DLB are kept unchanged (DLC14, DLC15, DLC23, DLC32, DLC33, and DLC42). Simulated time is not reported because it is not a strict requirement for the reduced DLB, and it can be chosen according to the aero-servo-elastic models used. Controller faults dependent load cases (DLC22) are not considered for the time being, as they were not included as design load cases for the DTU 10-MW RWT. These DLCs will be included in a future development of the reduced DLB.

7.2.2   Integration of the reduced DLB in an MDO framework

The reduced DLB concept can be integrated in an optimization problem for the design of a wind turbine blade. As shown in details in the next section, the envelopes obtained through the computation of the reduced DLB are similar in shape to the one obtained from a full DLB, but different in magnitude. For this reason, the reduced DLB can be used directly in the MDO as an indicator of the load variations following the scheme depicted in Figure 7.3. A detailed description of the steps of the integration process are highlighted in the figure's caption.

The optimization problem is supplied with blade load envelopes coming from a full DLB. Then, a correction, based on the load variations caught by the reduced DLB, is applied to every cost function evaluation. The deterministic nature of the reduced DLB does not compromise the optimization process, which is quickly provided with new ultimate blade load envelopes at each step. The most time-consuming part of the process (the estimation of envelopes with a full DLB) is done outside of the optimization loop.

7.2.3 Results

The purpose of this section is to show that an ultimate loading variation estimated through a reduced DLB is similar to load variations estimated by a much more computationally expensive DLB. If this assumption is verified, the reduced DLB can be suitable for ultimate blade load envelopes estimation in an MDO process, and the scheme described in Figure 7.3 can be applied.

Figure 7.4 shows a comparison between ultimate load envelopes (plot on the top left) of the Baseline and of the Step 1 designs extracted using the full and the reduced DLBs. The Step 1 is a blade design resulting from the first cost function evaluation of an MDO, where the design variables include both aeroshape and internal structure of the blade. The load envelopes are calculated at a blade radial station located at approximately 51m. Along with the envelopes, the ultimate loads projected in 4 directions (maximum and minimum flapwise moments, 0° and 180° respectively, maximum and minimum edgewise moments, 90° and -90° respectively) are compared. The bar plot at the bottom of the figure shows the ultimate loading variations in these 4 directions obtained with the full and the reduced DLBs. The latter plot shows how the reduced DLB is able to capture the quality of these variations.

A full overview of the projected ultimate flapwise and edgewise loads in both directions for each section of the blade is shown in Figure 7.5. The plots compare the variations between maximum and minimum flapwise and edgewise loads calculated using a full standard DLB and the reduced DLB, respectively. The variations in percent are estimated as $\mathbf{V}(r) = (\mathbf{E}_{S1}/\mathbf{E}_{BASE} - 1) * 100$, where r is the blade radius.

The reduced DLB approach is able to replicate the trend of the load variations computed using a standard DLB especially in the outer part of the blade. The reduced DLB overestimates the decrease in loading observed for the minimum flapwise direction (second plot of Figure 7.5). More discrepancies between the loads computed by the two DLBs can be observed in the inner part of the blade in both the edgewise directions. These differences depend on the fact that the
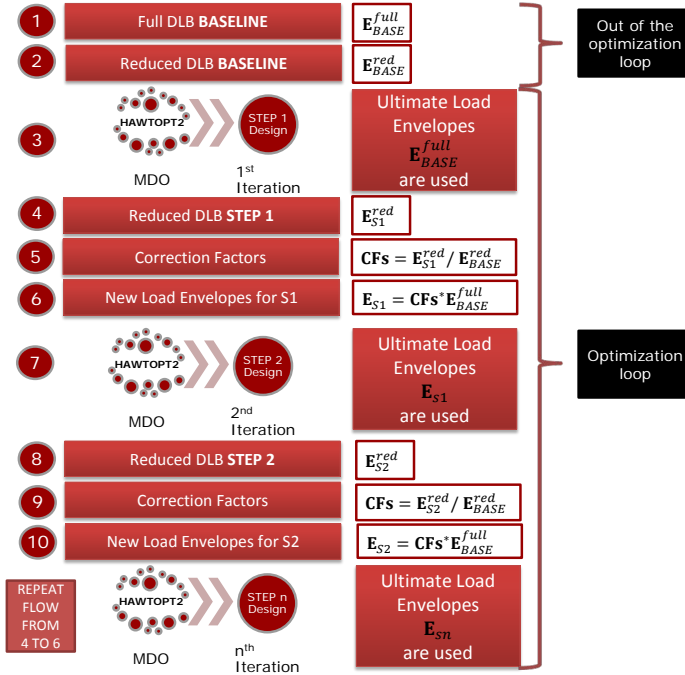
Figure 7.3: Description of the integration of the reduced DLB concept in an MDO framework. 1 - Out-of-the-optimization-loop estimation of ultimate load envelopes with full DLB for the starting design ($\mathbf{E}_{BASE}^{full}$ is a matrix containing cross sectional forces and moments for each envelope point and each blade section). 2 - Out-of-the-optimization-loop estimation of ultimate load envelopes with reduced DLB for the starting design ($\mathbf{E}_{BASE}^{red}$). 3 - Starting from the baseline design, the MDO is carried out until it reaches a new design (Step 1 design). The baseline full DLB ultimate load envelopes ($\mathbf{E}_{BASE}^{full}$) are used. 4 - The load envelopes are estimated with the reduced DLB on the Step 1 design ($\mathbf{E}_{S1}^{red}$). 5 - Correction factors **CFs** are obtained from the baseline reduced envelopes and the step 1 design ones (see equation). 6 - The correction factors are used to calculate the envelopes at the next cost function evaluation ($\mathbf{E}_{S1} = \mathbf{CFs} * \mathbf{E}_{BASE}^{full}$). 7 - The corrected ultimate blade loads are ready to be applied on the next iteration of the optimizer, which will produce a new design (Step 2 Design). 8/10 - Same procedure from point 4 to 6 is applied on Step 2 design [Paper F].
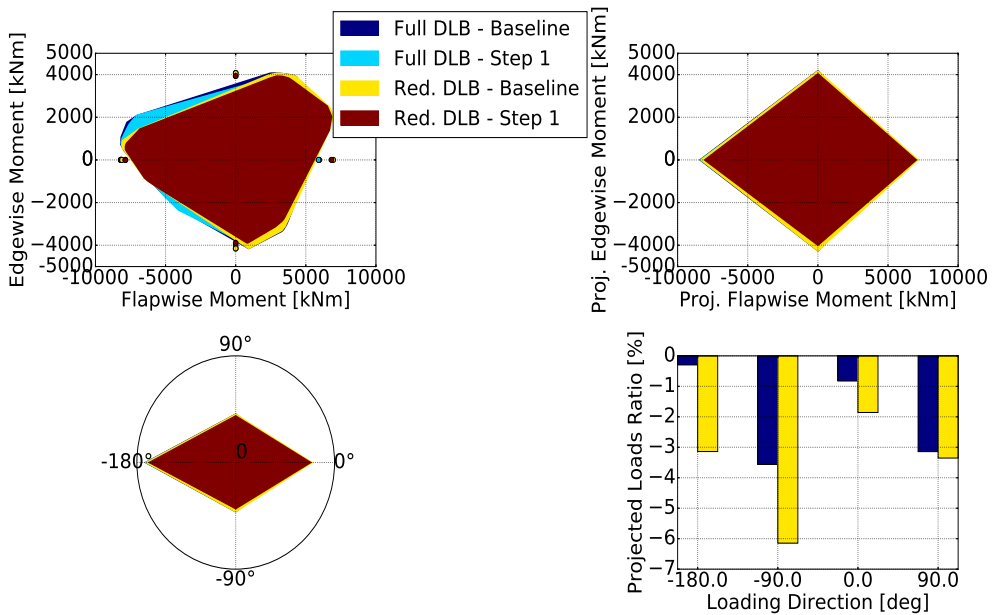
Figure 7.4: Comparison of ultimate load variations calculated between Baseline and Step 1 design using the full and the reduced DLB. The load envelopes are calculate for a section located at 51m along the blade length. The plot on the top left describes the envelopes, while the plot on the top right describes the ultimate loading projections along 4 directions, also plotted on the bottom-left plot. The bar plot shows the variations in ultimate loading in the 4 directions listed for the full and the reduced DLB [Paper F].

ultimate loads in the directions listed are driven by the DLC 1.3, where an extreme turbulence model is used to evaluate loads in a standard DLB. The reduced DLB can only mimic the effect of turbulence, and it is not able to fully capture the loading driven by an extreme turbulent load case. Specifically, in turbulent inflow conditions, wind speed and direction might vary considerably along the blade span, causing loading variations difficult to replicate with the simplified approach proposed in this work. Nonlinear dynamics of the system and behaviour of the controller add further complexity when it comes to mimic the effects of turbulence.

Despite these problem, the reduced DLB approach captures the quality of these variations along all the blade span very well. The custom-made shear zone is
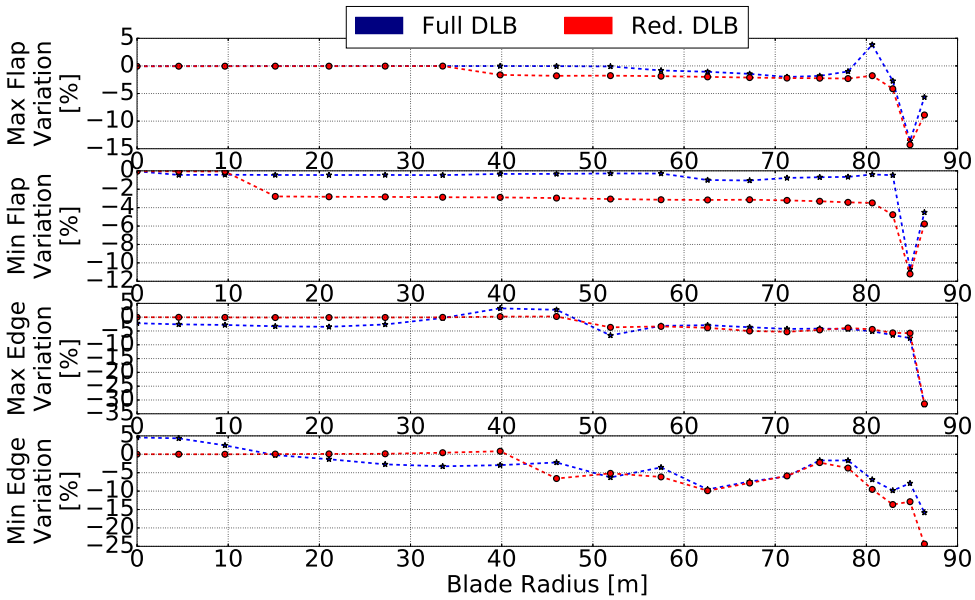
Figure 7.5: Comparison of ultimate load variations calculated between Baseline and Step 1 design using the full and the reduced DLB. The plots are listed in this order proceeding from top to bottom: maximum pure flapwise load variations along the blade radius; minimum pure flapwise load; maximum pure edgewise and minimum pure edgewise [Paper F].

able to replicate well the 1P loading excitation that is the main load contribution for a wind turbine undergoing turbulent DLCs. The extreme operating gusts are sufficient to capture the wind speed variations in the parked and maintenance load cases.

The reduced DLB method is applied for the design optimization of wind turbine blades employing passive loads control. The next part of the chapter is dedicated to the description of the passively controlled blades obtained through MDO. Specifically, the preliminary design of a wind turbine blade employing passive loads control strategies is formulated as an optimization problem. In the section that follows, we describe the numerical model behind the MDO problem. In the final part of the chapter, we demonstrate how each of the passive loads control techniques previously listed can be implemented and successfully deployed in the design process.

7.3   The Optimization Problem Formulation

The MDO process allows us to define clear objectives for the final blade design, and the ultimate goal is the reduction of the levelised cost of energy. For this reason, in the final part of this chapter, we are going to perform aeroelastic optimizations of swept blades where the objective of the process is to minimize blade mass and fatigue loads. We continue switching to an objective more effective for the reduction of the LCOE: the maximization of the AEP. In the latter case, in order not to increase capital investments on the wind turbine, the mass of the rotor is constraints together with the loads from another fundamental wind turbine component such as the tower. The final part of this chapter describes the MDO of a wind turbine blade that employs all the three categories of passive loads control simultaneously.

Before diving into the MDO applied to the design of wind turbine blades with passive loads control, we provide a description of the optimization problem formulation and a discussion on the issues related to the solution of this numerical problem.

7.3.1   Description of the Optimization Problem

In general, while we provide a full description of the different cost functions used for the problem formulation, we report only a brief overview of the constraints and design variables used. For detailed explanations, the reader can refer to the second part of this thesis in Papers F and G.

The numerical optimization problem formulated for the current work is the same as the one defined in ref. [18, p.3-6]. For the sake of clarity, the problem definition is reported in Equation 7.4, followed by a brief description of the variables, parameters, and constraints involved.

$$
\begin{aligned}
\underset{\mathbf{x}_p, \mathbf{x}_s}{\text{minimize}} \quad & f(\{\mathbf{x}_p, \mathbf{x}_s\}, \mathbf{p}, w) \\
\text{subject to} \quad & \mathbf{g}(\mathbf{x}_p) \leq \mathbf{0}, \\
& \mathbf{h_g}(\mathbf{x}_s) \leq \mathbf{0}, \\
& \mathbf{h_s}(\{\mathbf{x}_p, \mathbf{x}_s\}) \leq \mathbf{0}, \\
& \mathbf{k}(\{\mathbf{x}_p, \mathbf{x}_s\}) \leq \mathbf{0}
\end{aligned}
\tag{7.4}
$$

The cost function f depends on two sets of variables $\{\mathbf{x}_p, \mathbf{x}_s\}$, a set of constant parameters $\mathbf{p}$, and a weighting factor w.

The design variables (DVs) include the definition of the outer shape of the blade and the definition of the internal geometry of each blade section. The first set, $\mathbf{x}_p$, is constituted by the chord, the twist, the relative thickness distribution, and passive loads control design variables, such as sweep. The $\mathbf{x}_s$ variables include the thickness of the material layups in different regions of the blade sections and, again, passive loads control variables, such as fibres angles and position of the caps. Free form deformation splines (FFD) with numbers of control points (CPs) appropriate to the variable selected are used to parametrize the distribution of the design variables along the blade length. A complete overview of the blade parametrization used by HAWTOpt2 is provided in ref. [18, p.2-3] and [19, p.35-37]. The DVs are all normalized such that when they are equal to zero they correspond to the value of the baseline.

The parameters $\mathbf{p}$, which are kept unaltered throughout the optimization, include the definition of the other components of the wind turbine and its operational characteristics. A detailed overview of the blade geometry $\mathbf{x}_p$, blade layups $\mathbf{x}_s$, and parameters $\mathbf{p}$ for the DTU 10-MW RWT, used as starting design for the MDO, are reported in [83].

As shown in Equation 7.4, the constraints, to which the cost function is subjected, are divided according to their DVs dependency. The $\mathbf{g}$ constraints are connected to the definition of the planform DVs. They include limits for the chord, the twist, the relative thickness, and the blade sweep. The bounds for the thickness and fibres angles of the blade layups, and caps locations are defined in the constraints $\mathbf{h_g}$. The blade strength constraints are represented by the vector $\mathbf{h_s}$. Finally, the constraints $\mathbf{k}$ depend on both the blade planform and structural design variables. These constraints are evaluated by the aeroelastic solver, and they include: rotor loads, tip deflection, lift coefficients, aeroelastic frequencies, and blade root fatigue DEL.

7.3.2   Issues related to the Solution of the Optimization Problem

From the description provided above, we show the high complexity of the problem at hands. The amount of design variables and constraints involved in the optimization problem is very high (the DVs are usually around 60, while the constraints can reach up to a few hundreds). Because of this complexity, the aim of the optimization studies is not to find a global optimum, extremely difficult to reach seen the dimensions of the design space. The main goal is, for the time being, to use MDO to reach for better blade designs defined by a relevant improvement of the cost function considered. For this reason, the optimizations presented in the current chapter are not reaching for global optima, but they

are directed to a local optimum that could still ensure a blade design with an improved cost function and all the constraints within the standard design requirements.

Even though we are aiming to a local optimum, we are interested in a rapidly and smoothly converging solution. As we mentioned in the first section, the underlying codes that are used in the framework do not provide analytic gradients, and finite difference is therefore needed to compute the gradient of the objective and constraints. The accuracy of the gradients is critical to get a rapidly and smoothly converging optimization, which requires careful scaling of all design variables and a correct selection of the finite difference step size.

Concerning the scaling of the design variables, some of the DVs are normalized with respect to a reference value, while some others are scaled with user defined constants. The aim is to bring all the DVs closer to the a common interval defined by the dimension of the finite difference step, as values too far below or too far above the FD step can provide gradients of different quality compromising the stability of the optimization.

The selection of the FD step is a fundamental passage to ensure the stability of the optimization. Figures 7.6 and 7.7 show two examples of gradients computed for the aeroelastic workflow; one is the gradient of the objective function (AEP, in this case) with respect to the design variables describing the position of the upper cap (DV index $0, 1, 2, 3$ represent the control point of the location of the upper cap at 25%, 50%, 75%, and 100% of the blade length, respectively); the other is the gradient of the tower clearance with respect to the blade sweep (DV index $0, 1, 2$ represent the control point of the sweep at 50%, 75%, and 100% of the blade length, respectively). Both gradients require the fully coupled aeroelastic analysis. Neither set of gradients converge fully for decreasing step sizes (the one in Figure 7.7 better than the one in 7.6), although both exhibit fairly smooth convergence. In this case, all parameters were scaled to match a step size of $dx = 0.01$ based on these results.

The latest release of OpenMDAO allows the MPI parallelization of the evaluation of the finite difference gradients. At the upper level, the entire workflow is parallelised. All of the gradients computations are parallel and thus this scales linearly with the number of CPUs available. A typical optimization will use 20 cores per objective function evaluation, and be parallelised according to the available resource with n number of concurrent FD gradient evaluations. For the studies presented in this chapter, 30 concurrent FD evaluations were used. An iteration of the optimizer required approximately 15/20 minutes using a total of 600 cores. Usually, it takes around 10 hours (around 35 iterations of the optimizer) to see the cost function converging to a local optimum. This process would have been highly inefficient without the availability of an HPCC.
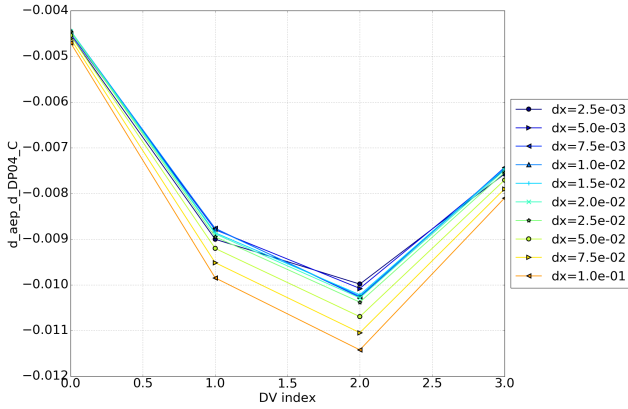
Figure 7.6: Finite difference gradient evaluations for different step sizes on the quantities AEP with respect to the control points for the location of the upper cap. DV index $0, 1, 2, 3$ represent the control point of the location of the upper cap at 25%, 50%, 75%, and 100% of the blade length, respectively
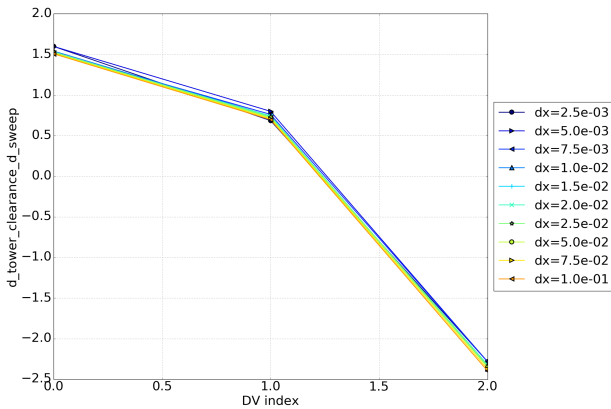
Figure 7.7: Finite difference gradient evaluations for different step sizes on the quantities tower clearance with respect to the control points for the blade sweep. DV index $0, 1, 2$ represent the control point of the sweep at 50%, 75%, and 100% of the blade length, respectively.

7.4 Aeroelastic Optimization of Swept Blades

The first investigation focuses on the first of the three categories of passive loads control discussed in the previous chapter. The key aspect of this investigation is the inclusion of sweep as a design variable in the formulation of an MDO problem (see Paper G). Fibres angle and location of the caps are not included as design variables in this study.

The introduction of sweep as a design variable gives more flexibility to the optimization process in the distribution of the loading on the blades, allowing the MDO to reach for further improvements of the merit function. To further stress the focus of the optimization on the variation of the loads, the minimization of the blade root flapwise fatigue moment is added to the cost function, taking the place of the AEP objective, which is enforced as a constraint in the problem formulation, i.e. an optimized design must have the same AEP as the baseline wind turbine.

The cost function is defined as

$$f(\{\mathbf{x}_p, \mathbf{x}_s\}, \mathbf{p}, w) = (1 - w)\frac{M(\{\mathbf{x}_p, \mathbf{x}_s\}, \mathbf{p})}{M(\{\mathbf{0}, \mathbf{0}\}, \mathbf{p})} + w\frac{DEL(\{\mathbf{x}_p, \mathbf{x}_s\}, \mathbf{p})}{DEL(\{\mathbf{0}, \mathbf{0}\}, \mathbf{p})} \qquad (7.5)$$

where M is the total mass of the blade, and DEL is the blade root flapwise damage equivalent load. $M(\{\mathbf{0}, \mathbf{0}\}, \mathbf{p})$ and $DEL(\{\mathbf{0}, \mathbf{0}\}, \mathbf{p})$ are the blade mass and the blade root fatigue DEL of the baseline design. The weighting factor w defines toward which of the two objectives the optimization is biased. A more detailed description regarding how the evaluation of the DELs is performed in the framework is provided in [96]. As previously mentioned, the full list of constraints and design variables can be found in Paper G.

In the performed MDOs, w is a vector defined $[0.0, 0.25, 0.5, 0.75, 1.0]$, where $w = 0.0$ defines an optimization purely aimed at the minimization of blade mass, and $w = 1.0$ defines an optimization purely aimed at the minimization of blade root flapwise fatigue DEL. Figure 7.8 shows the resulting optimized designs and how their blade mass and blade root DEL relates to the baseline design.

The MDOs result in two Pareto fronts: the blue solid line with star symbols traces the last optimized straight designs while the red solid line with square symbols delineates the last optimized swept designs. The x-axis of the plot indicates the blade root flapwise DEL normalized with respect to the baseline starting design (highlighted by the red arrow). The y-axis shows the evolution of the blade mass for the different designs normalized with respect to the mass of the DTU 10 MW. The small circles represent the designs chosen by the op-

timizer at each cost function evaluation. They are connected by dashed lines. The blue-shaded colours are used for the straight blades, while the red-shaded colours are used for the swept designs.

In general, the MDO is able to reduce blade mass by approximately 27% (see red squares on the bottom side of the plot) and fatigue DEL by approximately 25% (see red squares on the left side of the plot) for the best designs between the two sets obtained. When the blade sweep is added as a design variable in the optimization process, further reduction of the compound objective is obtained. The optimized swept blade designs achieve further reduction of the blade mass when the cost function is biased towards mass minimization ($w = [0.0, 0.25]$). Compared to the respective optimized straight designs (the two blue stars at the bottom of the plot), the mass is reduced by an extra 2-3% (see the difference on the y-axis between the two blue stars and the two red squares on the bottom of the plot), registering a load alleviation for both design sets between 10 and 15%. The DEL biased swept designs ($w = [0.75, 1.0]$) mitigate the blade root flapwise fatigue DEL by a further 8% compared to the optimized straight blades (see the
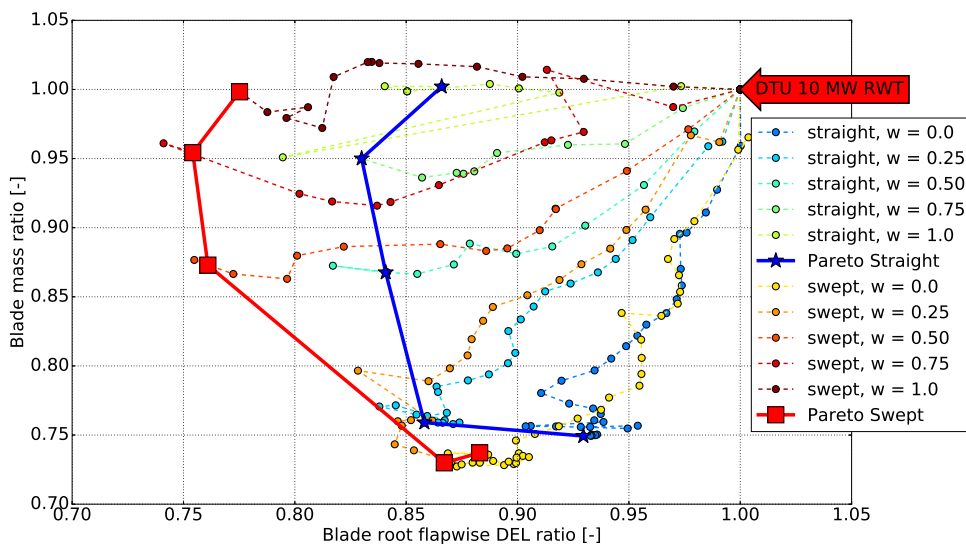
Figure 7.8: Evolution of the cost function for the optimization of the DTU 10-MW RWT. The blade mass is described by the abscissas and the blade root flapwise fatigue DEL by the ordinates. Blue-shaded colours: optimized straight blade designs; red-shaded colours: optimized swept blade designs [Paper G].

difference on the x-axis between the two blue stars and the two red squares on the left of the plot).

To provide a visual overview of the sweep selected by the optimization process, Figure 7.9 shows the curved geometry of the optimized swept design $w = 0.5$. Even though the sweep can vary closer to the inner part of the blade, the optimizer focuses the change in sweep only closer to the outer part of the blade. The sweep is purely backward to enhance the load alleviation potential of this passive loads control method, and it starts at 80% of the blade radius with a maximum backward sweep at the tip of approximately 2 m. This result is in line with the observations made in Paper C.

Detailed discussions related to the properties of the optimized designs can be found in Paper G. In this section, we are going to report only one of the most interesting results related to this first investigation: the complete standard DLB load analysis comparison between an optimized straight blade and an optimized swept one.

Figures 7.10 and 7.11 shows the baseline-normalized extreme loads and lifetime equivalent fatigue loads (LTEFL) of the optimized designs with $w = 0.5$. The loads are reported in radar-charts to provide an overview on different significant sensors, such as blade root, tower top, and tower bottom moments. On the extreme radar-chart, tower clearance and AEP are also reported (right side of the chart).

The annual energy production of the optimized wind turbines is extremely close to that of the baseline turbine (a loss of 0.3% is registered for the swept-bladed rotor). The tower clearance of the optimized swept turbine is higher than the baseline and the optimized straight design due to the beneficial load alleviation effect on the flapwise tip displacement around rated wind speed brought by the bend-twist coupling. The tower clearance of the optimized straight tur-
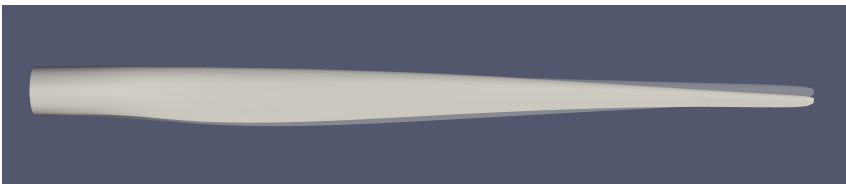
Figure 7.9: Overview of the planform swept geometry of the optimized swept design ($w = 0.5$). The planform is compared with the baseline one which is shown transparent on the plot [Paper G].

bine is slightly lower than the baseline (approximately -4%). Considering that a steady-state linear model was used in the optimization to estimate the tower clearance, a value out of 4% (but still within the standard requirements [41, 42]) is considered acceptable.

The benefits of adding the sweep as a design variable are particularly evident on the blade root fatigue flapwise extreme and LTEFL. The total reduction of this loads with respect to the baseline is around 20% for the optimized swept design. Moreover, the load alleviation effect of the structural coupling brings an extra reduction of approximately 8% compared to the optimized straight-bladed turbine. This 8% was already highlighted by the Pareto fronts shown in Figure 7.8.

As a consequence of the blade root flapwise load alleviation, tower top fore-
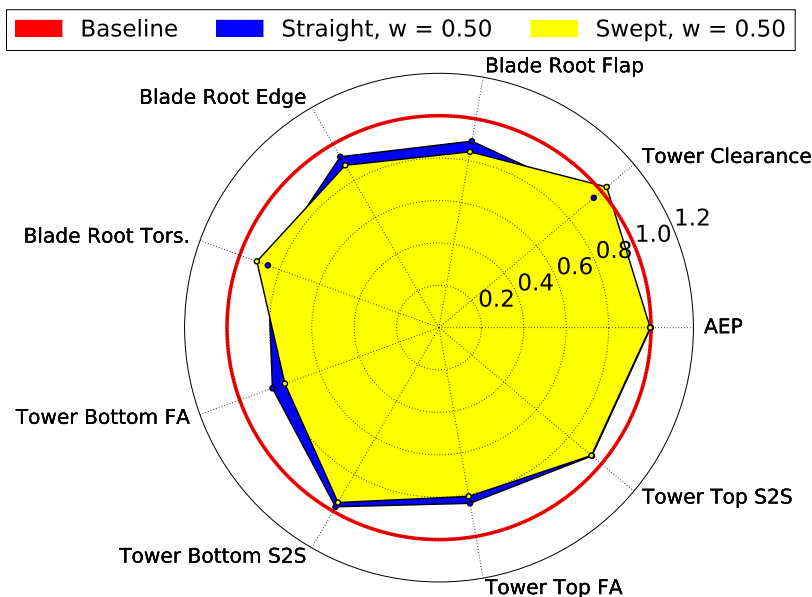
Figure 7.10: DLB extreme loads reported in radar-chart plots. Load results are provided for the following sensors: blade root, tower top, and tower bottom. In the extreme radar-chart also AEP and tower clearance are reported (right side of the chart). The optimized straight blade design (blue) and the optimized swept one (yellow) are normalized with respect to the baseline loads (red line). "FA" stands for fore-aft, "S2S" for side-to-side, and "Tors." for torsional [Paper G].
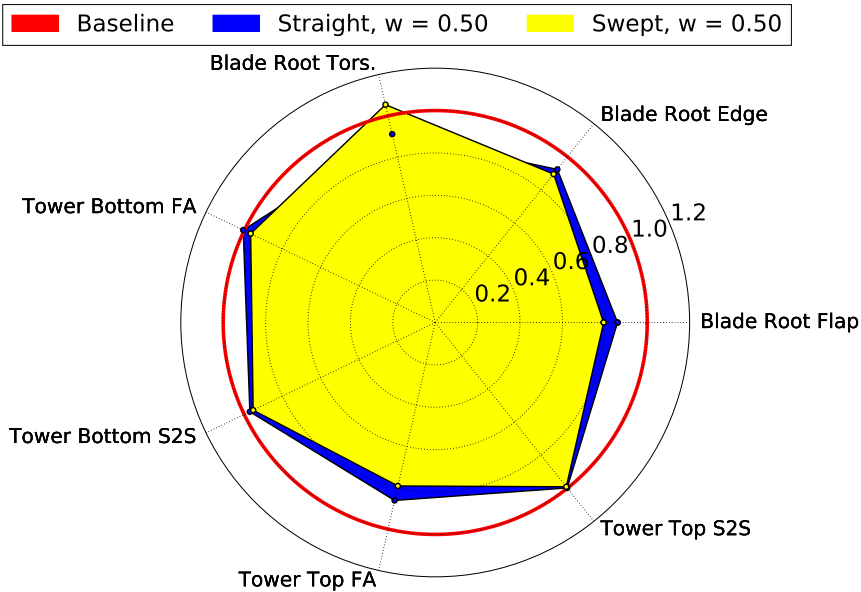
Figure 7.11: DLB life-time equivalent fatigue loads reported in radar-chart plots. Load results are provided for the following sensors: blade root, tower top, and tower bottom. In the extreme radar-chart also AEP and tower clearance are reported (right side of the chart). The optimized straight blade design (blue) and the optimized swept one (yellow) are normalized with respect to the baseline loads (red line). "FA" stands for fore-aft, "S2S" for side-to-side, and "Tors." for torsional [Paper G].

aft extreme and LTEFL are also consistently reduced. Once more, the addition of the sweep pays off by providing a total reduction of approximately 20% with respect to the baseline, 5% extra extreme load alleviation, and 8% extra fatigue load alleviation in relation to the optimized straight design. Similar variations are registered for the tower bottom fore-aft extreme loads. The tower bottom fore-aft LTEFL of the optimized designs is not considerably reduced (it is actually slightly higher for the optimized straight design, +0.5%, and lower for the swept rotor, -3.4%). The beneficial reduction of tower bottom fore-aft loading registered for the swept rotor, is caused by lower variations of the rotor thrust force triggered by the use of passive loads control.

The extreme and fatigue blade root edgewise loads are considerably reduced for both optimized designs due to the decrease in total blade mass. The allevi-

ation is in the order of 10-13%, hence comparable to the total mass reduction shown in Figure 7.8.

The optimized designs tower side-to-side loading is generally lower than the baseline turbine because of the reduction in total blade mass achieved by the MDO.

Even though the blade root torsional loads are higher for the swept blade compared to the straight one, they remain within the constraint imposed by the MDO (the extreme load is lower than the baseline, and the LTEFL is approximately only 5% higher than the reference value).

In general, the benefits of adding the sweep as a design variable are evident for the further load reductions that can be obtained especially on the blade root flapwise moment and, consequently, on the tower fore-aft moment. These alleviations, as previously highlighted, are due to the structural coupling between bending and torsion specifically tailored for the blades. The price to pay for the extra load alleviation effect is a slightly higher blade root torsional fatigue moment.

7.5   Aeroelastic Optimization of Blades using Material BTC

As a further step, we performed an MDO of a wind turbine blade employing material bend-twist coupling for passive loads control. This case includes the orientation of the fibres in the spar caps as a design variable during the optimization process (this time, other passive loads control design variables such as sweep and location of the spar caps are not considered). The MDO of a wind turbine blade with biased fibre orientation in the caps was initially used as an application case for the reduced DLB concept (see last section of Paper F). We decided to report the characteristics of this optimized design because it represents an interesting application of passive loads control methods in a wind turbine blade MDO. Furthermore, as previously introduced at the beginning of this section, we used a different objective for the blade optimization.

The cost function is the maximization of the annual energy production. To achieve the objective, the blade can stretch, increasing the rotor diameter and the energy captured. The design is further challenged by adding the orientation of the fibres in the spar caps as a design variable. The optimizer can exploit the bend-twist coupling towards feathering, hence dynamically decreasing the angle of attack to control the loading on the wind turbine [15]. As the fibres in the

spar caps start to rotate to create the structural coupling, the bending stiffness
of the blade decreases. The blade design becomes more prone to ultimate fail-
ure due to the increase of the loading as the rotor diameter stretches to harvest
more energy. Moreover, the rotation of the fibres in caps can compromise the
tower clearance required by the standard. To accommodate the ultimate fail-
ure requirements, the blade mass is allowed to increase by 5% compared to the
baseline design. The pre-bending of the blade can increment to fulfil the tower
clearance constraint. A full description of the design variables and constraints
is reported in Paper F.

The final design has a longer blade radius and, consequently, the wind turbine
has a higher AEP (+4.4%). The blade mass is slightly increased (+1.2%) to
sustain the higher loading and improve the strength of the blade, counteracting
the negative effects caused by turning the fibres of the unidirectional material in
the caps. The tower clearance requirement is kept within the given constraints.
Table 7.1 shows a summary of these characteristics with respect to the original
design.

Figures 7.12 and 7.13 provide an overview of the strength and loads of the final
design obtained from the MDO process, respectively.

Figure 7.12 shows the maximum failure indices for each cross section along
the blade. The failure indices are evaluated applying loads obtained from a full
standard DLB simulated at the end of the optimization on the final design. The
ultimate loads are selected from the envelopes projecting flapwise and edgewise
moments in twelve directions (not only in four directions shown in Figure 7.4).
The reduced DLB is able to drive the ultimate loads calculation in the right di-
rection during the MDO, as the final design can withstand a full DLB ultimate
loads respecting the given constraints. In fact, no failure is detected along the
blade according to the strain criteria.

Regarding the estimation of fatigue loads, the current MDO does not include

Table 7.1: Overview of the general characteristics of the final optimized design.
Results are shown in percent variation from the baseline design
[Paper F].

	Variation from Baseline
AEP	+4.4%
Blade radius	+7.7%
Blade mass	+1.2%
Blade tip pre-bending	+85.8%
Tower Clearance	+2.1%
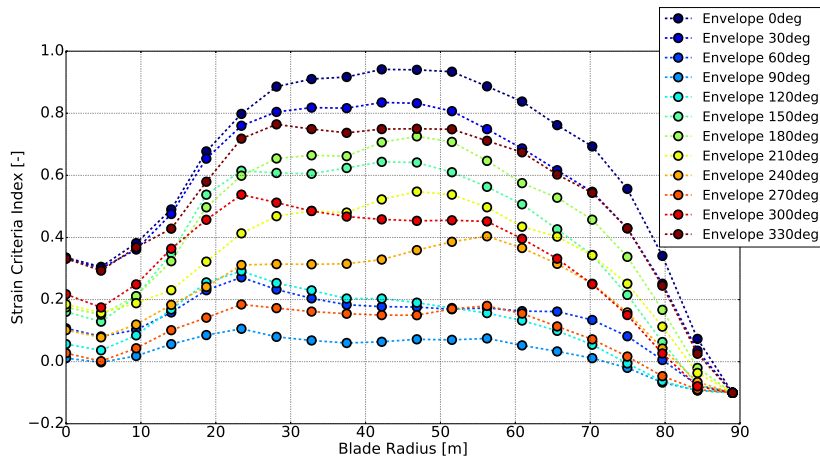
Figure 7.12: Maximum sectional failure indices. Failure indices are computed for twelve load cases extracted from ultimate sectional blade load envelopes [Paper F].

DEL constraints as done for the case reported in the previous section. The reason is that HawcStab2, the tool used to calculate DEL in the frequency domain, does not support the anisotropic beam element [12] needed to model material BTC. Hence, to improve these results even further, constraints on fatigue loads will be included in future studies.

Figure 7.13 shows the variation of life-time equivalent fatigue moments for the blade root and tower registered for the optimal design. Even though no constraints were imposed to control these loads, the bend-twist coupling effect generated by the material structural coupling helps to contain the increase. Figure 7.14 shows the bend-twist coupling parameter along the blade length. The flapwise bend-twist coupling coefficient β is calculated along the blade length in accordance to the method described in [9].

Except for the blade root torsional moment, which increases by approximately 15% due to the increase in the blade pre-bending, all the other fatigue loads register a maximum increase of approximately 4%.

To summarize, not only the annual energy production is greatly increased, but also the increase in blade mass and tower loading are contained. In the last part of this chapter we are going to show the results from an MDO where all the three categories of passive loads control are included simultaneously.
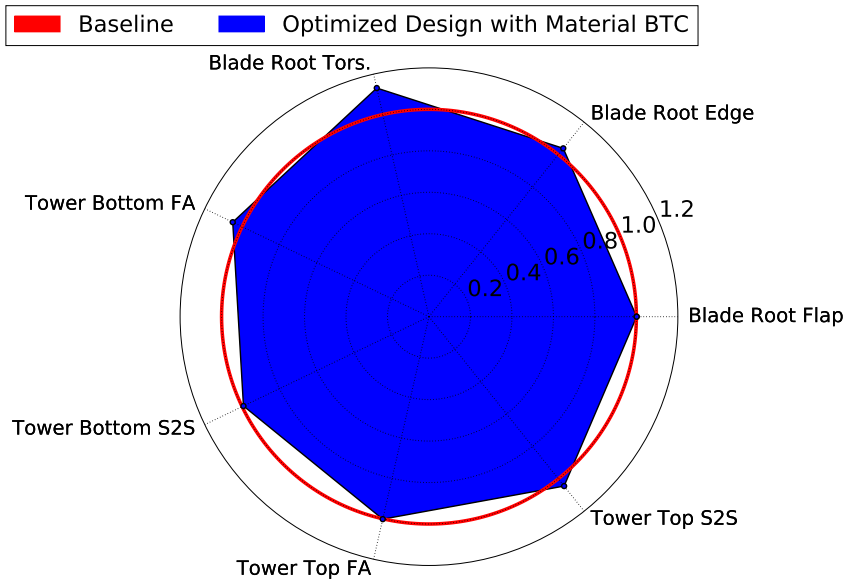
Figure 7.13: Life-time equivalent fatigue loads. The optimal blade design (blue) is normalized with respect to the baseline loads (red line). "FA" stands for fore-aft, "S2S" for side-to-side, and "Tors." for torsional [Paper F].
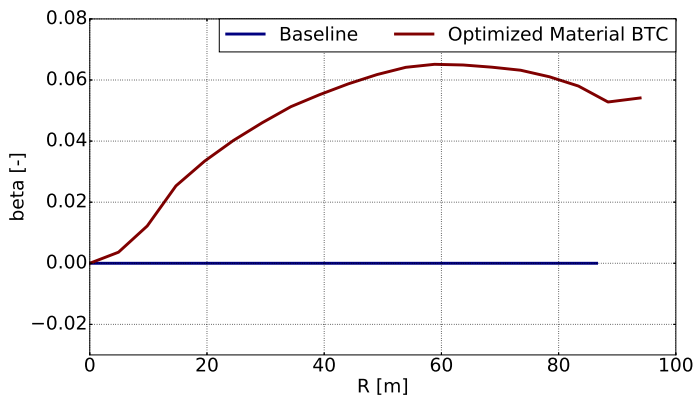
Figure 7.14: Bend-twist coupling parameter along the blade span [Paper F].

7.6   Aeroelastic MDO of a Fully Coupled Blade

The last step is to perform an aeroelastic MDO of a wind turbine blade where all the three categories of passive loads control discussed so far are included as design variables. Specifically, together with the set of design variables listed in the optimization problem formulation, the MDO takes into account: blade sweep, location of the spar caps, and orientation of the fibres in the unidirectional layers of the caps. We saw in the pure material BTC MDO of Paper F, that the large increase of the pre-bending design variable caused a large increase in blade root torsional fatigue load. To avoid this increment, the blade pre-bending is not considered as a design variable in the current MDO.

Additional constraints are also added to control the variations of the passive loads control design variables: the maximum sweep has to be lower than half of the maximum chord to allow the blade to be transported to the installation site (see also the constraints in Paper G); the ratio between the width and thickness of the spar caps are constrained to avoid originating caps with shapes more prone to buckling (see constraints in [18]); as the spar caps move relatively away from each other, the webs are not perpendicular to the caps and the new angles between webs and caps are constrained (specifically the webs need to be parallel to each other within a 20° tolerance, and the new angle with the spar caps has to be within 25° of the initial value); the fibres of the unidirectional material in the spar caps can be offset by an angle between -20° and +20° (see also the constraints in Paper F). As for the MDO described in the previous section, fatigue loads cannot be constrained following the method used in Paper G and depicted by Tibaldi in [96]. Future developments of HAWTOpt2 are going to take fatigue constraints into account, so that the results shown thereafter can be improved.

Figures 7.15, 7.16, and 7.17 provide a visual overview of the optimized blade.

Figure 7.15 shows the swept planform. As for the optimized swept blade shown previously in Figure 7.9, the change in blade planform starts at approximately 80% of the optimized radius. The maximum backward sweep is 2.4 m, which corresponds to approximately 2.5% of the total blade length. This result is in line with the observations made in Paper C.

Figure 7.16 provides an overview of the changes brought by the optimizer to the location of the caps. The spar caps are offset relative to each other, with the upper cap moved aft of the pitch axis towards the leading edge. This change in the location of the caps triggers a structural coupling between bending towards the tower and twist towards feather due to the rotation of the principal bending axes and the movement of the shear centre.

Figure 7.17 shows the bend-twist coupling parameter β along the blade length in accordance to the method described in [9]. Compared to the pure material BTC optimized blade (See Figure 7.14), the coupling parameter is much lower, especially in the inner part of the blade, where β is very close to zero. As shown in Figure 7.12, the inner part of the blade has the highest failure indices due to
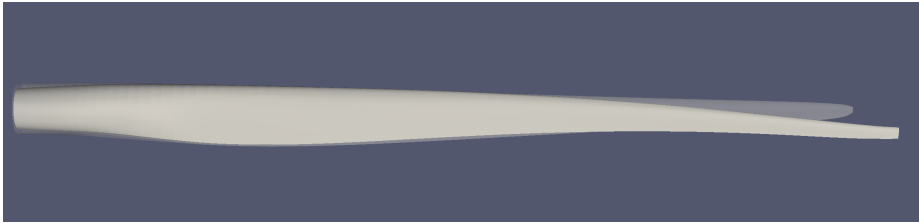
Figure 7.15: Overview of the planform swept geometry of the optimized fully coupled design. The planform is compared with the baseline one which is shown transparent on the plot.
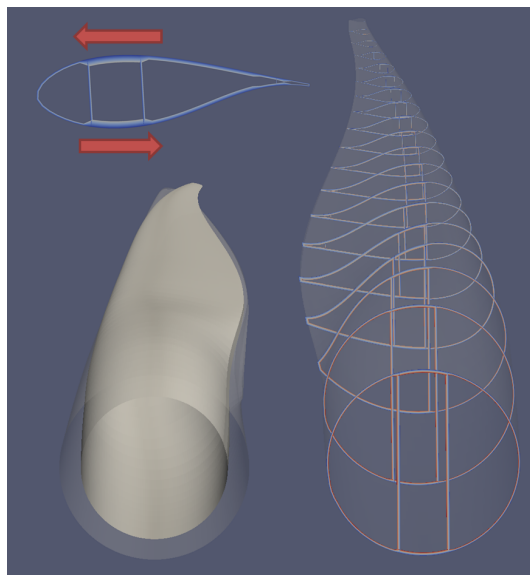
Figure 7.16: Overview of the internal structure of the optimized fully coupled design. The red arrows in the plot on the top left show in which direction the location of the caps moved compared to the baseline design.
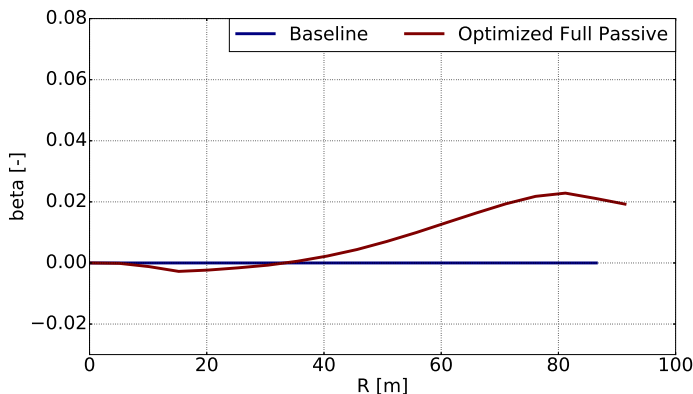
Figure 7.17: Bend-twist coupling parameter along the blade span for the fully coupled blade.

pure flapwise (0°) or 30° combined ultimate loading. Biased fibres in the spar caps degrade the strength of the blade for this type of loading. For this reason, the optimizer prefers other passive loads control methods to achieve the necessary load mitigation effect, keeping the fibres orientation in the caps unbiased towards the inner part of the blade.

The final rotor design produces a much higher AEP (+6.0%) compared to the baseline and to the optimized material BTC blade (see Table 7.1). The blade mass is slightly increased (+0.8%) to sustain the higher loading and improve the strength of the blade. The tower clearance requirement is kept within the given constraints. Table 7.2 shows a summary of these characteristics with respect to the original design. The use of passive loads control creates an additional positive effect: the decrease of the pitch actuator duty cycle. This reduction is caused by the passive loads control effect of coupled blades, which use the structural coupling to respond to turbulent fluctuations in the wind inflow. Consequently, the controller can pitch the blades less often, reducing the effort of the pitch actuator system [15].

Figure 7.18 shows the maximum failure indices for each cross section along the blade. The failure indices are evaluated applying loads, as obtained from a full standard DLB simulated at the end of the optimization, on the final design. The blade is able to withstand ultimate loads, as all the maximum failure indices for each loading direction and each blade section are less than one.

Figure 7.19 shows the variation of life-time equivalent fatigue moments for the

blade root and tower registered for the optimal design. Even though no constraints were imposed to control these loads, the bend-twist coupling effect generated by the combination of all the passive loads control strategies helps to contain the increase. In general, fatigue loads are alleviated except for: the blade root torsional moment which increases by approximately 7% due to the presence of the sweep; the blade root edgewise moment which increments by approximately 8% due to the increase in blade mass and blade mass moment (see Table 7.2); the tower fore-aft moment which is very close to the baseline value (slight increase of 1.5%). The peak in fatigue load mitigation is reached by the tower top fore-aft moment (approximately -15%) and by the blade root flapwise moment (-11%). Even though fatigue loads could not be constrained, the results obtained thanks to the combination of all the passive loads control strategies are satisfactory.

Table 7.2: Overview of the general characteristics of the final optimized fully coupled design. Results are shown in percent variation from the baseline design.

	Variation from Baseline
AEP	+6.0%
Blade radius	+5.8%
Blade mass	+0.8%
Blade mass moment	+4.5%
Tower Clearance	+36.2%
Pitch Actuator Duty Cycle	-2.8%
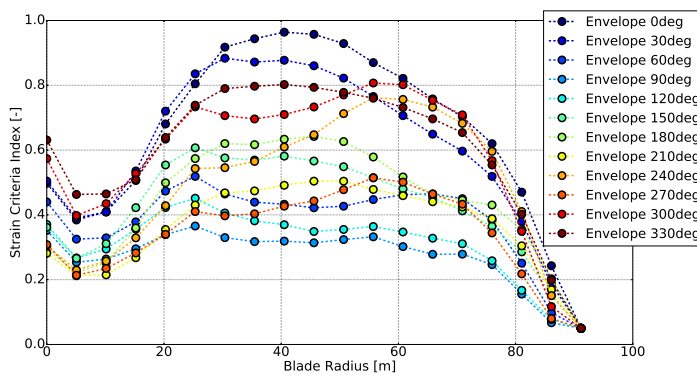
Figure 7.18: Maximum sectional failure indices of the full coupled optimized blade. Failure indices are computed for twelve load cases extracted from ultimate sectional blade load envelopes.
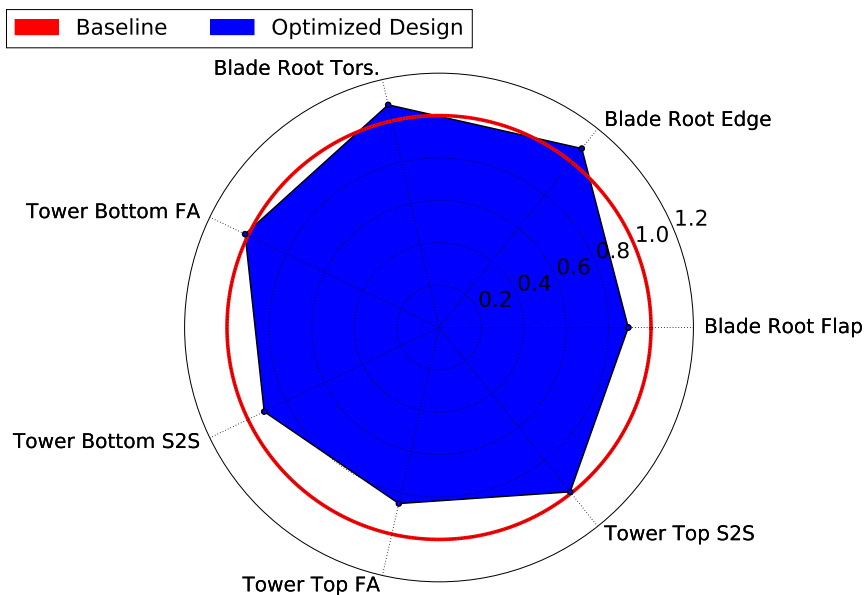
Figure 7.19: Life-time equivalent fatigue loads of the fully coupled optimized blade. Fatigue load results are provided for the following sensors: blade root, tower top, and tower bottom. The optimal blade design (blue) is normalized with respect to the baseline loads (red line). "FA" stands for fore-aft, "S2S" for side-to-side, and "Tors." for torsional.

Multidisciplinary design optimization is the best methodology to implement passive loads control strategies on wind turbine blades. The final MDO, which combined all the three categories of passive loads control, produced a blade design with a considerable increase in annual energy production. The blade mass almost matches the value of the baseline design, while the blade can withstand ultimate loading. The increased blade root edgewise and torsional fatigue loads are contained. Peaks of load alleviation are registered for the blade root flapwise and tower top fatigue moments. The design has potential for a substantial reduction in the cost of energy.

Needless to say, the optimized blade resulting from the optimization process is a preliminary design. The strong limitation of the work depicted through these pages is the absence of considerations related to a more detailed design that could take into account manufacturing constraints. We demonstrated that

passive loads control has the potential for reducing the LCOE and that multidisciplinary design optimization is the best choice to explore this potential. Future work has to take into consideration the successive steps in the design process that brings a wind turbine blade to manufacturing. A view on the problems that the industry faces in the design and manufacturing process of wind turbine blades is fundamental to further improve the methodology behind the implementation of passive loads control strategies, making them a more widely used design feature for operational wind turbines.

CHAPTER 8

Conclusions

8.1 Contributions

In the course of the research described in this thesis, we have provided a number of novel contributions to the state of the art. We have investigated the design problem of a wind turbine rotor employing passive loads control techniques, and developed methodologies for the implementation of this type of control in the preliminary and conceptual design process of a wind turbine blade.

After a validation of the accuracy of the structural component of the aero-servo-elastic framework used to perform the analyses in the current work, we investigated the interactions between the disciplines involved in the design of a wind turbine rotor. For instance, the decrease in angle of attack triggered by the use of passive loads control is beneficial in terms of load alleviations. However, it has a negative impact on the power output below rated wind speed. Furthermore, the connection between the employment of a passive loads control technique and the dynamics of a closed-loop wind turbine system plays an important role in the correct estimation of the load mitigation potential of blades designed with tailored structural couplings. We also made recommendations regarding the comparison of an initial design and a design with passive loads control: the wind turbines analysed have to produce the same amount of energy and need to have the same controller dynamics to provide a fair estima-

tion of the load alleviation potential of the passive loads control strategy chosen.

In an effort to evaluate the potential of different implementations of passive loads control methodologies in the wind turbine blade design process, we performed a series of parametric studies, always taking into account the inherit interactions between aerodynamics, structural dynamics, and control theory. Such studies are helpful to investigate the effects on the wind turbine loading of different combinations of passive loads control, but they do not provide any management on the numerous design requirements established by the standards. Furthermore, as highlighted by an analysis of the levelised cost of wind energy, load mitigations can have a favourable impact on the reduction of the LCOE, but these reductions in loading need to be translated to a decrease in blade mass and/or increases in annual energy production. In this context, the formulation of a passively controlled blade design as an optimization problem allows the designer to satisfy simultaneously several constraints while evaluating trade-offs between conflicting objectives.

We have implemented passive loads control techniques in a multidisciplinary design optimization framework. To overcome the issue of running a multitude of computationally expensive aero-servo-elastic simulations on every iteration of the optimization process, we developed a method to provide a fast estimation of the ultimate blade load envelopes and we used a frequency domain method for the estimation of fatigue loads.

The use of passive loads control design parameters as variables in the optimization process is our main contribution to the use of MDO for wind turbine blades. We have demonstrated that when passive loads control design variables are included in the design process, further improvements of the cost function can be achieved.

A final optimized design employing all the categories of passive loads control can substantially increase the annual energy production while either maintaining or decreasing the blade and the tower loads. The levelised cost energy can be then considerably reduced, opening the path to the systematic employment of passive loads control as a conceptual design feature for modern wind turbine blades.

8.2　Perspective and Opportunities for Further Research

The employment of passive loads control on the design of modern multi-megawatt wind turbine blades has the potential to bring about substantial reductions to the cost of energy. In fact, part of the wind energy industry already employs passive loads control techniques [109, 110]. What is missing is a set of methodologies that can facilitate the systematic employment of passive loads control in the design process of wind turbine rotors. We analysed and developed such methodologies, but further research work needs to be conducted. First, we need to further ensure the accuracy of the tools used to model structural couplings. Second, we need to improve the multidisciplinary optimization framework to include a more precise estimation of the aeroelastic loads and manufacturing constraints. Finally, multidisciplinary design optimization frameworks can be expanded to consider not only the design of a single component such as the blades, but also to consider the wind turbine as a system.

Regarding the first point, the aero-servo-elastic tools developed are providing an important aid to the systematic inclusion of passive loads control in the design process of wind turbine blades. We conducted a validation of two of these tools in Paper A, but, as the turbine rotor keeps increasing in size and flexibility, it is important to carry out investigations involving real wind turbine blades and experimental data. Specifically, measuring the structural behaviour of blades with bend-twist coupling is extremely challenging, and dedicated research and experimental campaigns are crucial to provide realistic data to validate the aero-servo-elastic models used to design wind turbine blades.

In relation to the improvements of MDO frameworks, in Paper F we describe a method to estimate ultimate loading on a wind turbine blade during an optimization process. We highlight that the method can capture the quality of the loading variations, but it cannot accurately simulate the magnitude of the ultimate blade loads. For this reason, the MDO problem cannot find a global optimum solution due to the simplified load analysis approach. Future research needs to address different methodologies, such as multi-fidelity techniques and surrogate-based methods, such as the creation of Approximation Model Management Frameworks (AMMF) [111, 112, 113].

Furthermore, as stated at the end of the previous chapter, future work needs to take into account all the steps of the design of a passively controlled blade, from the conceptual design to the production. If manufacturing constraints and industrial problems are taken into account in the framework from a preliminary phase of the design process, the methodologies for the implementation of passive

loads control can be improved and their applications made available to a larger audience.

The efficacy of passive loads control is not in question, but the manufactures face a wide variety of issues related to the specific approaches used to develop and produce their products. A framework for the design a wind turbine blade needs to be flexible enough to consider these issues. Our recommendation is that further research in the area of multidisciplinary design optimization of passively controlled blades has to be carried out together with the industry and looking at how real wind turbine blades are developed and produced.

In relation to future perspective for design frameworks, we have used MDO exclusively for the design of blades. The wind turbine is a system made of several components, each of them that has its own impact on the cost of energy. An interesting perspective is the possibility to include the design of other components in the MDO framework, using directly detailed LCOE models as a cost function (an example of combined tower-rotor optimization can be found in [114]). An MDO framework capable of handling the design of several wind turbine components can take into account not only the subtle and complex interactions arising due to the mutual effects of aerodynamics, structure, and control, but also the impact of each component on the cost of a wind farm project.

On a final note, we would like to emphasise how much throughout these pages we stressed the complexity of a wind turbine system and the importance of evaluating its impact in the real world with economic considerations. Wind energy technology is a mature field of research, where so much has been achieved in the last three decades. To produce a valuable impact on the society that surrounds us, future research on the implementation of passive loads control methodologies for wind turbine blade design has to look at the problems faced by industry, and at the factors that drive the manufacturing, production, and sale of wind farm projects, or, in two words, at the **bigger picture**.

Bibliography

[1] Taylor M, Daniel K, Ilas A and So E Y 2015 *Renewable Power Generation Costs in 2014* (Bonn, Germany: IRENA - International Renewable Energy Agency) URL www.irena.org/publications

[2] Ashwill T D 2009 Materials and innovations for large blade structures: Research opportunities in wind energy technology *50th AIAA Structures, Structural Dynamics, and Materials Conference* vol Palm Springs (AIAA) ISSN AIAA-2009-2407

[3] Bossanyi E A 2003 Individual blade pitch control for load reduction *Journal of Wind Energy* vol 6 nr 2 (John Wiley and Sons, Ltd.) pp 119–128 URL http://dx.doi.org/10.1002/we.76

[4] Barlas T K and Kiuk G V 2003 Review of state of the art in smart rotor control research for wind turbines *Progress in Aerospace Sciences* vol 46 nr 1 (Pergamon) pp 1–27 ISSN 0376-0421 URL http://dx.doi.org/10.1016/j.paerosci.2009.08.002

[5] Kooijman H December 1996 *Bending-torsion coupling of a wind turbine rotor blade* (Petten, Netherlands: ECN) ISBN ECN report 527 I-96-060

[6] Ashwill T, Veers P S, Locke J, Griffin I C D and Zuteck M D 2010 Concepts for adaptive wind turbine blades *Reno, Nevada, USA, 14–17 January 2002* vol Paper No. WIND2002-28 (ASME 2002 Wind Energy Symposium) URL 10.1115/WIND2002-28

[7] Ashwill T D 2009 Developments in large blades for lower cost wind turbines *50th AIAA Structures, Structural Dynamics, and Materials Conference* vol Palm Springs (AIAA) ISSN AIAA-2009-2407

[8] Knight and Carver Wind Group 2010 *Sweep-Twist Adaptive Rotor Blade: Final Project Report* (Albuquerque, New Mexico, USA: Sandia National Laboratories, SAND2009-8037)

[9] Fedorov V and Berggreen C 2014 Bend-twist coupling potential of wind turbine blades *Journal of Physics: Conference Series - The Science of Making Torque from Wind 2014* vol 524 (IOP Publishing) p 12035 URL http://dx.doi.org/10.1088/1742-6596/524/1/012035

[10] Ashwill T D 2004 Developments in large blades for lower cost wind turbines *Proceeding* (AWEA 2004) URL http://windpower.sandia.gov/other/041605C.pdf

[11] Hodges D H and Dowell E 1974 *Nonlinear Equations of Motion for the Elastic Bending and Torsion of Twisted Nonuniform Rotor Blades* (Ames Research Center and U.S. Army Air Mobility RandD Laboratory, Moffett Field, California 94035: NASA)

[12] Kim T, Hansen A M and Branner K 2013 Development of an anisotropic beam finite element for composite wind turbine blades in multibody system *Journal of Renewable Energy* vol 59 (Elsevier) pp 172–183 URL http://dx.doi.org/10.1016/j.renene.2013.03.033

[13] Wang Q, Johnson N, Sprague M A and Jonkman J 2015 Beamdyn: A high-fidelity wind turbine blade solver in the fast modular framework (Proceedings of the 33rd Wind Energy Symposium, AIAA 2015, Kissimmee, Florida)

[14] Verelst D R S and Larsen T J 2010 *Load consequences when sweeping blades - a case study of a 5 MW pitch controlled wind turbine* (Roskilde, Denmark: Risø-DTU, Technical Report Risø-R-1724)

[15] Bottasso C, Campagnolo F, Croce A and Tibaldi C 2013 Optimization-based study of bend-twist coupled rotor blades for passive and integrated passive and active load alleviation *Wind Energy* vol 16 nr 8 (John Wiley and Sons, Ltd.) pp 1149–1166 ISSN 1095-4244 URL http://dx.doi.org/10.1002/we.1543

[16] Bottasso C L, Campagnolo F and Croce A 2012 Multi-disciplinary constrained optimization of wind turbines *Multibody System Dynamics* vol 27 (Springer) pp 21 – 53 ISSN 1573-272X URL http://dx.doi.org/10.1007/s11044-011-9271-x

[17] Ning S A, Damiani R and Moriarty P J 2014 Objectives and constraints for wind turbine optimization *Solar Energy Engineering* vol 136 (ASME) URL http://dx.doi.org/10.1115/1.4027693

[18] Zahle F, Tibaldi C, Verelst D R, Bak C, Bitche R and Blasques J P A A 2015 Aero-elastic optimization of a 10 mw wind turbine *Proceedings - 33rd Wind Energy Symposium* vol 1 (American Institute of Aeronautics and Astronautic) pp 201–223

[19] Zahle F, Tibaldi C, Verelst D R, Bak C, Bitche R and Blasques J P A A 2015 *Rotor Design Optimization Tools and Cost Models* (Bremen, Germany: IQPC Workshop for Advances in Rotor Blades for Wind Turbines) URL http://orbit.dtu.dk/files/115528875/iqpc_hawtopt2.pdf

[20] Blanco M I 2009 The economics of wind energy *Renewable and Sustainable Energy Reviews* vol 13 nr 6–7 (Elsevier) pp 1372 – 1382 ISSN 1364-0321 URL http://dx.doi.org/10.1016/j.rser.2008.09.004

[21] Megavind Megavind lcoe model – guidelines and documentation URL http://megavind.windpower.org/megavind/lcoe_calculator_model.html

[22] Department of Trade and Industry - DTI 2007 *Study of the costs of offshore wind generation - A report to the Renewable Advisory Board (RAB) and DTI* (UK: URN Number 07/779)

[23] Krohn S, Morthorst P and Awerbuch S March 2009 *The Economics of Wind Energy - A report by the European Wind Energy Association* (EWEA - European Wind Energy Association) URL http://www.ewea.org/fileadmin/files/library/publications/reports/Economics_of_Wind_Energy.pdf

[24] Douglas-Westwood 2010 *Offshore Wind Assessment in Norway* (Oslo: The Research Council of Norway)

[25] Consulting M 2011 *Wind Turbine Trends* (UK: MAKE Consulting) URL http://www.consultmake.com/

[26] Griffith D T and Johanns W April 2013 *Large Blade Manufacturing Cost Studies Using the Sandia Blade Manufacturing Cost Tool and Sandia 100-meter Blades* (Albuquerque, New Mexico 87185 and Livermore, California 94550: Sandia National Laboratories) ISBN SAND2013-2734

[27] Paquette J and Veers P 2009 Increased rotor size through passive load control and weight reduction concepts *EWEC Proceedings* (European Wind Energy Conference and Exhibition)

[28] McKenna R, Hollnaicher S, P Ostman P, Leye V D and Fichtner W 2015 Cost-potentials for large onshore wind turbines in europe *Energy* vol 83 (Elsevier) pp 217–229 URL http://dx.doi.org/10.1016/j.energy.2015.02.016

[29] INNWIND Consortium Innovative wind conversion systems (10-20mw) for offshore applications URL http://www.innwind.eu/

[30] Bergami L, Gaunaa M, Poulsen N and Buhl T 2013 *Adaptive Trailing Edge Flaps for Active Load Alleviation in a Smart Rotor Configuration* (Denmark: DTU Wind Energy) ISBN DTU Wind Energy PhD-0020(EN), DTU Wind Energy PhD-0020

[31] Shirk M, Hertz T and Weisshaar T A 1986 Aeroelastic tailoring – theory, practice, promise *Journal of Aircraft* vol 23 (AIAA) pp 6–18

[32] Munk M 1949 *Propeller Containing Diagonally Disposed Fibrous Material* (U.S. Patent 2,484,308,1111)

[33] NASA X-29 forward swept wing technology demonstrator URL https://www.nasa.gov/centers/dryden/history/pastprojects/X29/index.html

[34] NASA Active aeroelastic wing (aaw) URL https://www.nasa.gov/centers/dryden/history/pastprojects/AAW/index.html

[35] Weisshaar T A 1978 *Aeroelastic Stability and Performance Characteristics of Aircraft with Advanced Composite Sweptforward Wing Structures* (AFFDL-TR-78-116, Air Force Flight Dynamics Laboratory, Wright-Patterson AFB, Ohio)

[36] Weisshaar T A 1979 *Forward Swept Wing Static Aeroelasticity* (AFFDL-TR-79-3087, Air Force Flight Dynamics Laboratory, Wright-Patterson AFB, Ohio)

[37] Weisshaar T A 1980 *The Influence of Aeroelasticity on Swept Composite Wings, Volume I Analysis* (AFWAL-TR-80-3137, Air Force Flight Dynamics Laboratory, Wright-Patterson AFB, Ohio)

[38] Weisshaar T A 1980 Divergence of forward swept composite wings *Journal of Aircraft* vol 17 (AIAA) pp 442–448

[39] Weisshaar T A 1980 Aeroelastic tailoring of forward swept composite wings *AIAA/ASME/ASCE/AHS 21st Structures, Structural Dynamics, and Materials Conference, Seattle, Washington* vol 17 (AIAA 80-0795) pp 442–448

[40] Librescu L and Thangjitham S 1988 The static aeroelastic behavior of sweptforward composite wing structures taking into account their warping restraint effect *Proc. 4th Japan-U.S. Conf. on Composite Materials, Washington, DC* (Technomic, Lancaster-Basel) pp 914–922

[41] Librescu L and Thangjitham S 1991 Analytical studies on static aeroelastic behavior of forward-swept composite wing structures *Journal of Aircraft* vol 28 (AIAA) pp 151–157

[42] Librescu L and Song O 1992 On the static aeroelastic tailoring of composite aircraft swept wings modelled as thin-walled beam structure *Composites Engineering* vol 2 (Elsevier) pp 497–512

[43] Jutte C V and Stanford B K 2014 *Aeroelastic Tailoring of Transport Aircraft Wings: State-of-the-Art and Potential Enabling Technologies* (NASA/TM–2014-218252, Langley Research Center, Hampton, Virginia)

[44] Larwood S and Zuteck M 2006 Swept wind turbine blade aeroelastic modeling for loads and dynamic behavior *Pittsburgh, USA, 4-7 June 2006* (Windpower 2006) p 17

[45] Ashwill T D, Kanaby G, Jackson K and Zuteck M 2010 Development of the swept twist adaptive rotor (star) blade *Orlando, Florida, 4-7 January 2010* (Proceedings of the 48th AIAA Aerospace Sciences Meeting)

[46] Zuteck M 2002 *Adaptive Blade Concept Assessment: Curved Planform Induced Twist Investigationt* (Albuquerque, New Mexico, USA: Sandia National Laboratories, SAND2002-2996)

[47] Hansen M H 2011 Aeroelastic properties of backward swept blades, *49th AIAA Aerospace Sciences Meeting. Orlando, Florida* (AIAA)

[48] Upwind Consortium 2011 *UpWind, Design limits and solutions for very large wind turbines* (EUPD - Sixth Framework Programme)

[49] Jensen P H 2010 *UpWind Activity Report year 4* (EUPD - Sixth Framework Programme)

[50] M Capuzzi A Pirrera P W 2014 A novel adaptive blade concept for large-scale wind turbines. part i: Aeroelastic behaviour *Energy* vol 73 (Elsevier) pp 15—-24 URL http://dx.doi.org/10.1016/j.energy.2014.06.044

[51] M Capuzzi A Pirrera P W 2014 A novel adaptive blade concept for large-scale wind turbines. part ii: Structural design and power performance *Energy* vol 73 (Elsevier) pp 25—-32 URL http://dx.doi.org/10.1016/j.energy.2014.04.073

[52] Karaolis N 1989 The design of fibre reinforced composite blades for passive and active wind turbine aerodynamic control *dissertation* (University of Reading, Department of Engineering)

[53] Karaolis N 1989 The design of fibre reinforced composite blades for passive and active wind turbine aerodynamic control *EWEC proceedings* (European Wind Energy Conference and Exhibition)

[54] Veers PS Bir G and Lobitz D 1998 Aeroelastic tailoring in wind-turbine blade applications *Proceedings* (Windpower '98 Meeting)

[55] Lobitz D and Veers P 1998 Aeroelastic behavior of twist-coupled hawt blades *ASME/AIAA proceedings* (ASME/AIAA Wind Energy Symposium, Reno, NV)

[56] Lobitz D and Laino D 1999 Load mitigation with twist-coupled hawt blades *ASME/AIAA proceedings* (ASME/AIAA Wind Energy Symposium, Reno, NV)

[57] Lobitz D W and Veers P S 2003 Load mitigation with bending/twist-coupled blades on rotors using modern control strategies *Wind Energy* vol 6 nr 2 (John Wiley and Sons, Ltd.) pp 105–117 ISBN 1099-1824 URL http://dx.doi.org/10.1002/we.74

[58] Berring P, Branner K and Berggreen C 2007 Torsional performance of wind turbine blades: Part i: Experimental investigation *Proceedings of the 16th International conference on composite materials* vol 2 (Japan Society for Composite Materials) pp 1118–1119 ISBN 978-4-931136-06-9

[59] Berring P, Branner K and Berggreen C 2007 Torsional performance of wind turbine blades: Part ii: Numerical validation *Proceedings of the 16th International conference on composite materials* vol 2 (Japan Society for Composite Materials) p 1432 ISBN 978-4-931136-06-9

[60] Internation Electrotechnical Commission 2005 *International Standard, IEC 61400-1 Third Edition 2005-08, Wind Turbines - Part 1: Design Requirements* (Reference Number IEC 61400-1:2005(EN))

[61] Germanischer Lloyd 2010 *Guideline for the Certification of Wind Turbines* (Standard)

[62] Timoshenko S and Goodier J N 1951 *Theory of Elasticity* (McGraw-Hill Book Company Inc.)

[63] Petersen J T 1990 *Kinematically Nonlinear Finite Element Model of a Horizontal Axis Wind Turbine* (Risø National Laboratory, Roskilde, Denmark)

[64] Larsen T J and Hansen A M 2015 *How 2 HAWC2, the user's manual* DTU Wind Energy Risø-R-1597(ver.4.6)(EN), Roskilde, Denmark

[65] DNV-GL Bladed wind turbine simulation tool URL https://www.dnvgl.com/services/bladed-3775

[66] Jonkman J M and Buhl M L 2005 *FAST v7 User's Guide* National Renewable Energy Laboratory Technical Report NREL/EL-500-38230, Golden, Colorado 80401-3393

[67] DTU Wind Energy Hawc2 URL http://www.hawc2.dk/

[68] Hansen M H, Gaunaa M and Madsen H A 2004 *A Beddoes-Leishman type dynamic stall model in state-space and indicial formulations* (Technical Report, Risø-R-1354(EN), Risø National Laboratory, Roskilde, Denmark)

[69] Leishman J and Beddoes T 1986 A generalized model for airfoil unsteady aerodynamic behaviour and dynamic stall using theindicial method *Proceeding of the 42nd Annual Forum of the American Helicopter Society* (AHS, Washington D.C.)

[70] Theodorsen T 1935 *General theory of aerodynamic instability and the mechanism of flutter* (NACA Report 435)

[71] Madsen H, Riziotis V, Zahle F, Hansen M, Snel H, Grasso F, Larsen T, Politis E and Rasmussen F 2012 Blade element momentum modeling of inflow with shear in comparison with advanced model results *Wind Energy* vol 15 (John/Wiley and Sons Ltd.) pp 63 – 81 URL doi:10.1002/we.493

[72] Popko W, Vorpahl F, Zuga A, Kohlmeier M, Jonkman J, Robertson A, Larsen T J, Yde A, Stertr K and et al K O Offshore code comparison collaboration continuation (oc4), phase i - results of coupled simulations of an offshore wind turbine with jacket support structure *Proceedings of the International Offshore and Polar Engineering Conference 2012* pp 337–346 rhodes, Greece, 17-23 June 2012

[73] Larsen T J, Madsen H A, Larsen G C and Hansen K S 2013 Validation of the dynamic wake meander model for loads and power production in the egmond aan zee wind farm *Journal of Wind Energy* vol 16 nr 4 pp 605–624 URL http://dx.doi.org/10.1002/we.1563

[74] Vorpahl F, Strobel M, Jonkman J M, Larsen T J and Passon P 2013 Verification of aeroelastic offshore wind turbine design codes under iea wind task xxiii *Journal of Wind Energy* URL http://dx.doi.org/10.1002/we.1588

[75] Jonkman J 2013 The new modularization framework for the fast wind turbine cae tool *Proceedings of the 51st AIAA Aerospace Sciences Meeting including the New Horizons Forum and Aerospace Exposition, Grapevine, Texas* (AIAA)

[76] INNWIND Consortium 2015 *Deliverable 2.21 - Part B: Benchmarking of aerodynamic and aeroelastic models* (EU 7th Framework Programme)

[77] AVATAR Consortium 2016 *Comparison of models with respect to Load analysis in extreme yaw of the INNWIND.EU and AVATAR RWT's* (EU 7th Framework Programme)

[78] Hansen M H and Henriksen L C 2013 *Basic DTU Wind Energy Controller* (Roskilde, Denmark: DTU Wind Energy, Technical Report-E-0018)

[79] Mann J 1998 Wind field simulation *Probabilistic Engineering Mechanics* vol 13 (Elsevier) p 269–282 URL doi:10.1016/S0266-8920(97)00036-2

[80] Hodges D H 2006 Nonlinear composite beam theory (AIAA)

[81] Yu W and Blair M 2012 Gebt: A general purpose nonlinear analysis tool for composite beams *Composite Structures* vol 94 nr 9 (Elsevier) pp 2677–2689 URL http://dx.doi.org/10.1016/j.compstruct.2012.04.007

[82] Wang Q, Sprague M A, Jonkman J and Johnson N 2014 Nonlinear legendre spectral finite elements for wind turbine blade dynamics (Proceedings of the 32nd ASME Wind Energy Symposium, National Harbor, Maryland)

[83] Bak C, Zahle F, Bitsche R, Kim T, Yde A, Henriksen L C, Natarajan A and Hansen M H 2013 *Description of the DTU 10 MW Reference Wind Turbine* (Roskilde, Denmark: DTU Wind Energy, Technical Report-I-0092)

[84] Mayo J, Garcıa-Vallejo D and Domınguez J 2004 Study of the geometric stiffening effect: comparison of different formulations *Multibody System Dynamics* vol 11 (Springer) pp 321–341 URL doi:10.1023/B:MUBO.0000040799.63053.d9

[85] Bathe K J and Bolourchi S 1979 Large displacement analysis of three-dimensional beam structures *International Journal for Numerical Methods in Engineering* vol 14 (John Wiley and Sons Ltd.) p 961–986 URL doi:10.1002/nme.1620140703

[86] Bauchau O A 2013 *Dymore User's Manual* Dymore Solutions http://dymoresolutions.com/dymore4 0/UsersManual/UsersManual.html

[87] INNWIND Consortium 2015 *Deliverable 2.21 - Part A: Results of the benchmark for blade structural models* (EU 7th Framework Programme)

[88] Sønderby I and Hansen M 2013 Open-loop frequency response analysis of a wind turbine using high-order linear aeroelastic model *Wind Energy* vol 17 (John/Wiley and Sons Ltd.) p 1147–1167 URL doi:10.1002/we.1624

[89] Tibaldi C, Henriksen L, Hansen M and Bak C 2014 Effects of gain-scheduling methods in a classical wind turbine controller on wind turbine aeroservoelastic modes and loads *Proceedings of the 52th AIAA Aerospace Sciences Meeting* (AIAA)

[90] Quarteroni A, Sacco R and Saleri F 2000, ISBN 0-387-98959-5 *Numerical Mathematics* (Springer-Verlag New York, Inc.)

[91] Hansen M H, Thomsen K, Natarajan A and Barlas A 2015 *Design Load Basis for onshore turbines - Revision 00* (Roskilde, Denmark: DTU Wind Energy, Technical Report E-0074(EN))

[92] Martins J R R A and Lambe A B 2013 Multidisciplinary design optimization: A survey of architectures *AIAA Journal* vol 51 (AIAA) pp 2049–2075

[93] Fuglsang P, Bak C, Schepers J, Bulder B, Cockerill T, Claiden P, Olesen A and Rossen R 2002 Site-specific design optimization of wind turbines *Wind Energy* vol 5 (John/Wiley and Sons Ltd.) pp 261–279 ISSN 1095-4244 URL http://dx.doi.org/10.1002/we.61

[94] Merz K O 2015 Rapid optimization of stall-regulated wind turbine blades using a frequency-domain method: Part 1, loads analysis *Wind Energy* vol 18 (John/Wiley and Sons Ltd.) pp 1703–1723 ISSN 1099-1824 URL http://dx.doi.org/10.1002/we.1786

[95] Ashuri T, Zaaijer M B, Martins J R R A, van Bussel G J W and van Kuik G A 2014 Multidisciplinary design optimization of offshore wind turbines for minimum levelized cost of energy *Renewable Energy* vol 68 (Elsevier) pp 893–905 URL http://dx.doi.org/10.1016/j.renene.2014.02.045

[96] Tibaldi C, Henriksen L, Hansen M and Bak C 2015 Wind turbine fatigue damage evaluation based on a linear model and a spectral method *Wind Energy* vol 18 (John/Wiley and Sons Ltd.) ISSN 1095-4244 URL http://dx.doi.org/10.1002/we.1898

[97] Tibaldi C 2015 *Concurrent Aeroservoelastic Design and Optimization of Wind Turbines* (PhD thesis, DTU Wind Energy)

[98] NASA Glenn Research Center Openmdao URL http://openmdao.org

[99] Moore K, Naylor B and Gray J 2008 The development of an open-source framework for multidisciplinary analysis and optimization *10th AIAA/ISSMO Multidisciplinary Analysis and Optimization Conference, Victoria, Canada* (AIAA)

[100] Gray J S, Moore K T and Naylor B A 2010 Openmdao: An open source framework for multidisciplinary analysis and optimization *13th AIAA/ISSMO Multidisciplinary Analysis and Optimization Conference, Fort Worth, Texas* (AIAA)

[101] Heath C M and Gray J S 2012 Openmdao: Framework for flexible multidisciplinary design, analysis and optimization methods *8th AIAA Multidisciplinary Design Optimization Specialist Conference (MDO), Honolulu, Hawaii* (AIAA)

[102] Perez R E, Jansen P W and Martins J R R A 2012 pyOpt: A Python-based object-oriented framework for nonlinear constrained optimization *Structures and Multidisciplinary Optimization* vol 45 (Springer) pp 101–118 URL http://dx.doi.org/10.1007/s00158-011-0666-3

[103] Gill P E, Murray W and Saunders M A 2002 Snopt: An sqp algorithm for large-scale constrained optimization *Journal on Optimization* vol 12 (SIAM) pp 979–1006 URL http://www.siam.org/journals/sirev/47-1/44609.html

[104] DTU Wind Energy Becas URL http://www.becas.dtu.dk/

[105] Blasques J P A A 2012 *User s manual for BECAS a cross section analysis tool for anisotropic and inhomogeneous beam sections of arbitrary geometry* DTU Wind Energy Technical Report, Roskilde, Denmark

[106] Blasques J P A A and Stolpe M 2012 Multi-material topology optimization of laminated composite beam cross sections *Composite Structures* vol 94 (Elsevier) p 3278–3289

[107] Lambe A B and Martins J R R A 2012 Extensions to the design structure matrix for the description of multidisciplinary design, analysis, and optimization processes *Structural and Multidisciplinary Optimization* vol 46 (Springer) pp 273–284 URL doi:10.1007/s00158-012-0763-y

[108] Zahle F, Tibaldi C, Pavese C, McWilliam M K, Blasques J P A A and Hansen M H 2016 Design of an aeroelastically tailored 10 mw wind turbine rotor *Journal of Physics: Conference Series - The Science of Making Torque from Wind 2016* vol 753 (IOP Publishing) URL http://iopscience.iop.org/article/10.1088/1742-6596/753/6/062008/pdf

[109] Siemens Siemens wind turbine blades URL http://www.siemens.com/global/en/home/markets/wind/turbines/technology/blades.html

[110] Vattenfall Pen y cymoedd wind farm URL https://www.flickr.com/photos/120047838@N03/

[111] Koziel S, Ciaurri D E and Leifsson L 2011 Surrogate-based methods *Computational Optimization, Methods and Algorithms - State of the art in Computational Optimization* vol 356 (Springer-Verlag Berlin Heidelberg) pp 33–59 URL http://dx.doi.org/10.1007/978-3-642-20859-1

[112] Simpson T, Toropov V, Balabanov V and Viana F 2008 Design and analysis of computer experiments in multidisciplinary design optimization: A review of how far we have come - or not *Multidisciplinary Analysis Optimization Conferences* (American Institute of Aeronautics and Astronautics) URL http://dx.doi.org/10.2514/6.2008-5802

[113] Queipo N V, Haftka R T, Shyy W, Goel T, Vaidyanathan R and Tucker P K 2005 Surrogate-based analysis and optimization *Progress in Aerospace Sciences* vol 41 (American Institute of Aeronautics and Astronautics) pp 1 – 28 ISSN 0376-0421 URL http://dx.doi.org/10.1016/j.paerosci.2005.02.001

[114] Bortolotti P, Bottasso C and Croce A 2016 Combined preliminary–detailed design of wind turbines *Wind Energy Science* vol 1 (Copernicus Publications on behalf of the European Academy of Wind Energy e.V) pp 71 – 88 URL http://dx.doi.org/10.5194/wes-1-71-2016

Part II

Publications

Paper A

HAWC2 and BeamDyn: Comparison Between Beam Structural Models for Aero-Servo-Elastic Frameworks

Authors:
Christian Pavese, Qi Wang, Taeseong Kim, Jason Jonkman, Michael A. Sprague

HAWC2 and BeamDyn: Comparison Between Beam Structural Models for Aero-Servo-Elastic Frameworks

Christian Pavese[1], Qi Wang[2], Taeseong Kim[1], Jason Jonkman[2], and
Michael A. Sprague[2]

Abstract

This work presents a comparison of two beam codes for aero-servo-elastic frameworks: a new structural model for the aeroelastic code HAWC2 and a new nonlinear beam model, BeamDyn, for the aeroelastic modularization framework FAST v8. The main goal is to establish the suitability of the two approaches to model the structural behaviour of modern wind turbine blades in operation. Through a series of benchmarking structural cases of increasing complexity, the capability of the two codes to simulate highly nonlinear effects is investigated and analyzed. Results show that even though the geometrically exact beam theory can better model effects such as very large deflections, rotations, and structural couplings, an approach based on a multi-body formulation assembled through linear elements is capable of computing accurate solutions for typical nonlinear beam theory benchmarking cases.

A.1 Introduction

Wind turbine blades are highly complex composite structures, and their design presents advanced challenges. In recent years, the development of multi-megawatt wind turbines has brought blade designers to explore different cost-effective solutions, including manufacturing larger, lighter, and more flexible wind turbine blades. The increase in size and flexibility in relation to the reduction in mass has augmented the importance of nonlinear effects related to the structural behaviour of the blades. These effects include large deflections and rotations along with structural couplings, such as bending-to-torsion. Hence,

---

[1]DTU Wind Energy, DK-4000, Roskilde, Denmark
[2]National Renewable Energy Laboratory, Golden, CO 80401

wind energy research started to focus on the necessity of developing models and tools able to accurately capture the response of these highly complex structures under aerodynamic loading.

In this paper, two beam models for aero-servo-elastic frameworks are presented, analyzed, and compared:

- A new linear anisotropic beam element implemented into the nonlinear aeroelastic multi-body code HAWC2 [1], developed by the Technical University of Denmark (DTU)

- A new nonlinear beam finite element (FE) model that uses the geometrically exact beam theory (GEBT), and for which spatial discretization is accomplished with Legendre spectral finite elements (LSFEs); the beam model is implemented as a module called BeamDyn [2][3] within the aeroelastic modularization framework FAST v8 [4], developed by the National Wind Technology Center at the National Renewable Energy Laboratory (NREL).

It is important to remark that even though the new HAWC2 beam element is based on a linear formulation, its implementation in a multibody system makes it possible to capture nonlinear effects, such as large rotations and translations. Hence, even if the structure in HAWC2 is modeled using several linear bodies, a comparison to the beam FE model implemented in BeamDyn can still be made even though the latter is based on a nonlinear formulation. Moreover, both of these structural codes have been separately verified and validated against results found in the literature and experimental data.

The purpose of this paper is not only to compare the accuracy of the two codes, but also to highlight the differences between the two approaches by setting up a specific series of benchmarking cases of increasing complexity. These cases involve only cantilever beams and an isolated wind turbine blade, whereas a full aeroelastic comparison will be presented in future works by the authors.

A.2   Approach

Highly flexible composite structures, such as wind turbine blades, can undergo large deflections without exceeding their specified elastic limit. Due to the geometry of their deformation, the behaviour of such structures is nonlinear and the solution becomes very complex. For this reason, and to face the complexity of these deformations, BeamDyn uses GEBT [5][6]. Exhaustive details related to the theory behind BeamDyn and its implementation in the FAST v8 state-space formulation are provided by [2][3]. This approach enables very high accuracy in

solving highly nonlinear structural problems, but it has a high computational cost. To address the computation cost, BeamDyn has been implemented with LSFEs, which characteristically have exponential convergence rates for smooth solutions, as opposed to low-order FEs that have algebraic convergence (requiring fewer nodes for the same accuracy). HAWC2 uses a different method to face nonlinear effects due to large deflections, large rotations, and structural couplings. As reported in the introduction, the beam model of HAWC2 is based on a multi-body formulation assembled with linear anisotropic Timoshenko beam elements. A detailed description of this type of element is provided by [1]. The accuracy of this approach is, in general, lower than that of the GEBT. The advantages, with respect to a nonlinear beam model, are the much lower computational cost required to model a nonlinear problem and the possibility of augmenting the accuracy by increasing the number of bodies.

These two methods are compared using a series of benchmarking cases. The main purpose is to evaluate the accuracy of the two structural codes against highly nonlinear problems. It is important to remark that the first four cases investigated in this work are "extreme." The deflections and rotations computed for these nonlinear problems are not comparable to those typical of operating wind turbine blades. Nonetheless, the two structural codes have been used to simulate these limit cases to prove the suitability of both approaches to provide valid solutions related to the behaviour of twisted and curved structures and composite beams with complex layups.

The cases are listed below:

- Case 1: Static analysis of a cantilever beam under five bending moments applied at its free end

- Case 2: Static analysis of an initially twisted and an initially curved beam

- Case 3: Static analysis of a composite beam with a force applied at the free end

- Case 4: Dynamic analysis of a composite beam with a sinusoidal force applied at the free end

- Case 5: DTU 10-MW reference wind turbine (RWT) [7] blade natural frequencies.

The analysis of the performances and responses of the two beam models start from a simple and very common case (static bending of a cantilever beam) and move to a complex tailored wind turbine blade. Except for the DTU 10-MW RWT blade natural frequencies, the cases were already used to verify BeamDyn and are presented by [2][3]. Nonetheless, these cases were selected as the basis for this study, because they are suited to demonstrate the capabilities of the

two codes to model structures that show nonlinear responses due to geometric and material couplings. The results obtained from the two codes were compared to results found in the literature or high-fidelity models generated using commercial, three-dimensional (3D), FE software such as ANSYS, Patran-Marc and Dymore.

A.3 Results

In this section, results for the each of the benchmarking cases are reported and discussed. Discrepancies between the two structural codes are highlighted and analyzed. The section is divided into five parts, one for each of the cases computed. Except for the last part of the study, which reports results concerning a wind turbine blade, very large displacements and composite beams with complex layups are taken into account.

A.3.1 Case 1: Static analysis of a cantilever beam under five bending moments applied at its free end

Case 1 concerns the static deflection of a cantilever beam that is subjected at its free end to a constant negative moment around the x_2 axis. A system schematic is shown in Figure A.1.

The length of the beam is 10 m and the input cross-sectional stiffness matrix is defined in Equation A.1. In this paper, the stiffness matrices are presented in the coordinate system adopted by [6].

$$K = 10^3 \begin{bmatrix} 1770 & 0 & 0 & 0 & 0 & 0 \\ 0 & 1770 & 0 & 0 & 0 & 0 \\ 0 & 0 & 1770 & 0 & 0 & 0 \\ 0 & 0 & 0 & 8.16 & 0 & 0 \\ 0 & 0 & 0 & 0 & 86.9 & 0 \\ 0 & 0 & 0 & 0 & 0 & 215 \end{bmatrix} \tag{A.1}$$

where the units associated with the stiffness values are $K_{i,j}$ (N) and $K_{i+3,j+3}$ ($\mathrm{N\,m^2}$) for $i,j = 1,2,3$. Further details on the data used are fully provided by [2]. The BeamDyn model is composed of two 5th- order LSFEs, whereas HAWC2 models uses 30 and 50 bodies, respectively. The negative moment applied around the x_2 axis is defined in Equation A.2.

$$M_2 = \lambda \pi \frac{EI_2}{L} \tag{A.2}$$

where λ is a parameter used to scale M_2, from 0 to 2; E is the Young modulus; I_2 is the moment of inertia with respect to the axis x_2, and L is the total length
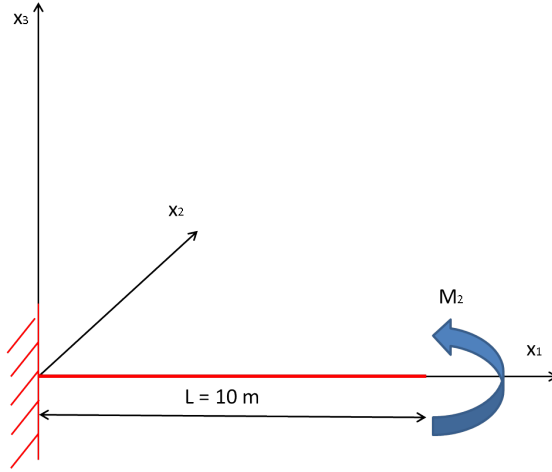
Figure A.1: Description of the beam and the coordinate system for Case 1.

of the beam. Table A.1 shows the tip displacements computed by BeamDyn and HAWC2 compared to the analytical solution. The solution, reported in Equation A.3, can be found in [8].

$$
u_1(x_1) = \rho \sin\left(\frac{l(x_1)}{\rho}\right) - l(x_1)
$$
$$
u_3(x_1) = \rho \cos\left(1 - \frac{l(x_1)}{\rho}\right)
$$

(A.3)

where $\rho = \frac{EI_2}{M_2}$ and u_1 and u_3 are the displacements along the x_1 and x_3 axes, respectively, calculated at each node $l(x_1)$.

In Table A.1, *Sol.* indicates the analytical solution, *BD* the beam model Beam-Dyn, and *H2-30b* and *H2-50b* the HAWC2 structural model assembled with 30 and 50 bodies, respectively. For $\lambda = 2$, because the analytical solution of u_1 is 0.0, the results are reported in absolute values instead of percentages.
Figure A.2 provides a visual representation of the beam displacement in longitudinal, x_3, and axial directions, x_1.
As the moment applied to the free end increases, the geometrically nonlinear effects of the benchmark problem become relevant. The tip displacement computed by BeamDyn is indistinguishable from the analytical solution; two 5th-order LSFEs is more than enough to achieve high accuracy and fewer nodes/elements is likely possible. Due to the use of linear elements, the structural model of HAWC2 is not fully able to catch this highly nonlinear behaviour. The increase in the number of bodies in HAWC2 to model the beam reduces the error and improves the accuracy of the computed displacements.

Table A.1: Comparison of the beam tip displacements for all the applied bending moments.

λ	Sol. (u_3)	BD	H2-30b	H2-50b
0.4	-2.432 m	0.0%	0.5%	0.2%
0.8	-7.661 m	0.0%	1.3%	0.5%
1.2	-11.56 m	0.0%	1.2%	0.4%
1.6	-11.89 m	0.0%	1.3%	0.5%
2.0	-10.00 m	0.0%	5.1%	2.0%
λ	Sol. (u_1)	BD	H2-30b	H2-50b
0.4	5.50 m	0.0%	0.1%	0.0%
0.8	7.20 m	0.0%	0.3%	0.1%
1.2	4.80 m	0.0%	4.5%	1.7%
1.6	1.37 m	0.0%	22.7%	9.7%
2.0	0.00 m	0.00	-0.008 m	-0.01 m

Figure A.2: Bending of the cantilever beam in the x_1-x_3 plane. Five growing negative bending moments around the x_2-axis are applied at the free end on the beam. Circles: HAWC2 beam model with 30 bodies. Triangles: HAWC2 beam model with 50 bodies.

A.3.2 Case 2: Static analysis of an initially twisted and an initially curved beam

Beams characterized by initial twists and curvatures are analyzed for Case 2. First, a straight beam with an initial twist is considered (Figure A.3). The beam is linearly twisted in the positive θ_1 direction from 0 degrees at the root to 90 degrees at the tip. Table A.2 shows the material properties for A36 steel, the beam geometry, and the force applied at the free end along the negative x_3 axis. As in Case 1, the beam in BeamDyn is meshed with two 5th-order LSFEs, and the HAWC2 beam model is meshed with 30 bodies.

The full description of the beam is also provided by [3]. The results for the twisted beam are shown in Table A.3 and compared to the baseline results obtained from an extremely refined 3D ANSYS SOLID186 elements model.

The second part of Case 2 involves an initially curved beam. The benchmark problem for pre-curved beams was proposed by Bathe in 1979 [9]. Figure A.4 shows the configuration of the curved cantilever beam. The beam lies in the plane defined by the positive x_1 direction and the negative x_2 direction. A force of 600 N is applied in the positive x_3 direction. The beam is defined by the 45-degree arc with 100-m radius centered at 100 m in the negative x_2 direction.
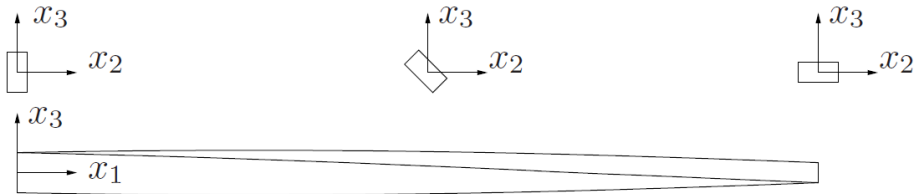
Figure A.3: Schematic of the twisted beam and the coordinate system for Case 2.

Table A.2: Material properties (A36 steel), geometry (rectangular section), and tip force applied on the beam.

Property	Value
Elastic Modulus	200 GPa
Shear Modulus	79.3 GPa
Height	0.5 m
Width	0.25 m
Length	10 m
Force	4000 kN

Table A.3: Comparison of the twisted beam tip displacements: ANSYS
SOLID186 Model, BeamDyn, and HAWC2.

	u_1 [m]	u_2 [m]	u_3 [m]
ANSYS	-1.134	-1.714	-3.584
BeamDyn	0.13%	0.04%	0.15%
HAWC2	2.42%	1.92%	1.05%

Figure A.4: Schematic of the initially curved beam and the coordinate system
for the second part of Case 2.

The beam has a square cross-section geometry. As in Case 1, the cross-sectional
stiffness matrix of the beam, computed using the geometry and the material
properties provided by [9], is diagonal. The computed displacements for the
static analysis are reported in Table A.4 and a comparison to the results pub-
lished by [9] is provided.

The tendency of the results computed by the two structural codes is the same for
both the pre-twisted beam problem and the pre-curved benchmark cases. With
the discretization applied, BeamDyn is able to better represent the nonlinear be-
haviour of twisted and curved beams (differences below 1%). HAWC2 computes
tip displacements that are between 2% and 3% away from the solutions. Even
though HAWC2 uses linear beam elements, the multi-body approach is able to
provide sufficiently accurate solutions for the large displacements considered in
these two geometrically nonlinear problems.

Table A.4: Comparison of the curved beam tip displacements: Ref.[9], Beam-Dyn, and HAWC2.

	u_1 [m]	u_2 [m]	u_3 [m]
Bathe-Bolourchi [9]	-23.7	-13.4	53.4
BeamDyn	0.8%	0.8%	0.0%
HAWC2	2.1%	3.1%	0.0%

A.3.3 Case 3: Static analysis of a composite beam with a force applied at the free end

The purpose of Case 3 is to compare the capability of HAWC2 to BeamDyn to simulate the behaviour of composite beams with an elastic coupling. A 10-m long cantilever composite box beam is considered. The coordinate system is the same as Case 1 (see Figure A.1). BeamDyn and HAWC2 use the same meshes described for Case 2 (BeamDyn: two 5th-order LSFEs; HAWC2: 30 bodies). The cross-sectional stiffness matrix is shown in Equation A.4.

$$K = 10^3 \begin{bmatrix} 1368.17 & 0 & 0 & 0 & 0 & 0 \\ 0 & 88.56 & 0 & 0 & 0 & 0 \\ 0 & 0 & 38.78 & 0 & 0 & 0 \\ 0 & 0 & 0 & 16.96 & 17.61 & -0.351 \\ 0 & 0 & 0 & 17.61 & 59.12 & -0.370 \\ 0 & 0 & 0 & -0.351 & -0.370 & 141.47 \end{bmatrix} \quad (A.4)$$

where the units associated with the stiffness values are $K_{i,j}$ (N), $K_{i,j+3}$ (N m) and $K_{i+3,j+3}$ (N m^2) for $i, j = 1, 2, 3$. A concentrated dead force of 150 N is applied in the positive direction of x_3 at the free tip of the beam. The displacements and rotations along the beam axis are plotted in Figure A.5 and Figure A.6, respectively. Due to the properties of the composite materials, coupling effects exist between the twist and the two bending modes (see Equation A.4). For this reason, a consistent rotation around the x_1 axis can be observed in Figure A.6.

The tip displacements and rotations are compared to Dymore [10], a finite-element-based multi-body dynamics code. Results are shown in Table A.5.

In Table A.5, p_1, p_2, and p_3 indicates the rotation of the free-end node of the beam around the axis x_1, x_2, and x_3 respectively. BeamDyn is able to perfectly match the displacements and rotations computed by Dymore. The tip deflections and rotations computed by the structural beam model of HAWC2 are in good agreement with Dymore, with a maximum discrepancy of approximately 3%.

Figure A.5: Displacements of the composite beam with respect to the nodal positions. Red: beam displacement of the nodes along the u_1 axis. Green: beam displacement of the nodes along the u_2 axis. Blue: beam displacement of the nodes along the u_3 axis. Triangles: HAWC2. Circles: BeamDyn.
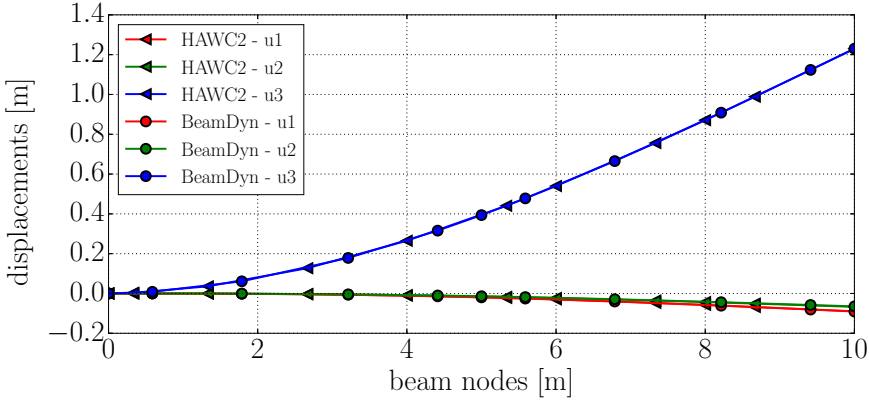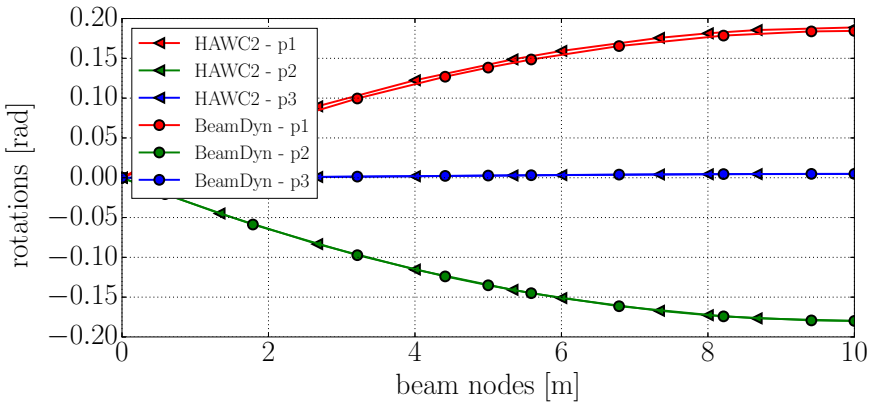

Figure A.6: Rotations of the composite beam with respect to the nodal positions. Red: beam rotation of the nodes around the u_1 axis. Green: beam rotation of the nodes around the u_2 axis. Blue: beam rotation of the nodes around the u_3 axis. Triangles: HAWC2. Circles: BeamDyn.

Table A.5: Comparison of tip displacements and rotations for Case 3.

	u_1 [m]	u_2 [m]	u_3 [m]
Dymore	-0.09064	-0.06484	1.22998
BeamDyn	0.0%	0.0%	0.0%
HAWC2	1.1%	3.7%	0.0%

	p_1 [rad]	p_2 [rad]	p_3 [rad]
Dymore	0.18445	-0.17985	0.00488
BeamDyn	0.0%	0.0%	0.0%
HAWC2	2.4%	0.01%	2.3%

A.3.4   Case 4: Composite beam with a sinusoidal force applied at the free end

The objective of Case 4 is to compare HAWC2 and BeamDyn to composite beams under dynamic loading. The cantilever beam used is the same as that described in Case 3 as are the meshes used for the beam models. The coordinate system is the same as that used in Case 1 and shown in Figure A.1. The cross-sectional mass matrix is presented in Equation A.5.

$$M = 10^{-2} \begin{bmatrix} 8.538 & 0 & 0 & 0 & 0 & 0 \\ 0 & 8.538 & 0 & 0 & 0 & 0 \\ 0 & 0 & 8.538 & 0 & 0 & 0 \\ 0 & 0 & 0 & 1.4433 & 0 & 0 \\ 0 & 0 & 0 & 0 & 0.40972 & 0 \\ 0 & 0 & 0 & 0 & 0 & 1.0336 \end{bmatrix} \tag{A.5}$$

The units associated with the mass matrix values are $M_{i,i}$ (kg s^2 m^{-2}) and $M_{i+3,i+3}$ (kg s^2) for $i = 1, 2, 3$. A sinusoidal point dead force is applied in the x_3 direction. The force is described by Equation A.6.

$$F_3(t) = A_F \sin \omega_F t \tag{A.6}$$

where the signal amplitude $A_F = 100$ N and the frequency $\omega_F = 10$ rad s^{-1}. The displacements and rotations along the beam axis are plotted in Figure A.7. Root forces and moments are plotted in Figure A.8.

On this dynamic benchmark case, BeamDyn and HAWC2 show good agreement, particularly in relation to the dynamics of the tip displacement and rotation in the direction where the force is applied. The most noticeable differences are registered for the displacement on the x_2 direction and the rotation around the x_3. These discrepancies are also the reason for the differences reported for the axial force F_1 (see Figure A.8). The forces are projected on a fixed coordinate system placed at the root of the beam. BeamDyn and HAWC2 compute slightly different rotations around the x_3 direction and slightly different
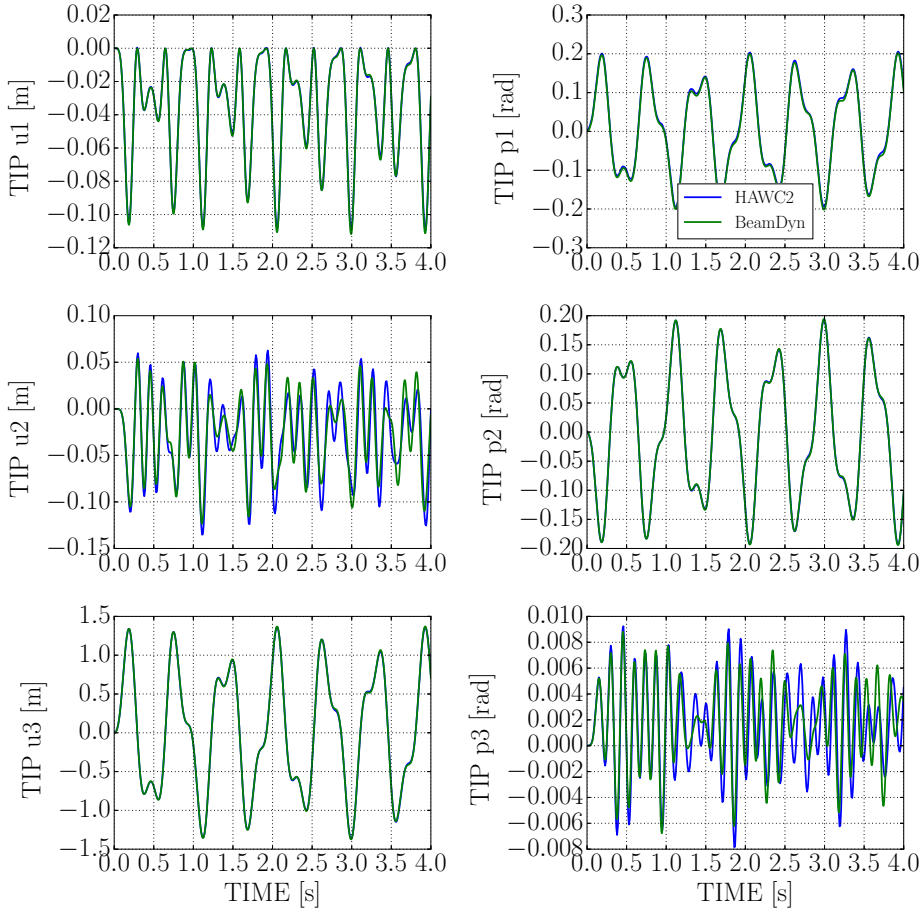
Figure A.7: Tip displacements (left side, u_1, u_2, and u_3 from top to bottom) and rotations (right side, p_1, p_2, and p_3 from top to bottom) for 4-second simulations.

deflections on the x_2 direction, and these have an impact on the component of the force projected on the x_1 axis. No other relevant discrepancies are registered between the forces and moments computed by HAWC2 and those computed by BeamDyn (see Figure A.8).
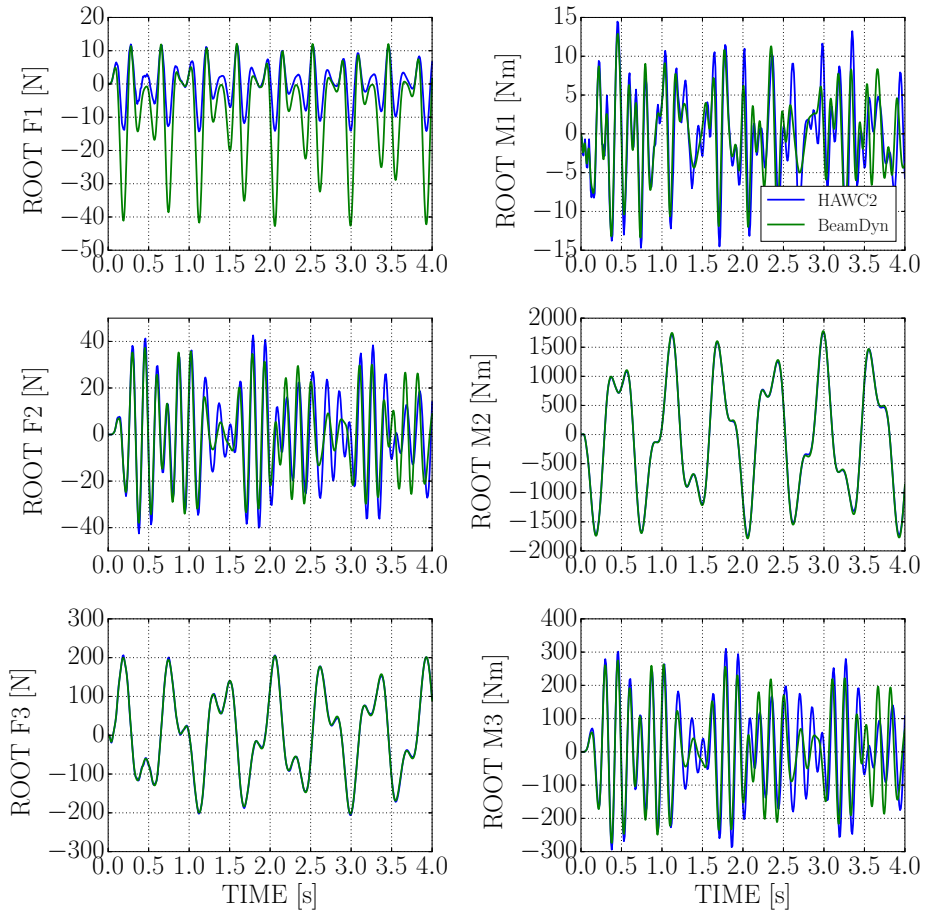
Figure A.8: Root forces (left side, F_1, F_2, and F_3 from top to bottom) and moments (right side, M_1, M_2, and M_3 from top to bottom) for 4-second simulations.

A.3.5   Case 5: DTU 10-MW RWT blade natural frequencies

For the last case, the natural frequencies of the isolated DTU 10-MW RWT blade [7] are compared. In HAWC2, the natural frequencies of the blade are obtained directly from its eigenvalue solver. The beam is assembled with 26 bodies. The version of BeamDyn used for the current work was not developed with an eigenvalue solver. Therefore, two impulse forces of 4 kN are applied on the blade tip in the edgewise and flapwise directions. Power spectral densities (PSDs) are then computed from the tip displacement time series. The beam is meshed assembling 13 2nd-order elements. For this case study, more elements than the previous cases were used to better represent the complexity of such a tailored structure. The results obtained from HAWC2 and BeamDyn are compared to the natural frequencies computed with a Patran-Marc 3D FE model (20-noded layered continuum elements).

Figure A.9 shows the PSDs of the two BeamDyn impulse test cases. Table A.6 identifies the natural frequencies using the Patran model compared to those computed by BeamDyn and HAWC2. The results show good agreement between
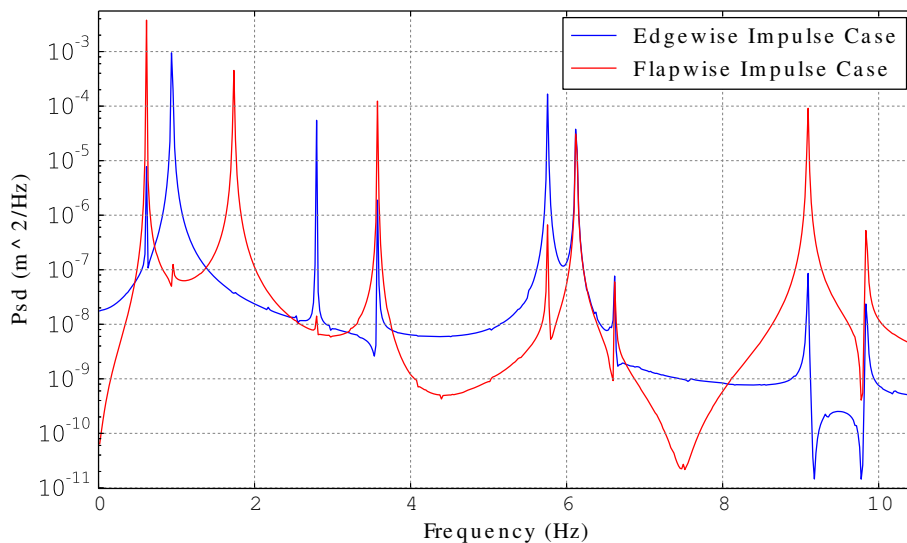
Figure A.9: BeamDyn PSD of tip displacement in flapwise and edgewise directions for impulse load case. Blue curve: Flapwise tip displacement for an impulse force applied on the tip in the flapwise direction. Red curve: Edgewise tip displacement for an impulse force applied on the tip in the edgewise direction.

Table A.6: Comparison of the DTU 10-MW RWT natural frequencies.

	FEM [Hz]	H2 [%]	BD [%]
1st Flap	0.615	-0.6%	0.0%
1st Edge	0.971	-4.2%	-3.8%
2nd Flap	1.764	-1.4%	-1.7%
2nd Edge	2.857	-3.7%	-2.2%
3rd Flap	3.592	-0.4%	-0.5%
1st Torsion	5.753	-1.7%	-0.1%
4th Flap	6.124	-1.1%	-0.1%
3rd Edge	6.151	-0.3%	-0.2%

HAWC2 and BeamDyn. The differences between the natural frequencies of the beam models from the full 3D FE model are in the same range. The largest discrepancy is registered for the first edgewise mode, with an approximate 4% difference between the beam models and the FE model. This discrepancy is because of the strategy used to model the trailing edge in the FE model, in which the 20-noded layered continuum elements allowed for a higher degree of tailoring compared to the input data provided in [7]. Consequently, this FE-modeling strategy resulted in a stiffer blade in the edgewise direction.

A.4   Conclusions

This paper presented a comparison between two new structural codes for aero-servo-elastic frameworks: one developed by DTU Wind Energy and implemented in the nonlinear aero-servo-elastic multi-body code HAWC2, and the other, a nonlinear beam FE based on GEBT and called BeamDyn, developed by the National Wind Technology Center at NREL as a module for the modular framework FAST v8. These new beam models were implemented with the purpose of better representing the complex structural behaviour of modern wind turbine composite blades. To analyze the capabilities of the two codes, ad hoc benchmarking cases were selected. To test the limit ability of the two beam models to simulate nonlinear structural behaviours, four extreme case studies, called Case 1 to Case 4, were chosen, along with a final modal analysis involving a wind turbine blade, called Case 5. The results obtained from the two codes were compared to analytical results or high-fidelity models generated using commercial 3D FE software such as Dymore, ANSYS and Patran-Marc.

Case 1 considered static bending of a cantilever beam under five constant bending moments applied at its free end. Case 2 investigated initially twisted and

initially curved beam with a force applied at the free end along the x3 axis direction. Both cases showed good agreement between HAWC2 and BeamDyn. In general, BeamDyn proved to have a greater capability to simulate extremely large displacements of beams subject to geometrical nonlinearities. HAWC2 demonstrated with sufficient accuracy its capability to model the first and second case, with the additional benefit of being able to increase the number of bodies for a more accurate solution without excessively compromising the computational cost. In Case 3 and Case 4, a composite beam with elastic coupling under static and dynamic loading, respectively, were analyzed. BeamDyn and HAWC2 were again in good agreement. Last, the isolated DTU 10-MW RWT blade case showed the capability of both models to accurately compute the natural frequencies of a complex structure such as a wind turbine composite blade. Given the results generated by both codes to simulate highly nonlinear structural problems, both approaches are considered suitable to properly model the complex behaviour of a wind turbine blade in operation.

Future work will provide an extensive comparison between the computational costs of the two structural codes. Full aeroelastic simulations will be taken into account, to provide a full overview regarding the capabilities of the two structural codes and the benefits that can be achieved with a full integration in aero-servo-elastic frameworks.

A.5   Acknowledgements

Bibliography

[1] Kim, T., Hansen, A. M., and Branner, K., *Development of an anisotropic beam finite element for composite wind turbine blades in multi-body system*, Journal of Renewable Energy, 2013, 59(2013) 172-183.

[2] Wang, Q., Sprague, M. A., Jonkman, J., and Johnson, N., *Nonlinear Legendre Spectral Finite Elements for Wind Turbine Blade Dynamics*, 32nd ASME Wind Energy Symposium, National Harbor, Maryland, January 13-17, 2014.

[3] Wang, Q., Johnson, N., Sprague, M. A., and Jonkman, J., *BeamDyn: A High-Fidelity Wind Turbine Blade Solver in the FAST Modular Framework*, 33rd Wind Energy Symposium, AIAA 2015, Kissimmee, Florida, January 5-9, 2015.

[4] Jonkman, J.M., *The new modularization framework for the FAST wind turbine CAE tool*, Proceedings of the 51st AIAA Aerospace Sciences Meeting including the New Horizons Forum and Aerospace Exposition, Grapevine, Texas, January, 2013.

[5] Hodges, D. H., *Nonlinear Composite Beam Theory*, AIAA, 2006.

[6] Yu, W. and Blair, M., *GEBT: A general-purpose nonlinear analysis tool for composite beams*, Composite Structures, Vol. 94, 2012, pp. 2677–2689.

[7] Bak, C., Zahle, F., Bitsche, R., Kim, T., Yde, A., Henriksen, L. C., Natarajan, A., and Hansen, M. H. *Description of the DTU 10-MW Reference Wind Turbine*, DTU Wind Energy Report-I-0092, July, 2013.

[8] Mayo, J.M., Garcıa-Vallejo, D., and Domınguez, J., *Study of the geometric stiffening effect: comparison of different formulations*, Multibody System Dynamics, Vol.11, 2004, pp.321–341.

[9] Bathe, K. J., and Bolourchi, S., *Large displacement analysis of three-dimensional beam structures*, International Journal for Numerical Methods in Engineering, Vol. 14, 1979, pp. 961–986.

[10] Bauchau, O.A., *Dymore User's Manual*, 2013, http://dymoresolutions.com/dymore4 0/UsersManual/UsersManual.html.

Paper B

Study on Controller Tuning of Wind Turbines with Backward Swept Blades

Authors:
Christian Pavese, Carlo Tibaldi, Taeseong Kim

Study on Controller Tuning of Wind Turbines with Backward Swept Blades

Christian Pavese[1], C. Tibaldi[1], Taeseong Kim[1]

Abstract

The objective of this study is to investigate the effects of backward swept blades on the dynamics of the controller of a wind turbine. When sweeping blades backward a coupling between flapwise bending toward the tower and torsion towards feathering is achieved. This coupling mitigates loads on the structure due to a decrease in the angle of attack. Changing the blade geometry can affect the behavior of the wind turbine controller. Hence, a detailed investigation of the effects generated by the blade sweep on the controller tuning is needed. Using the Basic DTU Wind Energy Controller, the aero-servo-elastic behavior of the 10 MW DTU Reference Wind Turbine (RWT) with swept blades is studied and considerations on the tuning of the controller are made in order to preserve and not compromise the dynamics of the system. This work focuses on understanding the interaction between the employment of backward swept blades and the dynamic behavior of the controller above rated wind speed. The purpose is to isolate loads variations due to the blade sweep from the loading differences brought by the controller's actions. This objective is achieved by re-tuning the controller of the wind turbine with swept blades according to the dynamics of the baseline regulator mode.

B.1   Introduction

As wind turbine capacities and dimensions increase, the necessity of reducing the costs of energy is a key concern for wind energy industries. The capability to mitigate loads on the structure maximizing wind yield and energy output, is central among the requirements. To this end, different techniques have been exploited in the last two decades to achieve load reduction on wind turbines,

---

[1]DTU Wind Energy, DK-4000, Roskilde, Denmark

and they can be generally categorized in two branches: active and passive control methods. The first consists of technologies able to reduce loads by actively controlling the machine e.g. blade pitch actuators and moving flaps. The second is based on the idea of designing a structure without any additional components that deforms so as to induce a load reduction when loaded.

Several studies, both numerical and experimental, were conducted to show the passive control potential of swept wind turbine blades. Larwood and Zuteck[1] use a 28 m blade model (STAR6) with 2.2 m of backward tip sweep to run aeroelastic simulations. Results are compared with a baseline 25 m straight-bladed turbine model. The swept rotor has a 25% wider area compared to the baseline in order to compensate the power loss below rated due to the sweep. The study shows that the swept-bladed turbine increases the amount of annual energy captured by 5-10%. The swept blade has similar or higher flapwise root bending moments than the original 25 m blade due to the coupling. Ashwill et al.[2] design, fabricate, and test a 27.1 m swept blade (STAR). They prove the capability of a sweep-adaptive blade to passively reduce operating loads. An increased production of energy is detected comparing the prototype to a baseline 23.5 m blade mounted on a 48 m diameter Zond 750 kW turbine. The new rotor shows an increase of 10-12% of the annual energy production without increasing the blade root bending moments. Verelst and Larsen[3] conduct a parametric study based on several swept blade configurations involving variations on both sweep curvature and sweep offset at the tip. The authors show that flapwise fatigue and extreme loads can be reduced up to 10 and 15% respectively for a backward swept blade, whereas the edgewise fatigue and extreme loads can increase by up to 6%. Verelst and Larsen also map the integrated pitch angle travel, registering a decrease of 10% in its activity for the Risø controller and an increase of 8% for the NREL controller. Hansen[4] investigates aeroelastic properties of backward swept blade using a linear model obtained from a nonlinear co-rotational finite beam element formulation coupled with the Blade Element Momentum method (BEM) including an unsteady aerodynamic model. He computes frequencies, damping, and mode shapes of the aeroelastic blade modes. Hansen concludes that the backward sweep creates torsion towards feathering for downwind flapwise deflection in the first flapwise bending mode. This torsional component is shown to cause the frequency of the first aeroelastic bending mode to increase compared to the corresponding structural frequency, and this increase is larger for larger sweep. Furthermore, Hansen finds that the frequency response of the flapwise blade root bending moment from wind excitation decreases below the increased first flapwise frequency. This drop of the flapwise blade root moment explains the reduced flapwise loads observed in other studies of backward swept blades.

Previous studies do not mention that a variation in the design of the rotor due to the introduction of swept blades affects the dynamics of the controller. Verelst and Larsen [3] collect information only on the traveled pitch angles. A more extensive analysis of the integration of passive and active load control is done by

Bottasso et al. [5]. A passive control method is implemented by exploiting the anisotropic properties of the blade layup by rotating the fibers away from the pitch axis. Integration of passive and active load control is studied using two different sets of gains of a cyclic pitch: the first has lower gains and moderate actuator duty cycle, whereas the second one has higher gains and more aggressive behavior. They conclude that the combination of passive and active methods leads to higher load reductions than one would obtain using separately only one of the two approaches. Effects on the dynamic behavior of the controller are not analyzed.

The purpose of this investigation is to offer a fair comparison between a baseline and passive-controlled wind turbines. This purpose can be achieved only if the load variations, estimated for the turbines with swept blades, are isolated from the influence of the controller. If the dynamic properties of the controller are the same for all the wind turbines benchmarked, a precise estimation of the load variations brought by the use of geometrical bend-twist coupling can be given. The aim of this study is to consider the effects of backward swept blades on the dynamics of the controller, highlighting how the dynamics of the mode that represents the controller are affected by variation of the geometrical properties of the blade. An analysis of the aeroelastic properties of the full wind turbine in closed loop is performed using a linear aero-servo-elastic model implemented in HAWCStab2[4] The interaction between the controller and the employment of backward swept blades, and the consequent effects on the dynamics of a wind turbine are discussed. Considerations on pole placement and tuning of the controller based on aero-servo-elastic modal analysis are presented.

DTU 10 MW RWT and the Basic DTU Wind Energy Controller are used as references. Results show that if the parameters of the controller are kept unchanged from the baseline, the regulator mode shows a variation in frequency and damping. The effects of using backward swept blades on the dynamics of the regulator are shown in this paper and controller tuning based on pole placement is implemented and discussed.

B.2   Model

In this investigation a linear and a nonlinear model are used. The linear aero-servo-elastic model implemented in HAWCStab2 for closed-loop eigenvalue analysis and the nonlinear aeroelastic model implemented in HAWC2 are used for response analysis in time domain. HAWCStab2 is based on a linearization of Timoshenko beam elements in a nonlinear co-rotational formulation coupled with an unsteady BEM method. Shed vorticity, dynamic stall and dynamic inflow are included in the aerodynamic model. A detailed description of the HAWCStab2 architecture is provided by Hansen[4]. Sønderby and Hansen[6] made an

exhaustive validation and analysis of the open-loop performances. A description of the linearized controller is given by Tibaldi et al.[7]. The structural model of HAWC2 is based on a multi-body formulation assembled using Timoshenko beam elements developed by Kim et al.[8]. The aerodynamic model, based also on a BEM method, handles dynamic inflow, dynamic stall, skew inflow, shear effects on the induction and effects from large deformation. Validation can be found in Vorpahl et al.[9], Popko et al.[10] and in Larsen et al.[11].

The DTU 10 MW RWT[12] is used as the baseline turbine in this study. Two different swept geometries are considered. Other properties of the turbine, such as structural properties, airfoil profiles, etc., are kept for the three configurations analyzed. The sweep geometries are described by a shape function similar to the one used by Verelst and Larsen[3] and Hansen[4]:

$$\mathbf{s} = \left\{ a\frac{z}{R_0} - b\left(\frac{z}{R_0}\right)^c, 0, z \right\}^T \quad z \in [0; R_0] \tag{B.1}$$

where s is the pitch axis as function of the blade length, z is the coordinate along the pitch axis of the blade, $R_0 = 89.166$ m is the blade length, a is a linear term for forward sweep added to compensate an otherwise large steady torque moment and b is the term for the backward sweep, which curve exponent is determined by c. Figure B.1 shows the x-coordinate of the pitch axis of the blade along the span for two different swept configurations. The parameters of Equation B.1 for the different blade shapes are:

- Swept Level 1 : $a = 5$, $b = 10$, $c = 2$

- Swept Level 2 : $a = 10$, $b = 20$, $c = 3$

The Basic DTU Wind Energy Controller[13] is used and its description with regard to the DTU 10 MW RWT is provided by Bak et al.[12]. In this work, the controller operates exclusively above rated wind speed, where power, torque and rotational speed are constant (Region 4). In this operational region a PI controller regulates the pitch angle, based on rotational speed measurements. HAWCStab2 is used to tune the PI controller using a method documented by Hansen et al.[14] and Tibaldi et al.[15]. In the closed-loop analysis described in this paper, the mode of the PI controller is called *speed regulator mode*. The rotational speed signal is filtered using a band stop notch filter and a second-order low pass filter. The poles of these two filters with respect to the DTU 10 MW RWT are reported by Hansen and Henriksen[13]. In the next section, discussion on the pole placement for the tuning of the PI controller is presented. These poles have to be distinguished from the poles of the rotational speed measurements filters, which are the same for all the wind turbine configurations benchmarked in this paper.
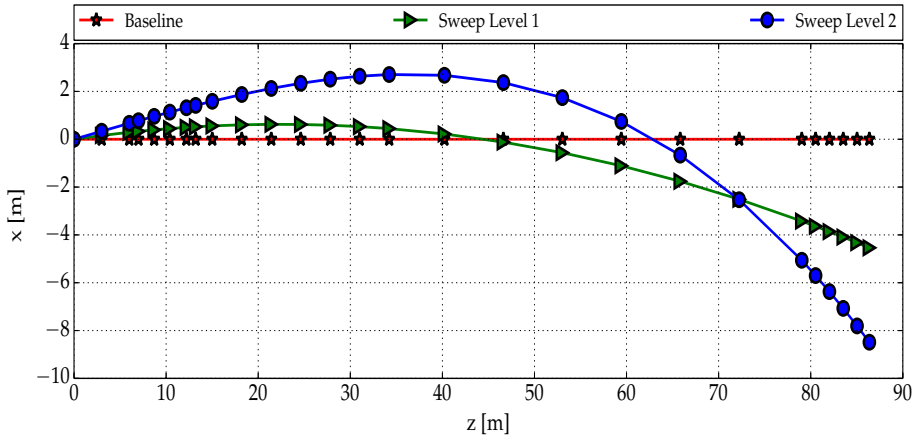
Figure B.1: Pitch axis coordinates for the baseline and the backward swept blades

The tuning of the PI controller is performed with a pole placement technique. This method requires selecting the a priori selection of the target frequency and a damping ratio of the speed regulator mode. The damping ratio is assigned to 70% for all the turbines benchmarked. The target frequency varies according to observation. More details are reported in the Results chapter.

B.3 Results

This section shows results from closed-loop analysis. First, the wind turbine aero-servo-elastic modes are analyzed. Following on from this, the investigation focuses on the regulator mode of the different wind turbine configurations studied. Finally, considerations on the controller tuning and pole placement of the regulator mode are made.

B.3.1 Closed-loop Wind Turbine Modes

Results are computed above rated wind speed where the action of the controller produces an effect on the turbine modes. Operational points are calculated for each of the benchmarked wind turbine.
Figure B.2 shows the first 11 aero-servo-elastic frequencies. The baseline model

(star symbol) is compared against the Level 2 swept configuration (circle). Only results for the most extreme swept shape, Level 2, are reported, since variations from the baseline are more pronounced and easier to spot than the differences registered for the mild case. However, the discrepancies of Level 1 frequencies with the baseline are qualitatively the same as to Level 2. Description of the modes can be found on the left part of the plot. Different colors help the association between descriptions and corresponding curves.

The first flapwise frequencies of Baseline and Level 2 show a different trends at $12 \mathrm{m\,s}^{-1}$ and $13 \mathrm{m\,s}^{-1}$. The difference is caused by the fact that the two configurations are using different operational points at $12 \mathrm{m\,s}^{-1}$ and $13 \mathrm{m\,s}^{-1}$. The backward sweep affects the first symmetric and the second asymmetric flapwise blade modes, drivetrain torsion and speed regulator mode more than tower, the first asymmetric flapwise and the first edgewise blade modes. The aero-servo-elastic frequencies of the first symmetric, the second backward and the second symmetric flapwise blade modes are increased when sweeping the blade, whereas the frequencies of the drivetrain torsion and the regulator mode decrease. An explanation concerning the differences reported for flapwise blade modes is given by Hansen[4]. The aerodynamic lift (which points mainly downwind) is reduced when the blades deflects toward the tower because of the structural coupling between torsion towards feathering and downwind flapwise deflection. Consequently, the lift acts as a stiffening restoring force. This results in increased aero-servo-elastic flapwise frequencies of the turbine with swept blades, as observed in Figure B.2. The modal frequencies of the drivetrain torsion mode of the swept configuration decrease compared to the baseline. Due to the change in geometry and the increase in length, the backward swept blade are heavier than the baseline. Therefore, the passive-controlled rotors have a higher inertia. The increase in rotor inertia justifies the drivetrain aero-servo-elastic frequency decreases.

Since the analysis focuses on the dynamics of the speed regulator mode, a detailed explanation of the differences in aero-servo-elastic frequencies of the tower, the first asymmetric flapwise and first edgewise blade modes will be the object of other more detailed studies.

Figure B.3 shows a comparison between the first 11 closed-loop aeroelastic modes dampings of the Baseline and the Level 2 sweep configuration. Damping ratios and modes are indicated in the same manner as in Figure B.2. Except for the flapwise blade modes and for the speed regulator mode, the damping of the wind turbine modes are almost unchanged by the sweep. The damping ratios of the regulator mode of the passive-controlled turbine increases close to the rated wind speed and decreases for high wind speeds. The damping ratios of the flapwise blade modes drastically decrease due to the sweep. As for the aeroelastic frequencies, a detailed explanation for the decreased damping of the flapwise modes is provided by Hansen[4]. For the Baseline, the torsional component of the flapwise blade modes is out of phase with the flapwise motion therefore adding to the damping. Wind turbines with backward swept blades

Figure B.2: Closed-loop frequencies of the aero-servo-elastic turbine modes as a function of the wind speed. Star: Baseline turbine modes . Circle: Passive-controlled (Sweep Level 2) turbine modes. Mode descriptions are labeled and distinguished by color.

have a torsional component of the flapwise blade modes around 180 degrees out of phase with the flapwise motion, therefore consistently reducing the effect of the torsional motion on the damping ratio of the flapwise blade modes.

The comparison between the aeroelastic frequencies and damping ratios of the speed regulator mode for the different configurations is discussed in detail in the next section.

B.3.2 Regulator Mode and Controller Tuning

The tuning of the PI collective pitch controller of the baseline wind turbine is performed using HAWCStab2. The gain-scheduling technique chosen, described by Tibaldi[15], assumes a quadratic variation of the partial derivatives of the
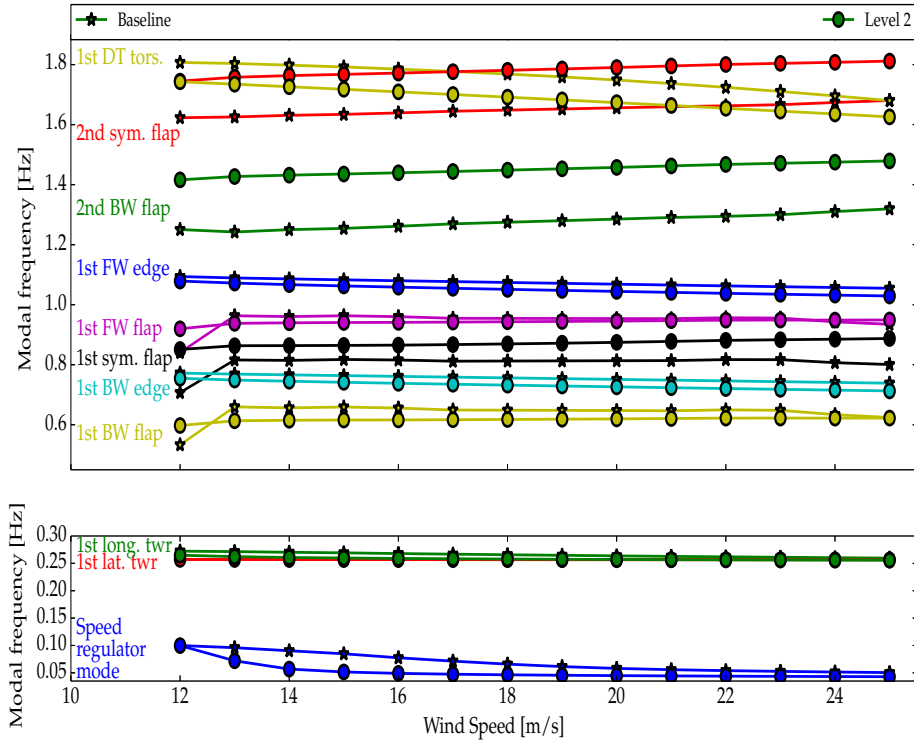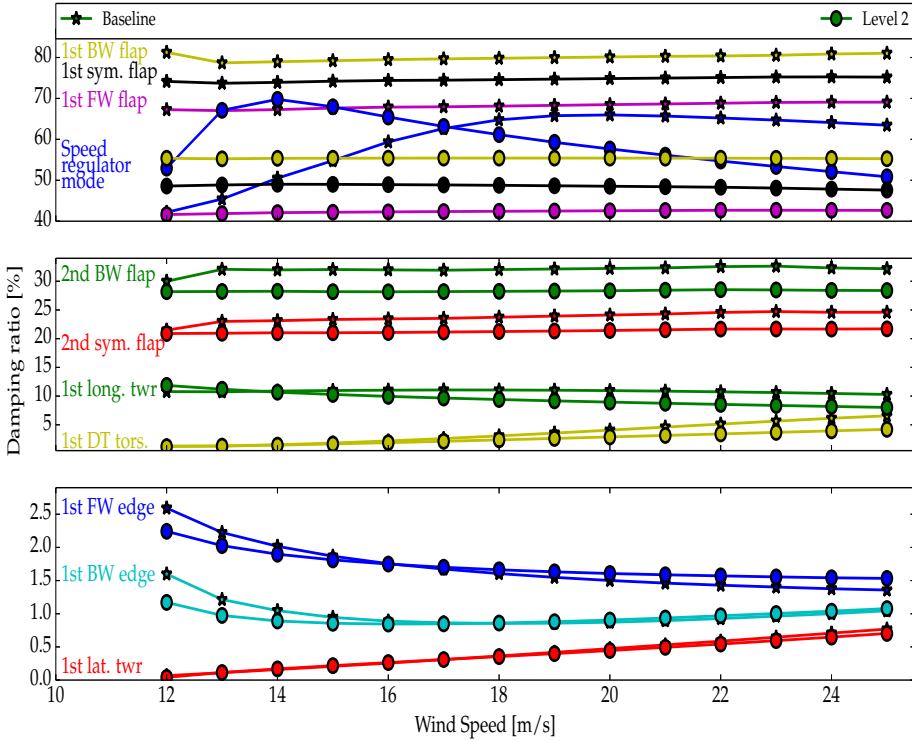
Figure B.3: Closed-loop damping ratios of the aero-servo-elastic turbine
modes as a function of the wind speed. Star: Baseline turbine
modes. Circle: Passive-controlled (Sweep Level 2) turbine modes.
Mode descriptions are labeled and distinguished by color.

aerodynamic torque with respect to the pitch angle (the so-called *aerodynamic gain*) and with respect to the rotor speed (the so-called *aerodynamic damping*).
The full load region poles are placed with the purpose of having, at rated wind speed, a regulator mode frequency of 0.1 Hz. The gains obtained tuning the baseline are initially also used for the other passive-controlled wind turbines.
Figure B.4 and Figure B.5 show respectively the modal frequencies and damping ratios of the regulator mode of the different configurations.
The baseline is denoted by a star symbol, while Sweep Level 1 and Sweep Level 2 are denoted by triangles and circles respectively. The three regulator modes start at 0.1 Hz. As the wind speed increases, the frequency of the regulator mode of the turbines with swept blades drops compared to the baseline. The effect, shown in Figure B.4, is increased for a larger sweep. The damping ratios of the regulator mode of the passive-controlled turbines increases close to the
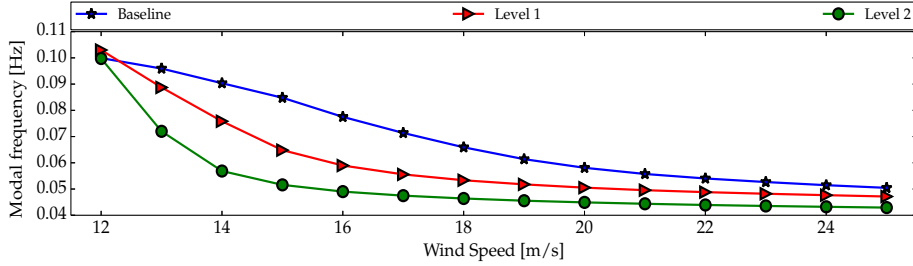
Figure B.4: Speed Regulator Mode frequency as a function of the wind speed. Star: Baseline regulator mode. Triangle: Sweep Level 1 configuration. Circle: Sweep Level 2 configuration - Baseline Controller Tuning.
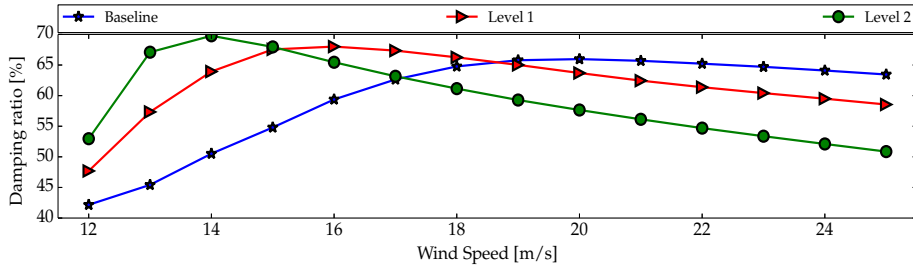
Figure B.5: Speed Regulator Mode damping as a function of the wind speed. Star: Baseline regulator mode. Triangle: Sweep Level 1 configuration. Circle: Sweep Level 2 configuration - Baseline Controller Tuning.

rated wind speed and decreases for high wind speeds. The explanation for the differences registered for the dynamic properties of the speed regulator mode lies in the aerodynamic gain and damping. The first, $\frac{\partial Q}{\partial \theta}$, is shown in Figure B.6, while the second, $\frac{\partial Q}{\partial \omega}$, is plotted in Figure B.7. Both partial derivatives are plotted with respect to the pitch angle. The higher the sweep level, the further is the difference in aerodynamic gains and damping from the baseline. These discrepancies are due to the variation of the pitch angle, which varies according to the amount of bend-twist coupling provided by different backward swept blade shapes. Because of the different aerodynamic gains and damping, the tuning process, done exclusively for the Baseline, has to be performed again for the passive-controlled wind turbines. In the next section, the gain scheduling technique used to tune the controller of the baseline is also performed for the wind turbines with swept blades. Results are discussed and observations on the pole placement are made.
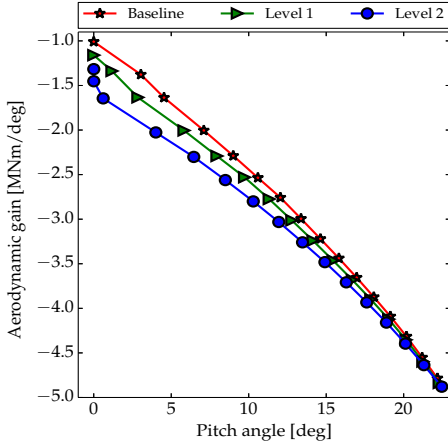
Figure B.6: Comparison of the aerodynamic gain of the different turbine configurations with respect to the pitch angle. Star: Baseline regulator mode. Triangle: Sweep Level 1 configuration. Circle: Sweep Level 2 configuration.
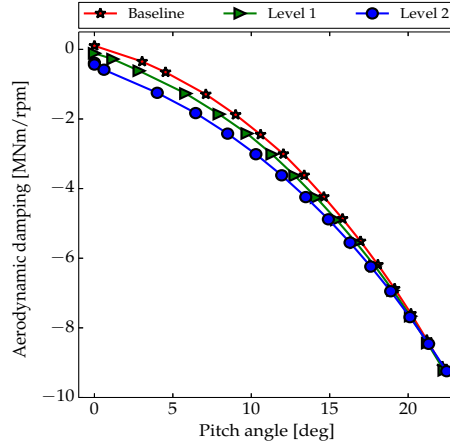
Figure B.7: Comparison of the aerodynamic damping of the different turbine configurations with respect to the pitch angle. Star: Baseline regulator mode. Triangle: Sweep Level 1 configuration. Circle: Sweep Level 2 configuration.

B.3.3   Pole Placement

Figure B.8 shows the frequency of the regulator mode for wind speeds above rated. The baseline and the passive-controlled wind turbine Sweep Level 1 regulator modes frequencies (star and triangle symbols respectively) are obtained with the gains reported for the DTU 10 MW RWT. For Sweep Level 1 Tuned configuration regulator mode frequencies (circle), HAWCStab2 is used to re-tune the controller. Poles are placed at the same frequency used for the baseline model. Finally, the regulator mode of the passive-controlled wind turbine is computed with a re-tuned controller and the pole placed in order to obtain a regulator mode frequency of 0.1 Hz at rated wind speed (frequencies denoted with the square symbol).

As mentioned in the previous section, the necessity of re-tuning for the swept configurations arises from the discrepancies registered in the aerodynamic gain and damping. As shown in Figure B.8, Level 1 Tuned (green circles) has a slope

Figure B.8: Comparison of Speed Regulator Mode frequencies as a function of the wind speed. Modes are computed varying the controller tuning. Star: Baseline frequencies. Triangle: Sweep Level 1 configuration with baseline tuning. Circle: Sweep Level 1 configuration re-tuned with HAWCStab2. Square: Sweep Level 1 configuration tuned with HAWCStab2 using a different pole placement.

closer to the Baseline (blue stars) than the swept configuration with baseline controller tuning (red triangles) for low wind speeds (12-16 $m\,s^{-1}$). Nonetheless, the aim is to obtain a regulator mode with dynamic behavior similar to the baseline. If the frequencies of the regulator mode of the various wind turbines analyzed are close, the controller has a similar impact on the dynamics of the full system. The result is a fair benchmarking that allows a more precise estimation of the load variations due to the employment of backward swept blades. Hence, the target frequency for the tuning of the PI controller is changed in order to obtain modal frequencies closer to the baseline (yellow squares).

Figure B.9 shows the regulator mode damping ratios. When the swept configuration controller is tuned to assign a frequency of 0.1 Hz and a damping ratio of 0.7 to the regulated pole, the damping ratios of the regulator mode match the baseline for low wind speeds. If the wind speed increases, the differences between the baseline and the re-tuned configuration with new poles are larger.

If the passive-controlled configuration controller is tuned using the described gain scheduling technique and the poles are placed accordingly, the discrepancies on the dynamic properties of the speed regulator mode are partially eliminated, as shown by Figure B.8 and Figure B.9. Still, relevant differences can be observed when the wind speed increases further away from the rated wind speed. The differences at high wind speeds are due to the gain scheduling technique used. A tuning method based only the aerodynamic gain and damping cannot accurately reproduce the behavior of the baseline controller for all the wind speeds.
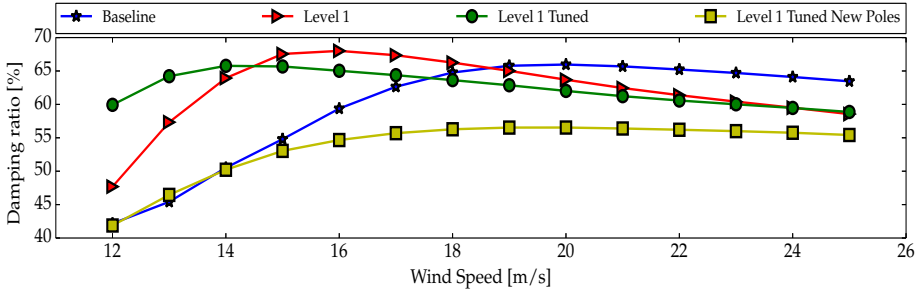
Figure B.9: Comparison of Speed Regulator Mode damping as a function of
the wind speed. Modes are computed varying the controller tun-
ing. Star: Baseline frequencies. Triangle: Sweep Level 1 configu-
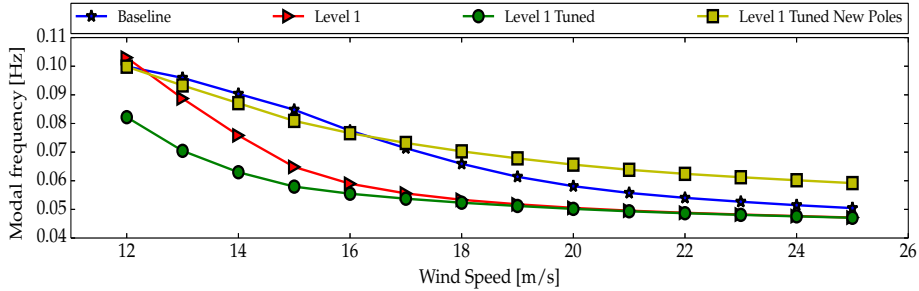ration with baseline tuning. Circle: Sweep Level 1 configuration
re-tuned with HAWCStab2. Square: Sweep Level 1 configuration
tuned with HAWCStab2 using a different pole placement.

B.3.4   Step Response

In this section, the full wind turbine dynamic response to a wind speed step
is computed using the high order nonlinear model. The baseline configuration
is compared with the Sweep Level 1 model, where the controller tuning is set
according to the considerations made in the previous section. Hence, for the
Level 1 turbine, aero-servo-elastic simulations are run taking into account the
following cases:

- Controller tuned on Baseline configuration

- Controller tuned on swept configuration, changing target frequency of the
  pole placement accordingly

Figure B.10 shows the wind step responses of the rotational speed (above)
and tower base fore-aft bending moment (below) for the configurations listed
above. Different settings of the controller parameters clearly affect the rota-
tional speed dynamics of the swept configurations in time domain. Re-tuning
the controller and varying the target frequency of the pole placement to face
the changes in structural properties brought by the employment of backward
swept blades is a necessary step to obtain controller dynamics close to the
ones defined for the baseline. In Figure B.10, the step response of Sweep
Level 1 Tuned with new poles (yellow line) at 14 m s^{-1} is closer to the baseline
compared to the other case. In fact, the frequency and the damping ratio of
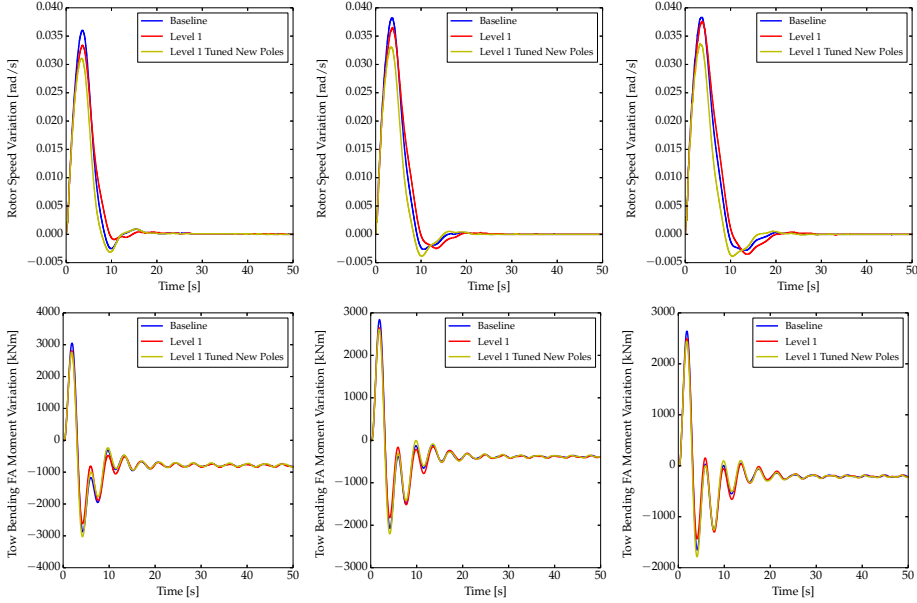
Figure B.10: Rotor speed (above) and tower base fore-aft bending moment variations (below) due to a wind speed step. Three wind steps performed at respectively 14 m s^{-1} (left plots), 18 m s^{-1} (center plots), 22 m s^{-1} (right plots). Comparison between: Baseline (blue line), swept blades turbine with baseline tuning (red line), swept blades turbine with tuned controller and ad hoc pole placement (yellow line).

Sweep Level 1 Tuned New Poles regulator mode at 14 m s^{-1} match the baseline values, as shown previously in Figure B.8 and B.9. As the differences between the regulator mode cases increase, the dynamic response of the rotational speed of Level 1 Tuned New Poles shows more discrepancies. Moreover, the uppermost plots of Figure B.10 show that the Baseline and Level 1 have the same dynamic behavior at high wind speeds (both 18 m s^{-1} and 22 m s^{-1}). In fact, frequencies and damping ratios of the passive-controlled configuration with baseline tuning are closer to the baseline than Sweep Level 1 Tuned with new poles, as shown in Figure B.8 and B.9. The amplitude of the step responses of Level 1 and Level 1 Tuned New Poles are slightly lower compared to Baseline. The differences between the maximum values are caused by the variation of the aerodynamic torque, which has a different dynamic behavior due to the blades sweep. The tuning of the controller affects the overshoot, as shown in the top plots of Figure B.10.

The tower base fore-aft bending moment is also affected by the choice of tuning

parameters. Three plots on the second line of Figure B.10 show the variation of tower base fore-aft bending moment due to a wind speed step for the different wind turbine configurations. The case with tuned controller and re-placed poles is close to the dynamic performance of the baseline, even though all the passive-controlled configurations show a very similar behavior. The small discrepancies registered for the maximum values of Level 1 and Level 1 Tuned New Poles with respect to Baseline can be explained with the different dynamic response of the aerodynamic thrust, which is affected by the use of backward swept blades. As previously observed for the rotor speed variation, the controller tuning has an effect on the amplitude of the overshoot of the tower bending fore-aft moment. When performing a benchmarking between turbines with passive control, it is important to properly select the procedure for tuning the controller, since the regulator mode performance has an effect on the overall dynamic response of the system. To provide a proper evaluation of the load variations brought by the passive control, the effects of the use of backward swept blades need to be separated from the influence of the controller. This can be achieved by ensuring that the dynamic properties of controllers of the benchmarked wind turbines are similar.

B.4 Conclusions

The effects of backward swept blades for wind turbine passive control on the dynamic behavior of the PI controller has been investigated. A linear aero-servo-elastic model provided closed-loop modal analysis to estimate the interaction between the regulator mode and the dynamics of wind turbines with swept blades. The modal analysis highlighted the impact of the dynamics of the controller and its tuning. Results showed that the frequencies and damping ratios of the speed regulator mode of a passive-controlled wind turbine are significantly different compared to a baseline. The discrepancies in aero-servo-elastic properties of the regulator mode of turbines with swept blades are due to differences in the aerodynamic gain and damping. Hence, the controller of the swept blades turbines needs to be re-tuned and the target frequency of the pole placement for the tuning needs to be changed. A high order nonlinear model has been used to compute step responses. The dynamic response of the controller of the turbines with swept blades and the baseline are closer for low wind speeds. Nevertheless, the gain scheduling technique used cannot guarantee that the frequencies and damping ratios of the regulator mode at high wind speeds match the baseline values.

Acknowledgments

Bibliography

[1] Larwood, S. and Zuteck, M., *Swept Wind Turbine Blade Aeroelastic Modeling for loads and dynamic behavior*, Windpower 2006, p.17, Pittsburgh, 4-7 June 2006.

[2] Ashwill, T. D., Kanaby, G., Jackson, K., and Zuteck, M, *Development of the swept twist adaptive rotor (STAR) blade*, Proceedings of the 48th AIAA Aerospace Sciences Meeting, 4-7 January 2010, Orlando, Florida

[3] Verelst, D.R.S. and Larsen, T.J., *Load consequences when sweeping blades - a case study of a 5 MW pitch controlled wind turbine*, Technical Report Risø-R-1724, Risø-DTU, May 2010, Roskilde

[4] Hansen, M. H., *Aeroelastic properties of backward swept blades*, Proceedings of the 49th AIAA Aerospace Sciences Meeting, 4-7 January 2011, Orlando, Florida

[5] Bottasso, C. L., Campagnolo, F., Croce, A. and Tibaldi, C. *Optimization-based study of bend-twist coupled rotor blades for passive and integrated passive/active load alleviation*, Journal of Wind Energy, 2013; 16:1149-1166. DOI:10.1002/we.1543

[6] Sønderby, I and Hansen, M.H., *Open-loop frequency response analysis of a wind turbine using high-order linear aeroelastic model*, Journal of Wind Energy, 2013, DOI: 10.1002/we.1624

[7] Tibaldi, C., Henriksen, L.C., Hansen, M.H. and Bak, C. *Wind turbine fatigue damage evaluation based on a linear model and a spectral method*, Under Review, 2014

[8] Kim, T., Hansen, A.M. and Branner, K., *Development of an anisotropic beam finite element for composite wind turbine blades in multibody system*, Journal of Renewable Energy, 2013; 59:172-183, doi:10.1016/j.renene.2013.03.033

[9] Vorpahl, F., Strobel, M., Jonkman, J.M., Larsen, T.J. and Passon, P., *Verification of aeroelastic offshore wind turbine design codes under IEA wind task XXIII*, Journal of Wind Energy, 2013; doi:10.1002/we.1588

[10] Popko, W., Vorpahl, F., Zuga, A., Kohlmeier, M., Jonkman, J., Robertson, A., Larsen, T.J., Yde, A., Stertr, K., Okstad, K.M., et al., *Offshore code comparison collaboration continuation (OC4), PHASE I - results of coupled simulations of an offshore wind turbine with jacket support structure*, Proceedings pf the International Offshore and Polar Engineering Conference 2012, 2012;337-346

[11] Larsen, T.J., Aagard Madsen, H., Larsen, G.C. and Hansen, K.S., *Validation of the dynamic wake meander model for loads and power production in the Egmond Aan Zee wind farm*, Journal of Wind Energy, 2013, 2013;16(4):605-624, doi:10.1002/we.1563

[12] Bak, C., Zahle, F., Bitsche, R., Kim, T., Yde, A., Henriksen, L.C., Natarajan, A. and Hansen, M.H., *Description of the DTU 10 MW Reference Wind Turbine*, DTU Wind Energy Report-I-0092, July 2013, Roskilde, Denmark

[13] Hansen, M.H. and Henriksen, L.C.,*Basic DTU Wind Energy Controller*, Technical Report DTU Wind Energy E-0018, DTU, 2013

[14] Hansen, M.H., Larsen, T.J., Øye, S., Sørensen and Fuglsang, P., *Control Design for a pitch-regulated, variable speed wind turbine*, Technical Report Risø-R-1500(EN), Risø National Laboratory, Roskilde, Denmark, 2005

[15] Tibaldi, C., Henriksen, L.C., Hansen, M.H. and Bak, C.*Effects of gain-scheduling methods in a classical wind turbine controller on wind turbine aeroservoelastic modes and loads*, Proceedings of the 52th AIAA Aerospace Sciences Meeting, 12-17 January 2014, National Harbor, Maryland

PAPER C

Design of a Wind Turbine Swept Blade Through Extensive Load Analysis

Authors:
Christian Pavese, Taeseong Kim, Juan Pablo Murcia

Design of a Wind Turbine Swept Blade Through Extensive Load Analysis

Christian Pavese[1], Taeseong Kim[1],Juan Pablo Murcia[1]

Abstract

The main focus of this work is to offer an extensive investigation regarding the use of backward swept blades for passive load alleviation on wind turbines. Sweeping blades backward produces a structural coupling between flapwise bending towards the tower and torsion towards feathering. This coupling mitigates loads on the wind turbine structure due to a decrease in the angle of attack. The load alleviation can be achieved by changing the blade geometry according to three parameters: starting point for the change of shape along the blade span, blade tip sweep, and blade forward sweep. A parametric study is carried out on a 10 MW wind turbine with the purpose of outlining the relation between load variations and three geometric parameters used to introduce passive control on wind turbine blades. The objective is to estimate and analyze extreme and fatigue loads, formulating suggestions for the design of a wind turbine that employs backward swept blades. From the investigation, it is concluded that mildly and purely backward swept shapes are the best option because they allow the wind turbine to achieve load alleviations without a large increase of the blade root torsional extreme and life-time equivalent fatigue moment. The efficacy of the design procedure provided with this work is proved through its application on a 5 MW wind turbine design.

C.1 Introduction

Reducing the cost of energy is a key concern for wind energy research and the ultimate goal for both academia and industry. An effective path to achieve this goal is to manufacture components that are lighter as the wind turbines capacities and dimensions increase [1]. According to "The Economics of Wind

---

[1]DTU Wind Energy, DK-4000, Roskilde, Denmark

Energy" [2], the rotor blades of a 5 MW onshore wind turbine contribute to the overall turbine cost with a share between 20 and 25%. For this reason, blade manufactures have taken up the challenge to scale down the increase in total mass of the blades, when designing and manufacturing rotors with increasing energy yield. In this context, the capability to mitigate loads on the structure during operation becomes an attractive characteristic for the design of modern wind turbine blades [3]. To this end, different techniques have been exploited in the last two decades to achieve load reduction on wind turbines, and they can be generally categorized in two branches: active and passive control methods. The first consists of technologies able to reduce loads by actively controlling the machine, e.g. blade pitch actuators [4], moving flaps [5], etc. The second is based on the idea of designing a structure that, without any additional components, deforms so as to induce a load reduction when it is loaded [6]. The work presented in this paper focuses only on passive control methodologies and, in particular, on the employment of swept blades. Sweeping blades backwards is considered a load alleviation technique. This methodology produces a structural coupling between flapwise bending towards the tower and torsion towards feathering. This coupling mitigates loads on the wind turbine structure due to a decrease in the angle of attack. Opposite effect is obtained sweeping the blade forward. For this reason, purely forward swept shapes are not taken into account in this work.

In the last two decades, several studies, both numerical and experimental, were conducted to show the potential of swept blades. The most complete study on the subject is called Sweep-Twist Adaptive Rotor Blade (STAR) and it was conducted by the Knight & Craver Wind Group in the SANDIA National Laboratories between 2004 and 2010 [7, 8, 9]. The project started after two feasibility studies: one by Ashwill et al. [10] and the other by Zuteck [11]. The STAR constitutes a complete study for swept blades involving aeroelastic simulations, manufacturing, and testing. The project showed that a swept-bladed turbine, with a wider rotor area compared to a straight-bladed baseline, increases the amount of annual energy captured undergoing similar or higher flapwise root bending moments. The implementation of this passive control methods and their potential on multi-mega watt wind turbines was not investigated. Parametric and conceptual studies were carried, but a full overview of the relation between different geometric parameters for the blade planform shape and load alleviations is missing. On a final note, the project cannot provide a "fair" comparison between the swept-bladed turbine and the baseline machine because of the substantial difference in rotor diameter and blade aeroelastic properties.

A detailed parametric study involving geometric parameters for swept blades was conducted by Verelst and Larsen [12]. This study is based on several swept blade configurations involving variations on both sweep curvature and sweep offset at the tip. The authors showed that flapwise fatigue and extreme loads can be reduced up to 10% and 15%, respectively, for a backward swept blade, whereas the edgewise fatigue and extreme loads can increase up to 6%. Verelst

and Larsen also mapped the blade root torsional moment, which registered an increase up to 400%. This parametric study is based on a simple load case (10-minute time series with fixed turbulence intensity of 0.18 and no wind shear), and it does not consider a full design load basis (DLB). Consequently, the work can provide only a rough estimation of load variations brought by the employment of swept blades. Instead, a load analysis based on full a DLB would have allowed observations focused on standard requirements for wind turbine design. Furthermore, Verelst and Larsen do not apply any method to compensate the loss in AEP below rated wind speed, and they do not take into account the interaction between the employment of swept blades and the dynamics of the pitch controller.

Hansen [13] investigated aeroelastic properties of backward swept blades, computing frequencies, damping, and mode shapes of the aeroelastic blade modes. The aeroelastic properties of backward swept blades were deeply investigated, but only a quality estimation of the load alleviations brought by the employment of geometric bend-twist coupling is provided.

Previous studies proved the potential for load alleviation of wind turbines that employ backward swept blades. The focus of the current numerical study is to investigate the design of swept blades through an extensive load analysis based on standard requirements for wind turbines construction and operation. The changes in blade geometry are classified through three parameters: location of the first control point of the Bezier polynomial used to implement the swept shapes, maximum blade tip backward sweep, and blade forward sweep. To ensure a "fair" comparison based on passive-controlled wind turbines with similar AEP and controller dynamics comparable to the baseline, the first part of this study is a pre-processing phase involving aero-servo-elastic modal analysis for controller tuning and aerodynamic twist optimization. Subsequently, a DLB is carried with the purpose of obtaining extreme and fatigue loads used for a realistic wind turbine design. The trends associated to the loading due to the variation of each geometric parameter are analyzed. The general observations provided are applied to the NREL 5 MW RWT [14] to prove the efficacy of the proposed extensive-load-analysis approach.

In the paper, the first section describes the parametric study architecture including details of the geometric parameters used and the workflow that each blade design is subject to. An extensive load analysis and a discussion of the results obtained through the parametric study follows in the next section. The last part of the paper is the application of the outcome of the parametric study on a different blade design, specifically, the blade of the NREL 5 MW RWT.

C.2 Parametric Study Architecture

This section shows the architecture of the parametric study, starting with a description of the different blade geometries considered. A detailed explanation of the models used is provided. At last, a description of the workflow and the DLB used are reported.

C.2.1 Swept Blades Shapes and Geometric Parameters

The blade shapes are obtained using Bezier polynomials [15], which provide the necessary flexibility to obtain the desired backward swept geometries. The control points for the polynomials are placed to avoid curves with very large sweep angles.

Three parameters are selected to describe the shape of the swept blades. Each of these parameters is associated to a letter (s, b or f) and a sequence of numbers having three (in this case, all three digits represent the integer part of the number) or four digits (three digits for the integer part and one for the fractional). The cataloguing system helps the classification of each blade shape, which can be described through a mix of three letters and three numbers representing the combination of the three parameters. The parameters are described as follows:

- *sxxx*: location of the first control point on the centerline; it roughly describes the spanwise length where the sweep starts;

- *bxxxx*: backward sweep at the tip in percentage of the total blade length;

- *fxxxx*: maximum forward sweep in percentage of the total blade length.

For example, the swept blade classified as *s080-b0025-f0005* has a shape where the sweep starts approximately at 80% of the blade length from the blade root, the backward sweep at the tip is 2.5%, and the maximum forward sweep is 0.5% of the total blade length.

The parametric study involves a total of 25 blade geometries, divided according to the spanwise location where the first control point for the polynomial is placed. The considered swept shapes are listed as follows:

- Family 1, the first control point for the Bezier function is placed on the pitch axis at 25% of the total blade length from the blade root;

- Family 2, the first control point for the Bezier function is placed on the pitch axis at 50% of the total blade length from the blade root;

- Family 3, the first control point for the Bezier function is placed on the pitch axis at 80% of the total blade length from the blade root;

- Family 4, the first control point for the Bezier function is placed on the pitch axis at 90% of the total blade length from the blade root;

- Family 5, the shapes are characterized by a different location of the maximum forward sweep along the blade span.

The only exception is the last family of shapes (Family 5), where the geometries are selected varying the location of the maximum forward swept part. Family 5 is included in the study to investigate whether the location of the maximum forward sweep has an influence on the variation of the blade root torsional moment.

Figure C.1 shows a sample of shapes that belongs to the Family 1, where the x-coordinate of the centerline are specified according to the coordinate system defined in the aeroelastic software HAWC2 [16].

C.2.2   Numerical Tools and Models Descriptions

In this work, linear and nonlinear models are implemented. Linear models are used in the pre-processing phase for the tuning of the controller of the swept-bladed wind turbines, and for the aerodynamic twist optimization needed to compensate the loss in AEP (see the next section for detailed explanations). The nonlinear models are used to perform the extensive load analysis that represents the core of the study.

Specifically, linear models are implemented in HAWCStab2 [17] and used for both closed-loop aero-servo-elastic eigenvalue analysis and aerodynamic twist
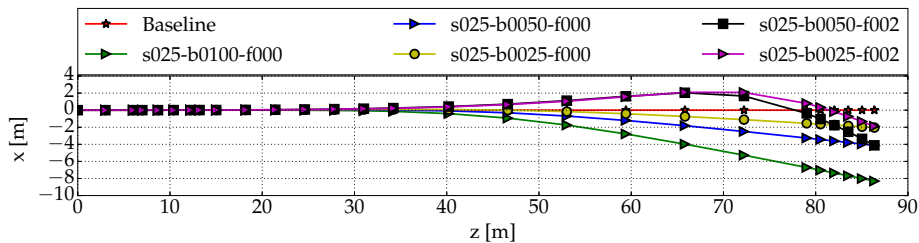

Figure C.1: Backward swept shapes of Family 1. z is the coordinate along the blade centerline, whereas x is the coordinate oriented in the edgewise direction. The first control point is located at 25% span of the total blade length.

optimization. The latter is carried out in the multi-disciplinary wind turbine analysis and optimization tool HAWTOpt2 [18, 19, 20, 21]. A detailed description of the HAWCStab2 architecture is provided by Hansen [13], and its validation can be found in [22]. A full description of the HAWTOpt2 framework and its application on aeroelastic optimization of a wind turbine is provided in [23]. The nonlinear models are implemented in the time-domain aero-servo-elastic code HAWC2 [16]. The description and the validation of the multi-body formulation used by the structural part of HAWC2 are reported in [24]. The validation of the unsteady BEM method used by the program can be found in [25, 26, 27]. The DTU 10 MW RWT [28] coupled with the Basic DTU Wind Energy Controller [29] are used as the baseline turbine.

C.2.3 Workflow and Simulations Set-Up

Two negative effects are associated with backward swept blades:

- due to the geometric structural coupling, turbines with backward swept blades have a lower AEP compared to a turbine with a straight-bladed rotor because of the decrease in the angle of attack along the blade span during operation [30];

- due to the changes in the structural and aerodynamic response of the blade, i.e. bend-twist coupling effect and change in the angles of attack, respectively, frequencies and damping ratios of the speed regulator mode of turbines with swept blades are significantly different compared to a baseline with straight blades [31].

Each blade design is pre-processed to overcome these two undesired outcomes. To compensate the loss of AEP below rated wind speed, the aerodynamic twist of each blade design selected is optimized using the HAWTOpt2 framework. The numerical optimization problem is defined as:

$$\begin{aligned} \max_{\mathbf{x}_p(\beta)} \quad & f(\mathbf{x}_p(\beta), \mathbf{p}) \\ \text{s.t.} \quad & \mathbf{g}(\mathbf{x}_p(\beta)) \leq \mathbf{0} \end{aligned} \tag{C.1}$$

The cost function f depends on a set of variable $\mathbf{x}_p(\beta)$ and a set of constant parameters $\mathbf{p}$. For this simple optimization, the design variables are exclusively the parameters that describe the aerodynamic twist of the blade β. A free form deformation spline (FFD) with 5 control points is used to parametrize the aerodynamic twist as a design variable. The parameters $\mathbf{p}$, including the blade planform, the layups of the blades, and the other components of the wind

turbine, are kept constant throughout the optimization. The design variables are normalized, such that when they are equal to zero they correspond to the baseline value.

The cost function, defined in Equation C.2, is subject to a set of nonlinear constraints **g**.

$$f(\mathbf{x}_p(\beta), \mathbf{p}) = \frac{AEP(\mathbf{0}, \mathbf{p})}{AEP(\mathbf{x}_p(\beta), \mathbf{p})} \tag{C.2}$$

$AEP(\mathbf{0}, \mathbf{p})$ is the annual energy production of the baseline design.
The constraints **g** include:

- the rotor thrust, so that the swept-bladed turbines cannot exceed the operational rotor thrust of the baseline;

- the operational lift coefficients that, along the blade span, are limited to avoid stall.

To face the second constraint, after the optimization loop, the controller of the turbines with swept blades is tuned. The tuning of the PI loop of the controller in Region 4 (constant power, torque, and rotational speed) is performed with a pole placement technique. HAWCStab2 is used to perform this tuning adopting a method documented in [32] and [33]. The target damping ratio and the target frequency for the pole of the speed regulator mode at $12 \mathrm{m\,s^{-1}}$ are 70% and 0.1Hz, respectively, for all the wind turbines that take part to the parametric study. The frequency of the pole placement for the tuning is changed according to a procedure reported by the authors [31].

A description of the workflow is shown in Figure C.2. On the left side of the figure, the tools and a summary of each step of the process are reported. On the right side, a description of the optimization loop explained above is shown.

Simulating the DTU DLB [34] for the design chosen is the last step of the parametric study workflow. The DTU 10 MW RWT was designed based on the IEC 61400-1 load basis [35], disregarding the controller dependent load cases. Therefore, the following modifications are made to the DTU DLB to have a load basis similar to the one used to design the baseline turbine:

- the controller dependent design load case DLC 2.2 is disregarded;

- the extreme values of the loading from DLC 1.1 are not determined using any statistical extrapolation because of the uncertainty related to the choice of an appropriate method; instead, the GL approach [36], which requires a partial safety factor of 1.35, is adopted.

Finally, a load analysis for each wind turbine configuration is carried. Extreme and life-time equivalent fatigue loads (LTEFL) for the blade root are analyzed,
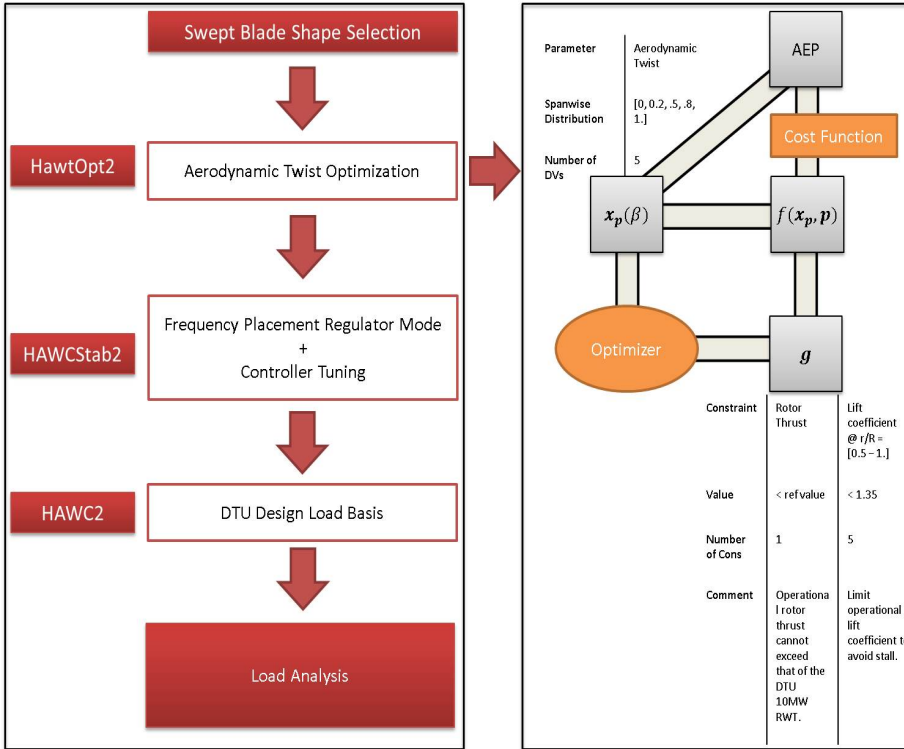
Figure C.2: Description of the workflow. The tools and a summary of each step of the workflow are listed on the left side of the figure. On the right side, the optimization loop for the aerodynamic twist is shown.

along with AEP and tower clearance. The trends associated with the variation of each of the geometric parameters are discussed in the next section, and conclusions on the design of backward swept blades are outlined.

C.3   Load Analysis Results

Numerical results from the load analysis depending on the swept geometries are reported and discussed in this section. In the first part of the section, the blade root extreme and fatigue loads are analyzed, with the purpose of investigating the impact of each geometric parameter of a swept blade. In the second part, AEP and tower clearance are analyzed.

C.3.1 Effects of the Location of the First Control Point, Parameter "sxxx"

The first geometric parameter analyzed is the first control point location along the centerline. This parameter is associated to the location along the blade span where the centerline shape starts to change. To examine the impact of this parameter on the extreme loading, the blades with the tip swept backward by 2.5% of the total blade length, *b0025*, and with no forward sweep, *f0000*, are taken into account. Four backward swept blades are considered: *s025-b0025-f0000*, *s050-b0025-f0000*, *s080-b0025-f0000*, and *s090-b0025-f0000*. The blade centerline of each design chosen is shown in Figure C.3.

Figure C.4 shows the normalized absolute maximum blade root bending moment distributions in the blade flapwise (left plot), edgewise (center plot), and torsional (right plot) direction, respectively. The distributions, shown in boxplots, include all the time-series considered in the DLB. To facilitate the comparisons, the loads are non-dimensionalized by the median of the respective baseline distribution. The lower edge of the blue box represents the first quartile, whereas the upper edge is the third quartile. The whiskers delimit the 5th and the 95th percentiles, respectively. Blue crosses are the outliers. The width of the blue box (the interquartile range, IQR), the location of the whiskers (1.8*IQR), and the spread of the outliers give an estimation of the statistical dispersion of the distribution. The uppermost values, highlighted with a green dashed line in Figure C.4, are the ultimate loads. The trend of these loads depends on the geometry of the blade selected. However, the ultimate loads are extracted from a single time-series, referring to a single point in the distribution shown in Figure C.4. Hence, a comparison between ultimate loads from different designs is deterministic, and it does not take into account the stochastic nature of the turbulent load cases. For example, it is not possible to establish whether the variation on the ultimate loads is caused by the change in blade geometry or the fact that the rotor sees a different turbulence field due to the changed struc-
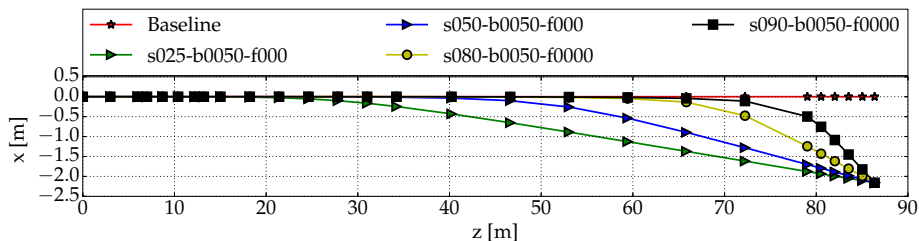

Figure C.3: The four backward blade shapes chosen to study the location of the first control point parameter.

tural and aerodynamic responses or due to tuning of the controller. Therefore in this study, the analysis of the extreme loads is based on the comparison of distributions of the absolute maxima instead of the ultimate loads. Specifically, the extreme load analysis focuses on:

- the medians, which retain information concerning the probability of a certain design having higher or lower absolute maxima across the DLB compared to the baseline;

- the IQR, which provides information on the variability of the absolute maxima across the DLB.

In Figure C.4, the median of the distribution is highlighted in red. The trend of the medians is described by a black dashed line.

One can notice the differences between the trend of the ultimate loads and the trend of the medians, especially for the extreme torsional blade root moment. To have a clear view on the medians, the boxes of the absolute maxima distribution are zoomed and reported in the bottom part of Figure C.4.

The "aggressive" shapes, i.e. with a change in geometry closer to the root (*s025-b0025-f000* or *s050-b0025-f000*), have a higher flapwise load alleviation potential because a larger portion of the blade is affected by the change in geometry resulting in the bend-twist coupling. The median and the IQR of the flapwise blade root moments decreases for the *s025-b0050-f0000* and *s050-b0050-f0000*, but it gets closer to the baseline for the shapes that have the first control point close to the blade tip (see Figure C.4, left plot). The decrease in IQR for the absolute maxima of the flapwise moment proves that the backward swept blades are able to reduce the peaks of the extreme blade root flapwise loads.

The median and the IQR of the distributions of the blade root edgewise moment are not significantly changed compared to the baseline (see Figure C.4, central plot). Furthermore, the variations of the medians in the edgewise direction are lower in value compared to the variations of the medians in the flapwise direction (compare bottom central and left plots of Figure C.4). Therefore, the variation of the first control point location parameter does not affect the blade root edgewise extreme loads.

As already shown in previous studies [9, 12], "aggressive" blade sweeps introduce the largest extreme blade root torsional moments. This effect is clearly shown in the right plot of Figure C.4: the medians and the IQRs are getting larger for more "aggressive" swept blades compared to the baseline. The first control point location parameter has a consistent influence on the blade root torsional extreme loads. Different conclusions can be drawn looking at the ultimate torsional loads, where the most "aggressive" shape (*s050-b0025-f000*) has the lowest ultimate torsional load. The latter observation highlights the importance of comparing

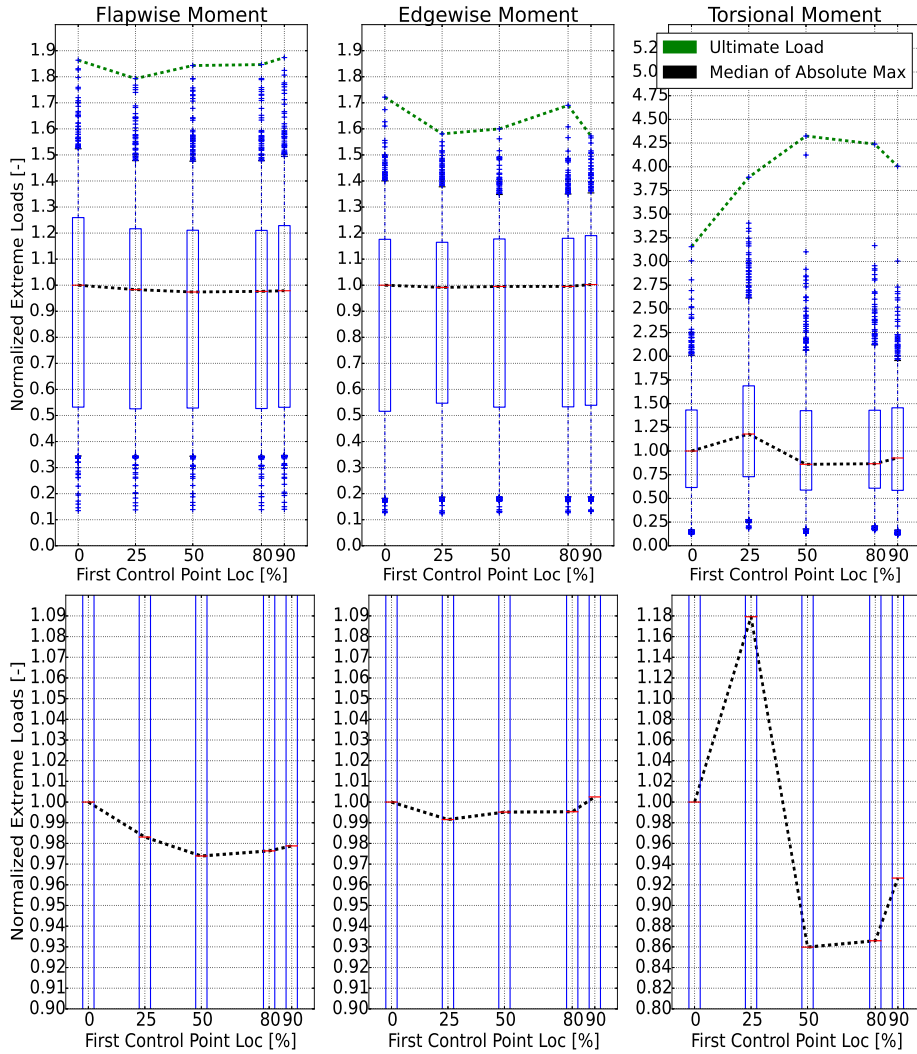**Figure C.4:** Normalized absolute maxima distributions for baseline and swept
blades with ascending first control point location along the blade
span. Extreme flapwise, edgewise, and torsional moments are
plotted on the left, center, and right, respectively. Bottom plots
show a close-up on the medians of the distributions. The loads
are non-dimensionalized by the median of the respective baseline
distribution.

extreme loads distribution instead of analyzing ultimate loads.

To investigate the impact of the parameter "sxxx" on LTEFL, a different set of four backward swept blades, with the blade tip swept backward is fixed at 5.0 %, is considered (see Figure C.5): *s025-b0050-f0000*, *s050-b0050-f0000*, *s080-b0050-f0000*, and *s090-b0050-f0000*. In this study, the computation of the life time equivalent fatigue loads is based on a life-time of 20 years.

Figure C.6 shows the LTEF blade root moments in the flapwise, edgewise, and torsional direction for the considered blade shapes shown in Figure C.5. The flapwise LTEFLs (blue circle dashed line) for the all swept blades are lower than the baseline. The edgewise LTEFLs are increased for all the shapes analyzed (red triangle dashed line), as opposed to the flapwise cases. The increases for the edgewise LTEFLs are caused by the increment in the total mass of the backward swept blades because the swept blades are longer than the baseline. The increase in curvilinear length results in more materials added, producing a design heavier than the baseline blade. An overview of the blade mass increase for all the designs analyzed with respect to the baseline is reported in Table C.1. Table C.1 shows that the *s090-b0050-f0000* has the largest increase in blade mass (1.22%) between the shapes selected and, consequently, the largest increase in edgewise LTEFL (approximately 3%).

The trend of the torsional LTEFL (green square dashed line) is similar to the one observed for the medians of the extreme loads distributions in Figure C.4, right plot. The highest torsional LTEFL is observed from the most "aggressive" shape, *s025-b0050-f0000* blade (approximately 68% LTEFL increase).

In conclusion, the main problem with the choice of the first control point location parameter to design an effective backward swept blade is the large increase in extreme and fatigue blade root torsional moments. Blade shapes that have a change in geometry that starts closer to the root are longer and heavier than the others and, consequently, present an increase of the edgewise LTEFL.
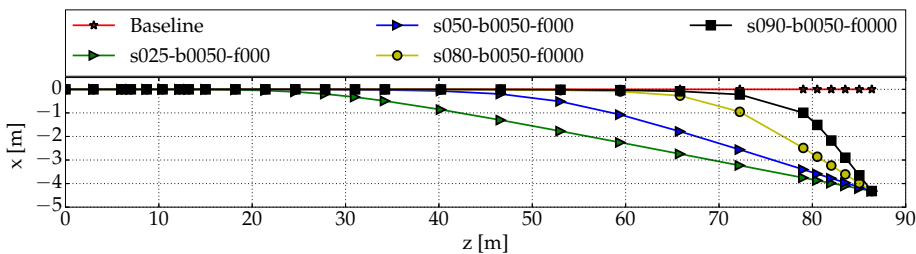
Figure C.5: The four backward blade shapes chosen to study the location of the first control point parameter.

Figure C.6: LTEFL blade root moments deviations in percentage from the baseline straight blade (blue circle - flapwise, red triangle - edgewise, green square - torsional). The backward sweep parameter at the tip is fixed at 5% of the blade length. No forward sweep is considered. Different blade radius along the span are taken into account.

C.3.2 Effects of Maximum Blade Tip Backward Sweep, Parameter "bxxxx"

The second parameter considered is the maximum blade tip backward sweep, "bxxxx". The other two parameters, "sxxx" and "fxxxx", are fixed to 80 and 0, respectively. Figure C.7 shows the considered swept blade geometries, that can be categorized as Family 3.

The absolute maximum load distributions of the considered swept blade geometries are reported in Figure C.8. In the figure, the medians and the IQRs of
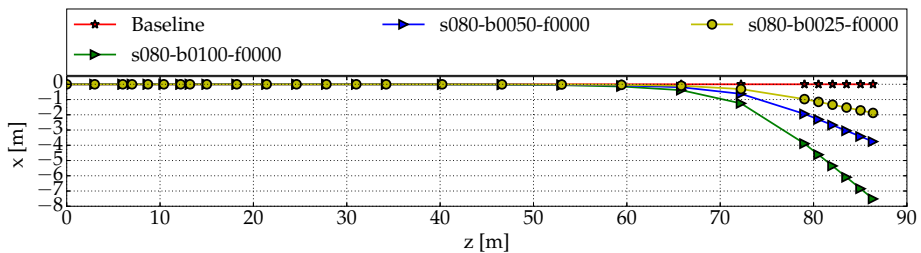
Figure C.7: Swept blade shapes of Family 3. First control point for the Bezier polynomial is located on the pitch axis at 80% of the total blade length.

Table C.1: Blade total mass variations for the designs analyzed. The baseline blade mass is reported in the second row of the table. The swept blades mass are reported as variation in percentage with respect to the baseline. The identification sequence for the swept blades is reported in the first column.

Shape	Blade Mass
BASELINE	41716 [kg]
s025-b0025-f000	0.2 [%]
s025-b0025-f002	0.9 [%]
s025-b0050-f000	0.3 [%]
s025-b0050-f002	1.6 [%]
s025-b0100-f000	1.0 [%]
s050-b0025-f000	0.2 [%]
s050-b0025-f002	1.0 [%]
s050-b0050-f000	0.5 [%]
s050-b0050-f002	2.0 [%]
s050-b0100-f000	1.5 [%]
s080-b0010-f0005	0.3 [%]
s080-b0025-f0000	0.2 [%]
s080-b0025-f0005	0.6 [%]
s080-b0050-f0000	0.5 [%]
s080-b0100-f0000	1.7 [%]
s090-b0005-f0000	0.1 [%]
s090-b0005-f0002	0.2 [%]
s090-b0010-f0000	0.2 [%]
s090-b0025-f0000	0.4 [%]
s090-b0050-f0000	1.2 [%]
spe1-b0008-f0005	0.2 [%]
spe2-b0010-f0005	0.2 [%]
spe3-b0010-f0005	0.2 [%]
spe4-b0008-f0005	0.2 [%]
spe5-b0005-f0002	0.1 [%]

the flapwise bending moments for the swept blades show a marginal load alleviation effect. The edgewise moment distributions are substantially unchanged, even though it appears that larger sweeps increase the medians due to the total weight increment (see Table C.1). Moreover, as shown in Figure C.8 on the right plot, increasing the maximum backward sweep at the tip of the blade produces higher medians and IQRs on the absolute maxima distributions of the blade
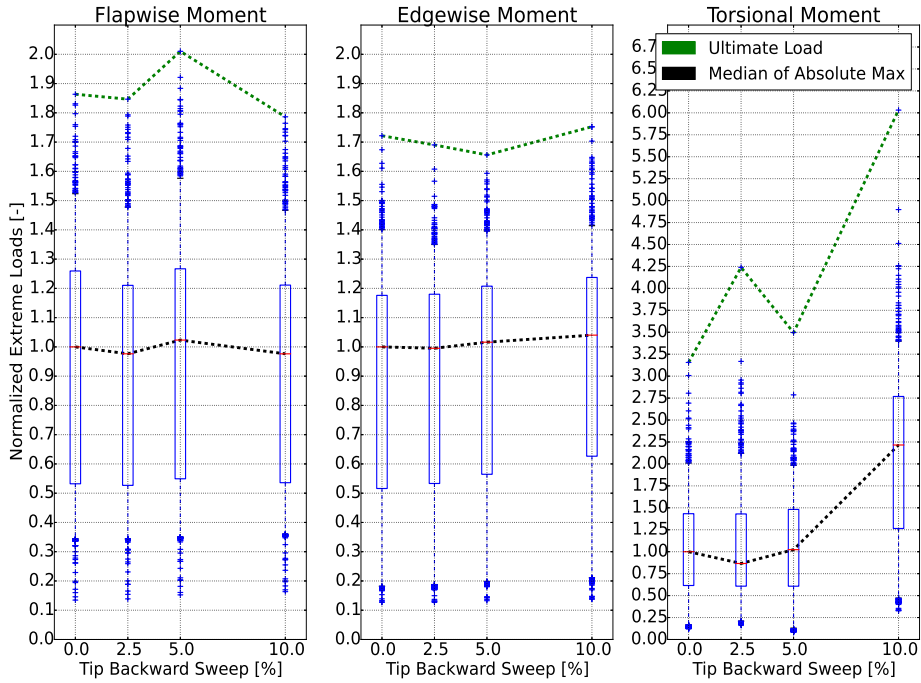
Figure C.8: Normalized absolute maxima distributions for baseline and swept blades with increasing maximum backward sweep at the tip. Extreme flapwise, edgewise, and torsional moments are plotted on the left, center, and right, respectively. The loads are non-dimensionalized by the median of the respective baseline distribution.

root torsional moment.

Figure C.9 shows the blade root LTEFLs. As the blade tip backward sweep increases, 1) the flapwise LTEFLs are reduced due to the higher load alleviation effect brought by larger sweeps, 2) the edgewise LTEFLs are increased due to increment of the total blade weight, and 3) the torsional LTEFLs are increased due to the increasing torque except the *s080-b0025-f0000*. In the latter case, the decrease in blade root torsional fatigue loading, not typical for backward swept blades, can be explained as a consequence of the annual energy production maximization and the change in aerodynamic twist.

The variation of the optimized twist along the blade span affects the distribution of the loading. For very mild swept shapes and very large variations of the aerodynamic twist (see the red curve in Figure C.10, where the largest variation of the twist is around 5°), it is possible to obtain a design that shows alleviations for both flapwise and torsional blade root fatigue loads. This property is diffi-
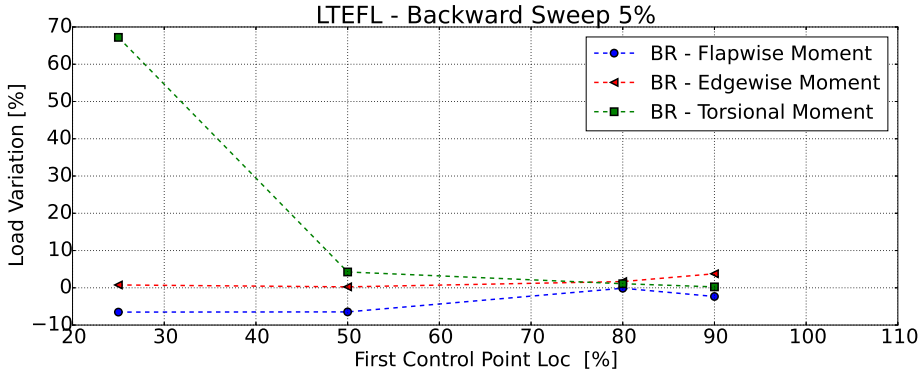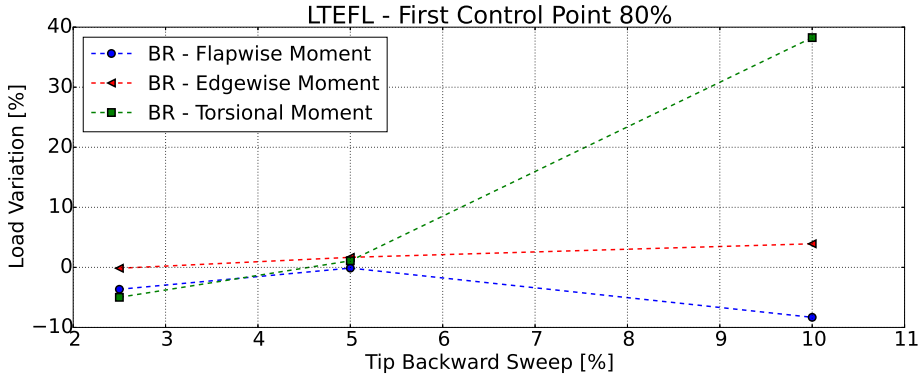
Figure C.9: Life Time Equivalent Fatigue Load blade root moments devia-
tions in percentage from the baseline straight blade (blue circle
- flapwise, red triangle - edgewise, green square - torsional). All
the shapes belong to Family 3. No forward sweep is considered.
The variation of the amount of backward sweep at the blade tip
is taken into account.
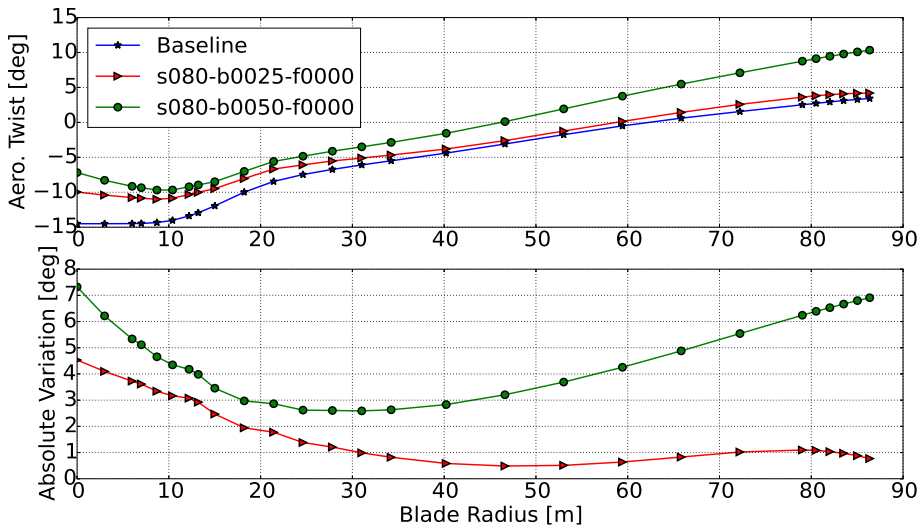
Figure C.10: Comparison of the aerodynamic twist of two blades: Baseline
(blue star) and *s080-b0025-f0000* (red triangle). Top plot shows
the aerodynamic twist in degree, while the bottom one shows
the absolute value of the variation of the twist of the two swept
blades with respect to the baseline blade.

cult to exploit through a parametric study, and it will be the subject of future work. Very large variations of the aerodynamic twist can also have an impact on the flapwise load alleviation potential of some designs. For example, the design *s080-b0050-f0000* shows no extreme and LTEF load alleviations compared to the baseline, the *s080-b0025-f0000*, and the *s080-b0100-f0000* (see Figures C.8 and C.9). The distribution of the flapwise loading is heavily affected by a large variation of the optimized aerodynamic twist, which shows an absolute difference of 7° at the tip compared to the baseline (see the green curve in Figure C.8). The changes in the distribution of the flapwise loading along the blade span have also an effect on the tower clearance. The latter problem is discussed in details in Section 3.4.

Conclusions regarding the analysis of the blade tip backward sweep parameter are similar to the ones reported in the previous section: the parameter has to be chosen considering the minimum increase in torsional extreme and fatigue loading, and taking into account the increase in blade mass due to the increment in blade length brought by the swept shape. Furthermore, it is important to consider that the aerodynamic twist optimization has an impact on the distribution on the aerodynamic loading along the blade span, which can result in a reduction of the blade root torsional moment. Future studies will be carried on the possibility of generating a design that shows alleviations for both flapwise and torsional blade root fatigue loads, as in the case of *s080-b0025-f0000*. Large variations of the optimized aerodynamic twist can also result in blade designs that show no load alleviation potentials in the flapwise direction.

C.3.3   Effects of Blade Forward Sweep, Parameter "fxxxx"

The last parameter considered is the presence of forward sweep and its location on a swept blade, "fxxxx". For this purpose, two swept blade shape families, Family 1 and Family 5, are used (see Figures C.1 and C.11). The main reason to implement the forward sweep on a backward swept blade is to reduce the large torsional moment at the root.

Figure C.12 shows the extreme blade root moment distributions for the shapes of Family 1 where the forward swept blades (*s025-b0025-f002* and *s025-b0050-f002*) are illustrated with red color. In general, the inclusion of forward sweep in the backward sweep jeopardizes the load alleviation effect on the extreme flapwise loading (compare medians of the blue and red boxes of the left plot of Figure C.12). The reason for this negative outcome lies behind the passive control mechanism used by swept blades. The benefits come from the increase in torsion along the blade length, and the consequent increase in twist towards feather to reduce the angle of attack. The efficacy of this mechanism is reduced if the shape is more "balanced" with a forward sweep. Moreover, the blades with forward sweep are longer and heavier than the respective purely swept shapes,
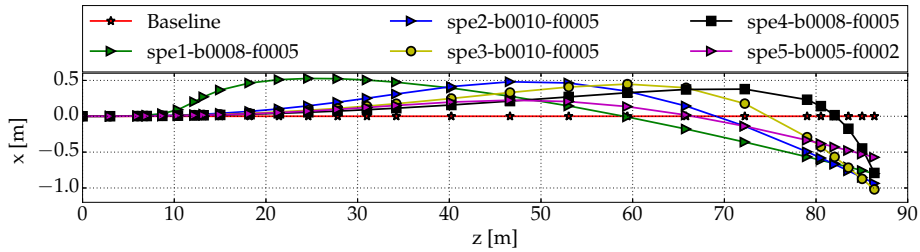
Figure C.11: Swept blade shapes of Family 5. Special set of shapes characterized by different locations of the forward swept portion of the blade.
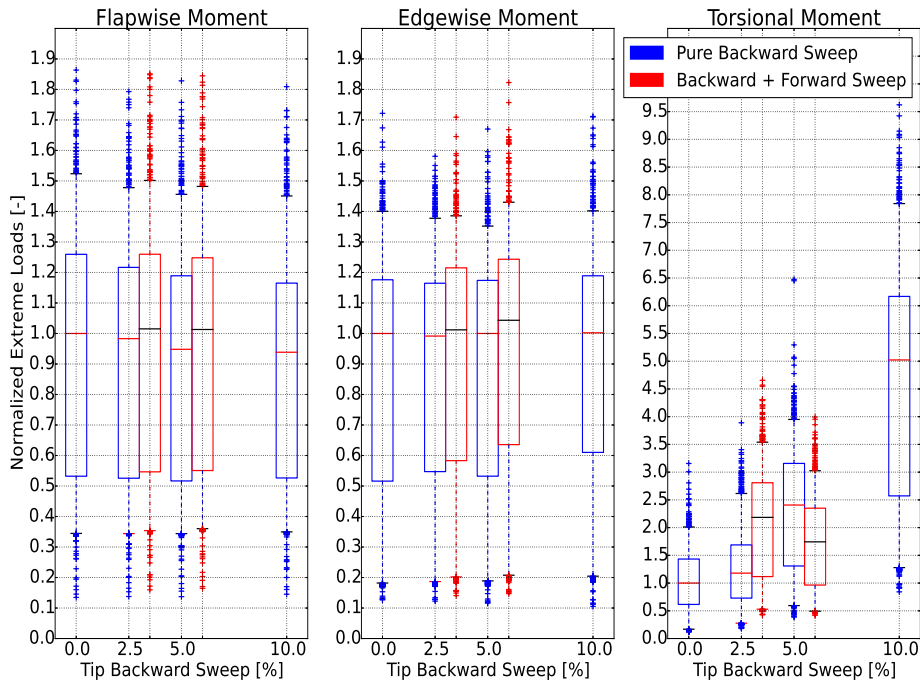
**Figure C.12:** Normalized absolute maxima distributions for baseline and swept blades of Family 1. Extreme flapwise, edgewise, and torsional moments plotted on the left, center, and right, respectively. The loads are non-dimensionalized by the median of the respective baseline distribution. Purely backward swept shapes are denoted using the blue colour. The shapes with forward sweep are highlighted in red.

generating an increase in extreme edgewise blade root loading (see medians of the red boxes of the central plot of Figure C.12). The torsional moments are also affected by the forward sweep. The right plot in Figure C.12 shows that the median and the IQRs can be reduced compared to the purely swept back blades (*s025-b0050-f000* and *s025-b0050-f002*).

Figures C.13 and C.14 show the blade root extreme and LTEFLs for the shapes of Family 5, respectively. The analysis of these figures is focused on the understanding of the impact that changing the location of the forward sweep has on the blade root loads.

The blade root flapwise extreme loads and LTEFLs are reduced, even though substantial forward sweep variations are introduced. The amount of LTEFL reductions is lower compared to the alleviations achieved varying the other two geometric parameters, "sxxx" and "bxxxx". The blade edgewise extreme loads and LTEFLs are not significantly affected by the forward sweep because the variation of blade mass for the shapes of Family 5 is very limited, as shown in Table C.1. The torsional extreme and LTEFLs are increased for all cases, as
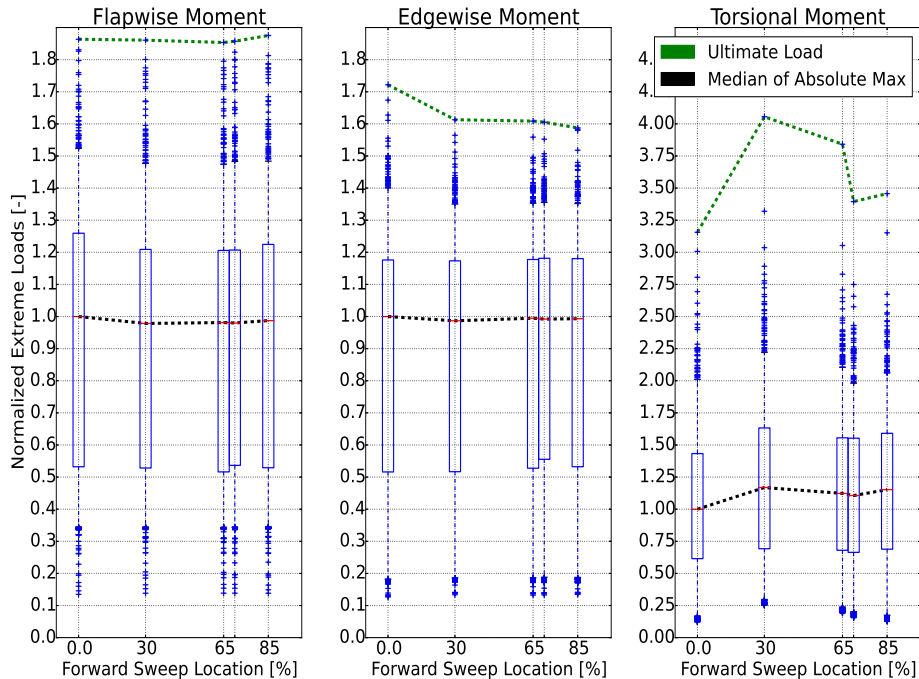
Figure C.13: Normalized absolute maxima distributions for baseline and swept blades of Family 5. The loads are non-dimensionalized by the median of the respective baseline distribution.
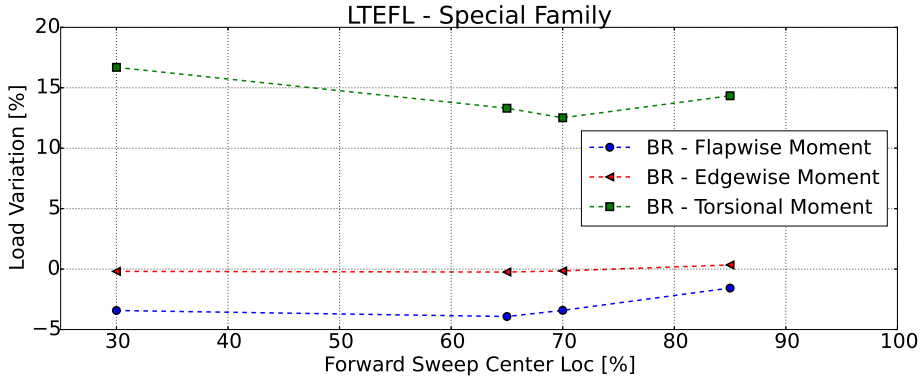
Figure C.14: Life Time Equivalent Fatigue Load blade root moments blade root moments deviations in percentage from the baseline straight blade (blue - flapwise, red - edgewise, green - torsional). All the shapes belong to Family 5. Load variations from the baseline are plotted against the location of the forward sweep.

shown on one side by the medians of the absolute maxima distributions (see Figure C.13, right plot), and on the other side by peaks between approximately 13 and 17% for the LTEFL (see Figure C.14). The amount of the increment is not significant compared to the previous geometric parameters variations analyzed (see Figures C.4, C.6, C.8, and C.9).

The conclusion is that there is a benefit in introducing forward sweep on backward swept blades. The blade torsional extreme loads and LTEFLs can be less affected by the backward sweep. On the other hand, the load alleviation benefits for the blade flapwise extreme loads and LTEFLs are reduced due to the forward sweep.

C.3.4 AEP and Tower Clearance

The annual energy production (AEP) and the tower clearance of all considered swept blades are reported in this section. Table C.2 shows the AEP and the tower clearance in percent difference from the baseline values.

The AEP of the backward-swept-bladed turbines are kept very close to the baseline value due to the aerodynamic twist optimization scheme implemented at the pre-processing phase (see Figure C.2). The variations of AEP are always below 1%, and the drops for the turbines with worse performances are never greater than 0.5%.

The tower clearance is calculated as the distance between the blade tip and

the closest outer section of the tower. The measured tower clearance window is between 175° and 185° azimuth, for a blade pointing upward at 0° azimuth. All the swept blade designs analyzed satisfy the requirement for tower clearance

Table C.2: AEP and tower clearance of the blade designs analyzed. The identification sequence for the swept blades is reported in the first column. The tower clearance results include also the identification sequence for the simulation that showed the minimum tower clearance: "dlc" denotes the Design Load Case, "wsp" the wind speed, "wdir" the wind direction and "s" the turbulence seed realization. The tower clearance takes into account the safety factors assigned by the DLB used.

Shape	AEP	Tower Clearance	
BASELINE	48.497 [GW h]	dlc13 wsp12 wdir350 s3005	3.656 [m]
s025-b0025-f000	0.0 [%]	dlc13 wsp12 wdir350 s3005	4.5 [%]
s025-b0025-f002	0.5 [%]	dlc13 wsp12 wdir000 s1005	-4.8 [%]
s025-b0050-f000	-0.5 [%]	dlc13 wsp12 wdir350 s3005	6.0 [%]
s025-b0050-f002	0.8 [%]	dlc13 wsp14 wdir000 s2006	-7.3 [%]
s025-b0100-f000	0.5 [%]	dlc13 wsp12 wdir350 s3005	1.3 [%]
s050-b0025-f000	-0.2 [%]	dlc13 wsp12 wdir350 s3005	1.5 [%]
s050-b0025-f002	0.7 [%]	dlc13 wsp12 wdir350 s3005	-1.0 [%]
s050-b0050-f000	0.1 [%]	dlc13 wsp12 wdir350 s3005	-4.6 [%]
s050-b0050-f002	1.0 [%]	dlc13 wsp14 wdir000 s2006	-4.1 [%]
s050-b0100-f000	0.7 [%]	dlc13 wsp12 wdir350 s3005	-1.6 [%]
s080-b0010-f0005	0.8 [%]	dlc13 wsp12 wdir010 s6005	-9.3 [%]
s080-b0025-f0000	-0.2 [%]	dlc13 wsp12 wdir350 s3005	1.8 [%]
s080-b0025-f0005	0.5 [%]	dlc13 wsp12 wdir350 s3005	0.1 [%]
s080-b0050-f0000	0.9 [%]	dlc13 wsp12 wdir350 s3005	-10.1 [%]
s080-b0100-f0000	0.8 [%]	dlc13 wsp12 wdir350 s3005	-5.8 [%]
s090-b0005-f0000	-0.3 [%]	dlc13 wsp12 wdir350 s3005	-3.3 [%]
s090-b0005-f0002	-0.3 [%]	dlc13 wsp12 wdir350 s3005	-3.9 [%]
s090-b0010-f0000	-0.3 [%]	dlc13 wsp12 wdir350 s3005	-2.2 [%]
s090-b0025-f0000	0.0 [%]	dlc13 wsp12 wdir350 s3005	-2.7 [%]
s090-b0050-f0000	0.8 [%]	dlc13 wsp12 wdir350 s3005	-3.1 [%]
spe1-b0008-f0005	-0.3 [%]	dlc13 wsp12 wdir350 s3005	4.1 [%]
spe2-b0010-f0005	-0.3 [%]	dlc13 wsp12 wdir350 s3005	4.5 [%]
spe3-b0010-f0005	-0.2 [%]	dlc13 wsp12 wdir350 s3005	3.0 [%]
spe4-b0008-f0005	-0.2 [%]	dlc13 wsp12 wdir350 s3005	3.3 [%]
spe5-b0005-f0002	-0.4 [%]	dlc13 wsp12 wdir350 s3005	2.7 [%]

demanded by the IEC standard [35]. The load alleviation effect brought by
the sweep reduces the flapwise displacement of the tip. Consequently, a higher
tower clearance is expected from all the turbines that takes part to the paramet-
ric study, but some of the designs show a substantial decrease of the minimum
tower clearance. The reason lies behind the optimization process where the op-
timizer might need to significantly increase the aerodynamic twist at the blade
tip to maximize the AEP, causing an increase in the angle of attack around rated
wind speed. The change in angle of attack introduces higher loads at rated wind
speed where the minimum tower clearance is registered. Figure C.15 shows the
aerodynamic twist distributions for two different swept blade cases and their
comparison with the baseline design. On one hand, the *s080-b0050-f0000* blade
(plotted in circle with green color) has a significant increase of the aerodynamic
twist at the blade tip (approximately 7° at the blade tip, as shown in the bottom
plot of Figure C.15) which results in a decrease of the tower clearance of approx-
imately 10%. On the other hand, the *s025-b0050-f000* blade design (plotted in
triangle with red color) shows an increase of tower clearance of approximately
6% whereas the aerodynamic twist at the tip of the blade is not significantly
increased (approximately 1° at the blade tip shown in the bottom plot of Figure
C.15).
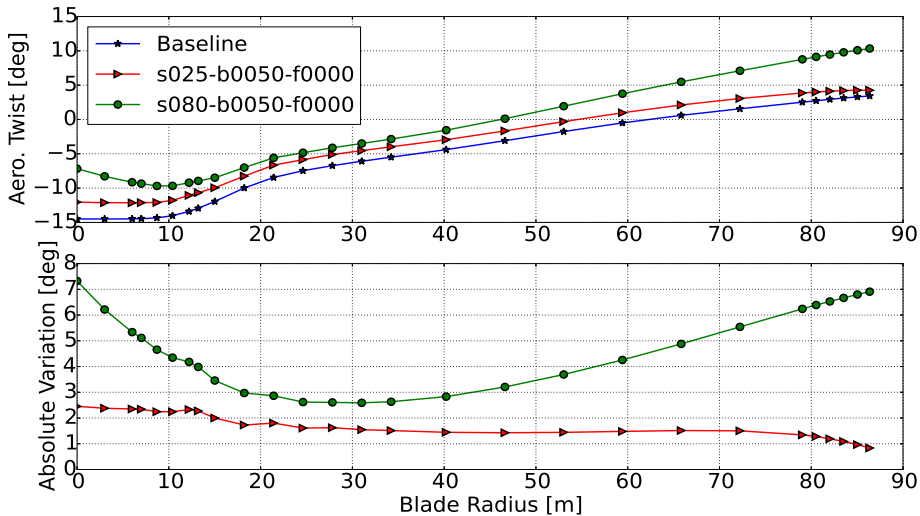
Figure C.15: Comparison of the aerodynamic twist of three blades: Baseline
(blue star), *s025-b0050-f000* (red triangle), and *s80-b0050-f0000*
(green circle). Top plot shows the aerodynamic twist in degree,
while the bottom one shows the absolute value of the variation
of the twist of the two swept blades with respect to the baseline
blade.

To keep or increase the tower clearance, the aerodynamic twist should be constrained during the optimization. An alternative is to pitch the blade towards stall below rated wind speed, to compensate for the reduction in the angle of attack generated by the sweep [30]. The latter solution has the advantage of being less computationally expensive than the optimization routine. Particular attention must be paid to avoid stall along the blade span below rated wind speed.

C.4   Swept Blade Design Application: the NREL 5MW RWT

In this section, one of the obtained swept blade designs from the DTU 10 MW RWT is applied to a different class turbine blade to verify its performances. In this study, the NREL 5 MW RWT is used [14] with the Basic DTU Wind Energy Controller [29].
The *s080-b0025-f0000* backward swept blade is selected for this study based on the investigations made in the previous sections:

- avoid forward sweep in any part of the blade because it reduces (or completely eliminate) the load alleviation effect;

- let the backward sweep start closer to the blade tip (80% or 90% of the total blade length) to avoid an excessive increase in blade root torsional moment;

- contain the maximum backward sweep at the tip within 5% of the total blade length to avoid a very large blade root torsional moment;

- optimize the aerodynamic twist or pitch the blade towards stall below rated wind speed to compensate the loss in AEP due to the decrease in the angle of attack; be aware of the risks of the two strategies: the optimization of the aerodynamic twist to maximize the AEP can increase the loading at the blade tip around rated wind speed reducing the tower clearance; pitching the blade towards stall below rated wind speed can drive part of the blade into stall.

The considered blade is pitched towards stall below rated wind speed to compensate the loss in AEP compared to the baseline design. This approach is preferred to the aerodynamic twist optimization because it does not have the negative impact on the tower clearance described earlier, and it is computationally cheap.
The same design load cases based on [34] with the modifications reported in Section 2.3 are considered.

C.4.1   AEP and Tower Clearance

Table C.3 shows the comparison of AEP and tower clearance between the baseline wind turbine and the swept-bladed one. The passive-controlled wind turbine has approximately the same annual energy production of the baseline, registering a very small loss of 0.04%. An increase in tower clearance can be observed (3.5%).

C.4.2   Extreme bending and torsional loads

Figure C.16 shows the blade root load comparisons between the baseline and the considered swept blade. The extreme blade root flapwise load is decreased, as median and IQR of the distribution of *s080-b0025-f0000* highlight. This reduction is qualitatively in agreement with the variation observed for the DTU 10 MW (see Figure C.8).
The median of blade root torsional moment distribution increases whereas the torsional moment distribution for the respective swept blade design of the DTU 10 MW is more similar to the its baseline (see Figure C.8), with a slightly lower median. The differences between the extreme blade root torsional loading of the NREL 5 MW and the DTU 10 MW are due to the different strategies used to compensate the loss in AEP. The choice between the aerodynamic twist optimization and the pitching towards stall has an impact on the distribution of the loading along the blade span, as already remarked in Section 3.2 (see Figure C.10).
The median of the edgewise loading increases due to the increase in blade mass,

Table C.3: AEP and tower clearance of the NREL 5 MW RWT with straight and backward swept blades (*s080-b0025-f0000*). The AEP and tower clearance for the baseline blade are reported in the second row of the table. The tower clearance results include also the identification sequence for the simulation that showed the minimum tower clearance: "dlc" denotes the Design Load Case, "wsp" the wind speed, "wdir" the wind direction and "s" the turbulence seed realization. The tower clearance takes into account the safety factors assigned by the DLB used.

Blade Design	AEP	Tower Clearance	
NREL 5MW RWT	24.197 [GW h]	dlc13 wsp12 wdir010 s5005	1.767 [m]
s080-b0025-f0000	-0.04 [%]	dlc13 wsp12 wdir010 s5005	+3.5 [%]
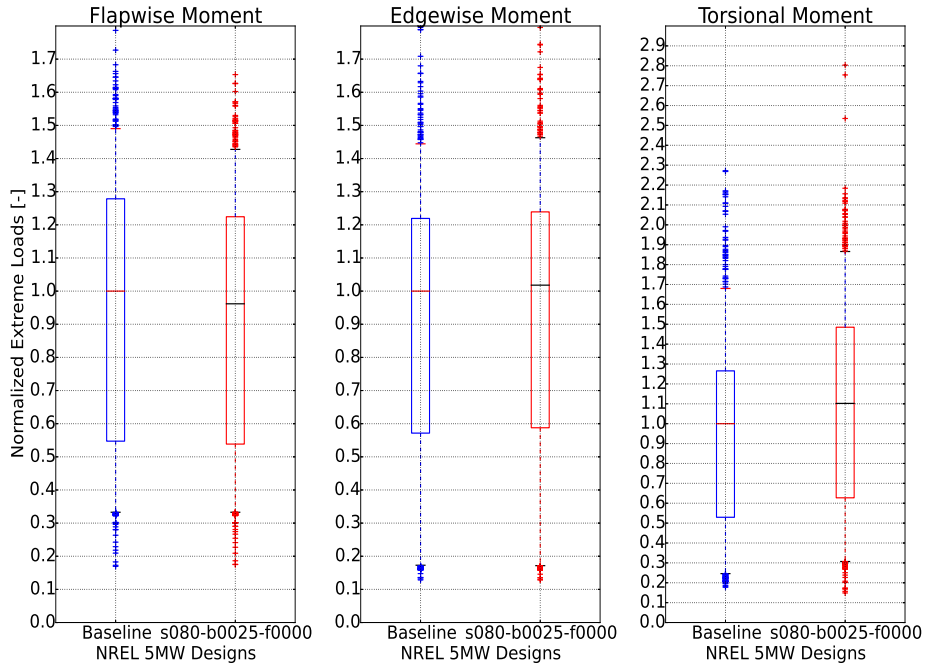
Figure C.16: Normalized absolute maxima distributions for baseline and swept blade of the NREL 5MW. The loads are non-dimensionalized by the median of the respective baseline distribution.

reported in Table C.4. The *s080-b0025-f0000* of the DTU 10 MW RWT benefits less from the backward sweep due to the optimization of the aerodynamic twist which affects the blade loading at the tip to compensate for the loss in AEP. The *s080-b0025-f0000* of the NREL 5 MW RWT shows improved load alleviation characteristics on the flapwise direction compared to the 10 MW, driven by a larger extreme torsional loading (compare Figures C.8 and C.16).

Table C.4: Blade mass of the NREL 5 MW RWT with straight and backward swept blades (*s080-b0025-f0000*). The mass of the swept blade loads is reported as variation in percentage from the baseline.

Blade Design	Blade Mass
NREL 5MW RWT	17740 [kg]
s080-b0025-f0000	+0.19 [%]

C.4.3 LTEF bending and torsional loads

Table C.5 shows the comparison of the blade root LTEFLs for the two designs. The loads for the baseline are reported in absolute value, whereas the LTEFLs for the *s080-b0025-f0000* are reported in percent variation. The variations of LTEFLs reported for the swept blade design of the NREL 5 MW are in agreement with the observations made from Figure C.9 where the LTEFLs of the flapwise and torsion directions are reduced while the edgewise LTEFL is increased.

Table C.5: LTEFL blade root moments of the NREL 5 MW RWT with straight and backward swept blades (*s080-b0025-f0000*). In the three rightmost columns, the blade root flapwise moment, the blade root edgewise moment, and the blade root torsional moment are respectively reported. The fatigue loads for the baseline blade are reported in absolute values in the second row of the table. The fatigue loads for the swept blade are reported as variation in percentage from the baseline.

Blade Design	LTEFL BR Flap	LTEFL BR Edge	LTEFL BR Tors.
NREL 5MW RWT	10092.379 [kN m]	7218.318 [kN m]	184.232 [kN m]
s080-b0025-f0000	-6.3 [%]	+0.2 [%]	-2.8 [%]

From the investigation with the NREL 5 MW RWT, it can be concluded that the outcomes of the extensive load analysis of the DTU 10 MW RWT can be applied to other wind turbines, ensuring the creation of a swept blade design able to provide beneficial passive load alleviations.

C.5 Conclusions

This paper studies extensive load analyses to investigate the backward swept blade designs for passive load alleviation on multi-megawatt wind turbines. To introduce various swept geometries, three representative parameters are considered:

- position along the blade span where the sweep starts;

- maximum backward sweep at the blade tip;

- maximum forward sweep.

Based on these three parameters, 25 shapes divided in 5 families were selected. The blade of the DTU 10 MW RWT was used as baseline. In general, the backward swept blades produce less electrical energy compared to the straight blade. Therefore, all the considered swept blades were pre-processed to provide the same amount of the annual energy production (AEP). An optimization approach was introduced. The aerodynamic twist was updated for each swept blade design to maximize the annual energy production, compensating the AEP loss below rated wind speed. After that, the tuning of the controller according to a specific frequency placement of the regulator mode was performed as well. A full design load basis was adapted and analyzed for each of the swept designs selected.

The variation of each geometric parameter was analyzed separately producing the following observations:

- "sxxx": the choice of the first control point location parameter is driven by the large increase in extreme and fatigue blade root torsional moment, and the increase of the edgewise LTEFL due to the increase in blade length more pronounced as the sweep starts closer to the root;

- "bxxxx": the parameter has to be chosen considering the minimum increase in torsional extreme and fatigue loading, and taking into account the increase in blade mass due to the increment in blade length brought by the swept shape;

- "fxxxx": the presence of forward sweep helps compensating excessive increments of the torsional moment, but it also reduces or cancels the beneficial effects due to the sweep; moreover, the location of the forward sweep along the blade span does not have a relevant influence on the loading.

To summarize, mildly and purely backward swept shapes are the best option for the design of passive-controlled wind turbines because they can achieve load alleviations without causing large increases in blade root torsional moment.

Annual energy production and tower clearance were monitored as well. The optimization of the aerodynamic twist to maximize AEP produces negative effects on the tower clearance of some of the designs analyzed. The optimizer increases the aerodynamic twist at the blade tip to fulfil the loss in AEP below rated wind speed, resulting in higher angles of attack and higher loads at the tip around rated wind speed compared to the baseline design. This process causes a reduction of the tower clearance with respect to the RWT and a different distribution of the loading along the blade span.

The observations obtained through the load analysis of all the DTU 10 MW RWT were applied to a different wind turbine, specifically, the NREL 5 MW

RWT. From this study similar trends between the DTU 10 MW RWT and the NREL 5 MW RWT were observed. The outcome of the parametric study can be generally applied to produce a passive-controlled wind turbine with reduced flapwise extreme and fatigue loads, and inevitable increase in extreme and fatigue blade root torsional moment.

Acknowledgements

Bibliography

[1] Taylor, M., Daniel, K., Ilas, A. and So, E. Y. *Renewable Power Generation Costs in 2014*, IRENA - International Renewable Energy Agency, Bonn, Germany, 2015.

[2] Krohn, S., Morthorst, P. E. and Awerbuch, S. *The Economics of Wind Energy: A report by the European Wind Energy Association*, EWEA - The European Wind Energy Association, March 2009.

[3] Ashwill, T. D. *Materials and Innovations for Large Blade Structures: Research Opportunities in Wind Energy Technology*, in: 50th AIAA Structures, Structural Dynamics, and Materials Conference, pp. AIAA-2009-2407. Palm Springs, USA, May, 2009.

[4] Bossanyi, E. A. *Individual Blade Pitch Control for Load Reduction*, Journal of Wind Energy (2003) 119-128. Doi: 10.1002/we.76.

[5] Barlas, T. K. , Bergami, L., Hansen, M. H., Pedersen, M. M., Verelst, D., Thomsen, K. and Madsen H. A., *Load alleviation potential of the Controllable Rubber Trailing Edge Flap (CRTEF) in the INDUFLAP project*, DTU Wind Energy, DTU Vindenergi-E-0065(EN), Roskilde, December 2014.

[6] Kooijman, H. *Bending-torsion coupling of a wind turbine rotor blade*, ECN report I-96-060, Petten, December 1996

[7] Larwood, S. and Zuteck, M., *Swept Wind Turbine Blade Aeroelastic Modeling for loads and dynamic behavior*, Windpower 2006, p.17, Pittsburgh, 4-7 June 2006.

[8] Ashwill, T. D., Kanaby, G., Jackson, K., and Zuteck, M, *Development of the swept twist adaptive rotor (STAR) blade*, Proceedings of the 48th AIAA Aerospace Sciences Meeting, 4-7 January 2010, Orlando, Florida

[9] Knight and Carver Wind Group, *Sweep-Twist Adaptive Rotor Blade: Final Project Report*, Sandia National Laboratories, SAND2009-8037, Albuquerque, New Mexico, USA, 2010.

[10] Ashwill, T., Veers, P. S., Locke, J., Griffin, I. C. D. and Zuteck, M. D. *Concepts for Adaptive Wind Turbine Blades*, in: ASME 2002 Wind Energy Symposium, Paper No. WIND2002-28, pp. 56-69. Reno, Nevada, USA, 14-17 January 2002, doi:10.1115/WIND2002-28.

[11] Zuteck, M. *Adaptive Blade Concept Assessment: Curved Planform Induced Twist Investigation*, Sandia National Laboratories, SAND2002-2996, Albuquerque, New Mexico, USA, 2002.

[12] Verelst, D.R.S. and Larsen, T.J., *Load consequences when sweeping blades - a case study of a 5 MW pitch controlled wind turbine*, Technical Report Risø-R-1724, Risø-DTU, May 2010, Roskilde

[13] Hansen, M. H., *Aeroelastic properties of backward swept blades*, Proceedings of the 49th AIAA Aerospace Sciences Meeting, 4-7 January 2011, Orlando, Florida

[14] Jonkman, J., Butterfield, S., Musial W. and Scott, G. *Definition of a 5-MW Reference Wind Turbine for Offshore System Development*, National Renewable Energy Laboratories, Technical Report, NREL/TP-500-38060, Golden, Colorado, USA, February 2009.

[15] Quarteroni, A., Sacco, R. and Saleri, F. *Numerical Mathematics*, Springer-Verlag New York, Inc., 2000, ISBN 0-387-98959-5.

[16] Larsen, T. J. and Hansen, A. M. *How 2 HAWC2, the user's manual*, DTU Wind Energy, Risø-R-1597(ver.4.6)(EN), Roskilde, Denmark, 2015.

[17] Henriksen, L. C., Tibaldi, C. and Bergami, L. *HAWCStab2 User Manual*, DTU Wind Energy, Technical Report, Roskilde, Denmark, 2015.

[18] NASA, http://openmdao.org, 2012.

[19] Moore, K. T., Naylor B. A. and Gray, J. S. *The Development of an Open-Source Framework for Multidisciplinary Analysis and Optimization*, in: 10th AIAA/ISSMO Multidisciplinary Analysis and Optimization Conference. AIAA 2008-6069, Victoria, Canada, August 2008.

[20] Gray, J. S., Moore, K. T. and Naylor, B. A. *OPENMDAO: An Open Source Framework for Multidisciplinary Analysis and Optimization*, in: 13th AIAA/ISSMO Multidisciplinary Analysis and Optimization Conference. AIAA-2010-9101, Fort Worth, Texas, USA, August 2010, http://www.aric.or.kr/treatise/journal/content.asp?idx=134451.

[21] Heath, C. M. and Gray, J. S. *OpenMDAO: Framework for Flexible Multidisciplinary Design, Analysis and Optimization Methods*, in: 8th AIAA Multidisciplinary Design Optimization Specialist Conference (MDO), pp. 1-13. Honolulu, Hawaii, USA, 2012.

[22] Sønderby, I and Hansen, M.H., *Open-loop frequency response analysis of a wind turbine using high-order linear aeroelastic model*, Journal of Wind Energy, 2013, DOI: 10.1002/we.1624

[23] Zahle, F., Tibaldi, C., Verelst, D. R., Bak, C., Bitche, R. and Blasques, J. P. A. A. *Aero-Elastic Optimization of a 10 MW Wind Turbine*, in: AIAA SciTech - 33rd Wind Energy Symposium. Kissimmee, Florida, USA, 5-9 January 2015.

[24] Kim, T., Hansen, A.M. and Branner, K., *Development of an anisotropic beam finite element for composite wind turbine blades in multibody system*, Journal of Renewable Energy, 2013; 59:172-183, doi:10.1016/j.renene.2013.03.033

[25] Vorpahl, F., Strobel, M., Jonkman, J.M., Larsen, T.J. and Passon, P., *Verification of aeroelastic offshore wind turbine design codes under IEA wind task XXIII*, Journal of Wind Energy, 2013; doi:10.1002/we.1588

[26] Popko, W., Vorpahl, F., Zuga, A., Kohlmeier, M., Jonkman, J., Robertson, A., Larsen, T.J., Yde, A., Stertr, K., Okstad, K.M., et al., *Offshore code comparison collaboration continuation (OC4), PHASE I - results of coupled simulations of an offshore wind turbine with jacket support structure*, Proceedings pf the International Offshore and Polar Engineering Conference 2012, 2012;337-346

[27] Larsen, T.J., Aagard Madsen, H., Larsen, G.C. and Hansen, K.S., *Validation of the dynamic wake meander model for loads and power production in the Egmond Aan Zee wind farm*, Journal of Wind Energy, 2013, 2013;16(4):605-624, doi:10.1002/we.1563

[28] Bak, C., Zahle, F., Bitsche, R., Kim, T., Yde, A., Henriksen, L.C., Natarajan, A. and Hansen, M.H., *Description of the DTU 10 MW Reference Wind Turbine*, DTU Wind Energy Report-I-0092, July 2013, Roskilde, Denmark

[29] Hansen, M.H. and Henriksen, L.C., *Basic DTU Wind Energy Controller*, Technical Report DTU Wind Energy E-0018, DTU, 2013

[30] Pavese, C. and Kim, T. *Implementation of Passive Control Strategies through Swept Blades*, in: 10th PhD Seminar on Wind Energy in Europe. Orleans, France, 28-31 October 2014.

[31] Pavese, C., Tibaldi, C. and Kim, T. *Study on Controller Tuning of Wind Turbines with Backward Swept Blades*, in: AIAA SciTech - 33rd Wind Energy Symposium. Kissimmee, Florida, USA, 5-9 January 2015.

[32] Hansen, M.H., Larsen, T.J., Øye, S., Sørensen and Fuglsang, P., *Control Design for a pitch-regulated, variable speed wind turbine*, Technical Report Risø-R-1500(EN), Risø National Laboratory, Roskilde, Denmark, 2005

[33] Tibaldi, C., Henriksen, L.C., Hansen, M.H. and Bak, C.*Effects of gain-scheduling methods in a classical wind turbine controller on wind turbine aeroservoelastic modes and loads*, Proceedings of the 52th AIAA Aerospace Sciences Meeting, 12-17 January 2014, National Harbor, Maryland

[34] Hansen, M. H., Thomsen, K. Natarajan, A. and Barlas, A. *Design Load Basis for onshore turbines - Revision 00*, DTU Wind Energy, Technical Report E-0074(EN), Roskilde, Denmark, 2015.

[35] I. E. Commission, International Standard, *IEC 61400-1 Third Edition 2005-08, Wind Turbines - Part 1: Design Requirements*, Reference Number IEC 61400-1:2005(EN), 2005.

[36] G. Lloyd, *Guideline for the CertiFIcation of Wind Turbines*, Standard, July 2010.

PAPER D

Implementation of Passive Control Strategies Through Swept Blades

Authors:
Christian Pavese, Taeseong Kim

Christian Pavese[1], Taeseong Kim[1]

D.1   Introduction

The purpose of this study is to define guidelines for the benchmarking of wind turbines that use passive control methods to reduce extreme and fatigue loads on the structure. Passive control techniques can be divided in two branches: changes of the blade geometry and tailoring the material properties with blade layups. The objective of the current investigation involves exclusively the first type.

The core of the concept behind the passive control methodology considered in this study is to create a coupling between flapwise bending toward the tower and torsion towards feathering. This coupling has the capability to mitigate loads due to a decrease in the angle of attack. This beneficial effect is achieved changing the geometry of the blade creating a backward swept shape.

Information concerning the positive and negative effects on the loading of a wind turbine with swept blades can be found in literature [1, 2, 3, 4]. For example, the parametric study carried by Verelst and Larsen [2] provided a clear picture related to the quality of the load variation generated by the use of different swept blade configurations. Knowledge regarding an accurate estimation of the quantity of these load variations is missing. The reason is the differences in power output between the baseline and passive-controlled wind turbines. The geometrical bend-twist coupling effect reduces the angle of attack, and this reduction is responsible for a decrease in power output below rated wind speed. Hence, in order to properly quantify the load variations, the benchmarking has to be based on wind turbines with comparable power curves.

This study uses a simple method to provide the benchmarking of turbines with swept blades, with power curves comparable to a baseline with unswept blades. The method is based on a study conducted by Hansen [3]. In order to compensate the power loss below rated wind speed, new minimum pitch angle settings for the controller are evaluated. The swept blades are therefore pitched further towards stall with respect to the baseline blade in order to achieve similar power outputs.

The paper provides guidelines for this type of benchmarking with the final purpose of isolating the effects on the loading brought by the use of geometrical passive control methodology.

A comparison of wind turbines with various swept blades is reported. Results and methods to improve and better isolate passive control effects to quantify load variations are discussed.

---

[1]DTU Wind Energy, DK-4000, Roskilde, Denmark

D.2   Model

In this investigation, two in-house aeroelastic codes have been used: the linear aero-servo-elastic model for open- and closed-loop eigenvalue and frequency-domain analysis HAWCStab2 [3] and the nonlinear aeroelastic model for response in time domain HAWC2 [5, 6, 7].
The DTU 10 MW Reference Wind Turbine (RWT) [8] is used as a baseline for the current study.
As previously introduced, three different swept geometries are considered. All the properties of the wind turbines related to aerodynamic characteristics of the blade are kept the same for all the configurations analysed.
The sweep geometries are described by the following shape function:

$$s = \{a\frac{z}{R_0} - b\frac{z}{R_0}, 0, z\}^T \ z \in [0; R_0] \tag{D.1}$$

where s is the pitch axis as function of the blade length, z is the coordinate along the pitch axis of the blade, $R0 = 89.166m$ is the blade length in hub-coordinate system, a is a linear term for forward sweep added to compensate an otherwise large steady torque moment and b is the term for the backward sweep, which curve exponent is determined by c.
The pitch axes of the blade along the span for three different swept configurations are plotted in Figure D.1, whereas the parameters for the different configurations are:

- Swept Blade Level 1 : $a = 5$, $b = 10$, $c = 2$

- Swept Blade Level 2 : $a = 10$, $b = 20$, $c = 2$

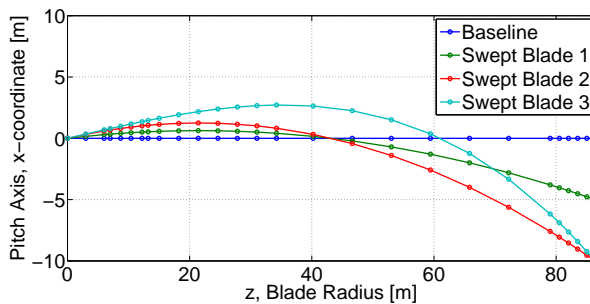- Swept Blade Level 3 : $a = 10$, $b = 20$, $c = 3$

Figure D.1: Pitch axis x-coordinate for the baseline and the backward swept blades.

A fair benchmarking has to be based on wind turbines with comparable power curves. New minimum pitch angle settings are calculated using HAWCStab2. The aim is to compensate the reduction of the angle of attack below rated wind speed pitching the backward swept blades toward stall. Figure D.2 shows the power curves of the baseline and the turbines with swept blades. The lower plot shows the relative error in percentage between the baseline and the three sweep levels. The dashed lines represent the difference in power curves when all the configurations have the same minimum pitch angle (zero degree) below rated wind speed. The solid lines shows the relative error when new minimum pitch angles have been used. The power losses have been significantly reduced and the maximum error is around 2This simple method for obtaining comparable power curves has an important downside: pitching the full blade below rated wind speed might push the part of the blade closer to the root to operate in stall condition. The coupling between flapwise bending toward the tower and torsion towards feathering produces a reduction of the angle of attack in the region of the blade closer to the tip. The angle of attack closer to the root is significantly less influenced by the coupling effect. Hence, when the backward swept blades are forced to pitch further toward stall below rated wind speed, the lift coefficient of the airfoils closer to the root, which work already at high angles of attack, approaches dangerously the stall region.

Lift coefficients along the blade span of the different DTU 10 MW RWT configurations used for the current benchmarking have been constantly monitored, to make sure that all the swept-blades wind turbines used for this study kept a behavior comparable to the baseline.

D.3 Results

The load case used for the benchmarking consist of 10 minute simulations with turbulent wind speed from 4 m/s to 26 m/s (single turbulence seed is considered), tower shadow and no wind shear. Extreme and fatigue loads acting on the wind turbines are computed. Two sets of simulations have been run: one where the minimum pitch angle below rated wind speed is kept equal (zero degree) for all the configurations, and the other one where a new minimum pitch angle has been selected for each of the cases to minimize the discrepancies between the power curves.

Extreme blade root flapwise bending moment for the different sweeps are reported in Figure D.3. The upper plot shows the values of this particular load for the different blade configurations. One bar (blue color) denotes the blade root flapwise bending moment for the set of simulations where the minimum pitch angles have been kept equal despite the blade geometry. The other bar (in red) shows the extreme blade root flapwise bending moment for wind turbine
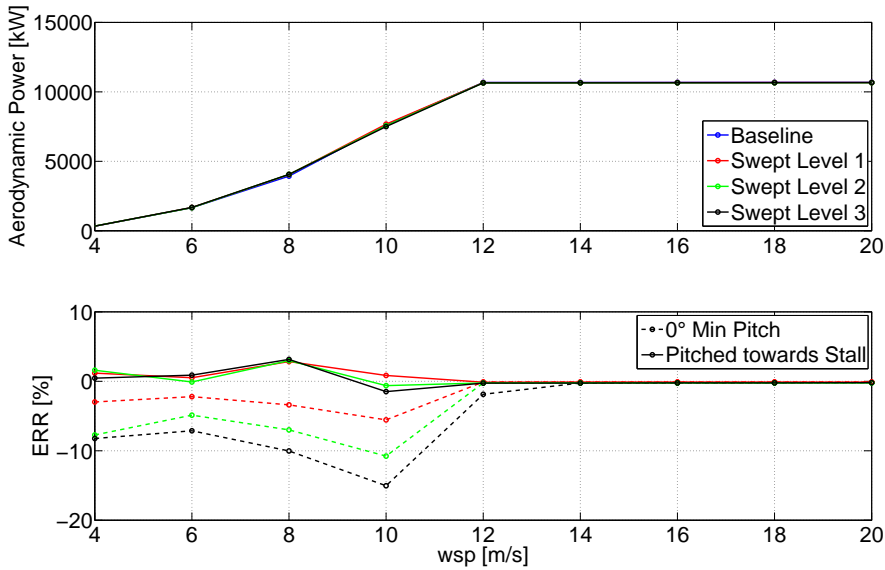
Figure D.2: Wind turbines Power Curves, Upper Plot - Relative Error between the power curves with comparison between configurations using same minimum pitch angles and HAWCStab2 new pitch settings below rated wind speed.

configurations with comparable power curves.

The lower plot shows the variation registered between the extreme loads calculated with and without taking into account wind turbines with similar power outputs. The maximum discrepancy in load variation from the baseline registered for the highest sweep level implemented with respect to extreme blade root flapwise moment is around 10%.

The maximum blade root torsional moment, shown in Figure D.4, increases dramatically when a swept geometry for the blades is introduced. A similar effect on the extreme load variation seen from Figure D.3 is reported. Torsional loadings are overestimated when a common pitch setting is used for all the configurations.

The extreme blade root flapwise bending and torsional moment are computed for wind speeds close to the rated. Therefore, the change in the minimum pitch angle below rated wind speed, introduced to compensate the power loss observed in wind turbines with backward swept blades, is responsible for the load variations observed between the two sets of simulations. Hence, a benchmarking without compensating the power losses of passive controlled wind turbines below rated wind speed brings to an overestimation of the extreme load allevi-

ations due to the use of backward swept blades.

Life time (20-years) equivalent fatigue loads for the blade root flapwise bending moment (Figure D.5) and for the blade root torsional moment (Figure 6 D.6) have been reported. Weibull distribution is considered. No relevant discrepancies between fatigue loads computed for the two sets of simulations are observed. For the blade root moments, the loading introduced by the action of the pitch actuator has the most relevant impact on the life time fatigue load, shadowing eventual effects due to a benchmarking done without considering turbines with lower power curves below rated wind speed.

The wind turbines with the backward sweep shapes chosen are characterized by excessive extreme and fatigue blade root torsional moments. Different changes in blade geometry must be investigated in order to overcome this issue.

It is important to remark that this type of benchmarking have to be based on wind turbines that produce the same power output below rated wind speed. The risk is a significant overestimation of the beneficial and negative effects brought by the use of geometrical bend-twist coupling. A load analysis that takes into account excessive discrepancies in the power curves cannot be trusted to evaluate the potential of passive control strategies.
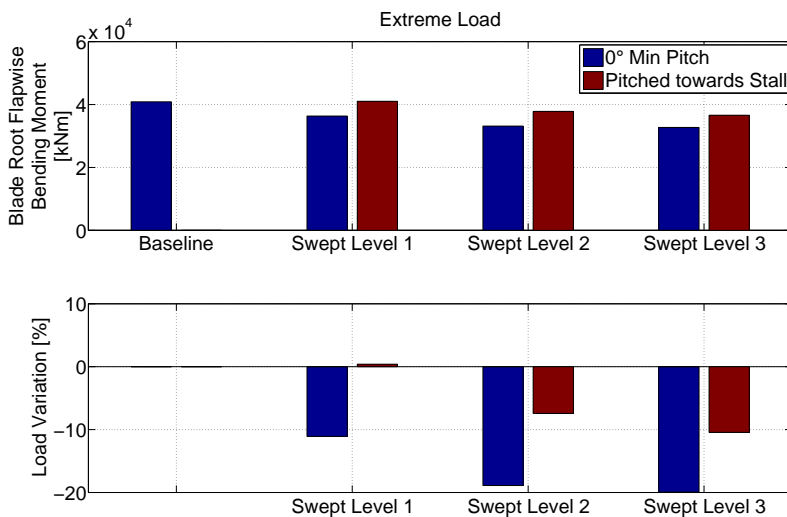
Figure D.3: Extreme blade root flapwise bending moment. Load variation with respect to the baseline (lower plots) according to the configurations using the same minimum pitch angles (blue) and new pitch angles (red).
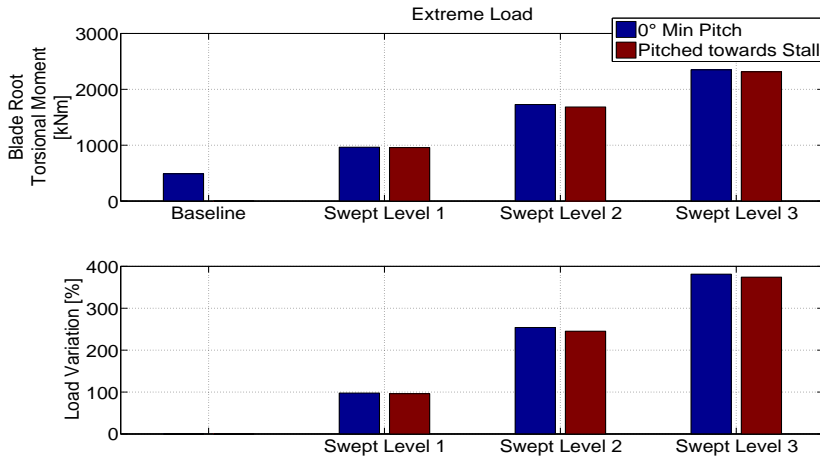
Figure D.4: Extreme blade root torsional moment. Load variation with respect to the baseline (lower plots) according to the configurations using the same minimum pitch angles (blue) and new pitch angles (red).
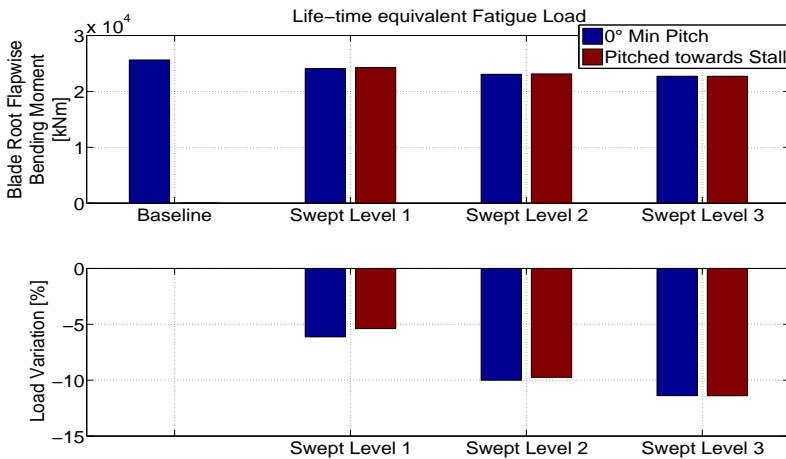
Figure D.5: LTE Fatigue blade root flapwise bending moment. Load variation with respect to the baseline (lower plots) according to the configurations using the same minimum pitch angles (blue) and new pitch angles (red).
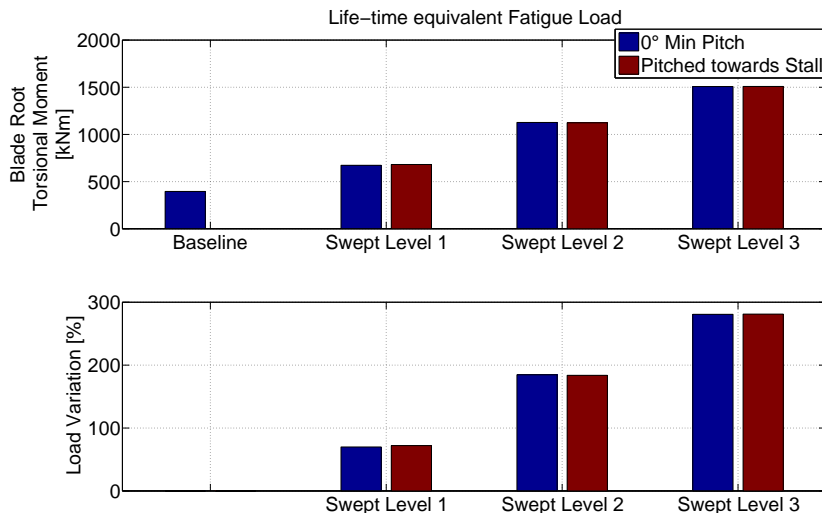
Figure D.6: LTE Fatigue blade root torsional moment. Load variation with respect to the baseline (lower plots) according to the configurations using the same minimum pitch angles (blue) and new pitch angles (red).

D.4   Conclusions

The current study showed the importance of providing definite guidelines for the benchmarking of wind turbines that use geometry-type passive control. Results have been reported with the purpose of comparing different configurations of wind turbines with backward swept blades. Main difference between the sets of simulations proposed was the implementation of a simple scheme able to provide the benchmarking with wind turbines characterized by comparable power curves. If the wind turbines used for the benchmarking produce less power below rated wind speed than the baseline, the beneficial load alleviations brought by the passive control method chosen can be overestimated. In order to give a correct estimation of the load variations brought by the passive control methodologies isolating its effects, the recommendation is that the benchmarking has to be based on wind turbines with similar power curves.

Bibliography

[1] Ashwill, T. D. *Passive Load Control for Large Wind Turbines*, in: 48th AIAA Meeting, Orlando, Florida, 2010

[2] Verelst, D.R.S. and Larsen, T.J., *Load consequences when sweeping blades - a case study of a 5 MW pitch controlled wind turbine*, Technical Report Risø-R-1724, Risø-DTU, May 2010, Roskilde

[3] Hansen, M. H., *Aeroelastic properties of backward swept blades*, Proceedings of the 49th AIAA Aerospace Sciences Meeting, 4-7 January 2011, Orlando, Florida

[4] Zuteck, M. *Adaptive Blade Concept Assessment: Curved Planform Induced Twist Investigation*, Sandia National Laboratories, SAND2002-2996, Albuquerque, New Mexico, USA, 2002.

[5] Larsen, T. J. and Hansen, A. M. *How 2 HAWC2, the user's manual*, DTU Wind Energy, Risø-R-1597(ver.4.6)(EN), Roskilde, Denmark, 2015.

[6] Larsen, T.J., Aagard Madsen, H., Larsen, G.C. and Hansen, K.S., *Validation of the dynamic wake meander model for loads and power production in the Egmond Aan Zee wind farm*, Journal of Wind Energy, 2013, 2013;16(4):605-624, doi:10.1002/we.1563

[7] Kim, T., Hansen, A.M. and Branner, K., *Development of an anisotropic beam finite element for composite wind turbine blades in multibody system*, Journal of Renewable Energy, 2013; 59:172-183, doi:10.1016/j.renene.2013.03.033

[8] Bak, C., Zahle, F., Bitsche, R., Kim, T., Yde, A., Henriksen, L.C., Natarajan, A. and Hansen, M.H., *Description of the DTU 10 MW Reference Wind Turbine*, DTU Wind Energy Report-I-0092, July 2013, Roskilde, Denmark

New lightweight structural blade designs and blade designs with build-in structural couplings - New Structural Solutions, sec. 2.3

Authors:
Christian Pavese, Vladimir Fedorov, Kim Branner

Christian Pavese[1], Vladimir Fedorov[1], Kim Branner[1]

E.1   State of the Art and Motivation

As wind turbines capacities and dimensions increase, blade designers and manufactures have taken up the challenge of designing and building blades that are stronger and lighter. The capability of efficient load mitigation on the structure during operation becomes an attractive characteristic for the design of modern wind turbine blades. To this end, different techniques have been exploited in the last two decades to achieve load reduction on wind turbines. In particular, the so-called "passive control methods" represent an interesting possibility for wind turbine blade designers. These types of methods are based on the idea of designing a structure that deforms so as to provide a load reduction during operation.

Passive control methods can be implemented by e.g. using the following mechanisms:

- employment of backward swept blades;

- bend-twist coupling (BTC) due to anisotropic properties of fiber-reinforced composite materials.

The objective of the implementation of these control strategies is the same: to introduce a structural coupling between bending toward the tower and torsion toward feather that has the effect of decreasing the angle of attack along the wind turbine blade, thus mitigating the loads on the structure.

In the last two decades, several studies have been conducted to show the passive control potential of either swept wind turbine blades [1, 2, 3, 4, 5, 6] or bend-twist coupled blades [7, 8]. So far, the research within wind energy field has been focused on the development of blade designs that employs only a single passive control strategy at a time. The current work aims at studying the load alleviation potential for a combination of passive control methodologies with the final goal of proposing new and innovative concepts for lightweight wind turbine blade designs.

In the present investigation, several designs involving both modification of geometry of an originally straight blade and modification of the blade structure, i.e. orientation of blade materials are considered. A single-shear web design is also proposed. The initial idea related to the use of a single shear web design

---

[1]DTU Wind Energy, DK-4000, Roskilde, Denmark

was to enhance the effects of backward swept blades and BTC due to a consistent decrease of blade torsional stiffness. Later analysis showed that a blade design with decreased torsional stiffness presents characteristics very similar to a blade with passive control. Due to the use of cambered airfoils, when the single-shear-web blade bends toward the tower it has the tendency of twisting toward feather, hence decreasing the angle of attack. For this reason, the single shear web design is considered as a passive control itself in this work.

Three passive control strategies are evaluated and combined in different blade designs. Blade stiffness and strength properties for each of the chosen blade design are analysed and reported. Full design load bases (DLB) are carried with the purpose of evaluating extreme and fatigue loads on the blades based on standard requirements for wind turbine construction and operation. The computed loads are compared to the DTU 10MW Reference Wind Turbine [9], which is used as a baseline for the studied passively controlled wind turbines. General observations are provided with the intention of gathering knowledge regarding the efficiency of each control strategy alone and their combinations.

The first section of the report describes the considered passive control methods for blade designs and the motivation behind the work. Models and tools used throughout the investigation are reported in the second section, along with a brief description of the baseline wind turbine, its controller and the DLB considered. Results for the modified blade configurations, including blade structural properties and strength characteristics, blade loads, annual energy production and tower clearance are presented and discussed in the following section. The last part of the chapter includes conclusions and future work.

E.2   Brief Description of the Concept

Three passive control strategies are taken into account: blades with backward sweep, blades with BTC and blades with single shear web. The final goal is first to study the effects of each of these methods separately, and then in different combinations. Extensive load and strength analyses are performed in order to prove the possibility of exploiting the synergies between these methods. The idea is to enhance the benefits from each of the strategy applied alone and to reduce the negative effects by combining the methods. A summary of the passive methods considered here is given in Figure E.1.

Each column in Figure E.1 describes a different method, classified by a three letters code (SSW for the blade design with single shear web, SWP for the swept blade and BTC for the blade with bend-twist coupling). The rows contain information regarding:

- application zone - area where the control strategy is applied according to the

span-wise position;

- mechanism of the passive control strategy;

- outcome - the qualitative effect of each control strategy;

- required design corrections - general design adjustments to be considered for implementing the method into the blades.

The following points have to be highlighted in order to clarify some of the presented choices for the passive control strategies applied in each blade design:

- the application zones for the different methods have been chosen based on the analysis of the possible outcomes;

- the application of the SSW on the full blade span is bounded to manufacturing constraints

	Single Shear Web (SSW)	Sweep (SWP)	Bend-twist coupling (BTC)
Application zone	Full Blade	Blade tip - s80-b0025-f0000 (80% radius, 2m tip back)	UD layers of spar caps - 8° UD bias for entire blade
Mechanism	Twist to feather due to lower torsional stiffness	Twist to feather by extra torque	Twist to feather due to bending moment and BTC
Positive Outcome	Passive load alleviation due to decreased angles of attack in operation, Slightly higher tower clearance	Passive load alleviation due to decreased angles of attack in operation, Higher tower clearance	Passive load alleviation due to decreased angles of attack in operation, Higher torsional stiffness (potentially positive)
Negative Outcome	Risk of aeroelastic instabilities Structural stability (buckling)	Higher torque load along the blade length Higher torque load at the pitch actuator	Lower tower clearance due to lower bending stiffness Lower strength of the biased UD layers
Required Design corrections	Pitch toward stall to compensate AEP loss below rated wind speed Check for buckling	Pitch toward stall to compensate AEP loss below rated wind speed	Pitch toward stall to compensate AEP loss below rated wind speed

Figure E.1: Passive control methods description.

- the swept blade design is selected according to a parametric study performed by the authors, taking into account load alleviation potential and a restrained increase in extreme and fatigue blade root torsional loads (to be published);

- the shape for the swept blade is chosen to be a pure backward sweep where the change in the shape starts at 80% of the blade length with the maximum sweep of around 2m at the tip;

- the application zone for the BTC is chosen after preliminary consideration of the blade strength and structural properties;

- after few design iterations, there was selected an angle of 8° for biasing of the UD layers in the spar caps.

All the choices related to the control strategies are made with the general idea of exploiting the synergy between the three passive control methods. Consider for example the tower clearance: a backward swept blade is able to increase the tower clearance due to its structural properties, at the same time providing beneficial load alleviations on the blades. The BTC can reduce the loads acting on the structure, but it also decreases the bending stiffness of the blade, lowering the tower clearance. Hence, a combination of SWP and BTC can result into a favourable load alleviation effect still maintaining the tower clearance required by the design standards.

The full list of the wind turbine blade design analysed within the present investigation is reported hereby together with their acronyms in the parenthesis:

- Baseline straight blade

- Swept blade (SWP)

- Blade with BTC (BTC)

- Straight blade with single shear web (SSW)

- Swept blade with single shear web (SWP+SSW)

- Swept blade with BTC (SWP+BTC)

- Straight blade with single shear web and BTC (BTC+SSW)

- Swept blade with single shear web and BTC (SWP+BTC+SSW)

E.3   Models Description, Baseline Wind Turbine and DLB

Linear aero-servo-elastic models are implemented in HAWCStab2 and used for closed-loop eigenvalue analysis and controller tuning. Further, nonlinear aeroelastic models, implemented in HAWC2, are used for response analysis in time domain. Structural properties of the blade cross-sections are calculated using the in-house Beam Cross section Analysis Software –BECAS.

HAWCStab2 is based on a linearization of Timoshenko beam elements in a nonlinear co-rotational formulation coupled with an unsteady blade element momentum (BEM) method. Shed vorticity, dynamic stall and dynamic inflow are included in the aerodynamic model. A detailed description of the HAWCStab2 architecture is provided by Hansen [6]. Sønderby and Hansen [10] made an exhaustive validation and analysis of the open-loop performances. A description of the linearized wind turbine controller is given by Tibaldi et al. [11].

The structural model of HAWC2 is based on a multi-body formulation using Timoshenko beam elements developed by Kim et al. [8]. The aerodynamic model, also based on the BEM method, handles dynamic inflow, dynamic stall, skew inflow, shear effects on the induction and effects from large deformation. Validation can be found in Vorpahl et al. [12], Popko et al. [13] and in Larsen et al. [14].

BECAS [15] is a group of Matlab functions used for 2D analysis of stiffness and mass properties of generic beam cross sections. Two pre-processing scripts included in the BECAS package, Airfoil2BECAS [16] and Shelllexpander [17], have been used to generate the FE meshes that served as input into BECAS. They are two python scripts designed to generate 2D-meshes of blade crosssections with specified materials and their corresponding spatial orientations in BECAS format

. The DTU 10 MW Reference Wind Turbine (RWT) [9] is used as the baseline turbine in this study. The Basic DTU Wind Energy Controller [18] is used and its description with regard to the DTU 10 MW RWT is provided by Bak et al. [9].

The DLB used is the DTU Wind Energy Design Load Basis for onshore turbines [19], which is based on the third edition of the IEC 61400-1 standard [20]. The DTU DLB covers typical cases for assessment of extreme and fatigue loads on the turbine components. The DTU 10 MW RWT was designed before the formulation of the DTU DLB, using a slightly different IEC 61400-1-inspired load basis as reported by Bak et al. [9] in chapter 6.3 of the report. Therefore, the following modifications are made to the DTU DLB to have a load basis similar to the one used to design the baseline turbine:

- the controller dependent design case DLC 2.2 is disregarded;

- the extreme values of the loading from DLC 1.1 are not determined using any statistical extrapolation, because of the uncertainty related to the choice of an appropriate method; instead, the GL approach [21], which requires a partial safety factor of 1.35, is adopted.

E.4   Description of the Workflow

A summary of the workflow used to build the analysed passive-controlled blades is provided in Figure E.2. The programs and tools used for each step of the workflow and reported in the previous section have been described here they are highlighted in red boxes.

After selection of a blade design is made, 2D FE meshes for 100 cross-sections along the blade span are generated using the DTU 10MW RWT input data. Cross-sectional structural properties are calculated and used for generation of the blade beam model. Structural damping of the beam is set to 3% for both first flapwise and the first edge-wise modes. Before launching the DLB and proceed-
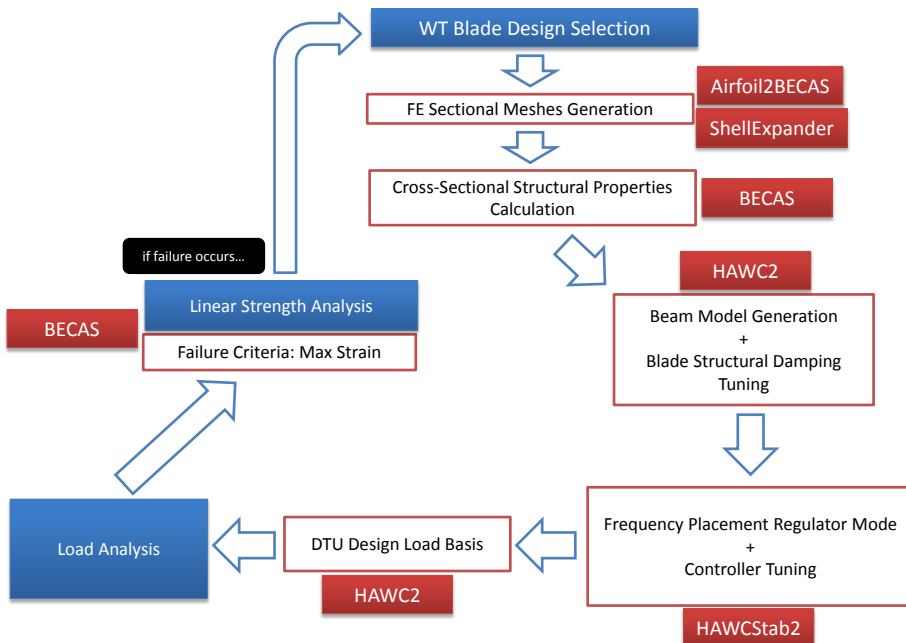
Figure E.2: Workflow diagram for input generation and analysis of selected blade designs.

ing with the load analysis of the passively controlled wind turbine blades, each design is pre-processed to balance the following two negative effects associated with the chosen passive control methods:

- frequencies and damping ratios of the speed regulator mode of turbines with a passively controlled blades can be significantly different compared to the baseline, due to the changes in structural properties and dynamic behaviour;

- due to the decrease in angle of attack due to the passive control, the turbine considered to have lower Annual Energy Production (AEP) at wind speeds below rated compared to the baseline configuration.

To overcome the first issue, tuning of the PI loop of the controller in Region 4 (constant power, torque and rotational speed) is performed with a pole placement technique. HAWCStab2 is used to perform this tuning adopting a method documented by Hansen et al. [18] and Tibaldi et al. [22]. The target damping ratio and the target frequency for the pole of the speed regulator mode at 12ms-1 are respectively 70% and 0.1Hz for all the wind turbines within this study.

To compensate for the loss of annual energy production at wind speeds below rated, the passively controlled blades are pitched further toward stall compared to the baseline configuration. This is done according to the amount of twist provided by the control strategy and to compensate for the decrease in the angle of attack.

Load analysis for each wind turbine configuration is then carried out. Extreme and life time equivalent fatigue loads for the blade root and tower top are analysed for each blade configuration, verifying the AEP is close to the original values, and the tower clearance is sufficient.

E.5   Results

Results from the load and strength analyses are reported and discussed in this section. The main focus is to establish the effects of combined passive control strategies, assuming that all the analysed blade designs fulfil standard design requirements.

In the first part of the section, an overview concerning the AEP and the minimum tower clearance for the wind turbines designed is presented. A discussion regarding the computed blades structural properties and their possible impact on the loads is reported. Strength analysis is carried out in the following part of the section and analysis of the blade root and tower top extreme and life time equivalent fatigue loads for all blade configurations is given in the last part of the section.

E.5.1 AEP and tower clearance

To keep performance and safety of the modified wind turbines at the original level, the annual energy production and minimum tower clearance are computed for each design and it is made sure they are not worse than of the baseline design. The values of the tower clearance include the GL safety factors [21]. In the DTU 10 MW RWT report [9] the authors state that the tower clearance has enough margin for all the load cases considered. The minimum tower clearance reported in [9] is provided by DLC 1.3 and its value, including safety factors, is 5.86 m. The baseline tower clearance calculated using the workflow and tools of the present study is also provided by DLC 1.3 and its value is 5.63 m without safety factors. Therefore, the minimum clearance registered for the baseline turbine satisfies only the IEC standard requirements [20], since still clearance between blades and tower is left applying a safety factor of 1.35 indicated by the DLB used. The clearance left is 3.66 m. The guidelines given by GL [21] are not satisfied, since they require a 30% of the total tower clearance for the operation load cases (from DLC 1.x to DLC 5.x). The total tower clearance for the DTU 10 MW RWT is 18.26 m and the minimum tower clearance registered (3.66 m) for the DLB including the safety factors which is only 20% of the total. For this reason, the tower clearance required for the passively controlled wind turbines has to satisfy only the IEC standard.

A summary of the annual energy production and the minimum tower clearance computed for each of the designs considered within the present study is reported in Table E.1. Results are given as variations in percent from the values for the baseline design. The annual energy production variations from the baseline are always lower than 0.5%. This is due to efficient strategy of pitching the blades toward stall at wind speeds below rated. Omitting this pitch angle tuning would cause a consistent drop in AEP level due to the nature of passive control mechanism to reduce the efficient angles of attack along the blade.

The tower clearance requirement according to the IEC standard is satisfied

Table E.1: AEPs and tower clearances compared to the baseline wind turbine.

Blade Design	AEP	Tower Clearance
Baseline	**48.564** GW h	**3.656** m
SSW	-0.3%	+1.3%
SWP	-0.1%	+4.9%
SWP + SSW	-0.4%	+8.6%
BTC	+0.04%	-5.7%
BTC + SSW	+0.3%	-11.6%
SWP + BTC	-0.1%	-4.0%
SWP + BTC + SSW	-0.3%	-1.0%
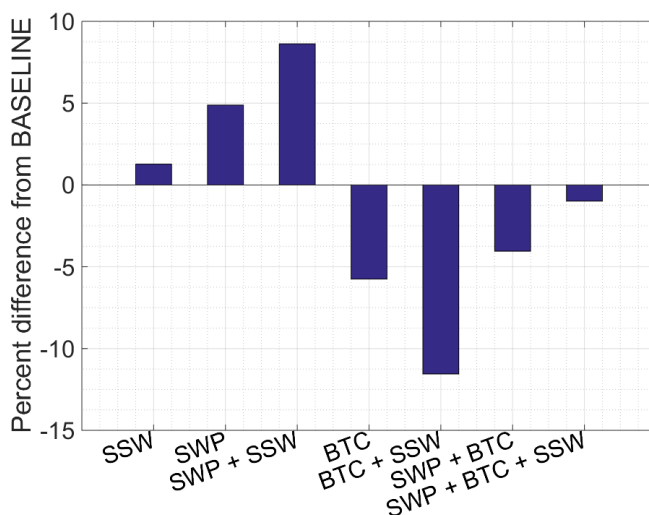
Figure E.3: Variation of the tower clearance of considered blade designs compared to the baseline configuration.

for all the passive-control designs, since none of the blades touches the tower for the implemented DLB. A diagram visualizing the differences in minimum tower clearances is given in Figure E.3. The blade designs incorporating BTC generally show a substantial drop in minimum tower clearance, due to decrease in the blade flapwise bending stiffness caused by the biasing of the fibers of the UD layers in the spar caps. As expected, the swept blades demonstrate lower tip displacements, which are reflected in a consistent increase of the minimum tower clearance. The combination of BTC and backward sweep in the blade design (SWP+BTC) helps compensating the negative effect of BTC on tower clearance, even though an increase of only 4% with respect to the baseline is registered. The combination of all three passive control methods produces a blade design with a minimum tower clearance very similar to the one of the baseline blade (difference of 1%).

E.5.2   Blade stiffness properties

Here structural properties of the modified blades are presented. They are calculated by BECAS for each of the 100 cross-sections along the blades. Notice that stiffness properties of the swept blade configurations are not given as they are the same as for the straight blades. The sweep itself is assumed not to introduce any difference into the structural properties.

Stiffness properties of each of the considered blade configurations with passive control are compared to the ones of the baseline blade configuration. The results for flapwise stiffness are given in Figure E.4. It becomes clear that the introduction of the fiber biasing into the UD layers of the spar caps leads to significant drop in blade flapwise bending stiffness, up to 7-8%, see the "2SW BTC" curve. While the single shear web blade design alone leads to minor reduction in the blade flapwise bending stiffness, combination of the single shear web and fiber biasing in the same design leads to maximum drop in the bending stiffness, which is the reason for decreased tower clearance of ca. 11.6%, see Table E.1.

Figure E.5 demonstrates the variation of the blade torsional stiffness for different blade designs. The single shear web blade design possess much lower (up to 35%) torsional stiffness which could be a potential problem, e.g. in the run-away case where it might cause flutter, but this is not verified in the present investigation. Another interesting fact is that the fiber biasing according to the BTC design cannot provide any reasonable recovery of the torsional stiffness in the single shear web blade design, $+2..+3\%$ at maximum. This is confirmed with the torsional stiffness growth for the BTC only blade design. It can be an indication that the UD layers of the spar caps is not the best position for fiber biasing if one wants to increase the blade torsional stiffness.

The next interesting plot demonstrates the amount of BTC along the blades with biased fibers in the spar caps UD layers, see Figure E.6. The flapwise bending-twist coupling coefficient β is calculated along the blade length in accordance to the method described in [23]. The figure shows that generally higher coupling can be achieved for the original two-shear web blade than for the modified single shear web blade. This fact agrees well with the results obtained for the coupled box- and I-beams in [23]. Thereby, the BTC and single-shear web methods for passive load control seem to interfere with each other and can unlikely be recommended for combination in the same blade design when the BTC effects are prioritized.

E.5.3 Blade Strength

In order to ensure operational blade designs it is important to perform strength calculations on the blades. In the present investigation this is done for extreme load cases according to the DLB. This means that the blade strength is checked at the most critical loads expected to occur during the wind turbine lifetime, also taking into the account the safety factors prescribed by IEC standard.

Strength analysis was performed in BECAS for 27 cross-sections along the blade length. It was done for a number of critical load cases occurred in the aeroelastic simulations for each blade configuration. The failure criterion chosen for the strength analysis was the maximum strain criterion. The choice is dictated by
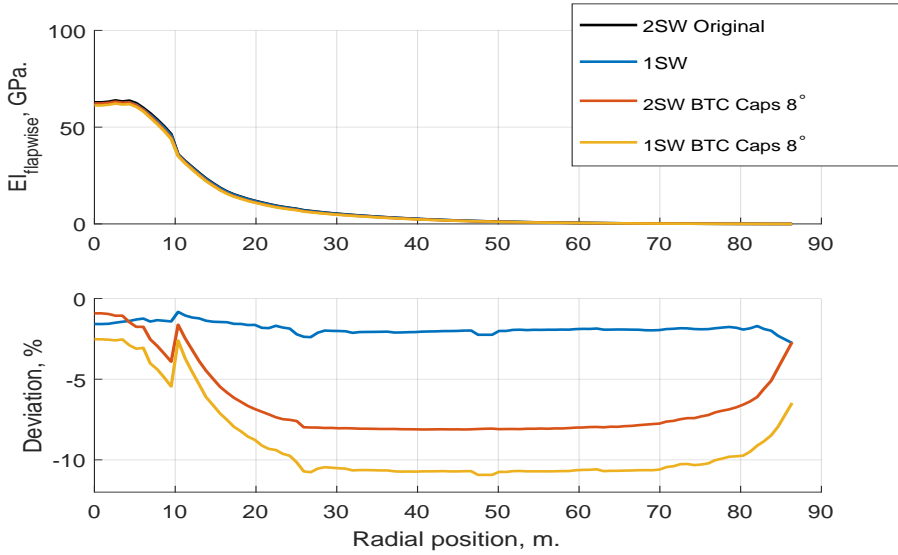
Figure E.4: Flapwise bending stiffness for different blade designs and its deviation from baseline blade characteristics.
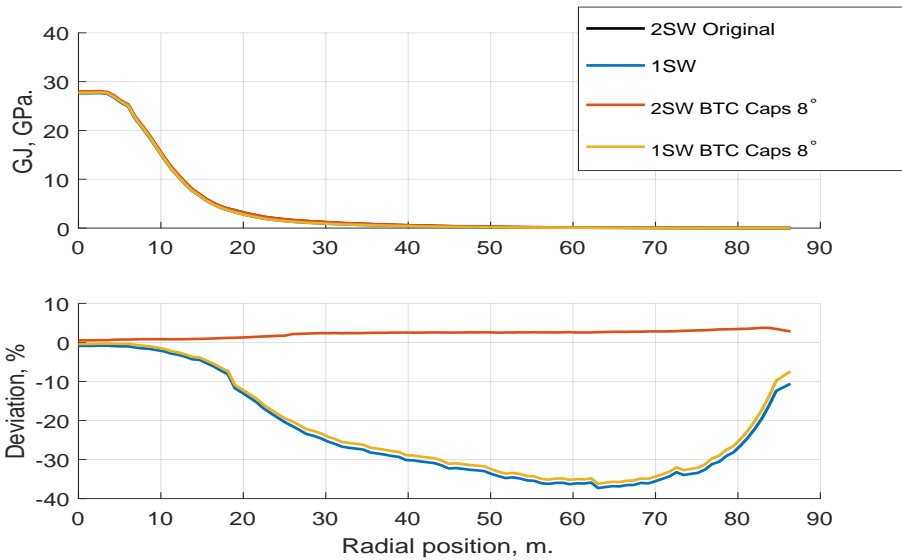
Figure E.5: Torsional stiffness for different blade designs and its deviation from baseline blade characteristics.
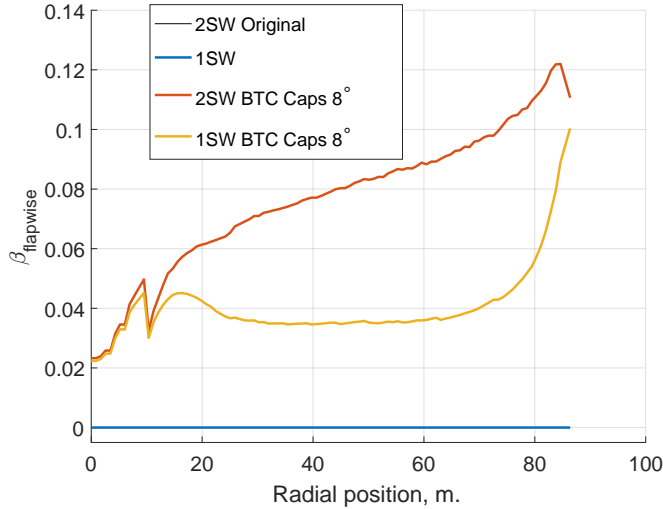
Figure E.6: Flapwise bend-twist coupling coefficient β for different blade designs.

the fact that this criterion was chosen to design the baseline DTU 10MW RWT blade. Selected results for the failure index, which shows how close is each of the sections to failure (FI = 1), are shown in Figure E.7.

As one can see from the results for failure indices, all the modified blade designs increase the failure index along the most of the blade length, except for the blade root. This is believed to be the case due to the positive effect of the passive load control which reflects lower extreme loads at the root and generally lower strength of the blade due to introduction of BTC and single shear web concepts. Generally, all the blade modifications are shown to be strong enough to resist the extreme lifetime loads.

E.5.4 Extreme and lifetime equivalent fatigue loads

Extreme and lifetime equivalent fatigue are reported in this section. The loads are calculated at two positions on the wind turbine: the blade root and the tower top.

Figure E.8/ E.9 and Figure E.10 show blade root bending and torsional loads respectively. In general, all passive control strategies produce alleviations for both extreme and fatigue bending loads in the range between 5 and 10%.

In the flap-wise case, the combination of all the three control methods demonstrates the highest drop in both extreme and fatigue loads (6% for extreme and
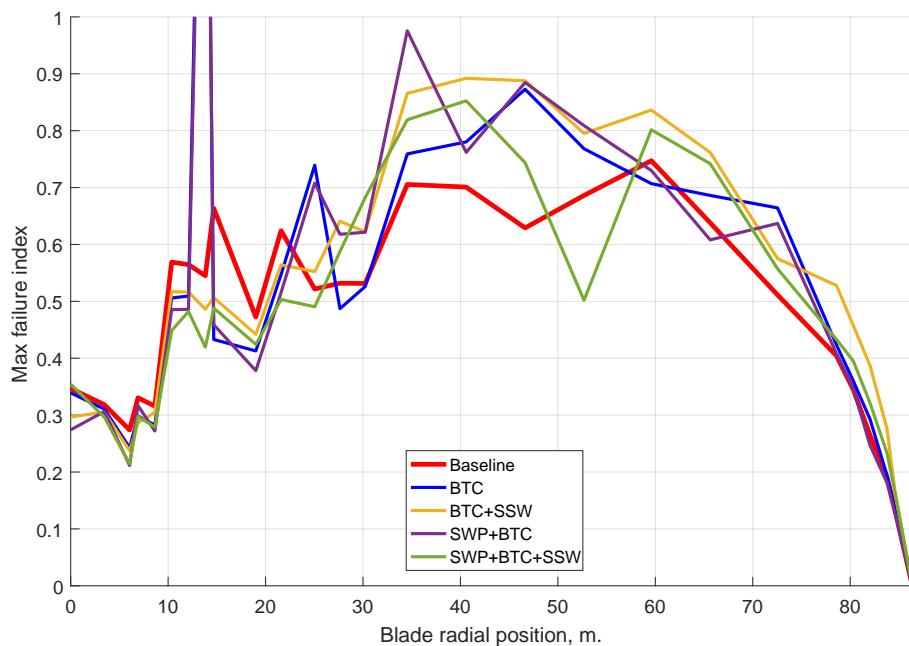
Figure E.7: Strength characteristics for some of the blade designs considered in the present investigation.

ca. 11% for fatigue values). The flap-wise load alleviation for the combined designs is stronger than for the isolated passive control designs.

The swept blade design is the most efficient for the extreme edgewise blade root loads. The single shear web design and its combinations prove to be the most effective choice for the lifetime equivalent blade root edgewise fatigue load. This outcome is due to the fact that these loads are mostly driven by gravity forces which are linked to the total mass of the blade. The SSW designs have lower blade mass, which is decreased by 7.5% compared to the DTU 10MW RWT blade due to the presence of only a single shear web against the three used for the baseline design.

It is worth mentioning here that the single shear web design will likely lead to a significantly lower buckling resistance of the blade and therefore the blades with single shear web configurations ideally have to be analyzed for this type of failure. Presently this type of analysis has not been performed as it requires modeling and computational recourses and is therefore planned for future work. The backward swept blade has a negative impact on the blade root torsional moment (1.5% increase in extreme and 5% increase in fatigue), due to the extra torque generated by the swept tip of the blade. BTC shows a strong alleviation of the extreme blade root torque (11%) and a large increase in the lifetime
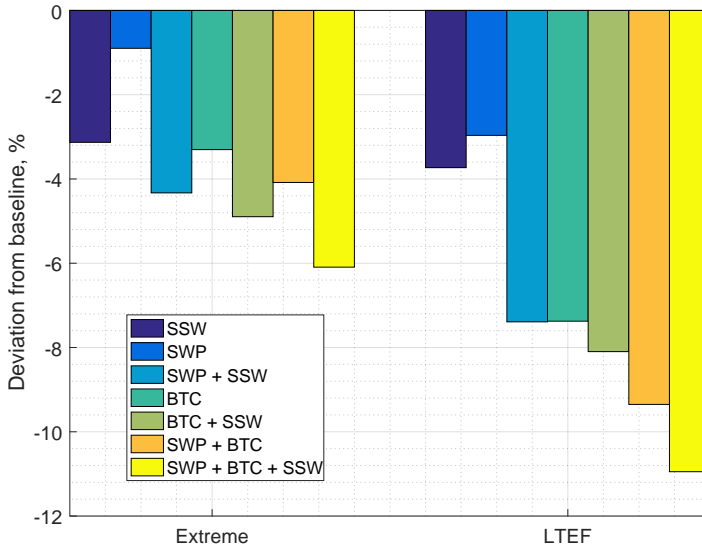
Figure E.8: Extreme and life-time equivalent fatigue (LTEF) flapwise bending moment for the blade root.
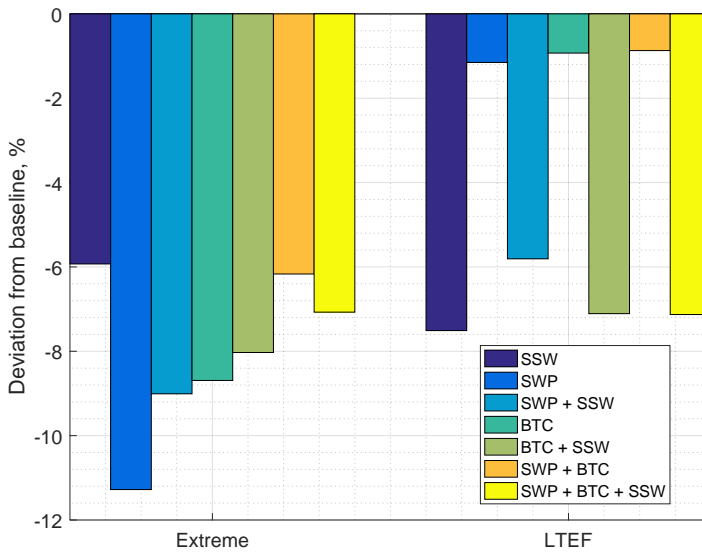
Figure E.9: Extreme and life-time equivalent fatigue (LTEF) edgewise bending moment for the blade root.
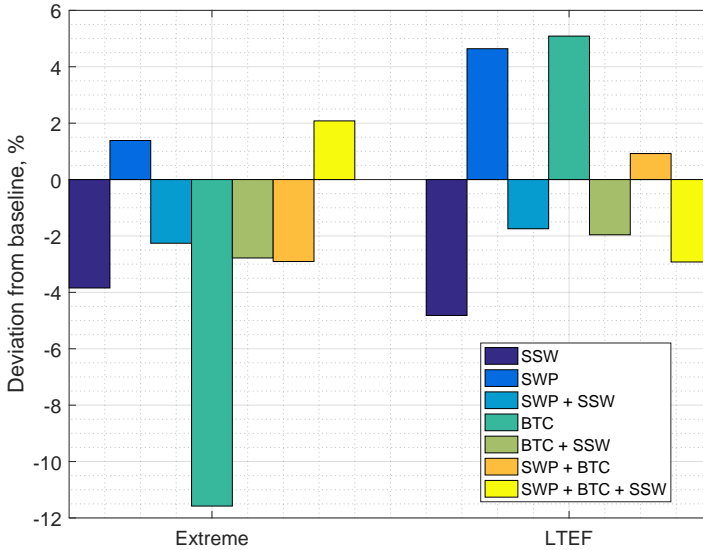
Figure E.10: Extreme and life-time equivalent fatigue (LTEF) torque values for the blade root.

equivalent fatigue load (around 5%). A clear reason for the latter is unknown. SSW alleviates both extreme and fatigue torsional moments. In general, while the results for blade root torque for the swept design have been expected, it was not possible to define a clear trend for the other passive control strategies and, consequently, for their combinations. Further investigations regarding the blade root torsional loads need to be performed, as well as eventual evaluation of the impact on the pitch controller and the aero-servo-elastic dynamics of the system.

Figure E.11 and E.12 shows the extreme and fatigue loads for the tower top, respectively. This is presented to demonstrate the load alleviation potential of the passive control strategies on other wind turbine components. The extreme fore-aft tower top moment decreases for all the considered designs. The alleviation reaches a maximum of around 9% for the case with all the three strategies combined. The result is in-line with the observations made regarding the blade root extreme flap-wise moment. The side-to-side extreme load does not show any considerable variation respect to the baseline design.

The two designs SWP+SSW and BTC have the most beneficial effects on the fore-aft tower top fatigue load, showing peak alleviations slightly higher than 9%. The combined designs are more efficient towards the side-to-side fatigue load reduction, where the SWPT+BTC+SSW and the BTC combined cases are able to reduce the lifetime equivalent load by almost 4%.
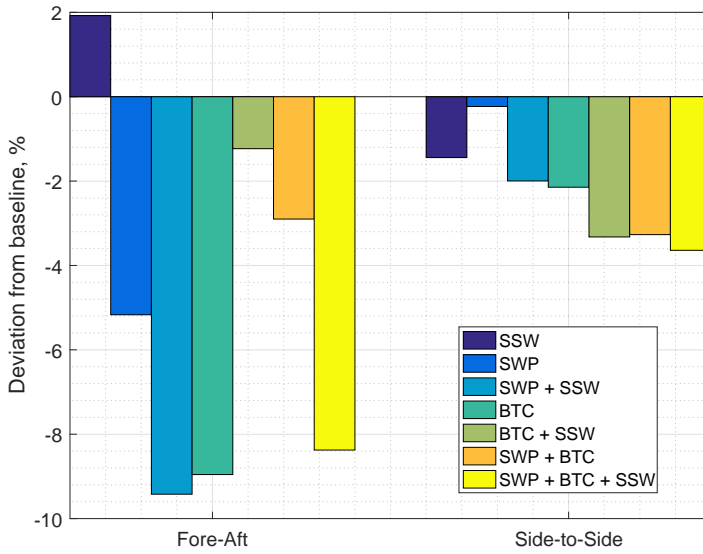
Figure E.11: Extreme values of the tower top fore-aft and side-to-side loads.
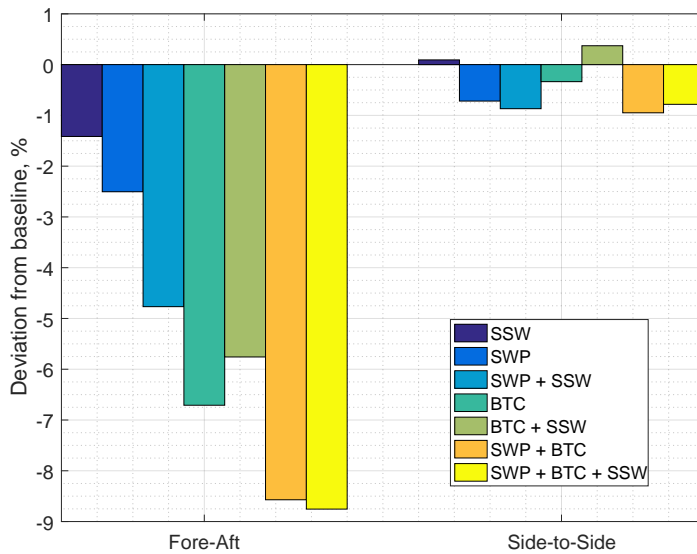
Figure E.12: Life-time equivalent fatigue (LTEF) values of the tower top fore-aft and side-to-side loads.

E.6 Conclusions and recommendations

Three passive control strategies for wind turbine blade design have been considered for the DTU 10MW reference wind turbine and the impact on loads and strength of the blades has been evaluated. The following passive control blade designs have been considered:

- backward swept blade, where change in the shape starts at 80% of the blade length with the maximum sweep at the tip at around 2m;

- BTC design, where the fibres of the UD layers in the spar caps are biased by 8°;

- single shear web design.

Several studies previously reported in the literature have already established the load alleviation potential of two of these passive control methods (blade sweep and material bend-twist coupling). Present work investigated synergies between these methods applying different combination of these passive controls strategies to a given blade design.

All the considered blade designs matched the requirements for blade strength and tower clearance. The deviation of the annual energy production from the baseline value was limited to lower than 0.5% design and it was kept at this level throughout the study.

The results showed that the right combination of passive control strategies can lead to a blade design capable of enhancing the load alleviations and diminishing negative effects from each of the passive control strategies. An example is the combination of the BTC and the backward sweep in the same blade, resulting in the blade root flap-wise fatigue loads being lower with respect to the baseline (4%) and with respect to the only-swept blade design (6% extra load alleviation) and the BTC-only design (2% extra load alleviation). At the same time, combining the swept blade design with the BTC helped to compensate the decrease in minimum tower clearance caused by the loss in bending stiffness due to the rotation of the fibres of the UD layers in the spar caps.

The single shear web design and backward sweep proved to be a good passive control combination for the reference blade. The load alleviation effects of the swept blade were enhanced by the lower torsional stiffness of the single shear web design. The blade root flap-wise life time equivalent fatigue loads for the single shear web design decreased by ca. 3.5% and the same load for the swept blade decreased by 2.5%, while combining the two designs brought a total load alleviation of 7%.

The single shear web design and BTC design combination did not produced the

desired boosting in terms of load alleviation. The reason lies in the bend-twist coupling parameter β, which is lower along the blade span for the combined BTC+SSW design, than for the BTC-only design. The consequence of lowering the coupling coefficient β was observed in the tower top fore-aft extreme and fatigue loads. The BTC design has much higher load alleviation than the combined BTC+SSW case.

The blade root edge-wise fatigue loads are driven by gravity and a blade with lower mass such as the single shear web design (7.5% lower mass than the baseline) and its combination can bring a 7% decrease in lifetime equivalent moment. The combination of all the three passive control strategies in the same reference blade is effective only with respect to the blade root flap-wise extreme and fatigue moments. For the blade root edge-wise loads and the tower top bending moments, the SWP+BTC+SSW design did not produce further load alleviations compared to the other combinations. The reason is the negative impact from the combination of BTC and single shear web design.

In general, all the passive control strategies and their combinations produced substantial changes in the structural properties of the blade. To better adapt these methods to exploiting their full potential, the blade has to be re-designed from the structural point of view, by e.g. moving materials and changing the thicknesses of the blade layups according to the needs. An optimization framework is seen to be used in the future studies to fulfil this purpose. Buckling analysis for the blade and stability analysis will also be provided in future investigations.

Bibliography

[1] Ashwill, T., Veers, P. S., Locke, J., Griffin, I. C. D. and Zuteck, M. D. *Concepts for Adaptive Wind Turbine Blades*, in: ASME 2002 Wind Energy Symposium, Paper No. WIND2002-28, pp. 56-69. Reno, Nevada, USA, 14-17 January 2002, doi:10.1115/WIND2002-28.

[2] Zuteck, M. *Adaptive Blade Concept Assessment: Curved Planform Induced Twist Investigation*, Sandia National Laboratories, SAND2002-2996, Albuquerque, New Mexico, USA, 2002.

[3] Ashwill, T. D., Kanaby, G., Jackson, K., and Zuteck, M, *Development of the swept twist adaptive rotor (STAR) blade*, Proceedings of the 48th AIAA Aerospace Sciences Meeting, 4-7 January 2010, Orlando, Florida

[4] Knight and Carver Wind Group, *Sweep-Twist Adaptive Rotor Blade: Final Project Report*, Sandia National Laboratories, SAND2009-8037, Albuquerque, New Mexico, USA, 2010.

[5] Verelst, D.R.S. and Larsen, T.J., *Load consequences when sweeping blades - a case study of a 5 MW pitch controlled wind turbine*, Technical Report Risø-R-1724, Risø-DTU, May 2010, Roskilde

[6] Hansen, M. H., *Aeroelastic properties of backward swept blades*, Proceedings of the 49th AIAA Aerospace Sciences Meeting, 4-7 January 2011, Orlando, Florida

[7] Bottasso, C. L., Campagnolo, F., Croce, A. and Tibaldi, C., *Optimization-based study of bend-twist coupled rotor blades for passive and integrated passive/active load alleviation*, Journal of Wind Energy, pp. 16:1149-1166. DOI:10.1002/we.1543, 2013.

[8] Kim, T., Hansen, A.M. and Branner, K., *Development of an anisotropic beam finite element for composite wind turbine blades in multibody system*, Journal of Renewable Energy, 2013; 59:172-183, doi:10.1016/j.renene.2013.03.033

[9] Bak, C., Zahle, F., Bitsche, R., Kim, T., Yde, A., Henriksen, L.C., Natarajan, A. and Hansen, M.H., *Description of the DTU 10 MW Reference Wind Turbine*, DTU Wind Energy Report-I-0092, July 2013, Roskilde, Denmark

[10] Sønderby, I and Hansen, M.H., *Open-loop frequency response analysis of a wind turbine using high-order linear aeroelastic model*, Journal of Wind Energy, 2013, DOI: 10.1002/we.1624

[11] Tibaldi, C., Henriksen, L.C., Hansen, M.H. and Bak, C., *Wind turbine fatigue damage evaluation based on a linear model and a spectral method*, accepted for publication on Journal of Wind Energy, 2014.

[12] Vorpahl, F., Strobel, M., Jonkman, J.M., Larsen, T.J. and Passon, P., *Verification of aeroelastic offshore wind turbine design codes under IEA wind task XXIII*, Journal of Wind Energy, 2013; doi:10.1002/we.1588

[13] Popko, W., Vorpahl, F., Zuga, A., Kohlmeier, M., Jonkman, J., Robertson, A., Larsen, T.J., Yde, A., Stertr, K., Okstad, K.M., et al., *Offshore code comparison collaboration continuation (OC4), PHASE I - results of coupled simulations of an offshore wind turbine with jacket support structure*, Proceedings pf the International Offshore and Polar Engineering Conference 2012, 2012;337-346

[14] Larsen, T.J., Aagard Madsen, H., Larsen, G.C. and Hansen, K.S., *Validation of the dynamic wake meander model for loads and power production in the Egmond Aan Zee wind farm*, Journal of Wind Energy, 2013, 2013;16(4):605-624, doi:10.1002/we.1563

[15] Blasques, J.P. and Bitsche, R., *User's Manual for BECAS*, DTU Wind Energy, Roskilde, Denamrk, 2014

[16] Bitsche, R. D. *Airfoil2BECAS: A preprocessor for the cross-section analysis software BECAS*, DTU Wind Energy, Roskilde, Denmark, 2014.

[17] Bitsche, R. *Shellexpander: A preprocessor for the cross-section analysis software BECAS*, DTU Wind Energy, Roskilde, Denmark, 2013.

[18] Hansen, M.H. and Henriksen, L.C., *Basic DTU Wind Energy Controller*, Technical Report DTU Wind Energy E-0018, DTU, 2013

[19] Hansen, M. H., Thomsen, K. Natarajan, A. and Barlas, A. *Design Load Basis for onshore turbines - Revision 00*, DTU Wind Energy, Technical Report E-0074(EN), Roskilde, Denmark, 2015.

[20] I. E. Commission, International Standard, *IEC 61400-1 Third Edition 2005-08, Wind Turbines - Part 1: Design Requirements*, Reference Number IEC 61400-1:2005(EN), 2005.

[21] G. Lloyd, *Guideline for the CertiFIcation of Wind Turbines*, Standard, July 2010.

[22] Tibaldi, C., Henriksen, L.C., Hansen, M.H. and Bak, C.*Effects of gain-scheduling methods in a classical wind turbine controller on wind turbine aeroservoelastic modes and loads*, Proceedings of the 52th AIAA Aerospace Sciences Meeting, 12-17 January 2014, National Harbor, Maryland

[23] Fedorov, V. and Berggreen, C., *Bend-twist coupling potential of wind turbine blades*, Journal of Physics: Conference Series - The Science of Making Torque from Wind 2014, IOP Publishing, 2014, doi: 10.1088/1742-6596/524/1/012035

Reduced Design Load Basis for Ultimate Blade Loads Estimation in Multidisciplinary Design Optimization Frameworks

Authors:
Christian Pavese, Carlo Tibaldi, Torben J. Larsen, Taeseong Kim, Kenneth Thomsen

Reduced Design Load Basis for Ultimate Blade Loads Estimation in Multidisciplinary Design Optimization Frameworks

Christian Pavese[1],Carlo Tibaldi[1], Torben J. Larsen[1], Taeseong Kim[1], Kenneth Thomsen[1]

Abstract

The aim is to provide a fast and reliable approach to estimate ultimate blade loads for a multidisciplinary design optimization (MDO) framework. For blade design purposes, the standards require a large amount of computationally expensive simulations, which cannot be efficiently run each cost function evaluation of an MDO process. This work describes a method that allows integrating the calculation of the blade load envelopes inside an MDO loop. Ultimate blade load envelopes are calculated for a baseline design and a design obtained after an iteration of an MDO. These envelopes are computed for a full standard design load basis (DLB) and a deterministic reduced DLB. Ultimate loads extracted from the two DLBs with the two blade designs each are compared and analyzed. Although the reduced DLB supplies ultimate loads of different magnitude, the shape of the estimated envelopes are similar to the one computed using the full DLB. This observation is used to propose a scheme that is computationally cheap, and that can be integrated inside an MDO framework, providing a sufficiently reliable estimation of the blade ultimate loading. The latter aspect is of key importance when design variables implementing passive control methodologies are included in the formulation of the optimization problem. An MDO of a 10 MW wind turbine blade is presented as an applied case study to show the efficacy of the reduced DLB concept.

---

[1]DTU Wind Energy, DK-4000, Roskilde, Denmark

F.1   Introduction

One of the key aspects for the design of a wind turbine blade is the estimation of ultimate loads. A reliable evaluation of ultimate loads is an intricate problem due to the stochastic nature of turbulence and the nonlinear dynamic behaviour of the system. To face the complexity of this issue, the standards require a large amount of simulations, which can represent an excessive computational effort. This effort becomes impractical when a turbine is preliminary designed with an MDO. In optimization frameworks, the computation of ultimate loads is of crucial importance when design variables implementing passive control methodologies are included in the process. These variables can produce substantial variations in the distribution of the loading on a wind turbine blade, requiring constant updates for the ultimate strength constraints. Consequently, there is a need of a scheme able to give a sufficiently accurate and quick estimation of the variation of the ultimate blade load envelopes during an MDO.

The wind turbine MDO frameworks developed in recent years already presented different solutions to this problem. Some of these frameworks assume that the blade load envelopes are *frozen* either at each step of the optimization process [1], either in a nested multi-stage MDO [2]. In general, a full DLB is computed outside the most computationally expensive loop, and the ultimate blade strength constraints remain unchanged throughout that MDO stage. The frozen loads assumption is valid if the load envelopes change slowly with respect to changes in the design variables, and if the optimization problem for a particular design is not exclusively driven by ultimate strength constraints. Another approach to simplify the calculation of ultimate blade loads is to use only a very restricted amount of design load cases (DLCs) [3, 4, 5]. The selection of these DLCs, which should represent the most strength-critical situations for the blade structure, is based on the experience of the designer.

In this paper, a fast method to compute ultimate blade load envelopes sufficiently accurate for an MDO is presented. The proposed scheme has the advantage of being so computationally cheap that can be included in the optimization loop, eventually dropping the frozen loads assumption. It can take into account all the effects that drive standard DLCs without exclusively relying on the designer experience, and without being dependent from the wind turbine design. The key behind the proposed ultimate blade load analysis strategy is the substitution of turbulent load cases with sets of "deterministic" DLCs. The effect of the turbulent inflow is mimicked using custom-made shear zones and extreme operating gusts. Consequently the amount of simulations and the simulation time are drastically decreased. Limitations connected to the substitutions of the turbulent DLCs need careful considerations.

The first section of this paper provides a description of the models used. The DTU 10 MW reference wind turbine (RWT) [6] is chosen as the baseline design for this study. The second section presents in details the methodology of the

reduced DLB concept. To test the efficacy of the latter, ultimate blade load envelopes are calculated for the baseline design and a design obtained after a generic MDO. The results section shows that the envelopes computed for a full standard design load basis (DLB) [7] and the reduced DLB for the two designs have similar characteristics that can be exploited following a workflow presented in the methodology section. Positive and negative outcomes behind the use of the reduced DLB approach are discussed. In the last section, a test case implemented in the DTU MDO framework HAWTOPT2 [1] is reported to provide an application for the reduced DLB approach.

F.2 Models

The nonlinear models used for the estimation of the load envelopes are implemented in the time-domain aero-servo-elastic code HAWC2 [8, 9]. The multibody formulation used by the structural part of HAWC2 is presented and validated in [10]. The description and the validation of the unsteady BEM method used by the program can be found in [11, 12, 13].

As mentioned in the introduction, the testing of the reduced DLB concept passes through the computation of a typical standard DLB. For this study, the "DTU Design Load Basis for onshore turbines - Revision 00" [7] is selected. The DTU 10 MW RWT [6] coupled with the Basic DTU Wind Energy Controller [14] are used as the baseline turbine.

The final test case presented in the last section is computed through an optimization process carried by the HawtOpt2 framework [1, 15]. Built on the platform provided by OpenMDAO (Open-source Multidisciplinary Design, Analysis, and Optimization Framework) [?, 17, 18, 19], the tool is used to handle the definition of the optimization problem, workflow, dataflow, and parallelization of simulation cases. OpenMDAO provides an interface to PyOpt [20], a container for several optimization algorithms. In this work, the gradient-based sequential quadratic programming optimizer SNOPT [21] is used.

F.3 Methodology

The stochastic nature of the turbulence adds complexity to the estimation of the ultimate loads. As briefly mentioned in the introduction, to face the intricate matter of simulating wind turbine loading in turbulent inflow conditions, a standard DLB requires an high amount of simulations (the DTU DLB counts up to 1880 DLCs). The number of simulations depends on the amount turbulence

seeds considered, which is usually as large as possible to obtain wind turbine loads with sufficient accuracy. Taking into account such a number of simulations in an MDO can become impractical due to the computational effort and time required to perform each cost function evaluation. Moreover, turbulent DLCs are lengthy simulations (usually the standard simulated time is 10 minutes), which can represent a further obstacle to keep the optimization time reasonable.

Another issue is the fact that the interaction of a changing turbine design with different parts of the same turbulent field during an MDO might compromise the quality of the optimization process [22].

In the light of these problems, the main idea behind the formulation of the reduced DLB for the estimation of ultimate loads in MDO frameworks is to use a "deterministic" set of load cases able to mimic the effects of turbulence on the blade loading. These "deterministic" DLCs are characterized by the presence of a custom-made shear zone or extreme operating gusts. A detailed description is provided in the next part of the section.

The absence of turbulence from the DLB gives the possibility to greatly shorten both the amount of simulations (no turbulence seeds need to be considered) and the simulation time of each DLC selected (without turbulence a simulated time of 10 minutes is no more a requirement). This translates in a consistent advantage with respect to computation time, which is consistently shortened for the aero-servo-elastic code used for the study. The time required to run an HAWC2 simulation of the reduced DLB is suited for efficient MDO.

In the next part of this section, a full description of the reduced DLB is provided, along with an explanation of "deterministic" set of load cases aforementioned. The section concludes with a part dedicated to how this reduced DLB concept can be integrated in an wind turbine blade MDO problem.

F.3.1 The Reduced DLB

The main characteristic of the reduced DLB is the substitution of turbulent load cases with a set of "determistic" ones. The substitution brings a significant reduction in the amount of the DLCs and simulation time. Moreover, as the presence of stochastic inflow conditions can compromise the results of the MDO process, the ultimate blade load envelopes are computed through simulations that use deterministic changes in the inflow. In this manner, a blade design changing during the MDO will always interact with the same wind field structure, ensuring a more robust evaluation of the variations in wind turbine loading due to a change in a design variable. At each cost function evaluation, the new design undergoes the same wind loading excitations than its predecessor ensuring, for example, that the optimization process is not depending on the position occupied by the blade in a stochastic inflow field.

Two wind flow conditions are used to substitute the turbulent inflow load cases:

- a custom-made shear for production, fault, start-up, and shut-down load cases;

- an extreme operating gust (EOG) for parked and maintenance DLCs.

Figure F.1 provides a visual representation of the first deterministic wind field variation used by the reduced DLB. When a blade rotates towards the upward positioning, it passes through a custom-made shear zone, formed by a combination of a linear horizontal shear and a linear vertical shear. At the center of the hub, the wind speed, defined by the coordinate system $< u, v, w >$ that follows the notation in the HAWC2 manual [9, p. 21], is equal to the uniform wind speed selected for the specific DLC ($u_1 = V_{hub}$ and $v_1 = V_{hub}$). Above the hub height, the wind speed increases towards the outer part of the rotor
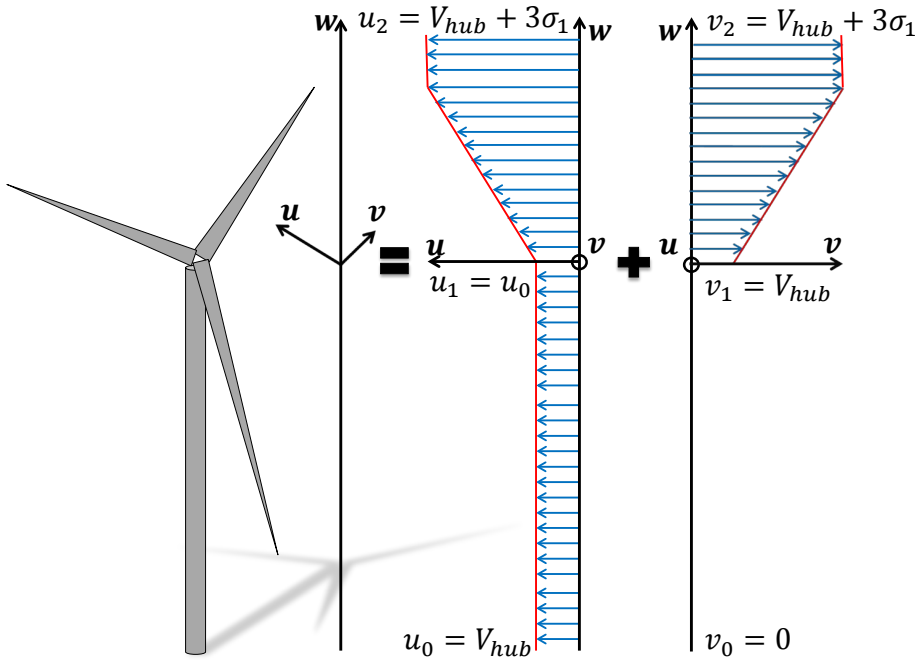

Figure F.1: Visual representation of the custom-made shear zone used to mimic ultimate blade loading generated by turbulent inflow. The sheared wind inflow is assembled by the combination of a linear horizontal shear and a linear vertical shear in the upper part of the rotor. Values of the wind speed in the different areas of the shear zone are highlighted in the equations.

until it reaches the value defined in Equation F.1. The rest of the wind inflow is uniform and it has a constant value of V_{hub}.

$$u_2 = V_{hub} + 3\sigma_1; \quad v_2 = V_{hub} + 3\sigma_1 \tag{F.1}$$

where V_{hub} is the wind speed at hub height selected for a specific DLC, and σ_1 is the representative value of the turbulence standard deviation as defined by the IEC standard [23, p.24-27] and reported in Equations F.2 and F.3 for normal and extreme turbulence models, respectively.

$$\sigma_1 = I_{ref}(0.75V_{hub} + b); \quad b = 5.6\text{m s}^{-1} \tag{F.2}$$

$$\sigma_1 = c \, I_{ref} \left[0.072 \left(\frac{V_{ave}}{c} + 3 \right) \left(\frac{V_{hub}}{c} - 4 \right) + 10 \right]; \quad c = 2\text{m s}^{-1}; \quad V_{ave} = 0.2 \, V_{ref} \tag{F.3}$$

where V_{ref} and I_{ref} are the reference wind speed and turbulence intensity, respectively, which depend on the turbine class. Since the DTU 10 MW RWT belongs to the class IA, $V_{ref} = 50\text{m s}^{-1}$ and $I_{ref} = 0.16$.

The idea behind the use of the described custom-made shear zone is to apply to each blade a loading with the highest peak at 1P both in the flapwise and the edgewise directions. This type of loading is typical for wind turbines due to shear, tower shadow, and nacelle tilt, and it represents the most important contribution to blade loads in turbulent inflow conditions. The wind profile in the custom-made shear zone (Equations F.1, F.2, and F.3) is selected to take into account the maximum wind speed variations present in the turbulence DLCs.

The second deterministic wind field variation is an EOG, which is implemented in the reduced DLB following the formulation provided by the IEC standard in [23, p. 26].

The effect of turbulence on the loads cannot be exactly replicated, but the maximum and minimum flapwise and edgewise blade loads can be caught with a sufficient accuracy, as shown in the next section. Furthermore, the proposed scheme to mimic turbulent DLCs is based on general observations of typical wind turbine loads, and it can be therefore applied to different wind turbine designs and classes.

A complete summary of all the load cases that constitute the reduced DLB used for the RWT is reported in Appendix A. Only the ultimate DLCs are part of the DLB (label "U" in [7, p. 7]). The partial safety factors used for each DLC are the same used in [7]. The load cases that do not consider turbulence in the DTU DLB are kept unchanged (DLC14, DLC15, DLC23, DLC32, DLC33, and DLC42). Simulated time is not reported because it is not a strict requirement for the reduced DLB, and it can be chosen according to the aero-servo-elastic models used. Controller faults dependent load cases (DLC22) are not considered for the time being, as they were not included as design load cases for the DTU

10 MW RWT. These DLCs are going to be included in a future development of the reduced DLB.

F.3.2 Intergration of the reduced DLB in an MDO framework

The reduced DLB concept can be integrated in an optimization problem for the design of a wind turbine blade. As shown in details in the next section, the envelopes obtained through the computation of the reduced DLB are similar in shape to the one obtained from a full DLB, but different in magnitude. For this reason, the reduced DLB can be used directly in the MDO as an indicator of the load variations following the scheme depicted in Figure F.2. A detailed description of the steps of the integration process are highlighted in the figure's caption.

The optimization problem is supplied with blade load envelopes coming from a full DLB. Then, a correction, based on the load variations caught by the reduced DLB, is applied every cost function evaluation. The deterministic nature of the reduced DLB does not compromise the optimization process, which is quickly provided with new ultimate blade load envelopes at each step. Moreover, the most time-consuming part of the process (the estimation of envelopes with a full DLB) is done outside the optimization loop.

F.4 Results

The purpose of this section is to show that an ultimate loading variation estimated through a reduced DLB is similar to load variations estimated by a much more computationally expensive DLB. If this assumption is verified, the reduced DLB can be suitable for ultimate blade load envelopes estimation in an MDO process, and the scheme described in Figure F.2 can be applied.

Figure F.3 shows a comparison between ultimate load envelopes (plot on the top left) of the Baseline and of the Step 1 designs extracted using the full and the reduced DLBs. The Step 1 is a blade design resulting from the first cost function evaluation of an MDO, where the design variables include both aeroshape and internal structure of the blade. The load envelopes are calculated at a blade radial station located at approximately 51m. Along with the envelopes, the ultimate loads projected in 4 directions (maximum and minimum flapwise moments, 0° and 180° respectively, maximum and minimum edgewise moments, 90° and -90° respectively) are compared.

Figure F.2: Description of the integration of the reduced DLB concept in an MDO framework. 1 - Out-of-the-optimization-loop estimation of ultimate load envelopes with full DLB for the starting design ($\mathbf{E}^{full}_{BASE}$ is a matrix containing cross sectional forces and moments for each envelope point and each blade section). 2 - Out-of-the-optimization-loop estimation of ultimate load envelopes with reduced DLB for the starting design ($\mathbf{E}^{red}_{BASE}$). 3 - Starting from the baseline design, the MDO is carried until it reaches a new design (Step 1 design). The baseline full DLB ultimate load envelopes ($\mathbf{E}^{full}_{BASE}$) are used. 4 - The load envelopes are estimated with the reduced DLB on the Step 1 design ($\mathbf{E}^{red}_{S1}$). 5 - Correction factors **CFs** are obtained from the baseline reduced envelopes and the step 1 design ones (see equation). 6 - The correction factors are used to calculate the envelopes at the next cost function evaluation ($\mathbf{E}_{S1} = \mathbf{CFs} * \mathbf{E}^{full}_{BASE}$). 7 - The corrected ultimate blade loads are ready to be applied on the next iteration of the optimizer, which will produce a new design (Step 2 Design). 8/10 - Same procedure from point 4 to 6 is applied on Step 2 design.

The bar plot at the bottom of the figure shows the ultimate loading variations in these 4 directions obtained with the full and the reduced DLBs. The latter plot shows how the reduced DLB is able to catch the quality of these variations. A full overview of the projected ultimate flapwise and edgewise loads in both directions for each section of the blade is shown in Figure F.4. The plots compare the variations between maximum and minimum flapwise and edgewise loads calculated using a full standard DLB and the reduced DLB, respectively.

The variations in percent are estimated as $\mathbf{V}(r) = (\mathbf{E}_{S1}/\mathbf{E}_{BASE} - 1) * 100$, where r is the blade radius.

The reduced DLB approach is able to replicate the trend of the load variations computed using a standard DLB especially in the outer part of the blade. The reduced DLB overestimates the decrease in loading observed for the minimum

Figure F.3: Comparison of ultimate load variations calculated between Baseline and Step 1 design using the full and the reduced DLB. The load envelopes are calculate for a section located at 51m along the blade length. The plot on the top left describes the envelopes, while the plot on the top right describes the ultimate loading projections along 4 directions, namely maximum and minimum flapwise moments, 0° and 180° respectively, maximum a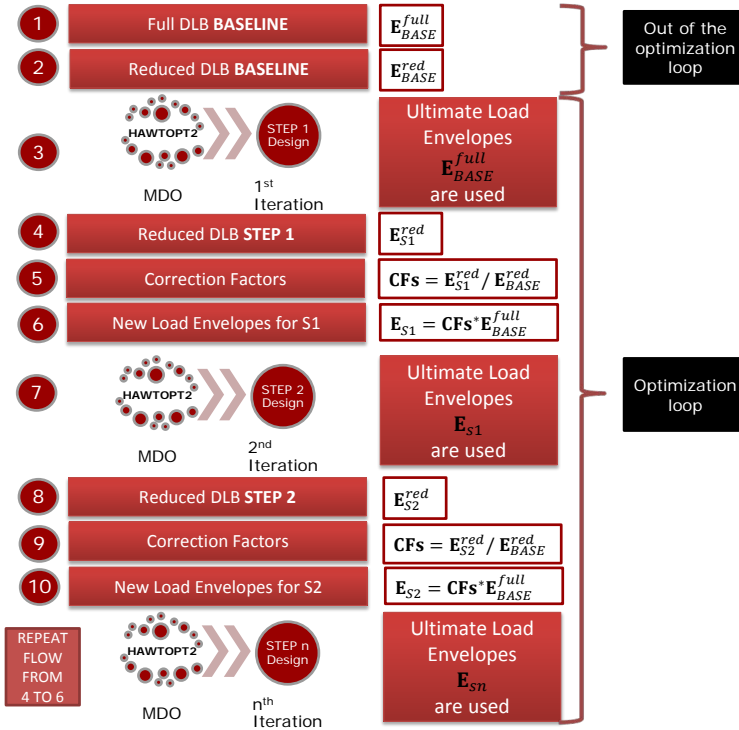nd minimum edgewise moments, 90° and -90° respectively (loading directions also plotted on the bottom-left plot). The bar plot shows the variations in ultimate loading in the 4 directions just listed for the full and the reduced DLB.

flapwise direction (second plot of Figure F.4). More discrepancies between the loads computed by the two DLBs can be observed in the inner part of the blade in both the edgewise directions. These differences depend on the fact that the ultimate loads in the directions just listed are driven by the DLC 1.3, where an extreme turbulence model is used to evaluate loads in a standard DLB. The reduced DLB can only mimic the effect of turbulence, and it is not able to fully catch the loading driven by an extreme turbulent load case. Specifically, in turbulent inflow conditions, wind speed and direction might vary considerably along the blade span, causing loading variations difficult to replicate with the simplified approach proposed in this work. Nonlinear dynamics of the system and behaviour of the controller add further complexity when it comes to mimic the effects of turbulence.

Despite these problem, the reduced DLB approach catches very well the quality of these variations along all the blade span. The custom-made shear zone is able to replicate well the 1P loading excitation that is the main load contribution for a wind turbine undergoing turbulent DLCs. The extreme operating gusts are enough to catch the wind speed variations in the parked and maintenance load

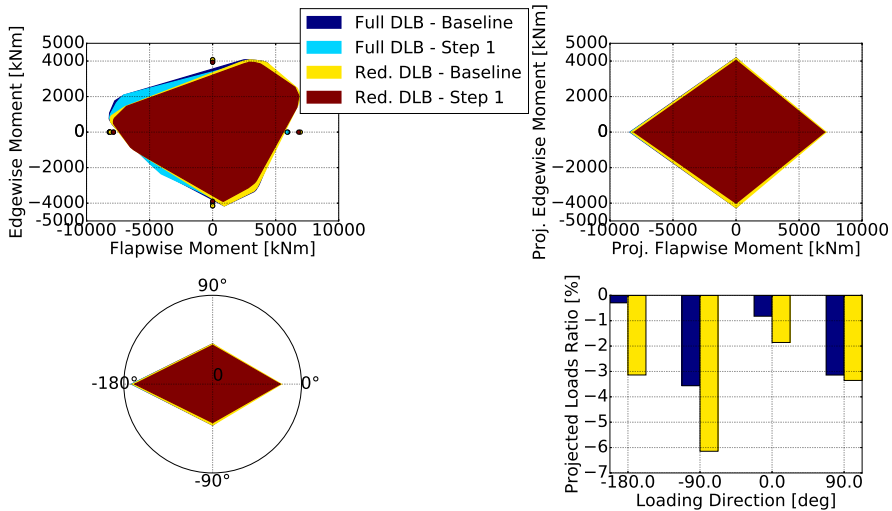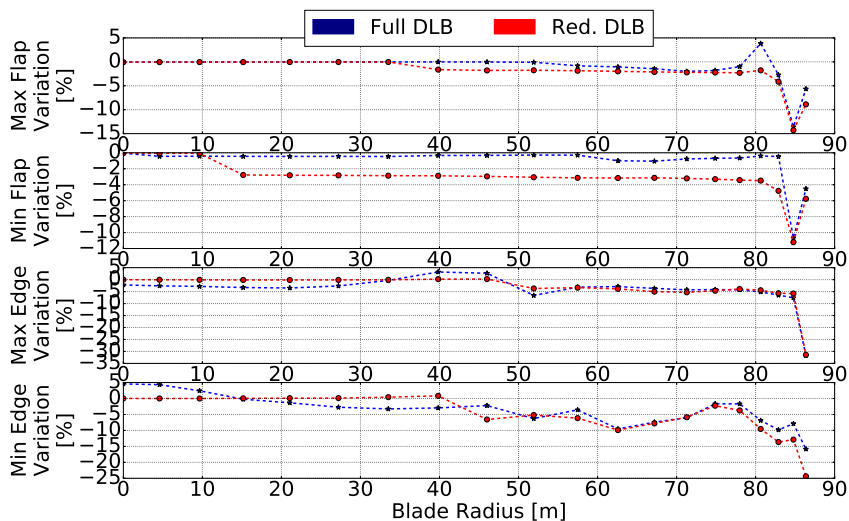**Figure F.4:** Comparison of ultimate load variations calculated between Baseline and Step 1 design using the full and the reduced DLB. The plots are listed in this order proceeding from top to bottom: maximum pure flapwise load variations along the blade radius; minimum pure flapwise load; maximum pure edgewise and minimum pure edgewise.

cases.

In the next section, the results from an optimization test case are reported to demonstrate the efficacy of the reduced DLB approach applied in an MDO framework.

F.5   Application on a Case Study

The reduced DLB concept is applied to a test case implemented in the MDO framework HawtOpt2 [1, 15]. For brevity, only an overview of the design variables and constraints is reported in this paper (see Appendix B). For the full description of the problem formulation and workflow used, the reader can refer to [1, p.2-6]. In the present study, the load estimation part of the workflow is done using the reduced DLB and not the steady state calculation method reported in [1]. Unlike the problem reported in [1], the cost function is the maximization of the annual energy production. To achieve the objective, the blade can stretch, increasing the rotor diameter and the energy captured. The design is further challenged by adding the orientation of the fibres in the spar caps as design variables. The optimizer can exploit the bend-twist coupling toward feather, hence decreasing dynamically the angle of attack to control the loading on the wind turbine [24]. As the fibres in the spar caps start to rotate to create the structural coupling, the bending stiffness of the blade decreases. The blade design becomes more prone to ultimate failure due to the increase of the loading as the rotor diameter stretches to harvest more energy. Moreover, the rotation of the fibres in caps can compromise the tower clearance required by the standard. It is therefore important to be able to properly catch the variations of the loads along the blade span, so that the optimizer can vary the design to conveniently accommodate the strength and tower clearance requirements.

The aim of the MDO problem formulated is to reach an improved design exploiting the possibility of catching the quality of the load variations through the use of the reduced DLB approach. In fact, due to the simplification in the load analysis brought by the absence of turbulence, the optimization cannot identify a global optimum for the design chosen. For the time being, the achievement of a better design compared to the baseline is considered satisfactory, but future work on better methodologies to estimate aeroelastic loads in an MDO is going to be carried out. At time being, surrogate-based methods with the creation of an Approximation Model Management Frameworks (AMMF) are explored [25, 26, 27].

A standard full DLB is computed on the optimal design coming out of the MDO. The wind turbine design characteristics and requirements such as AEP, tower clearance, and fatigue loads reported in Appendix C Table F.5 and Figures F.5 and F.6 are hence extracted from a full DLB to show the ability of the reduced

DLB to respect the design requirements set for the optimization.

The final design has a longer blade radius and, consequently, the wind turbine has a higher AEP (+4.4%). The blade mass is slightly increased (+1.2%) to sustain the higher loading and improve the strength of the blade, counteracting the negative effects caused by turning the fibres of the uniaxial material in the caps. The tower clearance requirement is kept within the given constraints. Table F.5 in Appendix C shows a summary of these characteristics with respect to the original design.

In Appendix C, Figures F.5 and F.6 provide an overview of the strength and loads of the final design obtained from the MDO process, respectively. Figure F.5 the maximum failure indices for each cross section along the blade. The failure indices are evaluated applying loads obtained from a full standard DLB simulated at the end of the optimization on the final design. The ultimate loads are selected from the envelopes projecting flapwise and edgewise moments in twelve directions (not only in four directions as done in Figure F.3). The reduced DLB is able to drive the ultimate loads calculation in the right direction during the MDO, as the final design can withstand a full DLB ultimate loads respecting the given constraints. In fact, no failure is detected along the blade according to the strain criteria.

In Appendix C, Figure F.6 shows the variation of life-time equivalent fatigue moments for the blade root and tower registered for the optimal design. Even though no constraints were put to control these loads, the bend-twist coupling effect generated by the material structural coupling helps to contain the increase. Figure F.7 in Appendix C shows the bend-twist coupling parameter along the blade length. The flap-wise bending-twist coupling coefficient β is calculated along the blade length in accordance to the method described in [28]. Except for the blade root torsional moment which increases by approximately 15%, all the other fatigue loads register a maximum increase of approximately 4%. To improve these results even further, constraints on fatigue loads are going to be included in future studies. The fatigue loads constraints are going to be computed using the method described in [29] and already used for optimization in [1].

F.6   Conclusions

The estimation of ultimate load envelopes is a central topic for wind turbine blade design. The calculation of these envelopes requires a great computational effort, which cannot be practically integrated into multidisciplinary design optimization frameworks. The solutions proposed in recent years to calculate ultimate loads in wind turbine blade optimization do not allow the use of design variables that have a large impact on the distribution of the loading along

the blade, i.e. blade sweep and orientation of the fibres in the layups. With the approach suggested by this study, the estimation of the ultimate blade load envelopes can be fast and accurate enough to be used in each cost function evaluation of an MDO. This approach is based on the formulation of a deterministic reduced DLB that can be computed quickly even by a "slow" aero-servo-elastic code. As the stochastic effect of turbulence might have dangerous consequences during an optimization process, the reduced DLB mimics the influence of turbulence on loading through a deterministic approach.

Results show that the ultimate load envelopes generated by the full and the reduced DLBs are similar, and the ultimate loading projected in the flapwise and edgewise directions vary along the same path.

An applied case study was reported, showing a design optimization process for the DTU 10 MW RWT blade. Blade radius and spar caps fibre orientation were included as design variables. The final optimal design is checked against a full standard DLB. An accurate estimation of the ultimate loads through the use of the reduced DLB at every cost function evaluation, produced a final design able to increase the AEP by 4.4%, withstanding increasing ultimate loads and without compromising the tower clearance. Life-time equivalent fatigue loads are not excessively incremented thanks to the material induced bend-twist coupling effect.

The MDO problem cannot spot a global optimum due to the simplified load analysis approach. The reduced DLB method can give a good estimation of the quality of the variations in loading, but not an accurate estimation of their magnitude. Future work is going to address different methodologies, such as surrogate-based methods including AMMF, to include accurate aeroelastic loads in an MDO with very fast computations.

Acknowledgements

F.7 Appendix A - Reduced DLB Overview

Table F.1: List of the DLCs included in the reduced design load basis used for the baseline wind turbine design. Part I.

Name	Description	WSP [$\mathrm{m\,s^{-1}}$]	Yaw [°]	Shear	Gust	Fault	Nr. Cases
DLC11	Normal production	4:2:26	0	Eqs. F.1-F.2	None	None	12
DLC13	Normal production	4:2:26	0	Eqs. F.1-F.3	None	None	12
DLC14	Normal production	$V_r \pm 2, V_r$ [a]	0	0.2	EDC [b]	None	3
DLC15	Normal production	4:2:26	0	0.2	EWS [c]	None	48
DLC21	Grid loss	4:2:26	0	Eqs. F.1-F.2	None	Grid loss at 10s	12
DLC23	Grid loss	$V_r \pm 2, V_r$	0	0.2	EOG	Grid loss at 3 times	12
DLC24	Large yaw error	4:2:26	-20/+20	Eqs. F.1-F.2	None	Large yaw error	24
DLC32	Start-up at 4 times	$V_{in}, V_r \pm 2, V_{out}$ [a]	0	0.2	EOG	None	16
DLC33	Start-up in EDC	$V_{in}, V_r \pm 2, V_{out}$	0	0.2	EDC	None	16
DLC42	Shut-down at 6 times	$V_r \pm 2, V_{out}$	0	0.2	EOG	None	18

[a] V_r, V_{in}, and V_{out} are the rated, cut-in, and cut-out wind speeds, respectively.
[b] Extreme direction change [60, p. 27].
[c] Extreme wind shear [60, p. 30].

Table F.2: List of the DLCs included in the reduced design load basis used for the baseline wind turbine design. Part II.

Name	Description	WSP [$\mathrm{m\,s^{-1}}$]	Yaw [°]	Shear	Gust	Fault	Nr. Cases
DLC51	Emergency shut-down	$V_r \pm 2, V_{out}$	0	Eqs. F.1-F.2	None	None	3
DLC61	Parked, extreme wind	V_{50} [a]	-8/+8	0.11	EOG	None	2
DLC62	Parked grid loss	V_{50}	0:15:345	0.11	EOG	Grid loss	24
DLC63	Parked large yaw error	V_1 [b]	-20/+20	0.11	EOG	Large yaw error	2
DLC71	Rotor locked extreme yaw	V_1	0:15:345	0.11	EOG	Rotor at 0:30:90°	72
DLC81	Maintenance	V_m [c]	-8/+8	0.2	EOG	Maintenance2	
						Total	278

[a] V_{50} is the extreme wind speed with 50-year recurrence period [60, p.25-26].
[b] V_1 is the extreme wind speed with 1-year recurrence period [60, p.25-26].
[c] V_m is the maintenance wind speed.

F.8   Appendix B - DVs and Constraints Overview for Case Study Section 5

Table F.3: Free form deformation spline (FFD) used in the optimization to define the blade design variables. The spanwise distribution is normalized with respect to the blade length.

Design Variables	CPs Distribution	DVs	Comment
Planform $\mathbf{x}_p$			
Blade length		1	Blade stretches.
Twist	[0.25, 0.45, 0.65, 0.9, 1]	5	Blade root fixed.
Blade pre-bend	[0.45, 0.65, 0.9, 1]	4	Blade root fixed.
Structure $\mathbf{x}_s$			
Spar Caps Uniax (SCU)	[0., 0.2, 0.45, 0.75, 0.95, 1.]	5	Pres./suc. side.
SCU fibre angle, pressure side.	[0., 0.2, 0.45, 0.75, 0.95, 1.]	5	[-20°, +20°]
SCU fibre angle, suction side	[0., 0.2, 0.45, 0.75, 0.95, 1.]	5	[-20°, +20°]
Total		25	

Table F.4: Constraints used in the MDO process.

Constraints	Value	Cons	Comment
Planform g			
max(pre-bending)	< ref. value	6	Maximum pre-bending limited according to scaled blade radius.
Structural $\mathbf{h_g}$			
min(blade mass)	< 1.05	1	The blade mass can increase by 5% compared to the one of the DTU 10MW RWT.
min(blade mass moment)	< 1.05	1	The blade mass moment can increase by 5%.

Constraints	Value	Cons	Comment
min(material thickness)	> ref. value	10	Ensure that the layups have realistic thicknesses depending on section region and material.
$t/w_{sparcap}$	> 0.08	38	Constraint for spar cap buckling.
Strength h_s			
Ultimate strain criteria	< 1.0	190	Material failure in each region of each blade section for ultimate load cases.
Aeroelastic k			
min(tower clearance)	> ref. value	1	Standard minimum tower clearance.
Total		267	

F.9   Appendix C - Results for Case Study Section 5

Table F.5: Overview of the general characteristics of the final optimized design. Results are shown in percent variation from the baseline design.

	Variation from Baseline
Blade radius	+7.7%
Blade mass	+1.2%
Blade tip pre-bending	+85.8%
AEP	+4.4%
Tower Clearance	+2.1%
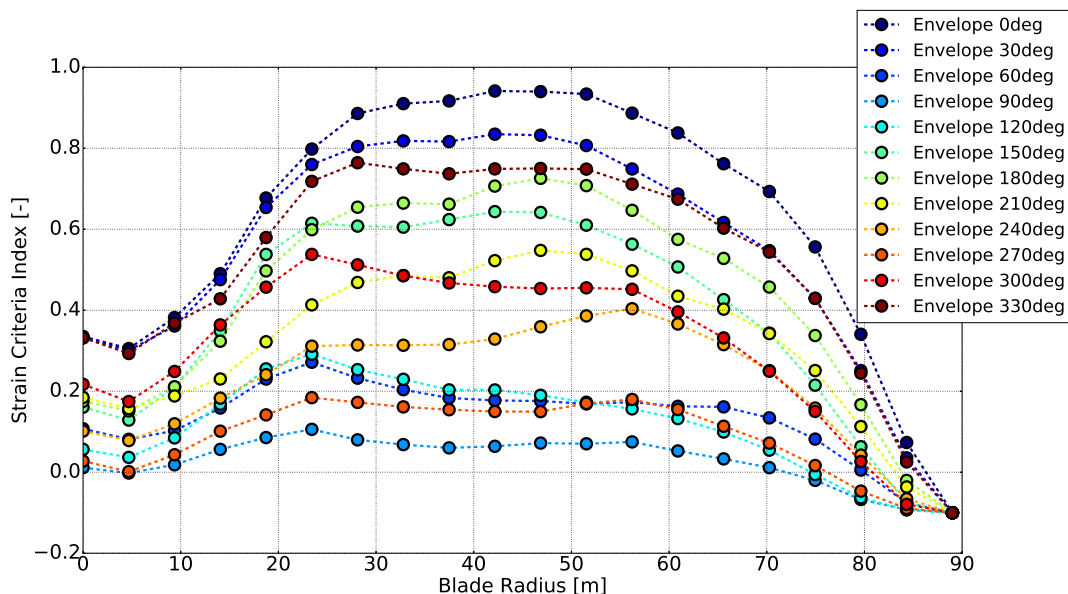
Figure F.5: Maximum sectional failure indices. Failure indices are computed for twelve load cases extracted from ultimate sectional blade load envelopes.
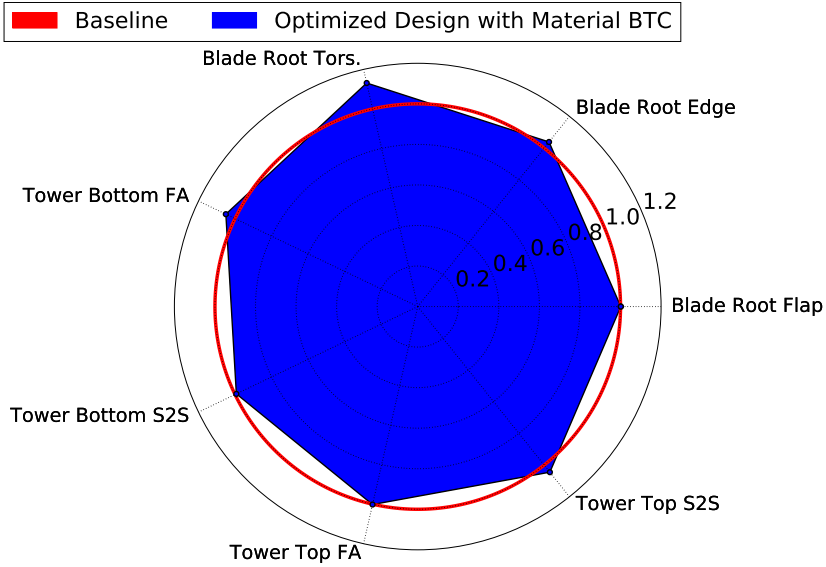
Figure F.6: Life-time equivalent fatigue loads. Fatigue load results are provided for the following sensors: blade root, tower top, and tower bottom. The optimal blade design (blue) is normalized with respect to the baseline loads (red line). "FA" stands for fore-aft, "S2S" for side-to-side, and "Tors." for torsional.
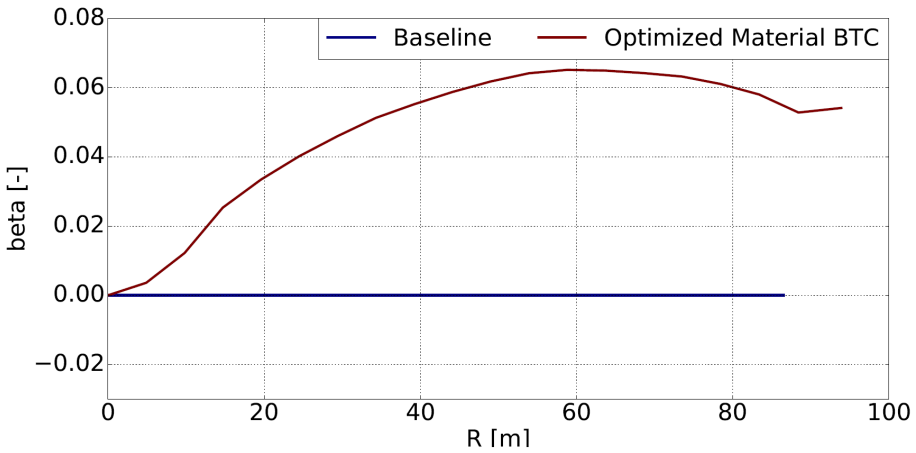
Figure F.7: Bend-twist coupling parameter along the blade span.

Bibliography

[1] Zahle, F., Tibaldi, C., Verelst, D. R., Bak, C., Bitche, R. and Blasques, J. P. A. A. *Aero-Elastic Optimization of a 10 MW Wind Turbine*, in: AIAA SciTech - 33rd Wind Energy Symposium. Kissimmee, Florida, USA, 5-9 January 2015.

[2] Bottasso, C. L., Campagnolo F., and Croce A. 2012 *Multi-disciplinary constrained optimization of wind turbines* Multibody System Dynamics vol 27 (Springer) pp 21-53 ISSN 1573-272X doi: 10.1007/s11044-011-9271-x

[3] Fuglsang P., Bak C., Schepers J., Bulder B., Cockerill T., Claiden P., Olesen A., and Rossen R. 2002 *Site-specific design optimization of wind turbines*, Wind Energy vol 5 (John/Wiley and Sons Ltd.) pp 261-279 ISSN: 1095-4244 doi: 10.1002/we.61

[4] Ashuri T., Zaaijer M. B., Martins J. R. R. A., Van Bussel G. J. W., and Van Kuik G. A. 2014 *Multidisciplinary design optimization of offshore wind turbines for minimum levelized cost of energy* Renewable Energy vol 68 (Elsevier) pp 893-905 doi: 10.1016/j.renene.2014.02.045

[5] Ning S. A., Damiani R., and Moriarty P. J. 2014 *Objectives and constraints for wind turbine optimization* Solar Energy Engineering vol 136 (ASME) doi: 10.1115/1.4027693

[6] Bak, C., Zahle, F., Bitsche, R., Kim, T., Yde, A., Henriksen, L.C., Natarajan, A. and Hansen, M.H., *Description of the DTU 10 MW Reference Wind Turbine*, DTU Wind Energy Report-I-0092, July 2013, Roskilde, Denmark

[7] Hansen, M. H., Thomsen, K. Natarajan, A. and Barlas, A. *Design Load Basis for onshore turbines - Revision 00*, DTU Wind Energy, Technical Report E-0074(EN), Roskilde, Denmark, 2015.

[8] DTU Wind Energy Hawc2 URL http://www.hawc2.dk/

[9] Larsen, T. J. and Hansen, A. M. *How 2 HAWC2, the user's manual*, DTU Wind Energy, Risø-R-1597(ver.4.6)(EN), Roskilde, Denmark, 2015.

[10] Kim, T., Hansen, A.M. and Branner, K., *Development of an anisotropic beam finite element for composite wind turbine blades in multibody system*, Journal of Renewable Energy, 2013; 59:172-183, doi:10.1016/j.renene.2013.03.033

[11] Larsen, T.J., Aagard Madsen, H., Larsen, G.C. and Hansen, K.S., *Validation of the dynamic wake meander model for loads and power production in the Egmond Aan Zee wind farm*, Journal of Wind Energy, 2013, 2013;16(4):605-624, doi:10.1002/we.1563

[12] Popko, W., Vorpahl, F., Zuga, A., Kohlmeier, M., Jonkman, J., Robertson, A., Larsen, T.J., Yde, A., Stertr, K., Okstad, K.M., et al., *Offshore code comparison collaboration continuation (OC4), PHASE I - results of coupled simulations of an offshore wind turbine with jacket support structure*, Proceedings pf the International Offshore and Polar Engineering Conference 2012, 2012;337-346

[13] Vorpahl, F., Strobel, M., Jonkman, J.M., Larsen, T.J. and Passon, P., *Verification of aeroelastic offshore wind turbine design codes under IEA wind task XXIII*, Journal of Wind Energy, 2013; doi:10.1002/we.1588

[14] Hansen, M.H. and Henriksen, L.C.,*Basic DTU Wind Energy Controller*, Technical Report DTU Wind Energy E-0018, DTU, 2013

[15] Zahle F., Tibaldi C., Verelst D. R., Bak C., Bitche. R, and Blasques J. P. A. A. 2015 *Rotor Design Optimization Tools and Cost Models* (Bremen, Germany: IQPC Workshop for Advances in Rotor Blades for Wind Turbines) URL http://orbit.dtu.dk/files/115528875/iqpc hawtopt2.pdf

[16] NASA, http://openmdao.org, 2012.

[17] Moore, K. T., Naylor B. A. and Gray, J. S. *The Development of an Open-Source Framework for Multidisciplinary Analysis and Optimization*, in: 10th AIAA/ISSMO Multidisciplinary Analysis and Optimization Conference. AIAA 2008-6069, Victoria, Canada, August 2008.

[18] Gray, J. S., Moore, K. T. and Naylor, B. A. *OPENMDAO: An Open Source Framework for Multidisciplinary Analysis and Optimization*, in: 13th AIAA/ISSMO Multidisciplinary Analysis and Optimization Conference. AIAA-2010-9101, Fort Worth, Texas, USA, August 2010, http://www.aric.or.kr/treatise/journal/content.asp?idx=134451.

[19] Heath, C. M. and Gray, J. S. *OpenMDAO: Framework for Flexible Multidisciplinary Design, Analysis and Optimization Methods*, in: 8th AIAA Multidisciplinary Design Optimization Specialist Conference (MDO), pp. 1-13. Honolulu, Hawaii, USA, 2012.

[20] Perez R. E., Jansen P. W., and Martins J. R. R. A. 2012 *pyOpt: A Python-based object-oriented framework for nonlinear constrained optimization* Structures and Multidisciplinary Optimization vol 45 (Springer) pp 101-118

[21] Gill P. E., Murray W., and Saunders M. A. 2002 *Snopt: An sqp algorithm for large-scale constrained optimization* Journal on Optimization vol 12 (SIAM) pp 979-1006

[22] Tibaldi C., Henriksen L., and Bak C. 2014 *Investigation of the dependency of wind turbine loads on the simulation time* proceedings of EWEA 2014 (European Wind Energy Association (EWEA))

[23] I. E. Commission, International Standard, *IEC 61400-1 Third Edition 2005-08, Wind Turbines - Part 1: Design Requirements*, Reference Number IEC 61400-1:2005(EN), 2005.

[24] Bottasso, C. L., Campagnolo, F., Croce, A. and Tibaldi, C., *Optimization-based study of bend-twist coupled rotor blades for passive and integrated passive/active load alleviation*, Journal of Wind Energy, pp. 16:1149-1166. DOI:10.1002/we.1543, 2013.

[25] Koziel S., Ciaurri D. E., and Leifsson L. 2011 *Surrogate-based methods Computational Optimization, Methods and Algorithms - State of the art* in Computational Optimization vol 356 (Springer-Verlag Berlin Heidelberg) pp 33-59 iSBN: 978-3-642-20859-1

[26] Simpson T., Toropov V., Balabanov V., and Viana F. 2008 *Design and analysis of computer experiments in multidisciplinary design optimization: A review of how far we have come - or not* Multidisciplinary Analysis Optimization Conferences (American Institute of Aeronautics and Astronautics) URL http://dx.doi.org/10.2514/6.2008-5802

[27] Queipo N. V., Haftka R. T., Shyy W., Goel T., Vaidyanathan R., and Tucker P. K. 2005 *Surrogate-based analysis and optimization* vol 41 pp 1–28 ISSN 0376-0421 URL http://www.sciencedirect.com/science/article/pii/S0376042105000102

[28] Fedorov, V. and Berggreen, C., *Bend-twist coupling potential of wind turbine blades*, Journal of Physics: Conference Series - The Science of Making Torque from Wind 2014, IOP Publishing, 2014, doi: 10.1088/1742-6596/524/1/012035

[29] Tibaldi C., Henriksen L., Hansen M., and Bak C. 2015 *Wind turbine fatigue damage evaluation based on a linear model and a spectral method* Wind Energy vol 18 (John/Wiley and Sons Ltd.) ISSN 1095-4244 doi: 10.1002/we.1898

Aeroelastic Multidisciplinary Design Optimization of a Swept Wind Turbine Blade

Authors:

Christian Pavese, Carlo Tibaldi, Frederik Zahle, Taeseong Kim

Aeroelastic Multidisciplinary Design Optimization of a Swept Wind Turbine Blade

Christian Pavese[1], Carlo Tibaldi[1], Frederik Zahle[1], Taeseong Kim[1]

Abstract

Mitigating loads on a wind turbine rotor can reduce the cost of energy. Sweeping blades produces a structural coupling between flapwise bending and torsion, which can be used for load alleviation purposes. However, the design of a swept-bladed rotor is a challenging task because of the interlaced disciplines involved in the process. To deal with the complex nature of swept blade design a multidisciplinary design optimization (MDO) problem is formulated including the blade sweep as a design variable. MDO has not been previously used to design coupled blades due to the large impact that varying the sweep has on the wind turbine loads and, consequently, on the optimization process. A multifidelity approach is used to confront the crucial effects of structural coupling on the estimation of the loads. During the MDO, ultimate and damage equivalent loads are estimated using steady state and frequency-domain based models, respectively. The final designs are verified against time-domain full design load basis aeroelastic simulations to ensure that they comply with the constraints. A 10 MW wind turbine blade is optimized by minimizing a cost function that includes mass and blade root flapwise fatigue loading. The design space is subjected to constraints that represent all the necessary requirements for standard design of wind turbines. The MDO is carried out with respect to the internal structure and outer shape of the blade. Simultaneous aerodynamic and structural optimization is performed with and without sweep as a design variable. When sweep is included in the MDO process, further minimization of the cost function can be obtained. To show this achievement, a set of optimized straight blade designs is compared to a set of optimized swept blade designs. Relatively to the respective optimized straight designs, the blade mass of the swept blades is reduced of an extra 2-3%, and the blade root flapwise fatigue DEL by a further 8%.

[1]DTU Wind Energy, DK-4000, Roskilde, Denmark

G.1   Introduction

When designing rotors with increasing energy yield, the designers have to face the challenge of scaling down the increase in total mass of the blades to reach the final goal of reducing the cost of energy (COE). To this end, the capability to mitigate loads on the structure during operation becomes an attractive characteristic for the design of modern wind turbine blades. The employment of swept blades is one of several different methodologies implemented in the design process to achieve load alleviation on a wind turbine. Sweeping blades falls under the category of passive control techniques, as it relies on the idea of designing a structure that, without any active mechanisms, deforms so as to reduce the unsteady loading generated by turbulent fluctuating wind inflow. Specifically, this passive control method produces a geometrical coupling between flapwise bending and torsion. According to the direction of the sweep, the induced coupling can either mitigate loads on the wind turbine structure due to a decrease in the angle of attack (backward sweep), or increment the wind turbine power production through an increase in the angle of attack (forward sweep).

In general, the effects produced by the adoption of sweep in the design of a wind turbine rotors are known. Several studies ranging from fully detailed numerical investigations [1, 2, 3, 4, 5, 6] to experimental campaigns [7, 8] were conducted in the past decade. The factor that relates this 10-year research is the observation that the design of swept blades is a complex process, involving a deep understanding of the interlaced disciplines involved. A modern wind turbine blade is subject to large deflections and non-negligible rotations driven by wind inflow conditions of stochastic nature. Moreover, the wind turbine has to be regulated to provide a prescribed performance. Aerodynamics, structural dynamics, and control theory are the interconnected disciplines that drive the design of a wind turbine blade. The multidisciplinary nature of blade design is a challenge from an early stage of the process, as it compels the designer to satisfy simultaneously several constraints while evaluating trade-offs between conflicting objectives.

In this context, a multidisciplinary design optimization (MDO) frameworks is used to develop wind turbine blades. Design parameters are optimized with respect to a cost function, subjected to constraints that encompass particular design requirements for wind turbines. These design parameters can be several and generally refer to different components of the wind turbine and its operational characteristics. If the focus of the MDO process is exclusively the wind turbine rotor, the design variables are the internal structure and the outer shape of the blades.

Several MDO frameworks have been presented in recent years. A common objective for these optimization frameworks is the minimization of the COE, or the maximization/minimization of its main drivers, such as annual energy production (AEP) and components mass. MDO of wind turbines can be done at several levels and using models of various fidelities. For example, the design

process of wind turbines can be done on a wind farm scale where the characteristics of the installation site are incorporated in the optimization [9]. In this case, the modelling of the components and costs are done based on simplified design principles to avoid the high computational costs that a more detailed model of the wind turbine would require. If the representation of the wind turbine system is done at high-fidelity, integrated aero/structural metrics can be used to reach for better designs [10]. Aeroelastic MDO requires a complex set of interfacing tools and computationally expensive procedures. In particular, the need of running a large amount of nonlinear aero-servo-elastic simulations constitutes a practical issue to successfully perform an MDO [11]. This challenge was tackled developing a multi-stage process that alternates between a purely aerodynamic blade optimization loop and a structural one, to then obtain a final optimum solution with the combination of the two [12]. As an alternative, the aeroelastic MDO can be done sequentially, stripping to a bare minimum the amount of aero-servo-elastic simulations involved [13].

Even though the MDO frameworks available today are robust enough to produce reliable wind turbine blade designs, the present authors have not found any previous work where sweep is used as a design variable for wind turbine blades optimization. In the past, an optimized passive-controlled wind turbine design was developed [14]. The loading on the rotor was mitigated through the employment of bend-twist coupled blades (orientation of the fibres in the layups is tailored to create structural coupling between flapwise bending and torsion), but the passive control method was imposed a priori and not as a variable in the MDO. This lack of research is due to the fact that varying the sweep of the blade has a large impact on the wind turbine loading [4]. A considerable amount of aeroelastic simulations is needed to properly catch the effect of the structural coupling induced by the sweep on the loads. The first issue is that a large number of simulations represent a too expensive computational effort for an optimization framework. The second problem is that large variations in wind turbine loading are not suited with the assumption that loads change slowly with respect to changes in the design variables (*frozen loads* assumption), i.e. a small change in the blade sweep can produce large loading modifications. In particular, an inaccurate estimation of the loads on a blade can produce a wrong evaluation of the strength constraints, compromising the quality of the final design.

The key aspect of this investigation is the inclusion of sweep as a design variable in the formulation of an MDO problem. The introduction of sweep as a design variable gives to the optimization process more flexibility in the distribution of the loading on the blades, allowing the MDO to reach for further improvements of the merit function. To further stress the focus of the optimization on the variation of the loads, the minimization of the blade root flapwise fatigue moment is added to the cost function, taking the place of the AEP objective, which is enforced as a constraint in the problem formulation, i.e. an optimized design must have the same AEP than the baseline wind turbine.

The optimization framework used for this paper is HawtOpt2 [15]. Previously, the framework used the *frozen loads* assumption for the estimation of the blade strength constraints. To deal with the issue mentioned in the previous paragraph, the version of HawtOpt2 used for the current work [16, 17] estimates ultimate loads and fatigue damage equivalent loads (DEL) through steady state and frequency-domain based models, respectively. Final designs obtained from the MDO and based on the loads from these models, are checked against a standard full design load basis (DLB) [18] of time-domain aeroelastic simulations.

The first part of the paper describes the formulation of the optimization problem. The description includes details on the workflow, models, and tools used by the framework. The cost function is discussed along with the design variables selected and the constraints to which the cost function is subjected to. The second part depicts the results from an aeroelastic optimization. As the cost function of the optimization problem is a combination of two objectives, the optimized blade designs are chosen based on a Pareto front. The DTU 10 MW reference wind turbine (RWT) [19] is used as baseline design for this case study.

G.2 Formulation of the Optimization Problem

This section describes the optimization problem, starting with a description of the used framework and models. The definition of the workflow is provided, along with a detailed exposition of the cost function, design variables, and constraints.

G.2.1 Framework and Models

The optimization process is implemented in the HawtOpt2 framework [15]. Built on the platform provided by OpenMDAO (Open-source Multidisciplinary Design, Analysis, and Optimization Framework) [20, 21, 22, 23], the tool is used to handle the definition of the optimization problem, workflow, dataflow, and parallelization of simulation cases. OpenMDAO provides an interface to PyOpt [24], a container for several optimization algorithms. In this work, the gradient-based sequential quadratic programming optimizer SNOPT is used [25].

The core of the MDO framework is constitued by two tools: a finite element cross sectional code, BECAS [26, 27, 28], and a linearized aeroelastic solver, HAWCStab2 [29, 30]. These two codes are connected to the optimization platform through interfaces that allow the state-of-the-art analysis required to tackle the complexity of the blade design process.

BECAS is a cross section analysis tool for anisotropic and inhomogenous beam

sections of arbitrary geometry. In the workflow, BECAS is used for the evaluation of the cross sectional stiffness and mass properties of the blade, and for the computation of stresses and strains. The geometry of each section is exactly described through a 2D finite element formulation, which allows a description of the various layups. The cross sectional stiffness and mass properties are used to extract the inputs for the linear Timoshenko beam element model implemented in a nonlinear co-rotational formulation in HAWCStab2. The latter tool is employed to compute steady-state aerodynamic states, structural deflections, and linearized models of the wind turbine. The linear high-order aero-servo-elastic model implemented in it uses an unsteady blade element momentum (BEM) model. A detailed description of the HAWCStab2 architecture is provided by Hansen [5, 31], and the validation of the open-loop performances can be found in [32].

The version of HawtOpt2 used for the MDO adopts a quasi-steady approach to update the ultimate loads at every cost function evaluation [16]. Also fatigue DEL are updated every iteration, and they are estimated using HAWCStab2 linear models and a frequency-domain based method described in [33]. Steady-state computations and frequency-domain based methods are preferred over standard turbulent time-domain simulations for two reasons: the first merely concerns computation time, which becomes usually impractical for MDO when time-domain aero-servo-elastic tools are employed; the second is the stochastic nature of turbulence because it can compromise a gradient-based optimization process with the interaction of a changing turbine design with different parts of the same turbulent field [34]. The loads obtained through the aeroealstic solver are provided back to BECAS, which has a stress recovery module that the framework uses for the blade strength and failure analysis.

Figure G.1 provides a visual overview of the general workflow. The connections between the tools aforementioned are highlighted. HawtOpt2 selects design variables (surface and internal geometry) based on a cost function subjected to constraints evaluated by the aeroelastic solver and the cross section analysis tool. Hence, the MDO is fully aeroelastic, as design variables that affect both aerodynamic and structural behaviour of the wind turbine are considered together in the same optimization problem. Specific details on the workflow and the related numerical optimization problem are reported in the next section.

The final blade designs obtained through the MDO are checked against nonlinear models implemented in the time-domain aero-servo-elastic code HAWC2 [35, 36]. The description and the validation of the multi-body formulation used by the structural part of HAWC2 are reported in [37]. The validation of the unsteady BEM method used by the program can be found in [38, 39, 40]. The aim of this final step is to ensure that the HawtOpt2 blades comply with constraints imposed by the design requirements provided by the standards [41, 42]. Hence, a typical DLB [18] is simulated using the nonlinear models.

The DTU 10 MW RWT, coupled with the Basic DTU Wind Energy Controller [43, 44], is used as the baseline turbine.
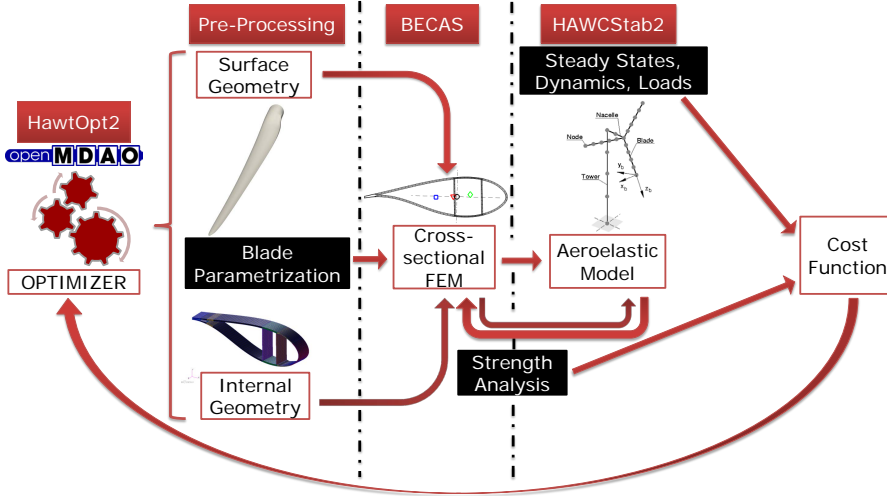
Figure G.1: General overview of the MDO framework. The link between the two tools (BECAS and HAWCStab2) and the pre-processing phase are highlighted.

G.2.2 Numerical Optimization Problem and Workflow

The numerical optimization problem formulated for the current work is the same as the one defined in ref. [15, p.3-6]. For the sake of clarity, the problem definition is reported in Equation G.1, followed by a brief description of the variables, parameters, and constraints involved.

$$
\begin{aligned}
\underset{\mathbf{x}_p, \mathbf{x}_s}{\text{minimize}} \quad & f(\{\mathbf{x}_p, \mathbf{x}_s\}, \mathbf{p}, w) \\
\text{subject to} \quad & \mathbf{g}(\mathbf{x}_p) \leq \mathbf{0}, \\
& \mathbf{h_g}(\mathbf{x}_s) \leq \mathbf{0}, \\
& \mathbf{h_s}(\{\mathbf{x}_p, \mathbf{x}_s\}) \leq \mathbf{0}, \\
& \mathbf{k}(\{\mathbf{x}_p, \mathbf{x}_s\}) \leq \mathbf{0}
\end{aligned}
\tag{G.1}
$$

The cost function f depends on two sets of variables $\{\mathbf{x}_p, \mathbf{x}_s\}$, a set of constant parameters $\mathbf{p}$, and a weighting factor w.
The design variables (DVs) include the definition of the outer shape of the blade and the definition of the internal geometry of each blade section. The first set, $\mathbf{x}_p$, is constituted by the chord, the twist, the relative thickness distribution, and the blade sweep. The $\mathbf{x}_s$ variables include the thicknesses of the material layups in different regions of the blade sections. Free form deformation splines

(FFD) with numbers of control points (CPs) appropriate to the variable selected are used to parametrize the distribution of the design variables along the blade length. A complete overview of the blade parametrization used by HawtOpt2 is provided in ref. [15, p.2-3] and [16, p.35-37]. The parametrization is part of the Framework for Unified Systems Engineering and Design of Wind Turbine Plants (FUSED-Wind) [45], developed as a collaboration between NREL and DTU Wind Energy. A summary of the planform and the structural design variables are provided in Table G.1. The DVs are all normalized such that when they are equal to zero they correspond to the value of the baseline.

The parameters $\mathbf{p}$, which are kept unaltered throughout the optimization, include the definition of the other components of the wind turbine and its operational characteristics.

A detailed overview of the blade geometry $\mathbf{x}_p$, blade layups $\mathbf{x}_s$, and parameters $\mathbf{p}$ for the DTU 10 MW RWT, used as starting design for the MDO, are reported in [19].

The control points for the FFD spline of the sweep variable (fourth line in Table G.1) are chosen based on a previous work by the authors [6]. This study underlined that the best compromise to efficiently exploit the potential of sweep is to focus the change in shape towards the outer part of the blade.

As shown in Equation G.1, the constraints, which the cost function is subjected to, are divided according to their DVs dependency. The $\mathbf{g}$ constraints are connected to the definition of the planform DVs. They include limits for the chord, the twist, the relative thickness, and the blade sweep. The bounds for the thickness of the blade layups are defined in the constraints $\mathbf{h_g}$. The blade strength constraints are represented by the vector $\mathbf{h_s}$. Finally, the constraints $\mathbf{k}$ depend on both the blade planform and structural design variables. These constraints are evaluated by the aeroelastic solver, and they include: AEP, rotor thrust, tip deflection, lift coefficients, aeroelastic frequencies, and blade root fatigue DEL. The blade root torsional DEL is allowed to be 20% higher than the one from the baseline to take into account the increase of torsional loading at the root typical of swept blades. This allowable 20% increase at the root is considered an extra loading that can be handled by the blade structure. Effects on the pitch actuator are not taken into account for the time being, and they will be the object of future investigations. An overview of all the constraints is provided in Table G.2.

The cost function is defined as

$$f(\{\mathbf{x}_p,\, \mathbf{x}_s\}, \mathbf{p}, w) = (1 - w)\frac{M(\{\mathbf{x}_p,\, \mathbf{x}_s\}, \mathbf{p})}{M(\{\mathbf{0},\, \mathbf{0}\}, \mathbf{p})} + w\frac{DEL(\{\mathbf{x}_p,\, \mathbf{x}_s\}, \mathbf{p})}{DEL(\{\mathbf{0},\, \mathbf{0}\}, \mathbf{p})} \qquad \text{(G.2)}$$

where M is the total mass of the blade, and DEL is the blade root flapwise damage equivalent load. $M(\{\mathbf{0}, \mathbf{0}\}, \mathbf{p})$ and $DEL(\{\mathbf{0}, \mathbf{0}\}, \mathbf{p})$ are the blade mass and the blade root fatigue DEL of the baseline design. The weighting factor w defines toward which of the two objectives the optimization is biased. A more detailed description regarding how the evaluation of the DELs is performed in

the framework is provided in [33].

Figure G.2 shows the extended design structure matrix [46] diagram of HawtOpt2 to give a final overview of the problem formulation, the models, and the tools involved. The tools used are highlighted in red boxes. HAWC2 is outside the matrix because it is used exclusevely to verify the final design after the optimization process is complete.

Design Variables	CPs Spanwise Distribution	DVs	Comment
Planform $\mathbf{x}_p$			
Chord	[0.0, 0.1, 0.2, 0.5, 0.85]	5	Tip chord fixed
Twist	[0.0, 0.1, 0.2, 0.5, 0.85, 1.0]	6	All control points included
Relative thickness	[0.1, 0.2, 0.5, 0.85]	4	Root and tip thickness fixed
Blade Sweep	[0.5, 0.85, 1.]	3	Inner blade geometry fixed
Structure $\mathbf{x}_s$			
Trailing edge uniax	[0.0, 0.1, 0.2]	3	Outer blade TE layups fixed. Pressure/suction side
Trailing edge triax	[0.0, 0.1, 0.2]	3	Outer blade TE layups fixed. Pressure/suction side
Trailing panel triax	[0.0, 0.1, 0.2, 0.5, 0.85, 1.0]	6	Pressure/suction side
Spar cap uniax	[0.0, 0.1, 0.2, 0.5, 0.85, 1.0]	6	Pressure/suction side
Leading panel triax	[0.0, 0.1, 0.2, 0.5, 0.85, 1.0]	6	Pressure/suction side
Leading edge uniax	[0.0, 0.1, 0.2, 0.5, 0.85, 1.0]	6	Pressure/suction side
Leading edge triax	[0.0, 0.1, 0.2, 0.5, 0.85, 1.0]	6	Pressure/uction side
Total		54	

Table G.1: Free form deformation spline (FFD) used in the optimization to define the blade design variables $\mathbf{x}_p$ and $\mathbf{x}_s$. The spanwise distribution of the control points is normalized with respect to the blade length.

Constraints	Value	Cons	Comment
Planform g			
max(chord)	< 6.2 m	1	Maximum chord limited for transport.
min(relative thickness)	> 0.24	1	Same airfoil series as used on the DTU 10MW RWT.
max(sweep at tip)	< 0.5*max(chord)	1	Maximum tip sweep limited to be lower than maximum chord for transport.
Structural h_g			
min(material thickness)	> one-ply thickness	36	Ensure that the layups have realistic thicknesses depending on section region and material.
$t/w_{sparcap}$	> 0.08	38	Basic constraint to avoid spar cap buckling.
Strength h_s			
Ultimate strain criteria	< 1.0	190	Material failure in each region of each blade section for ultimate load cases.
Aeroelastic k			
Annual Energy Production	> ref value	1	Annual Energy Production cannot be lower than that of the DTU 10 MW RWT.
Rotor thrust	< ref. value	1	Operational rotor thrust cannot exceed that of the DTU 10 MW RWT.
max(Flapwise tip deflection)	< ref. value	1	Maximum flapwise tip deflection cannot exceed that of the DTU 10 MW RWT.
max(Edgewise tip deflection)	< ref. value	1	Maximum edgewise tip deflection cannot exceed that of the DTU 10 MW RWT.

Table G.2: Constraints used in the MDO process.

Constraints	Value	Cons	Comment
Lift coefficient @ $r/R = [0.5-1.]$	< 1.35	5	Limit operational lift coefficient to avoid stall.
abs((Edge FW* mode frequency)/6P)	> 0.15	3	Aeroelastic frequency constraint to avoid resonance in three operational points.
Blade root edgewise DEL	$<$ ref. value	1	Blade root fatigue DEL cannot exceed that of the DTU 10MW RWT.
Blade root torsional DEL	< 1.20	1	Blade root torsional fatigue DEL can be 20% higher than that of the DTU 10MW RWT.
Total		280	

*FW stands for forward whirling.

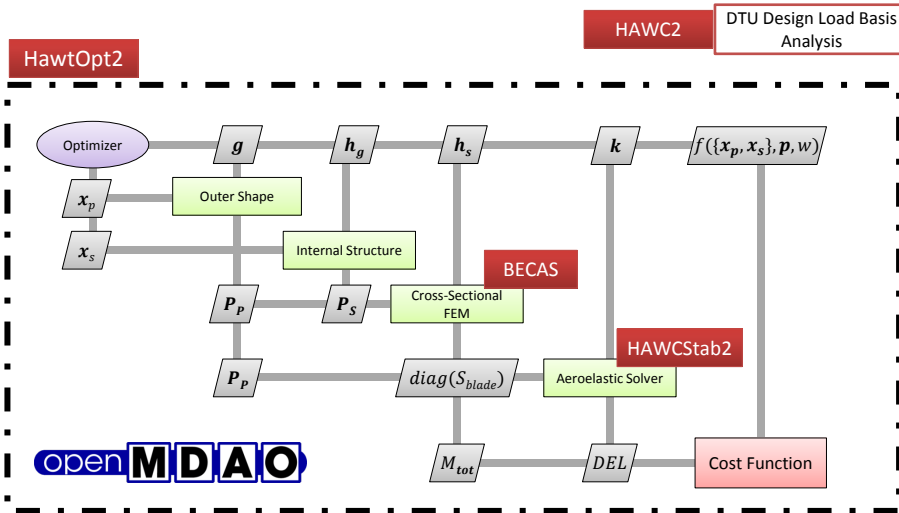**Table G.3:** Constraints used in the MDO process.

Figure G.2: Extended Design Structure Matrix diagram [46] of the workflow of HawtOpt2. The tools interfaced to the framework are highlighted by red boxes.

G.3 Results

Results from the MDO are presented in this section. The MDO process is carried out for two sets of blades: one straight and one where the blade sweep is included as a design variable in the optimization process. The aim is to offer a fair comparison, singling out the advantages of using sweep as a design variable relative to a blade design where the centreline shape is fixed. The first part of this section provides an overview of the designs obtained in terms of minimization of blade mass and blade root flapwise fatigue DEL. The designs resulting from this series of optimizations are shown in a Pareto front. One optimized straight blade design and one optimized swept blade design with same bias towards mass and DEL are picked from the Pareto fronts to analyse and compare in details the aerodynamic and structural properties of the new blades. In the last part of the section, extreme and fatigue loads evaluated through nonlinear models and standard DLB are discussed.

G.3.1 Pareto Fronts

As reported in the previous section in Equation G.2, the cost function is a compound objective that combines blade mass and blade root flapwise fatigue DEL. The weighting factor w presented in Equation G.2 defines whether the optimization process is biased towards mass or DEL. In the performed MDOs $w = [0.0, 0.25, 0.5, 0.75, 1.0]$, where $w = 0.0$ defines an optimization purely aimed at the minimization of blade mass, and $w = 1.0$ defines an optimization purely aimed at the minimization of blade root flapwise fatigue DEL. Figure G.3 shows the resulting optimized designs and how their blade mass and blade root DEL relates to the baseline design. The MDOs result in two Pareto fronts: the blue solid line with star symbols traces the last optimized straight designs while the red solid line with square symbols delineates the last optimized swept designs. On the x-axis of the plot is reported the blade root flapwise DEL normalized with respect to the baseline starting design (highlighted by the red arrow). The y-axis shows the evolution of the blade mass for the different designs normalized with respect to the mass of the DTU 10MW. The small circles represents the designs chosen by the optimizer at each cost function evaluation. They are connected by dashed lines. The blue-shaded colours are used for the straight blades, while the red-shaded colours are used for the swept designs.

In general, the MDO is able to reduce blade mass by approximately 27% (see red squares on the bottom side of the plot) and fatigue DEL by circa 25% (see red squares on the left side of the plot) for the best designs between the two sets obtained. When the blade sweep is added as a design variable in the optimization process, further reduction of the compound objective is obtained.
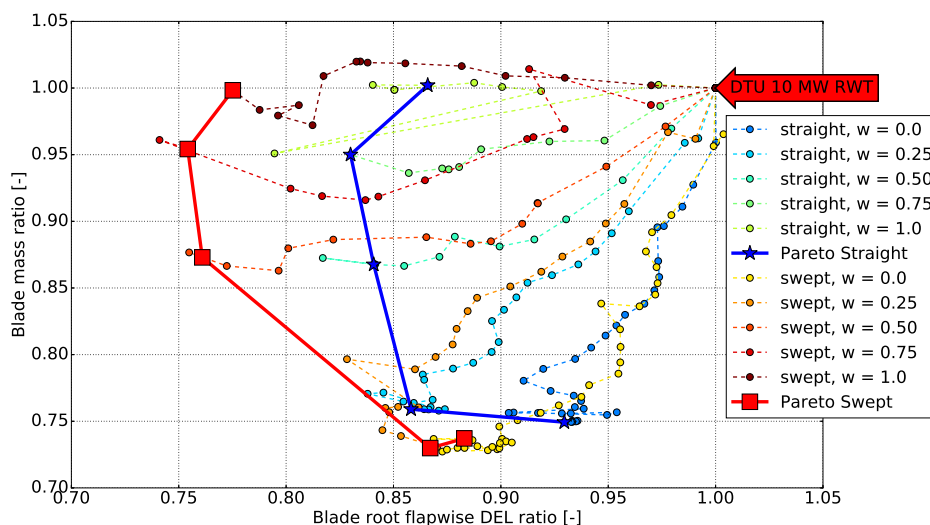
Figure G.3: Evolution of the cost function for the optimization of the DTU 10 MW RWT. The blade mass is described by the abscissas and the blade root flapwise fatigue DEL by the ordinates. Blue-shaded colours: optimized straight blade designs; red-shaded colours: optimized swept blade designs.

The optimized swept blade designs achieve further reduction of the blade mass when the cost function is biased towards mass minimization ($w = [0.0, 0.25]$). Compared to the respective optimized straight designs (the two blue stars at the bottom of the plot), the mass is reduced of an extra 2-3% (see the difference on the y-axis between the two blue stars and the two red squares on the bottom of the plot), registering a load alleviation for both design sets between 10 and 15%. The DEL biased swept designs ($w = [0.75, 1.0]$) mitigate the blade root flapwise fatigue DEL by a further 8% compared to the optimized straight blades (see the difference on the x-axis between the two blue stars and the two red squares on the left of the plot).

Table G.4 shows a list of the active constraints for each one of the optimized designs obtained. Annual energy production and blade tip displacements are active for all the designs. These two constraints are the main driver for the problem and the reason why the cost functions depicted in Figure G.3 could not be further improved in either of the two directions. The blade designs that are further biased towards mass reduction have also material thickness constraints activated. In particular, the optimization process has the tendency to reduce the TRIAX thickness.

Blade Design	Active Constraints			
Straight Blades	**Planform g**	**Structural h$_g$**	**Strength h$_s$**	**Aeroelastic k**
$w = 0.0$	None	- Leading panels TRIAX	None	- AEP - Flap/Edge tip displacements - Blade root edgewise DEL
$w = 0.25$	- Chord	- Leading panels TRIAX	None	- AEP - Flap/Edge tip displacements
$w = 0.50$	None	- Leading panels TRIAX	None	- AEP - Flap/Edge tip displacements - Blade root edgewise DEL
$w = 0.75$	- Chord - Relative thickness	None	None	- AEP - Flap/Edge tip displacements
$w = 1.0$	- Chord	None	None	- AEP - Flap/Edge tip displacements
Swept Blades	**Planform g**	**Structural h$_g$**	**Strength h$_s$**	**Aeroelastic k**
$w = 0.0$	None	- Leading panels TRIAX - Trailing panels TRIAX	None	- AEP - Flap/Edge tip displacements - Blade root edgewise/torsional DEL

Table G.4: Active constraints for the optimized blade designs.

Blade Design	Active Constraints			
$w = 0.25$	None	- Leading panels TRIAX - Trailing panels TRIAX	None	- AEP - Flap/Edge tip displacements - Blade root edgewise DEL
$w = 0.50$	None	- Leading panels TRIAX - Trailing panels TRIAX	None	- AEP - Flap/Edge tip displacements - Blade root edgewise DEL
$w = 0.75$	None	None	None	- AEP - Flap/Edge tip displacements
$w = 1.0$	None	None	None	- AEP - Flap/Edge tip displacements

Table G.5: Active constraints for the optimized blade designs.

As explained in more detail in a later section, removing the TRIAX causes the torsional stiffness of the blade to decrease, generating a load alleviation effect that allows further reduction of the blade mass. The decrease in blade mass has also consequences on the blade root edgewise DEL, which is active at the same time than the material constraints.

The following part of the section reports details regarding the planform and the structural properties of the optimized blades. Only the optimized designs with $w = 0.5$ are compared because they are considered the best compromise between the two parts of the compound objective. The general observations that will be made for the optimized straight $w = 0.5$ and the optimized swept $w = 0.5$ can be related to the other designs obtained in the MDO process.

G.3.2 Optimized Blade Planforms and Aerodynamic Forces

Figure G.4 shows a comparison between the planforms of the optimized blades and that of the baseline. Starting from the top left and proceeding clockwise, chord, absolute thickness, blade twist, and relative thickness are plotted.

The steady states distributed rotor aerodynamic normal and tangential forces, lift, and thrust coefficients at $10 \, \mathrm{m \, s^{-1}}$ are shown in Figure G.5 to facilitate the
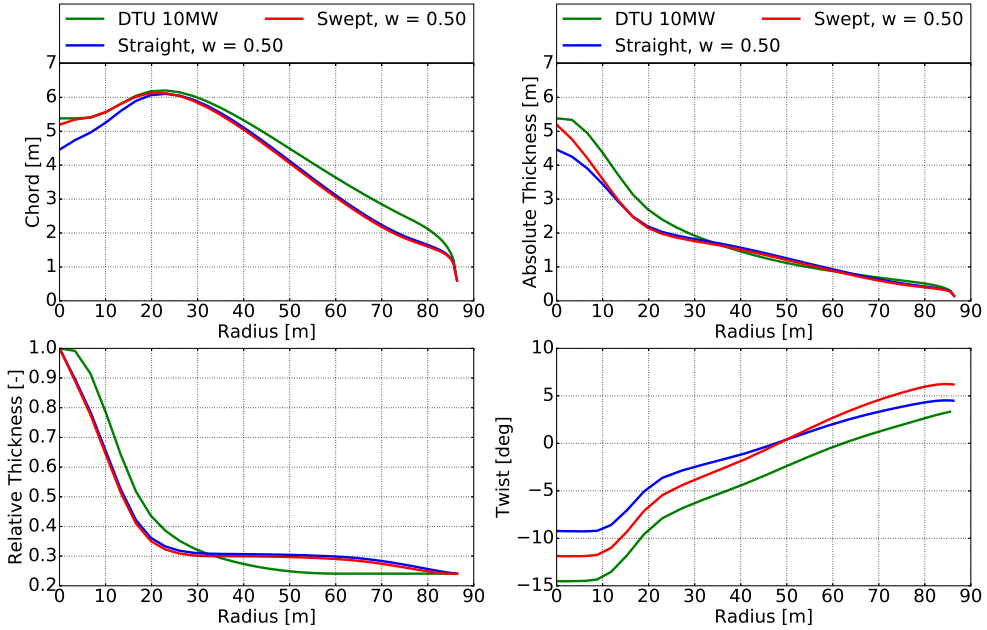
Figure G.4: Comparison between the optimized blade planforms (blue colour for optimized straight blade and red colour for optimized swept) and that of the DTU 10 MW RWT (green line). Starting from the top left and proceeding clockwise: chord, absolute thickness, blade twist, and relative thickness.

discussion on the evolution of the blade planform of optimized blade designs.
As already observed in previous aeroelastic optimization studies of the DTU 10 MW RWT [15] with active fatigue constraints, the two optimized designs have a reduced chord (see Figure G.4, top left plot) and operate at higher lift coefficients than the baseline design (see Figure G.5, bottom left plot).

As shown in the bottom left plot of Figure G.4, the relative thickness of the optimized design drops in the inner part of the blade and rises from 30 m radius on, to keep the same absolute thickness and, consequently, flapwise stiffness when reducing the chord.

The increase in absolute thickness and the decrease in chord are driven by the tip displacement constraints that are active around rated wind speed. To satisfy these constraints while reducing DEL and mass, the optimization curtails the loading at the blade tip. The distributed rotor normal force and, consequently, the rotor thrust coefficients plotted on the top left and the bottom right of Figure G.5, respectively, show the blade tip load curtailment effect.

Another important constraint that drives the optimization process is the AEP.
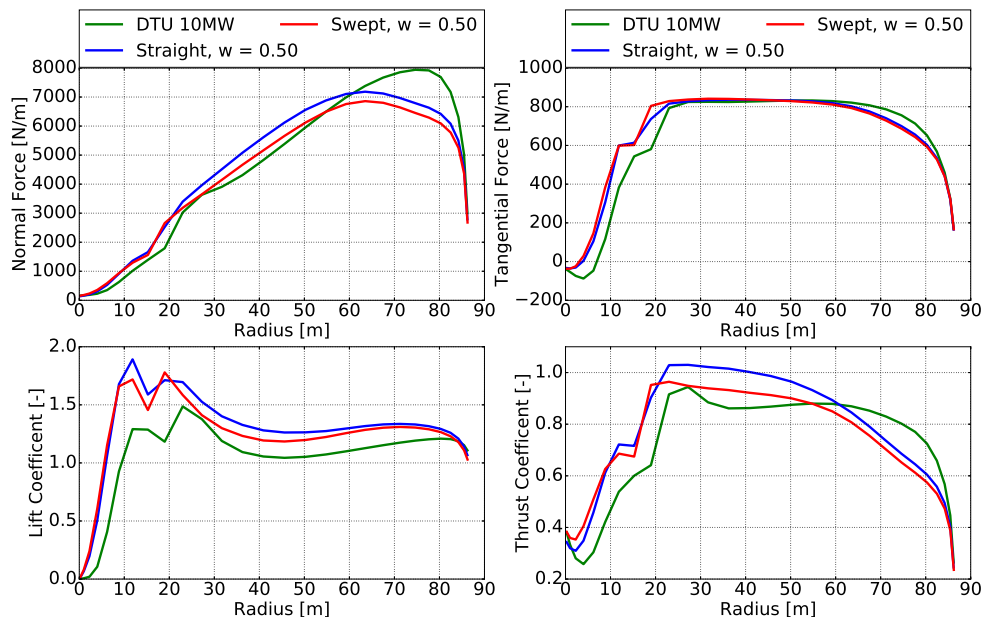
Figure G.5: Comparison between steady states at $10 \, \mathrm{m \, s^{-1}}$. Blue colour: optimized straight blade; red colour: optimized swept; green: DTU 10 MW RWT. Starting from the top left and proceeding clockwise: distributed rotor normal force, distributed rotor tangential force, thrust coefficents, and lift coefficents.

The blade planform twist is adjusted to ensure that the final designs satisfy the annual energy production required (see Figure G.4, bottom right plot). The optimized swept design is further twisted toward stall in the outer part of the blade compared to the optimized straight design. This adjustment is introduced to face the additional energy losses that swept blades undergo below rated wind speed due to the reduction in angle of attack caused by the structural coupling. It is possible to observe how the distributed normal and tangential forces, as well as the thrust coefficients, are lower on the optimized swept blade design than the optimized straight in the mid and outer part of the blade. The swept blade design achieves these reductions, not because of differences in chord and thickness, but because of the bend-twist structural coupling effect. Specifically, the relative thickness along the entire blade span and the chord and the thickness from 20 m radius on, are similar for both the optimized blades. The only difference lies at the root region, where the optimization process selects a larger root for the swept blade compared to the straight one. The reason is that swept blades have higher torsional loading at the root with consequently higher shear

forces to sustain compared to a straight blade. More details on extreme and fatigue loads are provided in the last part of this section.

Figure G.6 shows the steady state distributed angles of attack for the two optimized designs. The steady states are calculated at 5 (in blue), 11 (in red), and 20 m s^{-1} (in green). The left plot shows the absolute values of the angle of attack along the blade span. The right plot shows the variations of the optimized swept blade with respect to the optimized straight design.

The angle of attack in the inner part of the swept blade is reduced for all wind speeds due to the bend-twist coupling effect. At 5 m s^{-1} the angle of attack of the swept blade increases toward stall at the tip to compensate the loss in AEP due to the structural coupling toward feather (the blade is swept backward). At 11 the angle of attack decreases drastically, employing the load mitigation benefits of the sweep (see red line in the right plot of Figure G.6). At and 20 m s^{-1} (green line) the angle of attack decreases in the inner part of the blade where the loading is focused, increasing towards the tip to keep the a power performance similar to the straight blade.

Figure G.7 shows the curved geometry of the optimized swept design. The sweep at the tip fulfils the transportation constraint defined in Table G.2. Even though a control point for the sweep of the planform is placed at half of the blade radius, the optimizer focuses the change in sweep only closer to the outer part of the blade. The sweep is purely backward to enhance the load alleviation potential of this passive control method, and it starts at 80% of the blade radius
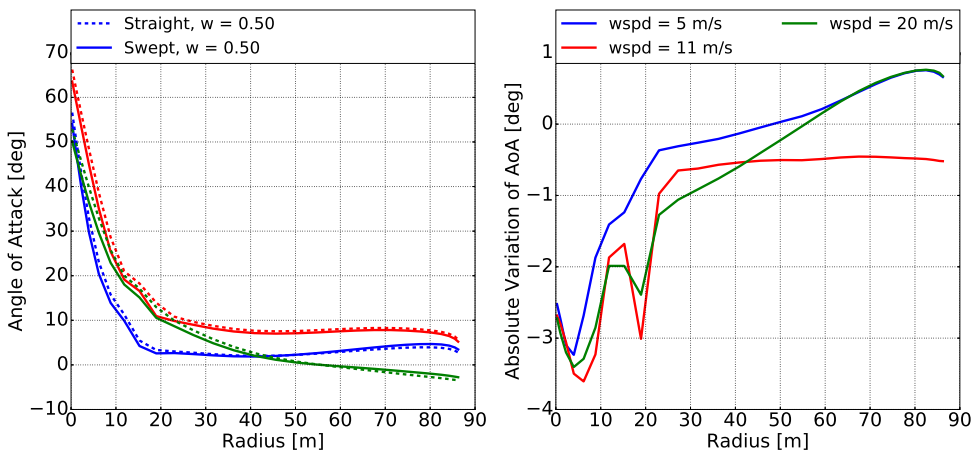

Figure G.6: Steady state distributed angles of attack at 5 (blue), 11 (red), and 20 m s^{-1} (green) for the optimized straight design (dashed lines) and the optimized swept blade (solid lines). The left plot shows the absolute values and the right plot shows the angle of attack absolute variations between the designs.
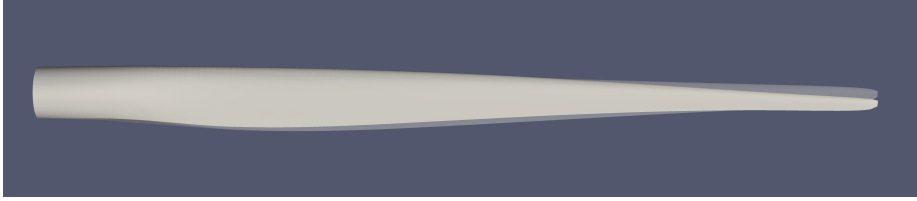
Figure G.7: Overview of the planform swept geometry of the optimized swept design ($w = 0.5$). The planform is compared with the baseline one which is shown transparent on the plot.

with a maximum backward sweep at the tip of approximately 2 m. This result is in line with the observations made in a previous work by the authors [6].

G.3.3   Optimized Blades Structural Properties

An overview of the structural properties of the optimized blade designs obtained from the MDO process is provided in this part of the section. The aim is to show the differences between the structural characteristic of an optimized swept blade compared to an optimized straight design. Figure G.8 shows the structural properties of the optimized blades normalized with respect to the baseline design. Flapwise and edgewise bending stiffness are reported in the top plots, while torsional stiffness and mass per length are plotted at the bottom of the figure.

In the blade root region, the optimization process selects a material distribution that provides higher stiffness, both bending and torsional, to the optimized swept blade than to the optimized straight one. The reason is again due to the high torsional loading and shear forces at the root caused by the introduction of the swept geometry.

For both the optimized designs, an increase in flapwise stiffness is registered in the central part of the blade. This increment is driven by the tip displacement constraints, as the optimizer looks for the best material distribution to minimize the total blade mass.

Large reductions in edgewise stiffness are obtained at the root and towards the outer part of the blade because of the reduction in chord (compare Figure G.8 top right plot with Figure G.4 top left plot).

In the central part of the blade, the optimized swept has a lower torsional stiffness compared to the optimized straight design (see Figure G.8 bottom left plot). A low torsional stiffness facilitates the load alleviation potential of the bend-twist coupling effect of the swept blade, as it is favourable for further angle
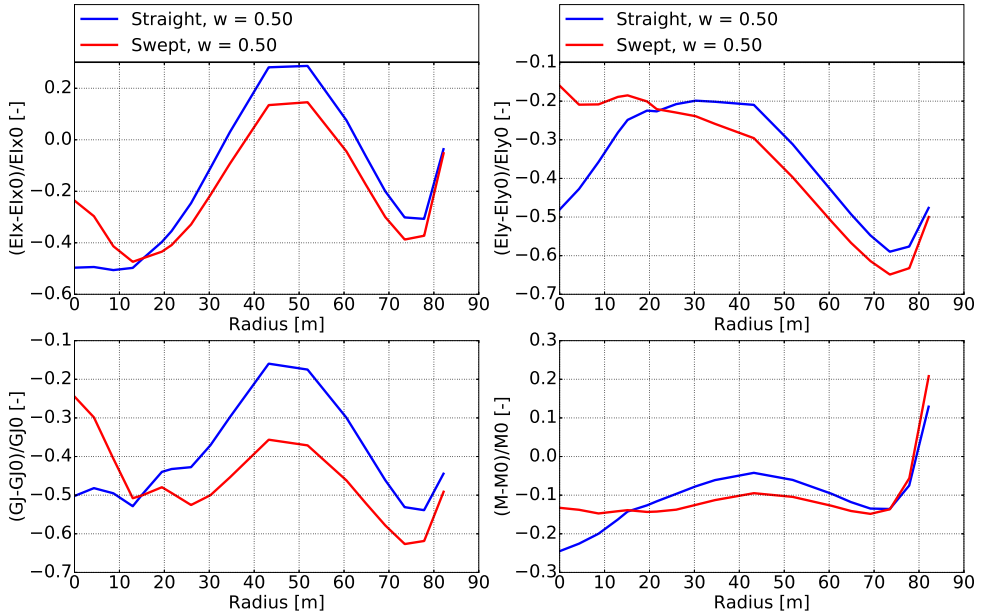
Figure G.8: Comparison between the optimized structural properties of the optimzed blades (blue colour for optimized straight blade and red colour for optimized swept) normalized with respect to the baseline design. Starting from the top left and proceeding clockwise: flapwise bending stiffness, edgewise bending stiffness, mass per length, and torsional stiffness.

of attack reductions during operation (see Figure G.6).

The decrease in total blade mass is comparable for the two optimized design analysed, as shown in the Pareto fronts of Figure G.3. The optimized swept blade has a higher mass per length in the root region compared to the straight blade to face the increased torsional loading (see Figure G.8, bottom right plot). In the central part of the blade, where the load alleviation effect of the sweep is more pronounced, the mass per length of the optimized swept design can be lowered further than a straight blade, as shown in the bottom right plot of Figure G.8.

G.3.4 Standard Design Load Basis Analysis

A standard DLB analysis is reported and discussed in this final part of the article. As previously mentioned, the optimized blades are modelled in HAWC2. An analysis of extreme and fatigue loads based on standard aero-servo-elastic simulations is carried out. The DLB and the post-processing methods for the loads used are reported in [18]. The purpose is to verify that the optimized designs obtained through the use of linear models, steady-state, and frequency domain-based load calculation methods fulfil the design requirements demanded by the standards [41, 42].

Figure G.9 shows the baseline-normalized extreme loads and Figure G.10 lifetime equivalent fatigue loads (LTEFL) of the optimized designs with $w = 0.5$. The loads are reported in radar-charts to provide an overview on different significant sensors, such as blade root, tower top, and tower bottom moments. On the extreme radar-chart also tower clearance and AEP are reported (right side of the chart).

The annual energy production of the optimized wind turbines is extremely close to the one of the baseline turbine (a loss of 0.3% is registered for the swept-bladed rotor). The tower clearance of the optimized swept turbine is higher than the baseline and the optimized straight design due to the beneficial load alleviation effect on the flapwise tip displacement around rated wind speed brought by the bend-twist coupling. The tower clearance of the optimized straight turbine is slightly lower than the baseline (approximately -4%). Considering that a steady-state linear model was used in the optimization to estimate the tower clearance, a value out of 4% (but still within the standard requirements [41, 42]) is considered acceptable.

The benefits of adding the sweep as a design variable are particularly evident on the blade root fatigue flapwise extreme and LTEFL. The total reduction of these loads with respect to the baseline is around 20% for the optimized swept design. Moreover, the load alleviation effect of the structural coupling brings an extra reduction of approximately 8% compared to the optimized straight-bladed turbine. This 8% was already highlighted by the pareto fronts shown in Figure G.3 and shows that the linearized model used to compute DELs is sufficiently accurate for multidisciplinary design optimization.

As a consequence of the blade root flapwise load alleviation, also tower top fore-aft extreme and LTEFL are consistently reduced. Once more, the addition of the sweep pays off providing a total reduction of approximately 20% with respect to the baseline, 5% extra extreme load alleviation, and 8% extra fatigue load alleviation in relation to the optimized straight design. Similar variations are registered for the tower bottom fore-aft extreme loads. The tower bottom fore-aft LTEFL of the optimized designs is not considerably reduced (it is actually slightly higher for the optimized straight design, +0.5%, and lower for the swept rotor, -3.4%). The beneficial reduction of tower bottom fore-aft loading

registered for the swept rotor, is caused by lower variations of the rotor thrust force triggered by the use of passive control.

The extreme and fatigue blade root edgewise loads are considerably reduced for both optimized designs due to the decrease in total blade mass. The alleviation is in the order of 10-13%, hence comparable to the total mass reduction shown in Figure G.3.

The optimized designs tower side-to-side loading is generally lower than the baseline turbine because of the reduction in total blade mass achieved by the MDO. As shown in the bottom left plot of Figure G.8, the optimized swept blade design has a heavier root compared to the optimized straight blade. Consequently, the swept blade has an higher mass moment compared to the straight one. A larger mass closer to the nacelle of the turbine helps reducing tower side-to-side large-amplitude vibrations and loading. This is the reason why the swept-bladed turbine has lower extreme and fatigue tower top and tower bottom side-to-side loading compared to the optimized straight design.
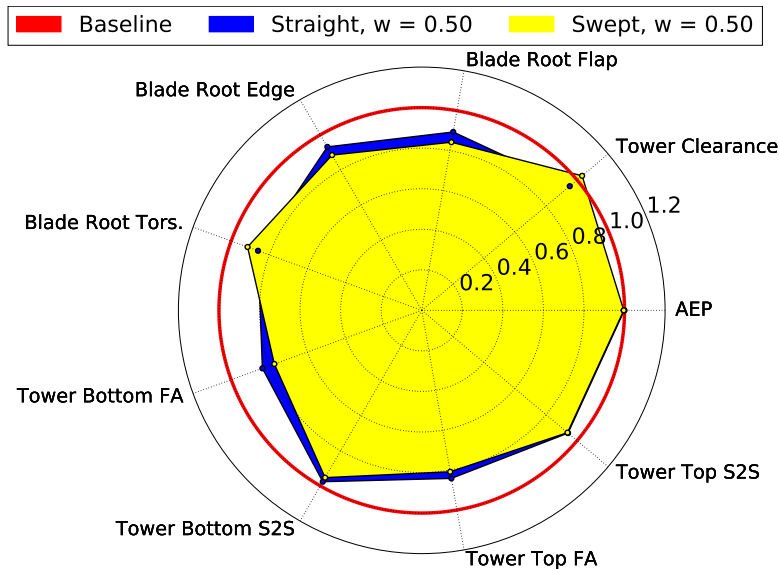

Figure G.9: DLB extreme loads reported in radar-chart plots. Load results are provided for the following sensors: blade root, tower top, and tower bottom. In the extreme radar-chart also AEP and tower clearance are reported (right side of the chart). The optimized straight blade design (blue) and the optimized swept one (yellow) are normalized with respect to the baseline loads (red line). "FA" stands for fore-aft, "S2S" for side-to-side, and "Tors." for torsional.
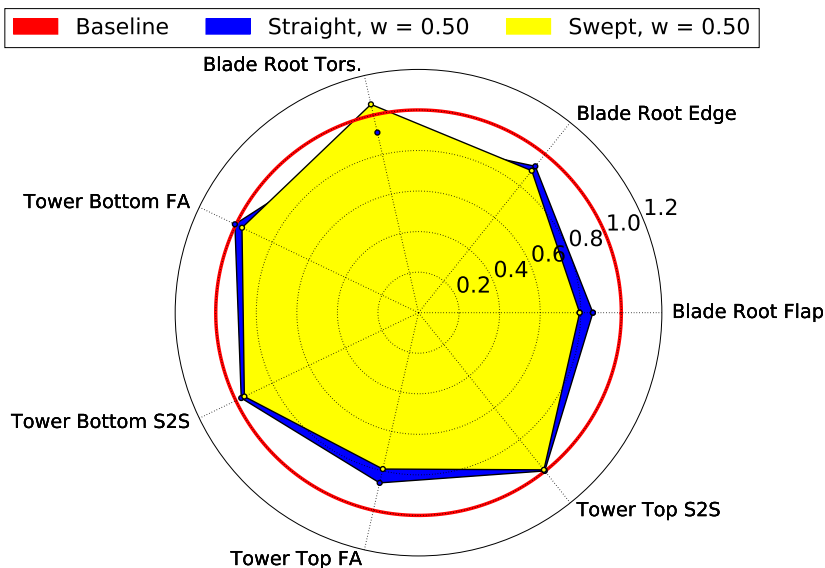
Figure G.10: DLB life-time equivalent fatigue loads reported in radar-chart plots. Load results are provided for the following sensors: blade root, tower top, and tower bottom. In the extreme radar-chart also AEP and tower clearance are reported (right side of the chart). The optimized straight blade design (blue) and the optimized swept one (yellow) are normalized with respect to the baseline loads (red line). "FA" stands for fore-aft, "S2S" for side-to-side, and "Tors." for torsional.

Even though the blade root torsional loads are higher for the swept blade compared to the straight one, they remain within the constraint imposed by the MDO (the extreme load is lower than the baseline, and the LTEFL is approximately only 5% higher than the reference value).

In general, the benefits of adding the sweep as a design variable are evident for the further load reductions that can be obtained especially on the blade root flapwise moment and, consequently, on the tower fore-aft moment. These alleviations, as previously highlighted, are due to the structural coupling between bending and torsion specifically tailored for the blades. The price to pay for the extra load alleviation effect is a slightly higher blade root torsional fatigue moment.

G.4   Conclusions

This paper includes blade sweep as a design variable in a wind turbine multi-disciplinary design optimization process. The introduction of sweep in a wind turbine blade generates a structural coupling between the flapwise bending and torsion. The effects induced by this structural coupling has an impact on the distribution of the loading along the blade span. If the MDO problem is formulated correctly, the blade sweep can be tailored to "passively" control the loads to reach for consistently better designs.

In this work, the internal structure and the outer shape of a 10 MW wind turbine blade is optimized by minimizing a compound objective including blade mass and blade root flapwise damage equivalent load. A weighting factor is set in the cost function to establish towards which of the two objectives the MDO process should be biased. The cost function of the optimization problem is subjected to constraints that represent all the necessary requirements for standard design of wind turbines. The MDO process carries out a simultaneous optimization of the aerodynamic and structural characteristics of the blade design.

The framework used performs aeroelastic optimizations of straight-bladed and swept-bladed rotors to show the effect adding the sweep as a design variable in the MDO. The Pareto fronts obtained by the two sets of optimization show that further minimization of the compound objective can be achieved when the sweep is included in the MDO process. Specifically, when the cost function is biased toward mass minimization, the blade mass of the swept blades are reduced of an extra 2-3% compared to the optimized straight designs. If the objective with the highest weighting factor is the blade root flapwise DEL, the use of sweep grants a further load reduction of approximately 8%.

To achieve the minimization of the cost function, the overall tendency of the MDO process is to increase relative thickness and operational lift coefficients, producing slender blade designs. The general aim is to shift the distributed blade loading from the tip to the inner part of the blade. The induced bend-twist coupling effect of the swept designs ensures more flexibility in the distribution of this loading, enabling the optimization process to consistently reach for better designs. A common factor in the design of optimized swept blades is that the root needs to be larger and heavier to support the inevitable increase in shear forces due to a higher torsional moment. Moreover, the torsional stiffness of the swept blade drops further than the one of a straight design as the bend-twist coupling effect is able to obtain more benefit from a less stiff structure in torsion.

As a final step, the results obtained from the MDO process are compared to non-linear models and standard aero-servo-elastic time-series simulations. Different sensors placed on blade root, tower top, and tower bottom are considered. The load analysis shows that the optimized designs inspected have generally lower extreme and fatigue loads while respecting the requirements for annual energy production and tower clearance. The optimized swept design achieves evident

load alleviations. The blade root extreme and fatigue loads reach peaks of 20% reductions compared to the baseline design, 8% more than what can be achieved by the optimized straight design. Also tower top and tower bottom loads are consistently reduced, where the effect of the sweep is more noticeable on the fore-aft direction than on the side-to-side. The optimized swept blade design pays a price on a slight increase of the blade root torsional moment, which raises by approximately 5% compared to the baseline.

In industrial applications, design concepts to mitigate loads on a wind turbine are exploited to stretch the length of the blade and increase the annual energy production. The possibility to increase the diameter of the rotor to harvest more energy while containing the increment in loading is not considered in this paper, and it will be the object of future investigations.

Acknowledgements

Bibliography

[1] Ashwill, T., Veers, P. S., Locke, J., Griffin, I. C. D. and Zuteck, M. D. *Concepts for Adaptive Wind Turbine Blades*, in: ASME 2002 Wind Energy Symposium, Paper No. WIND2002-28, pp. 56-69. Reno, Nevada, USA, 14-17 January 2002, doi:10.1115/WIND2002-28.

[2] Zuteck, M. *Adaptive Blade Concept Assessment: Curved Planform Induced Twist Investigation*, Sandia National Laboratories, SAND2002-2996, Albuquerque, New Mexico, USA, 2002.

[3] Larwood, S. and Zuteck, M., *Swept Wind Turbine Blade Aeroelastic Modeling for loads and dynamic behavior*, Windpower 2006, p.17, Pittsburgh, 4-7 June 2006.

[4] Verelst, D.R.S. and Larsen, T.J., *Load consequences when sweeping blades - a case study of a 5 MW pitch controlled wind turbine*, Technical Report Risø-R-1724, Risø-DTU, May 2010, Roskilde

[5] Hansen, M. H., *Aeroelastic properties of backward swept blades*, Proceedings of the 49th AIAA Aerospace Sciences Meeting, 4-7 January 2011, Orlando, Florida

[6] Pavese C., Kim T., and Murcia J. P. 2016 *Design of a wind turbine swept blade through extensive load analysis*, Journal of Renewable Energy, Elsevier, 2016; doi: 10.1016/j.renene.2016.10.039

[7] Ashwill, T. D., Kanaby, G., Jackson, K., and Zuteck, M, *Development of the swept twist adaptive rotor (STAR) blade*, Proceedings of the 48th AIAA Aerospace Sciences Meeting, 4-7 January 2010, Orlando, Florida

[8] Knight and Carver Wind Group, *Sweep-Twist Adaptive Rotor Blade: Final Project Report*, Sandia National Laboratories, SAND2009-8037, Albuquerque, New Mexico, USA, 2010.

[9] Fuglsang P., Bak C., Schepers J., Bulder B., Cockerill T., Claiden P., Olesen A., and Rossen R. 2002 *Site-specific design optimization of wind turbines*, Wind Energy vol 5 (John/Wiley and Sons Ltd.) pp 261-279 ISSN: 1095-4244 doi: 10.1002/we.61

[10] Ning S. A., Damiani R., and Moriarty P. J. 2014 *Objectives and constraints for wind turbine optimization* Solar Energy Engineering vol 136 (ASME) doi: 10.1115/1.4027693

[11] Merz K. O. 2015 *Rapid optimization of stall-regulated wind turbine blades using a frequency-domain method: Part 1, loads analysis* Wind Energy vol 18 (John/Wiley and Sons Ltd.) pp 1703–1723 ISSN 1099-1824 doi: 10.1002/we.1786

[12] Bottasso, C. L., Campagnolo F., and Croce A. 2012 *Multi-disciplinary constrained optimization of wind turbines* Multibody System Dynamics vol 27 (Springer) pp 21-53 ISSN 1573-272X doi: 10.1007/s11044-011-9271-x

[13] Ashuri T., Zaaijer M. B., Martins J. R. R. A., Van Bussel G. J. W., and Van Kuik G. A. 2014 *Multidisciplinary design optimization of offshore wind turbines for minimum levelized cost of energy* Renewable Energy vol 68 (Elsevier) pp 893-905 doi: 10.1016/j.renene.2014.02.045

[14] Bottasso, C. L., Campagnolo, F., Croce, A. and Tibaldi, C., *Optimization-based study of bend-twist coupled rotor blades for passive and integrated passive/active load alleviation*, Journal of Wind Energy, pp. 16:1149-1166. DOI:10.1002/we.1543, 2013.

[15] Zahle, F., Tibaldi, C., Verelst, D. R., Bak, C., Bitche, R. and Blasques, J. P. A. A. *Aero-Elastic Optimization of a 10 MW Wind Turbine*, in: AIAA SciTech - 33rd Wind Energy Symposium. Kissimmee, Florida, USA, 5-9 January 2015.

[16] Zahle F., Tibaldi C., Verelst D. R., Bak C., Bitche. R, and Blasques J. P. A. A. 2015 *Rotor Design Optimization Tools and Cost Models* (Bremen, Germany: IQPC Workshop for Advances in Rotor Blades for Wind Turbines) URL http://orbit.dtu.dk/files/115528875/iqpc hawtopt2.pdf

[17] Barlas A., Tibaldi C., Zahle F., and Aagaard Madsen H. 2016 *Aeroelastic optimization of a 10 mw wind turbine blade with active trailing edge flaps* Proceedings of the 34th Wind Energy Symposium (American Institute of Aeronautics and Astronautics)

[18] Hansen, M. H., Thomsen, K. Natarajan, A. and Barlas, A. *Design Load Basis for onshore turbines - Revision 00*, DTU Wind Energy, Technical Report E-0074(EN), Roskilde, Denmark, 2015.

[19] Bak, C., Zahle, F., Bitsche, R., Kim, T., Yde, A., Henriksen, L.C., Natarajan, A. and Hansen, M.H., *Description of the DTU 10 MW Reference Wind Turbine*, DTU Wind Energy Report-I-0092, July 2013, Roskilde, Denmark

[20] NASA, http://openmdao.org, 2012.

[21] Moore, K. T., Naylor B. A. and Gray, J. S. *The Development of an Open-Source Framework for Multidisciplinary Analysis and Optimization*, in: 10th AIAA/ISSMO Multidisciplinary Analysis and Optimization Conference. AIAA 2008-6069, Victoria, Canada, August 2008.

[22] Gray, J. S., Moore, K. T. and Naylor, B. A. *OPENMDAO: An Open Source Framework for Multidisciplinary Analysis and Optimization*, in: 13th AIAA/ISSMO Multidisciplinary Analysis and Optimization Conference. AIAA-2010-9101, Fort Worth, Texas, USA, August 2010, http://www.aric.or.kr/treatise/journal/content.asp?idx=134451.

[23] Heath, C. M. and Gray, J. S. *OpenMDAO: Framework for Flexible Multidisciplinary Design, Analysis and Optimization Methods*, in: 8th AIAA Multidisciplinary Design Optimization Specialist Conference (MDO), pp. 1-13. Honolulu, Hawaii, USA, 2012.

[24] Perez R. E., Jansen P. W., and Martins J. R. R. A. 2012 *pyOpt: A Python-based object-oriented framework for nonlinear constrained optimization* Structures and Multidisciplinary Optimization vol 45 (Springer) pp 101-118

[25] Gill P. E., Murray W., and Saunders M. A. 2002 *Snopt: An sqp algorithm for large-scale constrained optimization* Journal on Optimization vol 12 (SIAM) pp 979-1006

[26] DTU Wind Energy Becas URL http://www.becas.dtu.dk/

[27] Blasques J. P. A. A. 2012 *User's Manual for BECAS A cross section analysis tool for anisotropic and inhomogeneous beam sections of arbitrary geometry* DTU Wind Energy Technical Report, Roskilde, Denmark

[28] Blasques J. P. and Stolpe M. 2012 *Multi-material topology optimization of laminated composite beam cross sections* Composite Structures vol 94 (Elsevier) p 32783289

[29] DTU Wind Energy Hawcstab2 URL http://www.hawcstab2.vindenergi.dtu.dk/

[30] Henriksen L. C., Tibaldi C., and Bergami L. 2015 *HAWCStab2 User Manual DTU Wind Energy Technical Report*, Roskilde, Denmark

[31] Hansen M. H. 2004 *Aeroelastic stability analysis of wind turbines using an eigenvalue approach* Wind Energy vol 7 (John Wiley and Sons, Ltd.) pp 133–143 ISSN 1099-1824 URL http://dx.doi.org/10.1002/we.116

[32] Sønderby, I and Hansen, M.H., *Open-loop frequency response analysis of a wind turbine using high-order linear aeroelastic model*, Journal of Wind Energy, 2013, DOI: 10.1002/we.1624

[33] Tibaldi C., Henriksen L., Hansen M., and Bak C. 2015 *Wind turbine fatigue damage evaluation based on a linear model and a spectral method* Wind Energy vol 18 (John/Wiley and Sons Ltd.) ISSN 1095-4244 doi: 10.1002/we.1898

[34] Tibaldi C., Henriksen L., and Bak C. 2014 *Investigation of the dependency of wind turbine loads on the simulation time* proceedings of EWEA 2014 (European Wind Energy Association (EWEA))

[35] DTU Wind Energy Hawc2 URL http://www.hawc2.dk/

[36] Larsen, T. J. and Hansen, A. M. *How 2 HAWC2, the user's manual*, DTU Wind Energy, Risø-R-1597(ver.4.6)(EN), Roskilde, Denmark, 2015.

[37] Kim, T., Hansen, A.M. and Branner, K., *Development of an anisotropic beam finite element for composite wind turbine blades in multibody system*, Journal of Renewable Energy, 2013; 59:172-183, doi:10.1016/j.renene.2013.03.033

[38] Larsen, T.J., Aagard Madsen, H., Larsen, G.C. and Hansen, K.S., *Validation of the dynamic wake meander model for loads and power production in the Egmond Aan Zee wind farm*, Journal of Wind Energy, 2013, 2013;16(4):605-624, doi:10.1002/we.1563

[39] Vorpahl, F., Strobel, M., Jonkman, J.M., Larsen, T.J. and Passon, P., *Verification of aeroelastic offshore wind turbine design codes under IEA wind task XXIII*, Journal of Wind Energy, 2013; doi:10.1002/we.1588

[40] Popko, W., Vorpahl, F., Zuga, A., Kohlmeier, M., Jonkman, J., Robertson, A., Larsen, T.J., Yde, A., Stertr, K., Okstad, K.M., et al., *Offshore code comparison collaboration continuation (OC4), PHASE I - results of coupled simulations of an offshore wind turbine with jacket support structure*, Proceedings pf the International Offshore and Polar Engineering Conference 2012, 2012;337-346

[41] I. E. Commission, International Standard, *IEC 61400-1 Third Edition 2005-08, Wind Turbines - Part 1: Design Requirements*, Reference Number IEC 61400-1:2005(EN), 2005.

[42] G. Lloyd, *Guideline for the CertiFIcation of Wind Turbines*, Standard, July 2010.

[43] Hansen, M.H. and Henriksen, L.C.,*Basic DTU Wind Energy Controller*, Technical Report DTU Wind Energy E-0018, DTU, 2013

[44] DTU Wind Energy *Dtu wind energy controller* URL https://github.com/DTUWindEnergy/BasicDTUController

[45] DTU Wind Energy and NREL *Fusedwind* URL https://github.com/FUSED-Wind/fusedwind-dev

[46] Lambe A. B. and Martins J. R. R. A. 2012 *Extensions to the design structure matrix for the description of multidisciplinary design, analysis, and optimization processes* Structural and Multidisciplinary Optimization vol 46 pp 273–284 ISSN 1615-1488 URL http://dx.doi.org/10.1007/s00158-012-0763-y